CHARACTERIZATION AND POTENTIAL TECHNOLOGIES FOR HAZARD AND WASTE VOLUME REDUCTION FOR NORM-CONTAMINATED OILFIELD PROCESS VESSEL SOLIDS AND CONTAMINATED SOILS

By

MIYOUNG HAMMOND

Bachelor of Science
Texas A&M University
College Station, Texas
1987

Submitted to the Faculty of the
Graduate College of
Oklahoma State University
in partial fulfillment of
the requirements for
the Degree of
MASTER OF SCIENCE
July 1994

OKLAHOMA STATE UNIVERSITY

CHARACTERIZATION AND POTENTIAL TECHNOLOGIES
FOR HAZARD AND WASTE VOLUME REDUCTION
FOR NORM-CONTAMINATED OILFIELD
PROCESS VESSEL SOLIDS AND
CONTAMINATED SOILS

Thesis Approved:

William F. McTernan
Thesis Adviser

Gregory G. Wilkes

Thomas C. Collins
Dean of the Graduate School

ACKNOWLEDGMENTS

I must first express my gratitude to the chairman of my advisory committee, Dr. William F. McTernan for giving me the opportunity to work with such a fine group of people. Throughout my graduate career, he provided guidance, challenges, provoked thoughts, and gave me opportunities critical to my professional development. I would also like to thank the committee members, Dr. Gregory Wilber and Dr. John N. Veenstra.

Foremost, I thank Dr. J. B. Fisher for his constant encouragement and guidance throughout the preparation of this thesis. Special thanks are extended to Dr. N. P. Kemp and the Amoco Environmental Group for their patience and assistance. I appreciate the group's willingness to accept and support me during my research. Personnel at the Amoco facility were instrumental in putting together this thesis. I would like to express my sincere gratitude to Margie Meyer in Document Services. Graphics Services was also very helpful in providing all of my graphics needs.

Perhaps the greatest importance has been the love, support and patience of family and friends. I would like to thank my parents, Henry and Nancy Hammond, for their continued support and patience throughout my life which has enabled me to be where I am today. I extend sincere thanks to John Squire for his support and understanding along the way. I wish to acknowledge the help of my colleagues Karl Krieg, Alijeet Borole, Donna Lautzenhiser and Al Talley for discussions of new thoughts and ideas which have affected this work.

This work was primarily supported by Amoco Production Company. Field offices provided samples necessary for this research. The financial assistance by Amoco Production Company is greatly acknowledged.

TABLE OF CONTENTS

LIST OF TABLES

LIST OF FIGURES

Figure Page

CHAPTER 1

INTRODUCTION

Naturally Occurring Radioactive Materials (NORM)

The acronym NORM refers to naturally occurring radioactive material (NORM). Many radionuclides occur naturally at low levels. These materials are part of the natural radiation environment of the earth. For example, the radioactive isotope of potassium, K-40 comprises 0.012 percent of all potassium on earth and has a half-life of 1.28×10^9 years (Das, Faanhof, and Van Der Sloot, 1989). Radionuclides occur in nature either because the nuclide has a particularly long half-life (e.g., Rb-87, $t_{1/2} = 4.8 \times 10^{10}$ years), or because it is produced by a parent nuclide with a long half-life (e.g., Rn-222, $t_{1/2}$ = 3.84 days produced by the decay of U-238, $t_{1/2} = 4.5 \times 10^9$ years). Table I lists additional naturally occurring radioactive elements with long-lived NORM nuclides excluding uranium and thorium isotopes and their daughters.

Under the State of Louisiana regulations issued September 1989, NORM means any nuclide which is radioactive in its natural physical state (Louisiana NORM Regulations, 1989). Under these regulations, materials containing NORM which yield a radiation exposure rate greater than or equal to 25μR/hr at a distance of one centimeter, are subject to the handling and disposal provisions of these regulations (LADEQ, June 1992).

TABLE I
Additional Naturally Occurring Radioactive Elements

Nuclide	Decay Mode	Half-Life (yrs)
K-40	β	1.28×10^{9}
Rb-87	β	4.8×10^{10}
Cd-113	β	9×10^{15}
In-115	β	5.1×10^{14}
La-138	β	1.1×10^{11}
Nd-114	α	2.1×10^{15}
Sm-147	α	$1.0\,6x\ 10^{11}$
Sm-148	α	8×10^{15}
Gd-152	α	1.1×10^{14}
Lu-176	β	3.6×10^{10}
Hf-174	α	2×10^{15}
Re-187	β	4×10^{10}
Pt-190	α	6×10^{11}

Although the definition of NORM includes many isotopes, radionuclides produced by the decay of uranium and thorium isotopes are of special interest. Decay chains for U-238 and Th-232 are shown in Figure 1 (Anderson, 1990). In particular, radium (Ra) and radon (Rn) are the two radioactive elements of concern in the oil and gas industry. Although radium has over 25 isotopes, only Ra-226 produced by the decay of U-238 and Ra-228 produced by the decay of Th-232 will be considered here. These radioisotopes of Ra are of interest because of their relatively long half-lives (Ra-226, $t_{1/2}$ = 1,599 years; Ra-228, $t_{1/2}$ = 6.7 years). Similarly, Rn has a large number of isotopes, though only one, Rn-222, will be discussed here. All other isotopes of Rn have insignificantly short half-lives, and therefore cannot become widely dispersed.

Because both uranium and thorium occur naturally in underground formations and their radium decay products are slightly soluble, both Ra and Rn are produced with hydrocarbons, and hydrocarbon and water handling equipment can become contaminated by these nuclides and their decay daughters. Radium contamination can occur in any equipment which is exposed to produced water. Produced water refers to water that is produced from a well, along with oil and gas. Such contamination may be present in pipe scales, tank

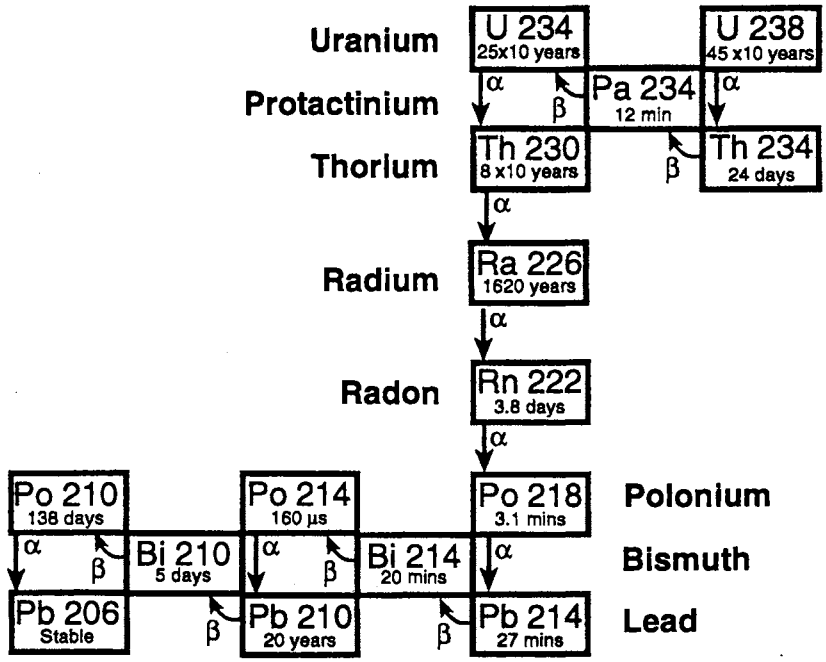

Principal decay scheme of Uranium 238

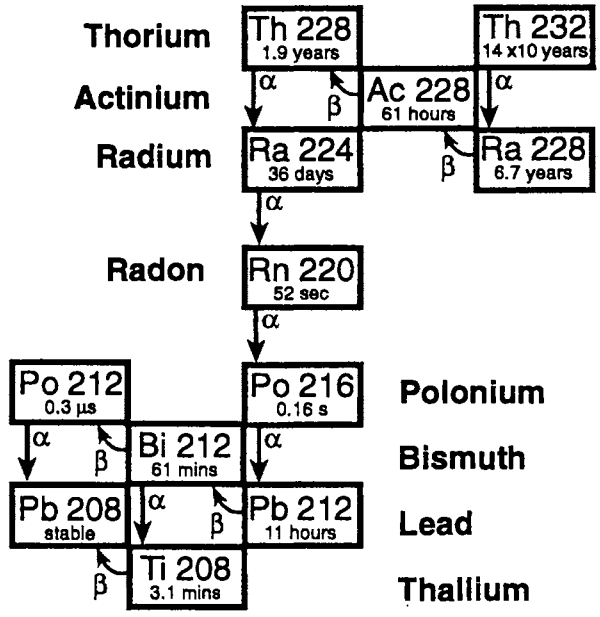

Principal decay scheme of Thorium 232

Figure 1. Decay chains for U-238 and Th-232 series.

bottom sludges, separator sands, and other precipitates arising from produced water. Radon, a noble gas, produces radioactive decay daughters (e.g., Pb-210, $t_{1/2}$ = 22.3 years) which can contaminate gas handling equipment. Since Rn has a boiling point of -61.8°C (-79.2°F), close to that of light hydrocarbon gases, it can become concentrated in cryogenically separated natural gas liquids (Gray, 1993).

Significance of NORM

Decaying atoms emit radiation in the forms of alpha particles (helium nuclei), beta particles (electrons), and gamma rays (high energy photons). These emissions are known to damage biological tissues are hazardous if a large dose of radiation is absorbed by the body (Mann, Rytz, Spernol, 1991). Because of this, strict health-based limits have been established for controllable human exposure to ionizing radiation.

Ingestion of these radionuclides in drinking water is the primary public health concern due to the long-term effects of radionuclide retention in the body (Conner et al., 1993). Maximum contaminant levels were set by the U.S. Environmental Protection Agency (EPA) in 1976 for Ra-226, Ra-228, and gross alpha and beta radiation levels in drinking water. Refer to Table II for maximum contaminant levels set by the 1976 National Interim Regulations for drinking water. Controlling NORM waste handling and disposal became a necessity to the oil and gas industry when state regulations were promulgated.

TABLE II

Maximum Contaminant Levels as Set by the 1976 National Interim Regulations

Gross alpha[a]	15 pCi/L
Radium-226 and -228	5 pCi/L
Gross beta	50 pCi/L
Man-made radionuclides	4 mrem

[a]Exclusive of contribution from uranium and radon, for which insufficient data were available to set regulations.

The EPA estimates that U.S. industry generates tens of billions of metric tons of low-activity waste each year, but the disposal options are limited (Geotimes, 1993). The EPA also estimates that petroleum operations in the U.S. generate approximately 456 x 10^3 tons of NORM wastes per year (413.7 x 10^9 grams)(EPA/SCA, 1991). Most NORM is stored, buried, disposed of on-site, or ignored (Gray, 1993). The EPA estimates that up to one-third of the oil and gas facilities in Louisiana have NORM contamination (Rutherford and Richardson, 1993). The Louisiana Department of Environmental Quality (LADEQ) estimates that over 20,000 facilities are NORM contaminated in Louisiana (Personal Communication, 1994). The disposal costs of NORM are high. The LADEQ estimates that the cost of storing these low level radioactive wastes could run about $175/cu ft (Gray, 1993). According to U.S. Ecology, the average oil field generates approximately 100 drums of NORM waste per site, and each of those drums cost anywhere from $185 to $600, depending on the concentration and type of NORM (Personal Communication, Frederick Gardner, 1993). The figures are independent of transportation costs and permitting costs. Amoco Production Company estimates onshore disposal cost to be approximately $350 per 55-gallon drum, which also includes lab work and packaging (Personal Communication, Angela Curry, 1994). Offshore disposal costs are much higher than onshore due to the cost of transportation. Amoco Production Company estimates $700 to $800 per barrel to dispose NORM waste for offshore. Cost of permitting is not included in these figures (Personal Communication, Bill Scaife, 1994).

Benefits of Achieving Workable Risk Reduction or Waste Separation Technologies

At present, there is no satisfactory solution to NORM waste disposal (Gray, 1993). The NORM-contaminated waste cannot be disposed of in ordinary landfills for oil and gas production wastes. Only a limited number of facilities are licensed to accept NORM waste, and the use of such facilities is very costly. Downhole disposal of NORM wastes is an option for low volume waste streams (e.g., pipe scale), but such disposal presents some

technical and logistic challenge, and is inappropriate for high volume waste streams (e.g., contaminated soils). For instance, the volume of a well that is 10,000 ft deep with an annular casing diameter of eight inches is approximately 622 barrels (26,000 gallons), and the volume of one acre-ft of land is approximately 7,758 barrels (326,000 gallons).

Independent of the disposal method, reduction of NORM waste stream volume is highly desirable, since only a small fraction of these NORM wastes is radioactive. Reduction of NORM waste volume would necessarily reduce future liability and reduce current costs. Further, reduction of NORM waste volume could make downhole disposal more attractive.

Objectives

The foci of the study were: (1) to perform a detailed characterization of NORM in vessel solids by evaluating chemical, physical, mineralogical, and radiochemical analyses of NORM, and (2) develop chemical and mechanical volume reduction techniques. Vessel solids include separator sands and tank bottoms. After the detailed characterization of the vessel solids, chemical and mechanical separation techniques were developed for waste volume reduction. The soil shielding experiment was performed to determine the effectiveness of various shielding materials. The radon emanation experiment was performed to mitigate radon exposure.

CHAPTER 2

BACKGROUND AND REVIEW OF LITERATURE

Occurrence of Oil Field NORM

The recognition that natural materials can emit ionizing radiation dates from Becquerel's observations of the effects of uranium-rich minerals on covered photographic plates (Becquerel, 1896) and the isolation of polonium and radium from pitchblende by the Curies (Curie, Curie and Bemont, 1898). Knowledge of the presence of natural radioactive substances in association with hydrocarbon production dates from the early twentieth century when radon was found in some Canadian natural gases (Satterly and McLennan, 1918). Since then, numerous workers have observed elevated levels of actinide decay series elements in oil, natural gas, pipe scales, and vessel solids (separator sands and tank bottoms). Published reports of these occurrences are available for the United States, the North Sea, and Russia (Anderson, 1990), but the ubiquity of U and Th in the earth's crust suggests that Ra-bearing scales will be common wherever produced water is salty, hot and depleted in sulfate. Varied formation and surface chemistries cause variations in radioactivity brought to the surface. The primary radioisotopes of interest in these so-called NORM (naturally occurring radioactive materials) contaminated materials are Ra-226 and Ra-228 in pipe scales and vessel solids, Rn-222 in natural gases, and Pb-210 deposits in natural gas handling equipment.

The widespread occurrence of actinide decay series elements is not surprising. Both parental elements, U and Th, are relatively abundant in earth solids. On a whole earth basis, U (18 ppb) and Th (65 ppb) are comparable in abundance to materials perceived as reason-

ably common (i.e., indium, 2.7 ppb; thallium, 4.9 ppb; mercury, 9.9 ppb; iodine, 17 ppb; cadmium, 21 ppb; tantalum, 29 ppb; beryllium, 56 ppb; cesium, 59 ppb; rhenium, 76 ng/g; silver, 80 ppb; and bromine, 135 ppb) (Ganapathy and Anders, 1974). Both U and Th are lithophilic elements, and consequently, both are substantially more abundant in the earth's crust than in the earth as a whole (crustal abundance: U = 2.7 ppm; Th = 9.6 ppm) (Taylor, 1964). Moreover, both U and Th are sometimes greatly concentrated in some sedimentary rock types (shales, coals, phosphatic rocks, some limestones and some sandstones) (API, 1990). Because of their chemistry, however, neither U nor Th are typically mobilized from hydrocarbon reservoirs and concentrated in scales and sludges. However, their radium decay products are slightly soluble (API, 1990). In contrast, their Ra and Rn decay daughters are mobilized from hydrocarbon reservoirs (API, 1990). Gas streams contain Rn, and gas handling equipment can become increasingly radioactive from the accumulation of Pb-210, a relatively long-lived ($t_{1/2}$ = 22 yr) decay daughter of Rn-222 (Gray, 1993). Mineral scales and sludges, particularly barite ($BaSO_4$), precipitated from produced water can become quite radioactive due to incorporation of Ra-226 ($t_{1/2}$ ~ 1,600 yr) and Rn-222 ($t_{1/2}$ ~ 3.8 days); decay daughters, respectively, of U-238 and Th-232. If produced water is discharged into earthen pits, as was sometimes past operating practice, soil in the pits may become contaminated with Ra as an exchange cation on clays, as a constituent in $BaSO_4$, and possibly otherwise.

The NORM accumulated in production equipment scales typically contains radium coprecipitated in barium sulfate. Sludges are dominated by silicates or carbonates, but also incorporate trace radium by coprecipitation. Typically, Ra-226 is in equilibrium with its decay products, but Ra-228 has subequilibrium decay products. Reduced concentrations of Ra-228 daughters result from the occurrence in the Th-232 decay chain of two radium nuclides separated by the 1.9-year half-life of Th-228. Thus, radium mobilized from the formation initially becomes depleted in Ra-224 (3.6 days) until more is generated by Ra-228 decay through the Th-228 intermediate (API, 1990).

Chemistry of Radium

Radium is an alkaline earth metal (Group IIA). The radiological significance of Ra is its incorporation in bony tissue. The chemical behavior of Ra is relatively simple. Only one oxidation state (+2) is known. It is a lithophilic element. It does not form minerals of its own. The atomic and ionic size of Ra are nearly equivalent to those of Ba. Consequently, its geochemical behavior is much like that of Ba. The key chemical characteristics of Ra in geologic settings of environmental interest (e.g., surface water, groundwater, seawater, soils and sediments) are its formation of highly insoluble sulfates and carbonates, lack of strong association with common natural ion pairing agents, and very strong binding by anionic solids. In short, Ra would not be expected to be a particularly mobile element in most natural earth surface environments. In the presence of clays or organic matter, Ra will be strongly associated with these anionic solids through cation exchange.

Radium is a polyisotopic element. Twenty-five Ra isotopes with mass numbers between 206 and 230 are known, but only four occur naturally (Weigel, 1977; Brown, Dairiki and Doebler, 1978). These naturally occurring isotopes, Ra-226, Ra-228, Ra-224 and Ra-223, are all intermediate members of the three natural actinide element decay series (Figure 1). They occur in nature only because they are continually produced by long-lived parents. Even the longest lived isotope, Ra-226, has a geologically brief half-life (1,599 yr). The half-lives of the other natural Ra isotopes are far shorter. As a consequence of its long half-life and the abundance of its long-lived parent, U-238, the most important Ra isotope in nature is Ra-226. Except for Ra-228, all of these isotopes decay via modestly energetic (~5 MeV) α emissions to yield an Rn isotope. In this process, relatively low energy γ photons (0.1 to 0.4 MeV) are also emitted. The exception, Ra-228, decays via a β emission to Ac-228, then via β emission to Th-228, and finally via α emission to Ra-224.

Since Ra is formed by the decay of U and Th isotopes, its distribution in earth materials is, to a first approximation, dependent on the distribution of U- and Th-bearing

minerals. Even so, observed ratios of Ra-226/U-238 (and ratios of Ra-224, Ra-228/Th-232) show deviations from secular equilibrium. A limiting case of radioactive equilibrium in which $\lambda_1 << \lambda_2$, and the parent activity does not decrease measurably during many daughter half-lives is known as secular equilibrium (λ is the charactistic decay constant for the species). This indicates that, as would be expected, Ra has distinctly different geochemical behavior from its long-lived parents, and thus travels through the environment via distinctly different pathways.

Because U and Th are widely distributed in the earth's crust, Ra is also widely distributed. As can be readily observed, Ra-226 is more abundant in silica-rich igneous rocks than in silica-poor rocks. Among igneous rocks, Ra-226 is more abundant in acidic rocks than in basic or ultrabasic rocks. Clay-rich, organic-rich, and phosphate-rich sedimentary rocks have far greater levels of Ra-226 than carbonate rocks which, in turn, are richer in Ra-226 than typical sandstones.

In normal uncontaminated soils, the abundance of Ra-226 appears to be controlled by the abundance of U and Th, and reported Ra-226 activities in these soils show a broad range (0.1 to 3/4 pCi/g) (Frissel and Koster, 1990; Iyengar, 1990). Soils associated with Th-rich monazite occurrences can contain 1,000 pCi/g Ra-226 (Khademi, Alemi and Nasseri, 1980), and under other special circumstances (a soil derived from highly weathered limestone associated with volcanic ash), levels of Ra-226 in excess of 300 pCi/g have been observed in uncontaminated soils (Marsden, 1963).

Typically, surface waters on continents have very low levels of Ra-226 activity. The estimated mean global value for rivers is approximately 0.07 pCi/L, but some drainage basins in North America, Europe, Asia and Africa have levels much greater than this (up to 7.9 pCi/L in a Czechoslovakian river) (Iyengar, 1990). The reasons for such elevations in Ra-226 activity reflect either local geology or anthropogenic inputs. Groundwater typically contains more Ra-226 than surface water, and Ra-226 activities measured in groundwater

are highly variable. Geothermal settings or association with U, Th or phosphate mineralization can yield very high levels of Ra-226. In Finland, for example, well water from a U- and Th-rich granite has been measured at just over 255 pCi/L Ra-226 activity (Asikainen and Kahlos, 1979).

Reported Ra-226 activity is low in all of the seawater data reviewed by Iyengar (1990). This is as expected due to the high SO_4^{-2} content of seawater. The highest value reported for seawater was just under 1.5 pCi/L. The general trend observed is for Ra-226 activity to increase with increasing water depth in the open ocean (increasing from about 0.03 pCi/L in surface waters to 0.1 pCi/L in deep waters). The apparent removal of Ra from surface seawater has been attributed to its association with siliceous organisms which, when they die and fall to the bottom, are known to scrub Ba from surface seawater. Coastal seawater Ra-226 activities are higher than open ocean surface activities and are comparable to those observed for deep oceanic water.

Observations of normal groundwater, surface water and seawater suggest that Ra is less mobile than U. Typically, the Ra/U ratio of these fluids indicates a deficiency of Ra. This is not true for high salinity deep subsurface waters produced with hydrocarbons. These waters (generally referred to as produced water or formation brine) can be highly enriched in Ra with respect to U, and the isotopic composition of the Ra indicates a variety of parental (i.e., U and Th) compositions for the Ra sources (Bobin, 1933; Komlev, 1933; Nikitin, 1933; Gott and Hill, 1953; Pierce, Mytton and Gott, 1955; Armburst and Kuroda, 1956; Kraemer and Reid, 1984; Kramer, 1981, 1985, 1986a, 1986b). Ostensibly, the high concentrations of Ra observed for produced water is due to the extremely high total salinity of these waters, their low SO_4^{-2} content, and high chloride content. Such waters may enhance the solubilization of Ra by virtue of inhibited ion exchange with clays, the lack of a low solubility precipitate, and possibly the formation of an Ra-Cl ion pair (Kraemer and Reid, 1984). Some workers have suggested that the abundance of Ra in hydrocarbon-as-

sociated waters is the result of enhanced Ra solubilization by unknown and unidentified organic-inorganic interactions (Filonov, 1964; Gustalo, 1964, 1967). Gustalo (1967) showed a fairly convincing correlation between Ra abundance and the quantity of hydrocarbon gas dissolved in subsurface waters in the Dnieper-Donets basin.

Ra is incorporated by both plants and animals in aquatic, marine and terrestrial environments. An enormous literature exists concerning Ra uptake by biota. This literature has been thoroughly reviewed in recent publications of the International Atomic Energy Agency (1990). In overview, the conclusion that can be drawn from this body of information is that although Ra is taken up by both plants and animals, it has a very poor transfer efficiency across trophic levels. Under normal environmental geochemical conditions, Ra is not substantially bioconcentrated in soft animal tissues.

Marine algae, zooplankton, molluscs, crustacea and fish incorporate radium from seawater into their tissues and concentrate it to varying degrees (concentration factors varying from ~10 to ~10^3 (Bonnoto, 1990; Iyengar and Rao, 1990). In general, lower trophic level organisms, such as phytoplankton, concentrate radium from seawater to a higher degree than higher trophic levels (e.g., fish). This is poor migration of Ra through the marine food chain. In addition, as would be expected, hard, calcified biological materials (shell, bone and chitin) are relatively richer in Ra than soft tissues (Iyengar and Rao, 1990).

In freshwater systems, planktonic and attached algae can accumulate Ra from water, and rooted macrophytes appear to be able to extract it from sediments. Observed concentration factors for both macrophytes and algae are small: (~10) for algae, and for macrophytes accumulating Ra from water, <<1 (0.014) (Williams, 1990). Freshwater porifera, molluscs (both gastropods and bivalves), arthropods (both crustaceans and insects), and fish can take up Ra from their environment (Jeffree, 1990; Justyn and Havlik, 1990). Uptake of Ra by aquatic animals depends on many factors including age, diet, nutritional status, levels of other alkaline earth metals and sex. As with marine animals, Ra

varies among tissues, but tends to be concentrated in hard calcium-rich biological materials. Concentration factors (with respect to water) for freshwater fish are comparable to those of marine fish (~1-5 x 10^2).

In general, terrestrial plants actively discriminate against incorporating Ra in their tissues. Terrestrial plants typically have bioconcentration factors <<1.0 (Simon and Ibrahim, 1990). An interesting exception to this overall behavior is the Brazil nut tree which notably concentrates Ra (~100 x soil concentrations) in its nut (i.e., endosperm) and to lesser but significantly large factors in other tissues. Interestingly, plants growing in soils with notably high Ra activities (both natural soils and uranium mill tailings) do not exhibit greater uptake, proportionally, than similar plants in normal soils. In fact, one of the surprising aspects of investigations of Ra uptake by terrestrial plants is the finding that bioconcentration factors can decrease exponentially with increasing Ra concentration.

Lastly, terrestrial primary consumers do not appear to easily transfer Ra to their soft tissues in normal environmental settings (Halbert et al., 1990). The fraction of Ra contained in food and water consumed by domestic animals that can be transferred to tissues used as food by humans is quite small (~10^{-3} maximum and typically ~10^{-4}).

Health Effects of Radiation Exposure, Biological Consequences of Radiation Exposure

If body tissue or organs are exposed to excessive radiation, biological damage can occur in the individuals exposed or in their offspring. The biological consequences of exposure to ionizing radiation include somatic effects such as anemia, fatigue, loss of hair, cataracts, skin rash, and cancer. Genetic effects include inheritable changes resulting from mutation in reproductive cells (Sawyer and McCarty, 1978).

External radiation sources can pose a threat to human health, but this threat can be easily mitigated. When naturally occurring radionuclides spontaneously decay, they emit ionizing radiation in the form of helium nuclei, electrons and high energy photons (referred

to as α, β and γ radiation, respectively). Despite their high energies, the external radiation threat to human health posed by α and β emissions can be readily mitigated by modest shielding. The energy of α particles is completely dissipated after traveling a few centimeters in air, and α particles cannot penetrate human skin. Although far more penetrating, β particles can be completely stopped by a thin aluminum sheet and can penetrate only the surface layer of human skin. In contrast, γ radiation can penetrate thick steel and can completely pass through the human body. This makes γ radiation the primary risk from an external radiation source.

Internal radiation sources pose a far greater risk to human health than external sources. Internal radiation sources, once in place, cannot be avoided. For the same degree of radioactivity, internal sources which emit α and β particles pose a greater health threat than γ emitting sources. This is because α and β particles deposit all their energy in tissues surrounding their source. The high energy photons comprising γ radiation do not interact as strongly with matter, and much of the energy from an internal γ source will pass harmlessly from the body.

Internal radiation sources derive from radioactive material that is either ingested or inhaled. After inhalation or ingestion, this radioactive material may remain as distinct foreign particles, or actually be metabolized and become incorporated in tissues. Depending on the physical and chemical nature of the inhaled or ingested material, it may or may not be able to pass from the body. The most damaging internal source materials, then, are those which are α and β emitters whose chemistry or physical size allow more or less permanent association with biological tissues.

Radium (Ra) isotopes and their decay daughters, especially radon gas (Rn), can be viewed as high health hazard materials. Most of the energy released from the decay of Ra and its decay daughter products is via the emission of α particles. The chemistry of Ra is similar to that of calcium (Ca). Consequently, Ra can become incorporated in bone and

other Ca-bearing tissues. When so incorporated, the radioactive decay of Ra and its daughter products will expose surrounding tissues to a high dose of ionizing radiation. Because it is a gas, Rn, if present in air, will be inhaled. More importantly, Rn decay yields radioactive metallic ions which may become associated with fine particles. If sufficiently fine, such particles may become lodged in deep lung tissue. In fact, inhalation of Rn-222 present in normal air is estimated to comprise the single largest radiation dose to the human population at large (Nero, 1989).

Regulatory Climate

In September 1989, the State of Louisiana became the first state to regulate NORM. The current Louisiana NORM regulations were promulgated in June 1992 (LAC 33:XV.14). These regulations contain a number of specific provisions which: (1) exempt specific materials from regulation, (2) specify radiation detector characteristics, (3) provide for general licensing of NORM producers and special licensing for NORM handlers and processors, (4) restrict the release of land contaminated by NORM, (5) specify worker protection requirements, (6) specify NORM waste storage and transfer requirements, and (7) dictate financial responsibilities for NORM transporters, treaters and storers.

The net effect of these regulations and their accompanying implementation document (LADEQ, 1992) has been the reengineering how the petroleum industry carries on normal production operations and property transfers in Louisiana. Surface equipment, piping and soil at each facility must be surveyed for radiation. Each NORM general license must submit a worker protection plan for approval by the LADEQ Radiation Protection Division. All NORM-contaminated areas must be clearly marked. Release of land for unrestricted use must pass a stringent radiation survey and a written request for release must be submitted to the Radiation Protection Division. Approval of NORM disposal options is conducted on a case-by-case basis. NORM-contaminated piping and equipment must be

given special handling, and decontamination of NORM-contaminated equipment and handling of NORM waste must be conducted by a specially licensed contractor.

Proposed and existing regulations in other states vary in detail, but are generally similar to those in force in Louisiana. At present, four states (Louisiana, Mississippi, Arkansas and Texas) have NORM regulations in force and thirteen states (Alabama, Kentucky, New Mexico, Oklahoma, Illinois, Michigan, Alaska, Kansas, Ohio, California, Colorado, North Dakota and Pennsylvania) either are reviewing and revising NORM regulation drafts or are studying the issue of NORM regulation. No federal regulations with specific reference to NORM are currently in force. Even so, this issue is under study at the federal level (EPA, 1991). Further, some materials containing elevated levels of NORM in the absence of a specific exemption could be regulated under Hazardous Materials Regulations 49CFR 171-179. Lastly, NORM wastes generated by operations regulated by the MMS (Minerals Management Service) are subject to MMS restrictions and guidance. As currently practiced, NORM waste management involves identification of NORM contamination, decontamination of tubulars (tubing), equipment and soil, packaging of NORM wastes, and disposal of NORM wastes. A general guidance document has been prepared by American Petroleum Institute (API) (API, 1992).

NORM contamination is identified using commonly available NZI scintillation detectors capable of μR resolution. Tubulars and equipment are decontaminated by water or air blasting techniques engineered to eliminate air emissions of particulates. Detailed decontamination may require hand scrubbing. Few soil decontamination projects have been attempted to date, but these have typically involved excavation. When possible, NORM-contaminated fines have been concentrated from inert coarse materials (e.g., shells). NORM waste packaging is somewhat variable. Often, NORM wastes are simply placed in 55-gallon steel drums, but "encapsulation" in lengths of steel casing or PVC pipe has become an increasingly practiced alternative (Hoover, 1994).

Both downhole and landfill disposal of NORM wastes are accepted alternatives (API, 1990). Because of a general fear of uncontrolled dispersion, NORM waste downhole injection has not been frequently practiced. More often, NORM wastes have been "entombed" as part of the material used in well plugging and abandonment operations. Since, in reality, landfill disposal of NORM wastes actually constitutes storage rather than disposal, it is a less desirable "disposal" option. Nevertheless, landfilling at the two sites in the United States which will accept NORM wastes is frequently practiced for purely logistical reasons (i.e., wells scheduled for plugging and abandonment are not always available).

CHAPTER 3

MATERIALS AND METHODS

Characterization of NORM Vessel Solids

Examples of vessel solids (tank bottoms and separator sands) were obtained from equipment located in the Gulf Coast region of the United States and from Trinidad. Upon receipt, these samples were divided into aliquots for specific analyses: oil, water and solids content, mineralogical composition, bulk chemistry, particle size, radionuclide identification and quantification, scanning electron microscopy and surface chemistry. Excess vessel solids were combined as a "composite vessel solids" sample which was used in the mechanical separation and dissolution experiments. Table III provides a summary of the analyses conducted and the methods employed. Table IV provides cursory information concerning the origin of the samples tested. The general scheme of sample processing and analysis is shown in Figure 2.

Radiation Screening

Before the samples were extensively processed, risks that might be associated with sample processing and shipping was assessed by screening each sample for emission of γ radiation. The γ radiation field at a distance of one inch from the sample was measured with a Ludlum Model 3-97 survey meter using the internal 1 in. x 1 in. NaI detector (Ludlum Measurements, Inc., Sweetwater, TX). Samples were received in plastic bags or glass jars. Measured radiation field intensities (adjusted for background radiation of approximately

TABLE III

Analyses Used in Vessel Solids Investigation

Analysis	Methods Used
Gross physical Examination	Visual Observation, Photography
Microscopic Examination	Optical Microscopy, Photomicrography, Scanning Electron Microscopy
Particle Size Characterization	Sieve Analysis, Laser Interferometry, Scanning Electron Microscopy
Surface Chemistry	Scanning Electroscopy, Energy Dispersive X-Ray Fluorescence, Electron Backscatter Imaging
Bulk Chemistry	Wavelength Dispersive X-Ray Fluorescence, Inductively Coupled Atomic Emission Spectroscopy
Mineralogy	X-Ray Diffractometry
Oil, Water, Solids Content	Gravimetric Thermal Retorting
Radiochemistry	HPGe Gamma Spectrometry Radiation Field Determination

TABLE IV

Geographic Locations and Sample Type

Sample	Geographic Location	Sample Type	Dose Rate* (μR/hr)
11374-2	Eugene Island	Separator Sand	900
11374-3	E. M. Watkins Lease	Separator Sludge	60
11374-4	Lacasine Old Thorwell Field	Pipe Scale	4,000
11374-5	South Florence Field	Tank Bottom	20
11374-7	Bickham No. 1	Separator Sand	10
11374-8	Bickham No. 2	Separator Sand	20
11374-9	South Florence (E. M. Watkins)	Separator Sand	10
11374-10	South Kaplan (E. M. Watkins)	Separator Sand	90
11374-11	Georgia Pacific, Livingston Parish	Separator Sand	1,000
11374-12	Georgia Pacific No. 3	Separator Sand	20
11374-57	Pennington No. 3	Separator Sand	95
11374-58	Trinidad	Sludge	25
11374-80	OCS 61248 MBD-0150	Separator Sand	150
11374-81	OCS 61248 MBD-0100	Separator Sand	160
11374-82	OCS 61248 MBD-0160	Separator Sand	28
11374-83	OCS 61248 M117	Separator Sand	170
11374-84	OBU Sample	Separator Sand	18

*Measured one inch from the sample

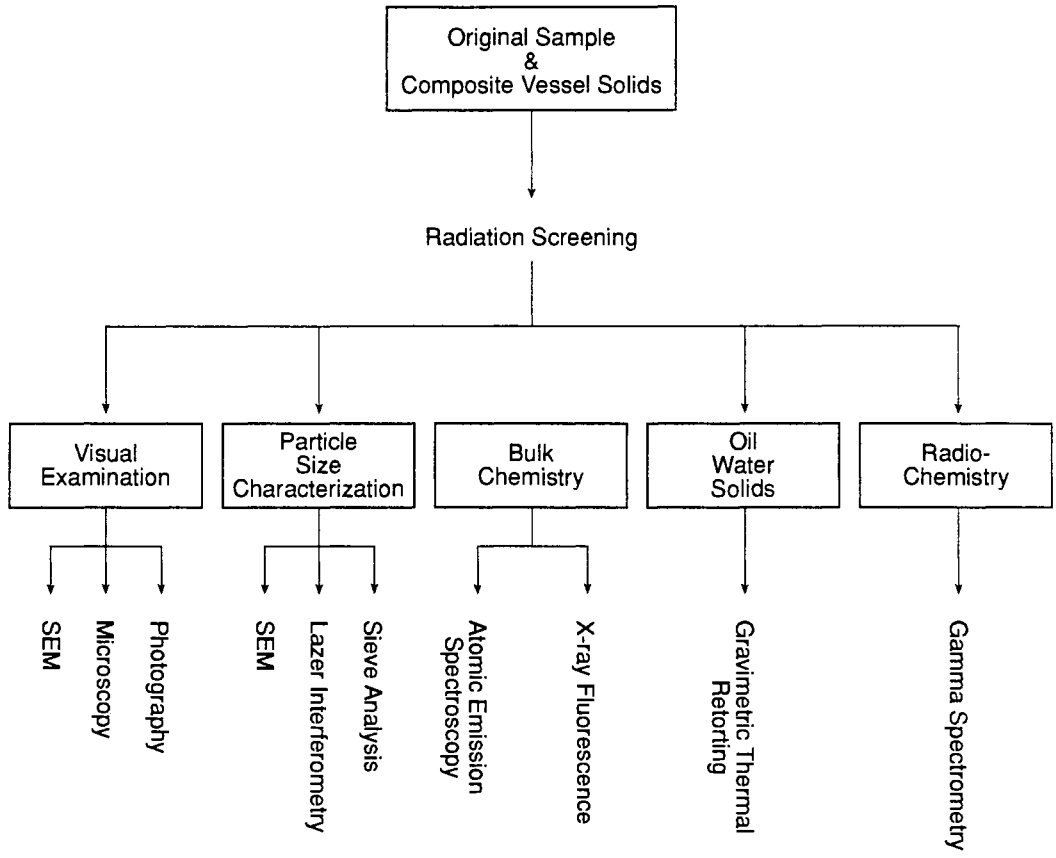

Figure 2. Schematic of sample processing and analysis.

10 μR/hr) ranged from 10 μR/hr to 4,000 μR/hr. None of the samples, therefore, could be considered especially hazardous. The exposure limit specified for the general public by the Nuclear Regulatory Commission is 0.5 rem/hr based on continuous exposure, 24 hours per day and 365 days per year.

Visual Examination and Surface Chemistry Determinations

All samples were examined optically using a stereomicroscope, and documentary photographs were made of all samples as received (normal photographs and photomicrographs). In addition, selected samples were examined by scanning electron microscopy (SEM) to obtain a photographic record of grain sizes and grain shapes. The distribution and associations of barite in these samples were investigated with the SEM by obtaining barium maps backscattered electron imaging. Gross chemistry of the viewing field was

also determined using an energy dispersive X-ray spectrometer (KEVEX (Unispec System 7000, San Carlos, CA). KEVEX results show the elements present in the vessel solids. All SEM work was conducted on samples which had been cleaned by dichloromethane reflux extraction to remove hydrocarbon. Samples were mounted on a carbon stub and sputter--coated with gold and palladium.

Oil, Water and Solids Content

The oil, water and solids content of the samples was determined using a Baroid 50 ml retort (Baroid Testing Equipment, Houston, TX). This device expels water and oil from the samples by heating a known mass of sample. The expelled water and oil are condensed and collected in a graduated tube which can be read to an accuracy of 0.5 ml. The volumes of expelled liquid are converted to masses through knowledge of their density. To insure that mass balance was maintained, original sample mass was compared to the sum of retorted sample mass plus expelled fluid mass (weighed). In all cases, mass was conserved.

Mineralogy

The mineralogy of each sample was determined by X-ray diffraction (XRD) using a Seimens D500 X-ray diffractometer and data analysis system (Seimens Instruments, Federal Republic of Germany). Samples were air dried, and any oil present in the sample was removed by reflux extraction with dichloromethane using a Soxtec System HT2 (Tecator, Hoganas, Sweden). Samples were ground to 50 μm or less prior to analysis as random powder mounts. The resulting diffractograms were interpreted by comparison to diffractograms obtained from standard solids. X-ray diffractometry can only examine crystalline materials present at percent levels. The method is completely blind to amorphous materials and is not sufficiently sensitive to detect crystalline phases present at less than ~1%.

Particle Size Characterization

Particle size analysis was conducted using two methods. The mass of particles larger than 180 μm was determined by sieving. The size distribution of particles finer than 180 μm was determined by laser interferometry using a Laser Optical Particle Sizer (Malvern Instruments, Malvern, England). Samples were cleaned by reflux extraction with dichloromethane prior to this analysis. A known mass of this dried material was placed in a 100 ml beaker containing 50 ml of a solution of sodium hexametaphosphate (.01%). This suspension was sonicated (Model W-380 Sonicator, Heat Systems-Ultrasonics, Inc., Farmingdale, NY) for 15 minutes to diaggregate and disperse particles. Particles larger than 180 μm were removed by set sieving. Particles retained on the sieve were dried and weighed. The size distribution of particles passing the sieve was then determined using the Laser Optical Particle Sizer following the protocol set out by the instrument manufacturer.

Bulk Chemistry

Samples for bulk chemistry were forwarded to the contract laboratory (XRAL, Don Mills, Ontario, Canada) as received. At the contract laboratory, the samples were cleaned and processed prior to elemental analysis by wavelength dispersive X-ray fluorescence (XRF) and inductively coupled plasma atomic emission spectroscopy (ICP-AES).

Quantification of Radionuclides

All radionuclide activity analyses were conducted using a Genie-PC Gamma Spectroscopy System (Canberra Nuclear, Meridian, CT). This system was comprised of an 18% efficiency HPGe (high purity germanium) capable of both 4π (i.e., well) and Marinelli counting geometries, a 4096K multichannel analyzer, and data handling software. All analyses were calibrated against an NBS traceable mixed gamma standard (Amersham Certificate Standard No. 792041). All analyses were conducted using a 4π geometry. Prior to analyses, all samples were cleaned using dichloromethane reflux extraction. A consis-

tent mass and geometry of sample was weighed into a 10 x 75 mm acrylic test tube and sealed. Typical counting times for these samples were 12 hours, but times were varied to accrue comparable total counts among samples. Quantification of Ra-226 was accomplished by measuring its direct γ at 186.21 keV. Interference at this energy from the primary U–235 γ at 185.71 keV was addressed by examining the spectra for other U-235 lines; none were found. Confirmation of Ra-226 was addressed by examining the spectrum for its decay series daughter Bi-214 at 609.31 keV; this energy was consistently present. Quantitation of Ra-228 was accomplished by measuring its short-lived ($t_{1/2}$ = 6.7 years) Ac-228 daughter at 911.6 keV. All counting experiments were conducted in a lead shield manufactured by Canberra Nuclear for this detector. All analyses were made on a background subtracted basis, corrections for detector efficiency, decay, etc., were made by the data analysis software.

Soil Shielding Experiment

The soil shielding experiment was conducted to determine the effectiveness of various commonly available covering agents to mitigate γ radiation from buried NORM material. A sample of barite scale obtained from the NORM Environmental Services Company (a special licensee) processing facility in Amelia, LA, was tumbled using a large sample tumbler (Model 1317, Associated Design and Mfg. Co., Alexandria, VA) to obtain a consistent, finely divided, and well packed mixture. This mixture was then formed into a confined rectangular source (11-1/2 x 12-1/2 x 5/8 inch) by first double-bagging it in one-gallon Ziploc^{TM} bags. This source was then placed in a plywood box with an acrylic front having dimensions of 12-1/2 x 13-1/2 x 8 inch. The specific activity of Ra isotopes present in the source as determined by γ spectroscopy was 1,085.2 pCi/g for Ra-226 and 111.1 pCi/g for Ra-228. The γ radiation field at various distances above the source were then measured with and without various thicknesses of fill material. A schematic diagram of the experimental setup is given in Figure 3. The fill materials used were: (1) marine

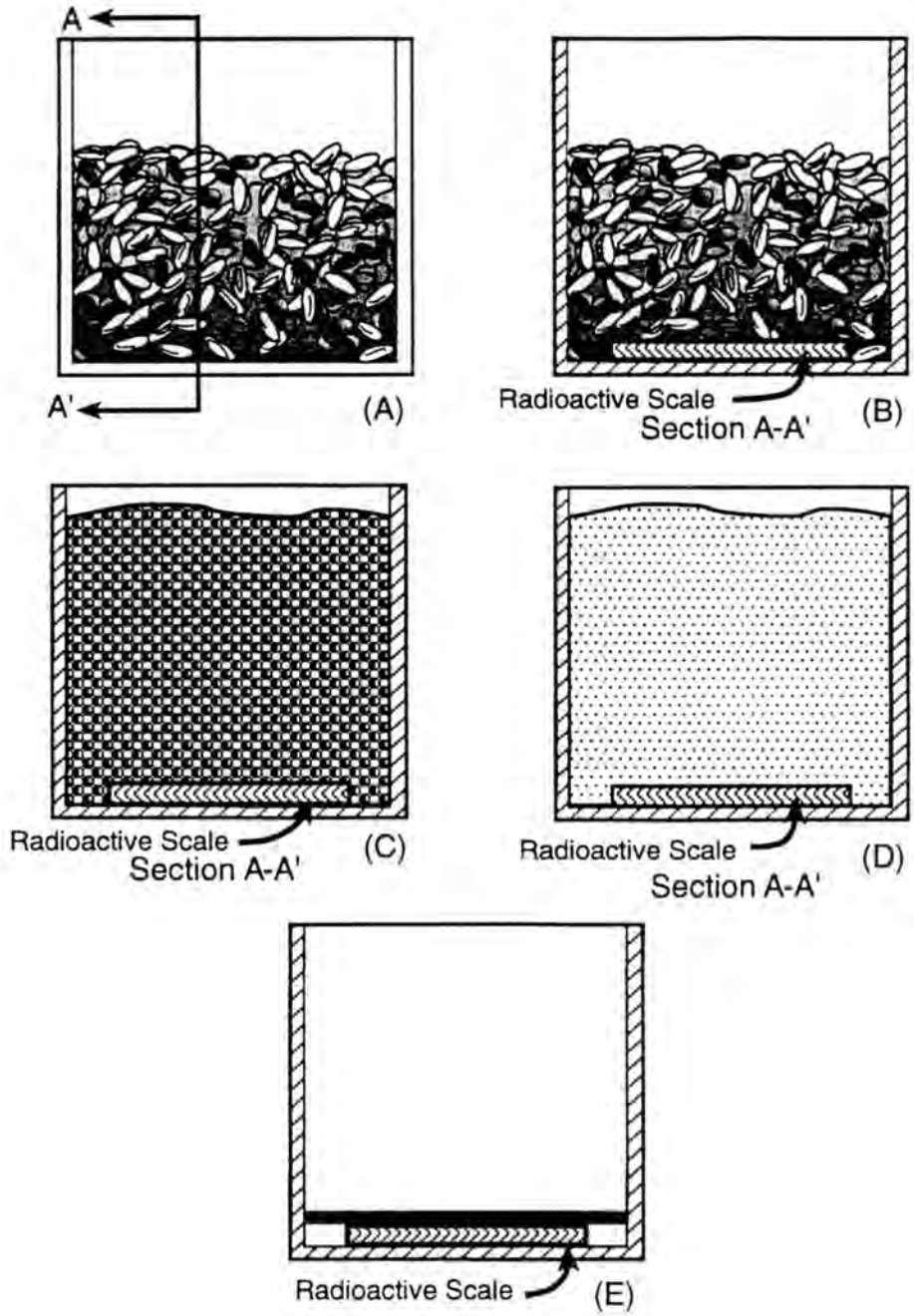

Figure 3. Experimental design of soil shielding. (A) Front view of mollusc shells. (B) Cross-section view of mollusc shells. (C) Cross-section view of limestone pellets. (D) Cross-section view of Ottawa sand. (E) Cross-section view of sheets of lead.

bivalve mollusc shells typically used for location paving in the Gulf Coast area, (2) standard Ottawa sand, and (3) limestone pellets. For reference, radiation field measurements were also made with a 0.125 inch lead sheet covering the NORM radiation source. The marine bivalve shells can be described as flat rectilinear grains having average dimensions of 4-1/2 x 4 x 1 cm. The standard Ottawa sand was obtained from VWR and is specified to be 30-40 mesh. The limestone pellets were manufactured by Revelle (Des Moine, IA) and are 15-20 mesh.

Radon Emanation Experiment

The radon emanation experiment was conducted to determine the effect of the presence of an activated charcoal absorbent to mitigate radon emanation. This experiment was conducted using the "accumulation method," and, overall, follows the procedure of Wilson and Scott (1992). Materials used were the NORMCO scale material (see above), standard Ottawa sand (30-40 mesh), and activated coconut charcoal (EM Science, Gibbstown, NJ), 8-12 mesh. The one-quart size paint can and its content used for this experiment are shown in Figure 4. Experimental design of the radon emanation experiment is shown in Figure 5. The samples containing lower percentages of scales represent contaminated soil. The 100% scale sample represents equipment scales.

Scale-sand mixtures were made by tumbling (48 hours) a weighed amount of Ottawa sand with a weighed amount of NORM-contaminated scale. The 100% scale experiments were conducted with the scale on an as-received basis. The scale was not subjected to tumbling, but was dried. Specific activities of both Ra-226 and Ra-228 were determined for each mixture and the pure scale sample.

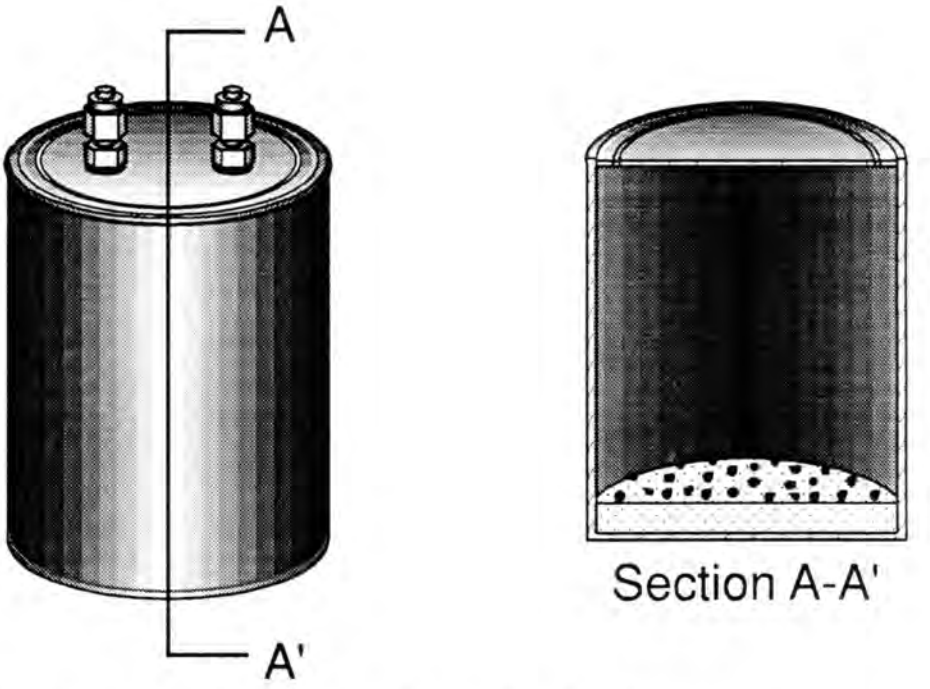

Figure 4. Cross-section view of sand, scale, or scale and sand mixture with activated charcoal addition.

Amount of Charcoal Added (g)	Amount of Scale Added* (g) 0	.5	1	100
0	3 Replicates	3 Replicates	3 Replicates	3 Replicates
1	3 Replicates	3 Replicates	3 Replicates	3 Replicates
2	3 Replicates	3 Replicates	3 Replicates	3 Replicates
4	3 Replicates	3 Replicates	3 Replicates	3 Replicates
8	3 Replicates	3 Replicates	3 Replicates	3 Replicates

* in 100 grams total

Figure 5. Experimental design of radon emanation.

The scale, sand, or scale-sand mixtures were sealed inside one-quart paint cans along with various amounts of activated coconut charcoal, completely degassed by vacuum, returned to atmospheric pressure, and then allowed to grow in Rn-222 for 30 days. At the end of this period, an aliquot of gas was removed from the can and assayed for total Rn activity. Radon analyses were conducted using gas scintillation counting. The specific equipment used was a Pylon Model AB-5 portable radiation monitor and Pylon Model 110A Lucas Cells (Pylon Electronics, Ottawa, Ontario, Canada).

Mechanical Separation Experiment

The mechanical separation experiment was conducted to determine if the finely divided NORM-contaminated barite in the vessel solids could be effectively separated from the nonradioactive components of the vessel solids. In all, six experiments were conducted. Experimental conditions used are outlined in Table V. The format of the tests involved mixing the composite vessel solids with water to achieve a 10% (by volume) slurry in a ten-gallon container. This slurry was fed through a hydrocyclone at a measured rate of 40 gpm using a 5-hp pump running at 3,520 rpm. Figure 6 shows the flow diagram of hydrocyclone experiment. Solids present in both the overflow and underflow streams from the hydrocyclone were collected and assayed for radioactivity.

TABLE V

Experimental Design for Hydrocyclone Experiment

Untreated Original untreated sample	**Dispersator Only** Slurried with water and sheared for 45 minutes	**Dispersant Only** DFLC was added to the slurry
Dispersator and Dispersant Sheared for 45 minutes with DFLC added	**Dispersant and Dispersator**** 	**Ultrasonic Probe** Sheared for one hour with DFLC added

**Underflow was collected and fed through the hydrocyclone. Additional water was added to make up the ten gallons. This was done to simulate hydrocyclones running in series.

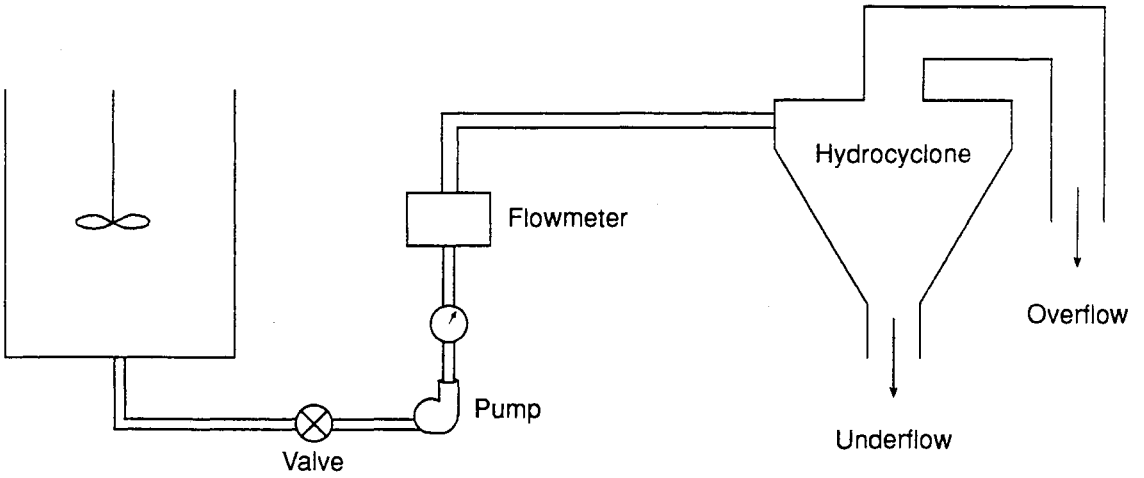

Figure 6. Flow diagram of hydrocyclone experiment.

Drillaid DFLC (Welchem, Inc., Houston, Texas) is a low molecular weight sodium polyacrylate. DFLC was used to disagglomerate vessel solids prior to being fed through the hydrocyclone. The dispersator (Premium Mill Corp., New York) is a high shear mixing device with variable speed control. The ultrasonic probe (Ultrasonic Liquid Processor, Model W-380, by Heat Systems- Ultrasonics, Inc., Farmingdale, New York) uses a wave frequency above the audible range to shear and disagglomerate particles.

Dissolution Experiment

The dissolution experiment was conducted to determine the possibility of separating the finely divided NORM-contaminated barite from the nonradioactive components of the vessel solids by dissolution. Two dissolution media were used in these experiments. The first dissolution media was Calnox-271, a commercial barite scale dissolver produced by Baker Chemical. The second dissolution media was a solution adjusted to a pH of 12 with KOH containing 196,700 mg/l DPTA (diethylaminepentaacetic acid) and 45,000 mg/l oxalic acid. Experiments were run in duplicate. In each experiment, unwashed composite vessel solids were combined with 60 ml of dissolution media in a 250-ml acrylic plastic jar and shaken for 24 hours. The samples were then removed from the shaker and allowed to

settle for 24 hours at room temperature. Solids were dried following separation from the liquid by decantation, centrifugation and filtration. Both solids and liquids were retained, and the specific activity of both solids and liquids was determined by γ spectroscopy. One set of experiments was conducted at room temperature. The other set of experiments was conducted at 75°C.

CHAPTER 4

RESULTS AND DISCUSSION

Introduction

This chapter presents and discusses results obtained from the NORM vessel solids characterization study, the soil shielding experiment, the radon emanation experiment, the mechanical separation experiment, and the chemical dissolution experiment. The goals of this work were to: (1) establish the chemical, mineralogical, and morphological nature of NORM-contaminated process vessel solids, (2) examine the effectiveness of common fill materials as radiation shields for γ radiation from NORM-contaminated materials, (3) determine the effectiveness of activated charcoal in reducing radon emanation from NORM-contaminated materials in soils, (4) explore the possibility of achieving an effective mechanical separation of NORM-contaminated barite from nonradioactive vessel solids components using a hydrocyclone, and (5) examine the efficiency of a barite scale dissolver in dissolving NORM-contaminated barite present in the vessel solids (Calnox S-271 or DTPA (diethylaminepentaacetic acid) and oxalic acid solution).

Characterization of NORM Vessel Solids

Overview

Extensive visual, physical, chemical, mineralogical, and radiochemical analyses were performed on the NORM-contaminated vessel solids to determine the applicability of various waste volume reduction approaches.

Particulate matter in NORM-contaminated vessel solids was a mixture of quartz, barite, and amorphous iron and manganese oxides. These particles ranged in size from fine to very fine sand to silt. Particle geometry is a function of composition. Barite particulates are angular plates, while quartz grains are subround to subangular spheroids. Barite is not exclusively present as discrete particulates, but is often found as microcrystalline patches and coatings on quartz grains. When present as grain coats, the geometry of the barite is similar to that described by Snodgrass (1986). Due to coprecipitation of radium with barium in these barites, some vessel solids were substantially radioactive. In addition to radium, other materials of environmental concern present were substantial levels of zinc, lead, copper, and arsenic.

Experimental Results

Gross Composition of Vessel Solids

The oil, water, and solids content of each sample was determined using a Baroid 50-ml retort. A mass balance was calculated for each experiment. Results of these mass balance calculations were never worse than 99%. The average vessel solid contained 78.51 weight percent solids, 15.97 weight percent water, and 5.52 weight percent oil. These data are given in Table VI.

Particle Size of Vessel Solids

The particle size distribution of the vessel solids was determined by wet sieve analysis and Malvern laser optical particle size analyzer. On average, 22.58 weight percent of particles were greater than 180 μm in diameter. The median grain size for particles less than 180 μm was 26.2 μm in diameter, and half of all particles finer than 180 mm were between 10.77 mm and 39.44 mm in diameter. Results of all particle size determinations are summarized in Table VI and given in detail in Appendix A.

TABLE VI.

Oil, Water and Solids Content, Mineralogy and

Particle Size Distribution for Vessel Solids

Sample	Oil	Water	Solids	Mineralogy from X-Ray Diffraction	Weight % Particles >180 mm	Size Distribution for Particles <180 mm		
	Weight %					Q1	Median	Q3
11374-2	2.61	4.71	92.68	Quartz, barite	57.72	5.66	16.76	29.00
11374-3	4.40	15.08	80.52	Quartz, barite, ferroan dolomite, calcite	29.02	6.05	13.45	22.46
11374-4	1.19	5.13	93.68	Quartz, barite (Sr substituted)	3.08	1.90	12.05	5.71
11374-5	7.75	7.75	84.50	Quartz, barite, albite, bassinite	18.82	10.39	26.78	44.85
11374-7	nd	nd	nd	Quartz, calcite	1.34	3.11	14.13	17.81
11374-8	2.20	11.63	86.17	Quartz, barite	30.76	2.03	11.15	8.42
11374-9	6.77	10.04	83.19	Quartz, barite	3.70	4.95	14.89	28.70
11374-10	11.96	28.13	59.91	Quartz, barite, calcite, celestite	6.23	29.51	16.73	13.90
11374-11	1.17	0.75	98.08	Barite, quartz	32.50	7.60	19.79	30.58
11374-12	0.65	15.56	83.79	Quartz, barite	22.72	9.93	28.98	57.44
11374-57	9.72	15.14	75.14	Quartz, barite, calcite, pyrite	7.72	4.66	15.68	48.74
11374-58	3.58	20.58	75.84	Quartz	36.51	2.33	34.19	7.78
11374-80	1.55	24.37	74.08	Quartz, barite, calcian albite	12.42	31.68	58.16	82.04
11374-81	5.99	10.75	83.26	Quartz, barite, calcian albite	11.62	12.81	34.49	65.65
11374-82	1.82	15.87	82.31	Quartz, calcian albite	23.30	32.75	69.88	106.22
11374-83	1.54	1.55	96.91	Barite	85.08	8.13	25.91	69.10
11374-84	23.47	68.42	6.11	Quartz, barite, calcian albite	1.36	9.61	32.36	32.12
Mean	5.52	15.97	78.51		22.58	10.77	26.20	39.44
Maximum	25.47	68.42	98.08		85.08	32.75	69.88	106.22
Q3	7.02	17.05	87.80		30.76	10.39	32.36	57.44
Median	3.10	13.36	83.23		18.82	7.60	19.79	30.58
Q1	1.55	7.10	75.67		6.23	4.66	14.89	17.81
Minimum	0.65	0.75	6.11		1.34	1.90	11.15	5.71

Identity of Crystalline Phases

X-ray diffraction, XRD, was used to determine the identity of crystalline phases present in the vessel solids. Minerals present in the vessel solids were principally quartz

and barite, with minor and infrequent occurrences of calcite, celestite, bassinite, calcium-rich albite, ferroan dolomite and pyrite. Mineralogy data obtained for the vessel solids are given in Table VI. It should be noted that XRD is blind to amorphous material, cannot detect crystalline materials present at less than about one weight percent abundance, and because of the specific X-radiation used, is less sensitive to iron-bearing crystalline materials than minerals not containing iron.

Bulk Chemistry of Vessel Solids

Elemental analysis of the vessel solids was done using both wavelength dispersive X-ray fluorescence (XRF), and inductively coupled plasma atomic emission spectrometry (ICP-AES).

The average bulk composition of the vessel solids was 46.92 weight percent SiO_2, 19.23 weight percent $BaSO_4 + SrSO_4$ (mostly $BaSO_4$), 4.67 weight percent Fe_2O_3, 2.13 weight percent CaO, 2.36 weight percent FeO, and 1.73 weight percent Al_2O_3. The average loss on ignition was 6.41 percent by weight. This high loss on ignition (LOI) may reflect the organic and the sulfur compound content of these materials. Table VII lists the major constituents of the vessel solids. Minor constituent data are given in Table VIII. Average concentrations of Zn, Pb, Cu, and As were 3,440 ppm, 2,804 ppm, 302 ppm, and 151 ppm, respectively. The samples also consistently contained tungsten (W). It is unlikely that W is naturally present in the samples. It is more likely a sample preparation artifact. Grinding equipment used to prepare the samples is made from or coated with W.

TABLE VII

Major Constituents of Vessel Solids

Sample	SiO_2	$BaSO_4$ + $SrSO_4$	Al_2O_3	CaO	MgO	Na_2O	K_2O	TiO_2	Cr_2O_3	P_2O_5	MnO	Fe_2O_3	FeO	LOI
							Weight %							
11374-2	22.30	40.32	0.21	0.13	<0.01	0.30	0.28	0.263	<0.01	0.02	0.02	0.17	0.10	1.77
11374-3	14.20	31.87	1.21	1.72	0.06	0.60	0.28	0.344	0.02	0.07	0.22	28.10	18.70	4.93
11374-4	2.07	45.34	0.36	0.92	<0.01	0.28	0.13	0.287	<0.01	0.05	0.11	13.70	1.90	2.70
11374-5	77.40	4.82	1.66	3.01	0.10	0.81	0.62	0.451	<0.01	0.05	0.05	2.78	1.10	5.65
11374-7	72.00	7.44	0.42	4.39	0.08	0.49	0.25	0.232	0.02	0.03	0.06	7.93	2.90	6.62
11374-8	87.00	3.30	0.43	0.61	0.17	0.52	0.26	0.426	<0.01	0.05	0.02	1.50	1.10	3.85
11374-9	82.80	1.08	3.85	2.93	0.19	1.23	1.05	0.380	0.03	0.05	0.07	0.84	0.40	4.50
11374-10	24.20	28.55	2.66	2.88	0.35	0.67	0.44	0.351	<0.01	0.26	0.13	10.70	5.90	18.80
11374-11	1.99	46.41	0.32	0.12	<0.01	<0.01	0.18	0.269	<0.01	0.02	0.04	2.44	0.90	1.23
11374-12	88.50	6.84	0.45	0.31	0.14	0.20	0.21	0.234	<0.01	0.03	0.01	0.40	0.20	1.45
11374-57	2.62	19.39	0.11	11.40	0.07	2.90	0.06	0.114	<0.01	0.50	0.48	3.66	2.60	7.70
11374-58	87.00	0.68	1.54	3.39	0.36	0.40	0.36	0.227	<0.01	0.05	0.03	1.59	0.80	7.54
11374-80	62.90	17.39	4.48	0.93	0.25	2.44	1.04	0.242	<0.01	0.04	0.03	0.75	0.30	2.70
11374-81	62.00	19.61	3.53	1.35	0.56	1.18	0.86	0.226	<0.01	0.04	0.03	0.83	0.50	2.16
11374-82	84.70	2.33	4.54	0.82	0.22	1.29	1.10	0.236	<0.01	0.05	0.03	1.24	0.60	2.08
11374-83	1.27	48.46	0.59	0.36	<0.01	0.56	0.04	0.262	<0.01	0.14	0.01	0.50	0.20	0.62
11374-84	24.70	3.14	3.12	1.01	1.31	7.22	0.67	0.269	<0.01	0.09	0.04	2.22	2.00	34.60
Mean	46.92	19.23	1.73	2.13	0.30	1.32	0.46	0.283	0.02	0.09	0.08	4.67	2.36	6.41
Maximum	88.50	48.46	4.54	11.40	1.31	7.22	1.10	0.451	0.03	0.50	0.48	28.10	18.70	34.60
Q3	82.80	31.87	3.12	2.93	0.35	1.25	0.67	0.344	0.03	0.07	0.07	3.66	2.00	6.22
Median	62.00	17.39	1.21	1.01	0.19	0.64	0.28	0.263	0.02	0.05	0.04	1.59	0.90	3.85
Q1	14.20	3.30	0.42	0.61	0.10	0.47	0.21	0.234	0.03	0.04	0.03	0.83	0.40	2.08
Minimum	1.27	0.68	0.11	0.12	0.06	0.20	0.04	0.114	0.02	0.02	0.01	0.17	0.10	0.62

Radium Occurrence in the Vessel Solids

The activities of radium isotopes in the vessel solids were determined by γ spectrometry. A high purity germanium well detector (HPGe) was used for all γ spectrometry experiments. The specific activity of both Ra-226 and Ra-228 was measured. Secular equilibrium was assumed to exist between Ra-228 and Ac-228. Radioactive equilibrium in which the parent activity does not decrease measurably during many daughter half-lives is known as secular equilibrium (Fredlander et al., 1981). Typical counting time for these

TABLE VIII

Minor Constituents of Vessel Solids

Sample	Rb	Co	Ni	Cu	Zn	Ga	As	Se	Y	Zr	Nb	Mo	Sn	Sb	Ta	W	Tl	Pb	B
	ppm																		
11374-2	12	12	31	295	103	<3	6	6	<2	<3	<2	5	<5	41	3	79	9	145	22
11374-3	11	45	146	528	3750	<3	50	10	<2	<3	<2	49	<5	27	<2	107	14	572	9
11374-4	11	20	216	591	1170	<3	41	<3	<2	<3	<2	43	<5	64	36	<5	<5	1080	<3
11374-5	16	47	25	105	1670	10	64	22	<2	696	12	<2	<5	15	4	302	<5	531	7
11374-7	<2	38	71	754	108	<3	11	54	<2	80	5	30	141	47	<2	768	<5	76	6
11374-8	5	78	35	64	2700	14	540	42	<2	156	20	16	<5	25	25	597	<5	4500	7
11374-9	31	77	17	2	8247	16	25	43	<2	578	11	<2	9	23	14	603	6	160	10
11374-10	7	34	115	713	10900	<3	234	7	<2	<3	<2	54	<5	73	<2	77	57	3950	<3
11374-11	<2	18	25	292	520	<3	6	<3	<2	<3	<2	53	<5	393	38	64	8	193	15
11374-12	<2	70	15	15	421	<3	37	40	<2	<3	7	<2	<5	<3	19	537	<5	306	<3
11374-57	8	31	90	353	21900	12	430	<3	<2	<3	<2	31	<5	<3	<2	<5	75	12300	11
11374-58	12	70	19	18	2310	<3	35	15	<2	276	9	<2	<5	17	12	578	<5	236	<3
11374-80	28	34	11	72	115	<3	67	8	<2	<3	4	<2	<5	36	17	259	<5	872	6
11374-81	25	35	29	731	271	<3	253	14	<2	<3	<2	<2	<5	30	14	494	<5	3480	<3
11374-82	32	86	32	91	204	<3	125	18	<2	213	7	<2	8	13	12	661	<5	919	<3
11374-83	14	15	52	404	291	<3	444	<3	<2	<3	<2	14	<5	48	79	55	<5	16200	26
11374-84	<2	28	56	82	11800	<3	192	10	<2	17	6	2	<5	3	<2	117	38	2150	<3
Mean	16	43	58	302	3440	13	151	22	na	288	9	30	53	33	23	353	30	2804	12
Maximum	32	86	216	754	21900	16	540	54	na	696	20	54	141	73	79	768	75	16200	26
Q3	25	70	71	528	2700	15	234	40	na	427	11	48	75	44	28	588	48	3480	14
Median	12	35	32	292	520	13	64	15	na	213	7	31	9	30	16	302	14	872	10
Q1	11	28	25	72	247	12	35	10	na	118	6	15	9	20	12	93	9	236	7
Minimum	5	12	11	15	103	10	6	6	na	17	4	2	8	3	3	55	6	76	6

samples was 12 hours, but times were varied to accrue comparable total counts. Table IX lists the concentrations of barium, strontium, barium to strontium ratios, concentrations of actinide elements, and specific activities of Ra-226 and Ra-228 in the vessel solids. The average activities of Ra-226 and Ra-228 were 62,201 pCi/g and 8,867 pCi/g, respectively. The median activities were 2,142 pCi/g for Ra-226 and 560 pCi/g for Ra-228. These activities are comparable to those obtained by Gott (1953) for highly radioactive barite scales in southeastern Kansas.

TABLE IX

Barium, Strontium, Barium:Strontium Ratio, Actinide Elements,

Ra-226 and Ra-228 in Vessel Solids

Sample	Ba	Sr	Ba/Sr	Si	Th	U	Ra-226	1 σ	Ra-228	1 σ
	ppm	ppm	mole ratio	ppm	ppm	ppm	pCi/g	pCi/g	pCi/g	pCi/g
11374-2	228,000	7,490	19.42	103,000	24	<2	2,142	107.0	1,208	13.7
11374-3	182,000	4,470	25.98	76,600	<2	<2	148	7.9	47	0.8
11374-4	231,000	29,000	5.08	105,000	16	<2	152,270	7,619.0	29,500	372.0
11374-5	26,800	1,270	13.46	14,400	9	3	53	3.6	17	0.4
11374-7	40,700	2,470	10.51	21,900	<2	2	1,054	78.4	160	9.4
11374-8	18,000	1,140	10.07	11,300	47	<2	29	2.1	11	0.3
11374-9	5,730	513	7.13	4,260	4	4	49	3.0	20	0.4
11374-10	162,000	4,820	21.44	80,600	46	<2	667	34.0	105	1.9
11374-11	260,000	10,600	15.65	116,000	<2	<2	2,648	134.0	560	7.0
11374-12	39,100	907	27.51	17,100	8	<2	386	51.1	63	7.9
11374-57	106,000	6,560	10.31	151,000	138	2	7	0.9	2	0.2
11374-58	3,520	382	5.88	6,770	3	3	6352	350.0	1,399	29.1
11374-80	101,000	1,070	60.23	43,300	12	<2	36,620	1,856.0	12,796	164.0
11374-81	110,000	4,380	16.02	48,400	38	<2	117,400	5,883.0	49,229	579.9
11374-82	12,900	650	12.66	5,530	13	<2	7,772	543.1	3,453	60.9
11374-83	247,000	30,900	5.10	121,000	178	<2	723,200	36,540.0	49,620	14,440.0
11374-84	17,800	535	21.23	63,100	20	<2	6,620	359.4	2,556	42.0
Mean	105,385	6,303	16.92	58,192	40	3	62,201.0		8,867.3	
Maximum	260,000	30,900	60.23	151,000	178	4	723,200.0		49,620.0	
Q3	182,000	6,560	21.23	103,000	44	3	7,772.0		3,453.0	
Median	101,000	2,470	13.46	48,400	18	3	2,142.0		560.0	
Q1	18,000	907	10.07	14,400	10	3	148.0		46.5	
Minimum	3,520	382	5.08	4,260	3	<2	7.1		1.5	

All samples exhibited higher Ra-226 activity than Ra-228 activity. The minimum activity ratio for Ra-226 to Ra-228 was ~50. Observations by Kraemer and Reid (1984) and Fisher (1994) of the Ra-226 to Ra-228 ratio in Gulf Coast region produced waters indicate that freshly precipitated barites should have a Ra-226 to Ra-228 ratio of approximately 0.4 to 1.2. The Ra-226 to Ra-228 values obtained from the samples showed strong depletion in Ra-228 relative to Ra-226. This is probably due to the age of the vessel solids.

Many of these samples were collected from out-of-service equipment. Length of out-of-service time was unknown. Ra-228 had a substantially shorter half-life than Ra-226. Consequently, if Ra-228 in the barite is not renewed by equilibrium exchange with produced water, it will decay to low activity levels much faster than Ra-226. This apparently accounts for the data observed in this effort.

Actinide Elements in the Vessel Solids

Thorium (Th) was found above detection level (<2 ppm) in all but three samples. In contrast, uranium (U) was found above detection level in only four samples. The average concentration of Th was 40 ppm, and the highest U concentration was 4 ppm. Based on the calculated averages shown in Table IX, the U to silicon (Si) ratio is approximately that expected for crustal rocks (Taylor, 1964). If the below detection units are taken into account, U can be considered depleted with respect to normal crustal rocks. In contrast, Th to Si ratio shows substantial enrichment with respect to crustal rocks, on the average by a factor of approximately 3.5. Neither Ra-226 nor Ra-228 activity appears to vary in response to either Th or U concentrations. The Ra isotopes present in the vessel solids are unsupported by their parental actinides.

Relationship of Barium and Strontium in the Vessel Solids

Average Ba and Sr concentrations in the vessel solids were 105,385 ppm and 6,303 ppm, respectively, and the average Ba to Sr mole ratio was 16.92. Both the samples displayed a wide range of Ba to Sr mole ratios. Samples enriched in Sr have Ba:Sr mole ratios less than ~10 (seven samples), while samples depleted in Sr have Ba:Sr ratios greater than ~10 and range to ~60. The quantitative results obtained by Hanor (1969) show that the Ba:Sr ratios for sea water and deep sea sediments was approximately two; however, sediment samples near East Pacific Rise were approximately seven. Barite-enriched samples from this experiment suggest that the general region of the samples had additional

sources of barium and mechanisms for the precipitation of barite. Perhaps commingling with the produced water may have resulted in more precipitation of barite.

SEM Analysis of Vessel Solids

Vessel solids were examined by SEM to obtain visual information on grain sizes and morphologies. SEM photographs indicate that barite in these vessel solids are present in two distinct geometric arrangements. Samples rich in barite contain fine to very fine sand size, angular, platy, massive clasts of barite. These clasts may have originated as scale particles detached from piping and subsequently deposited in separators and tanks. The barite-poor samples are comprised of angular to subrounded quartz grains, and the barite is typically present as grain coats and isolated patches. This barite habitat in the barite-poor vessel solids is similar to that described by Snodgrass (1986) in experimental studies of barite precipitation. In this work, small microcrystalline spherical patches of barite were found to preferentially precipitate on silicate grains. Figures 7 and 8 show the SEM photographs of these contrasting types of vessel solids.

Results of KEVEX analysis indicate all samples contain barium, silicon, and sulfur. KEVEX data also confirmed the presence of Zn in some samples. The origin of the zinc may be natural, or may arise from heavy zinc bromide completion fluids. Completion fluid is the liquid that is kept in the well as it is being completed. Figures 9 and 10 show the typical spectra obtained from KEVEX on dark material and bright material. The light material consisted of white or bright spots that appeared on the larger grain surfaces from the back-scattered imaging. Dark material seen from the photographs was smooth surface of grain. These light and bright materials were examined to determine the occurrences of barium. The light material consistently contained higher barium peaks in all the samples. The dark materials were examined to determine the occurrences of quartz. The dark materials showed higher silicon peaks.

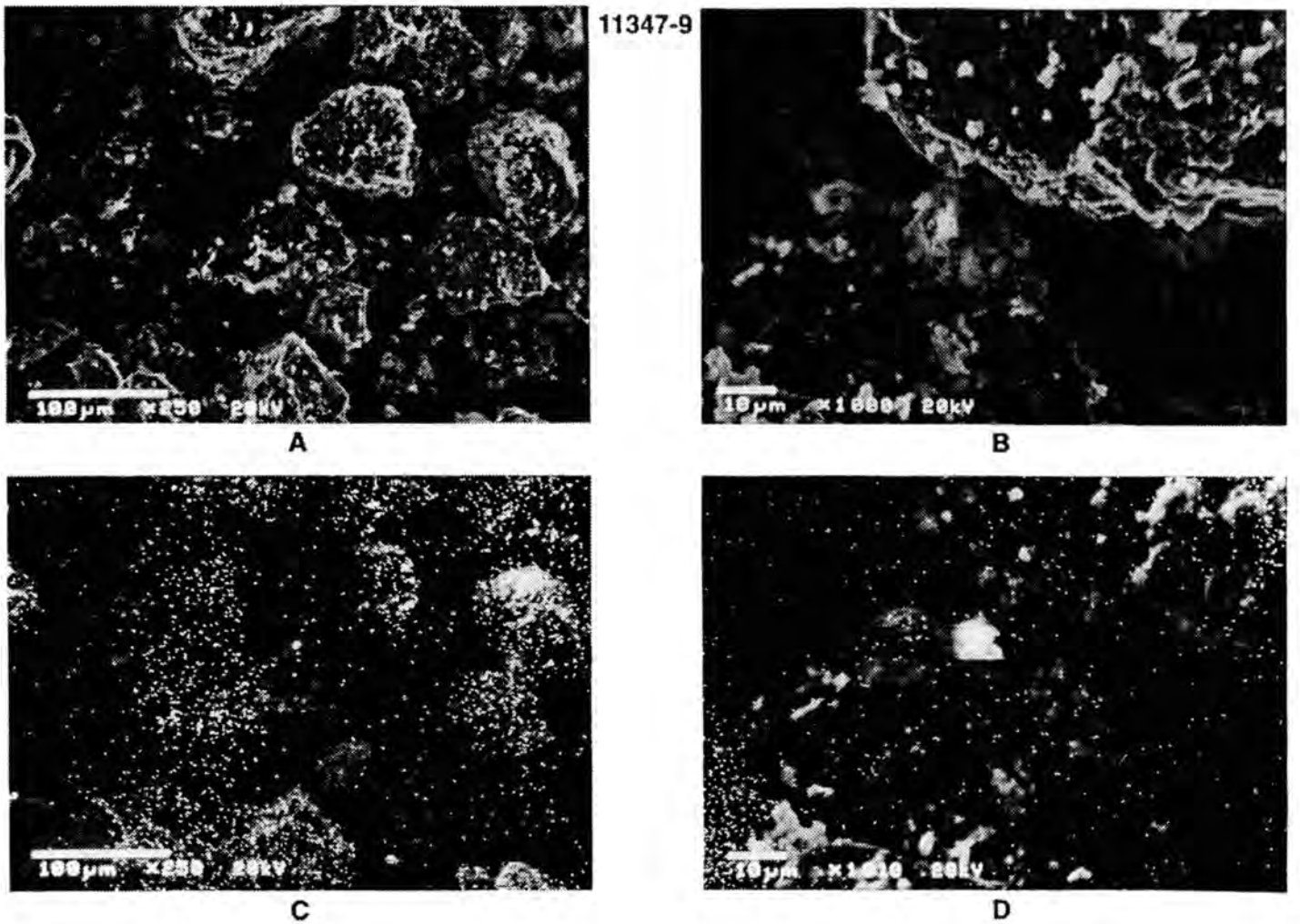

Figure 7. SEM photographs of barite-poor vessel solids (sample 11374-9). (A) X250 image showing particle morphologies. (B) X1000 image showing detailed particle morphologies. (C) X250 image showing barium X-ray map of image shown in (A). (D) X1000 image showing barium X-ray map of image shown in (B).

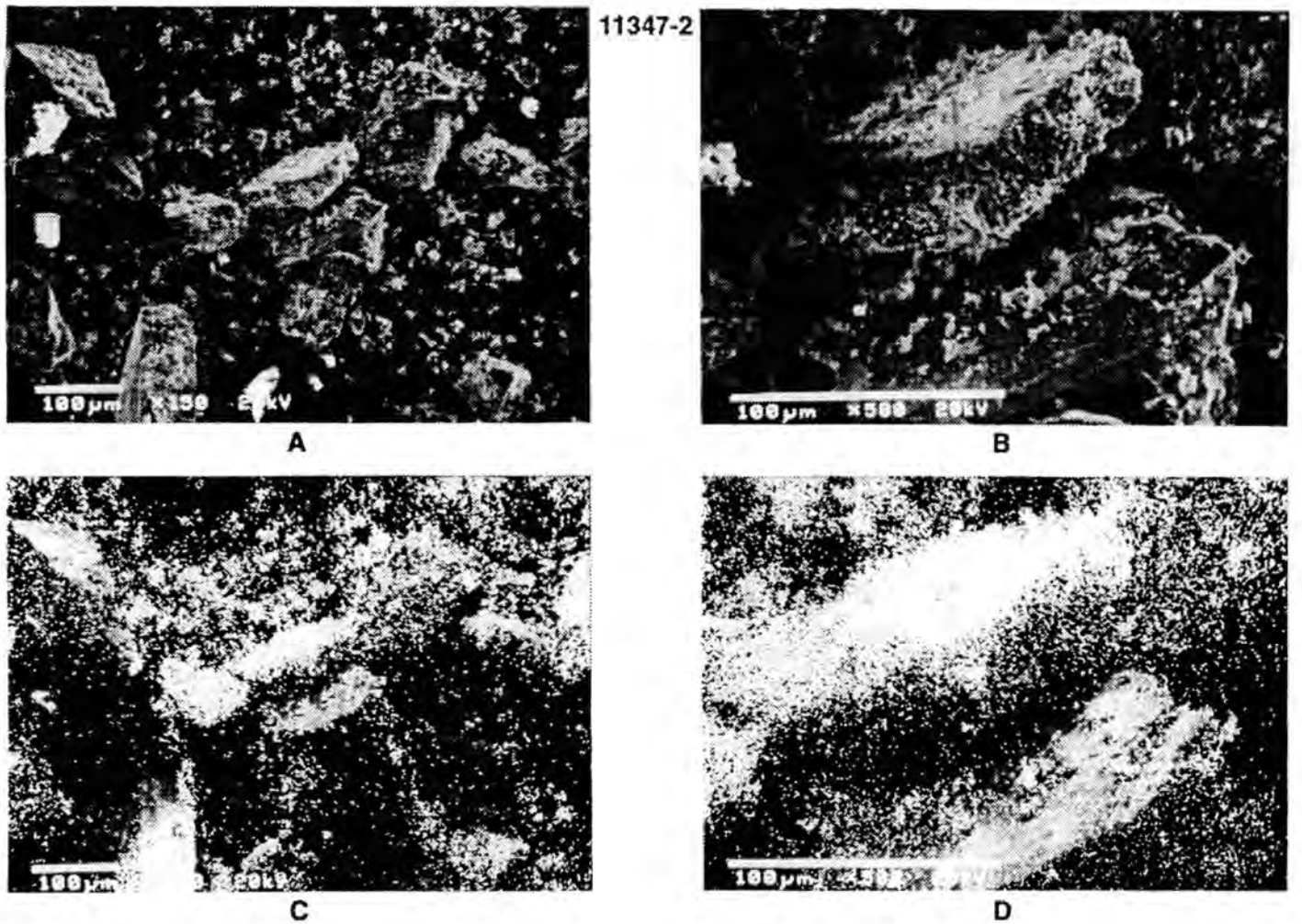

Figure 8. SEM photographs of barite-rich vessel solids (sample 11374-2). (A) X150 image showing particle morphologies. (B) X500 image showing detailed particle morphologies. (C) X150 image showing barium X-ray map of image shown in (A). (D) X1000 image showing barium X-ray map of image shown in (B).

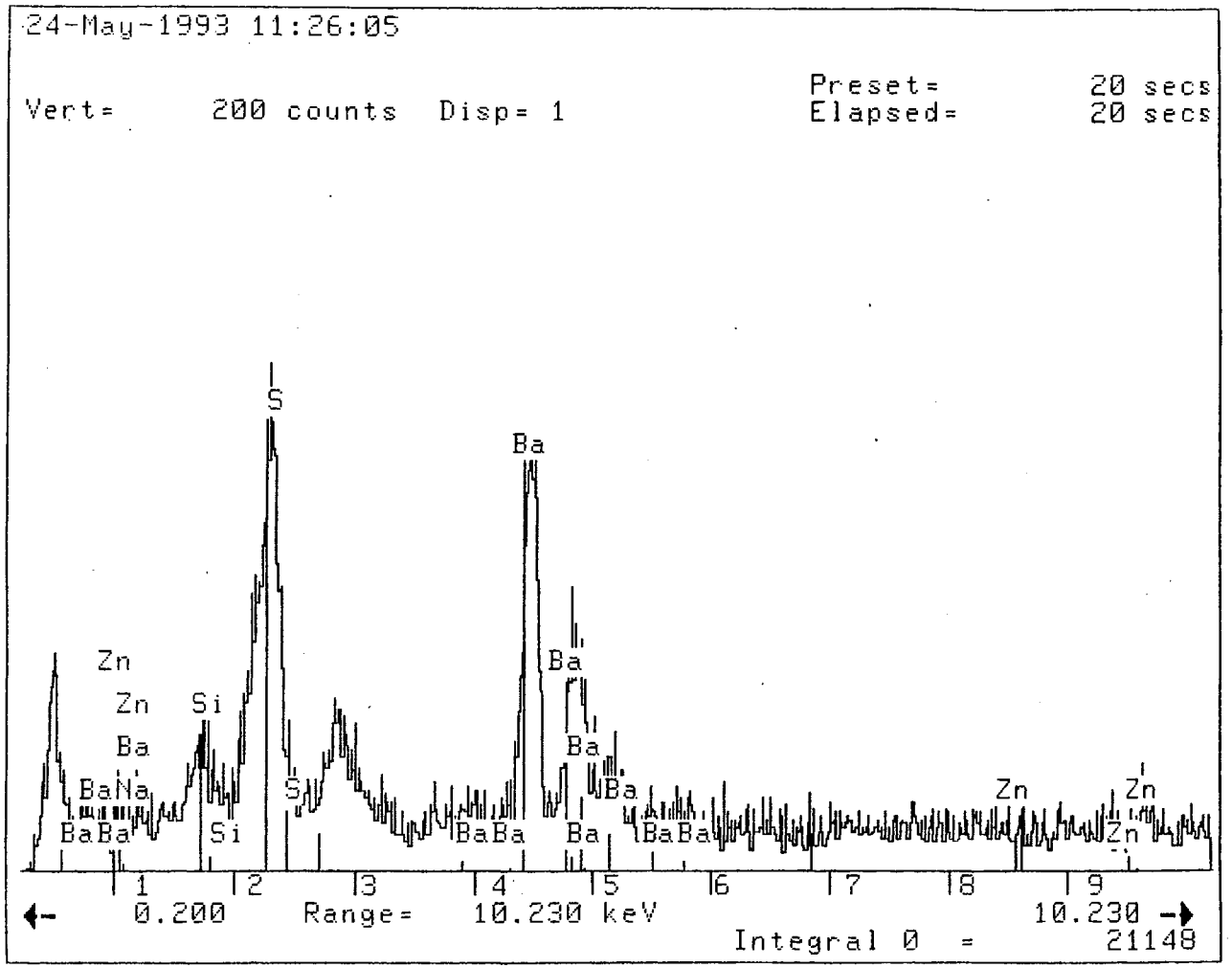

Figure 9. Spectra on bright material for sample 11374-2.

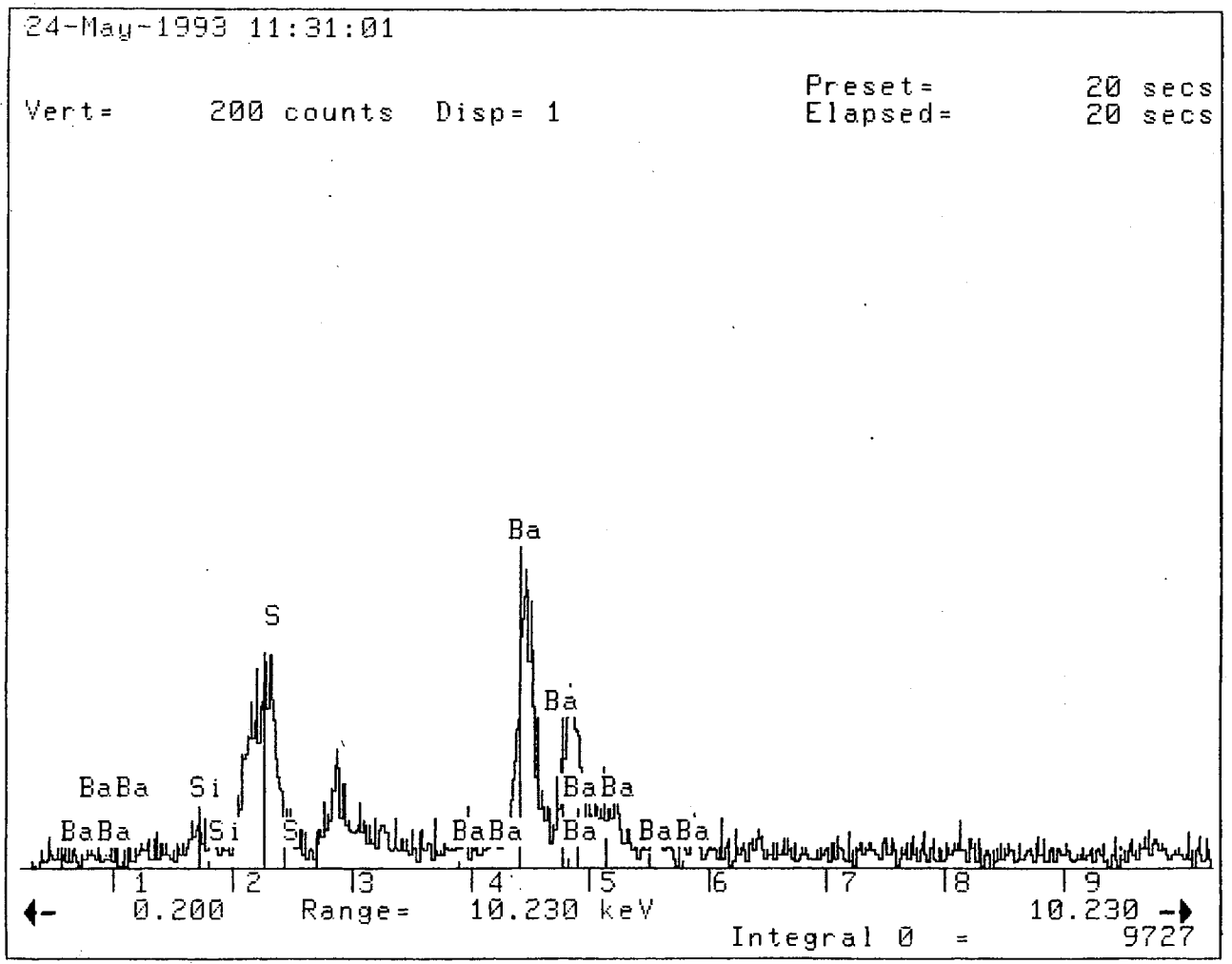

Figure 10. Spectra on dark material for sample 11374-2.

Summary

Average vessel solids contain ~6 weight percent oil, 16 weight percent water, and 79 weight percent solids. Vessel solids particulates were typically fine to very fine sand and silt sized quartz and barite. In addition to its occurrence as discrete particles, barite was also present as both diffuse and continuous grain coats and spherical microcrystalline patches on quartz grains. Amorphous iron and manganese oxides were also present as both coatings and discrete accumulations. Barite in these vessel solids was radioactive due to its content of Ra-226 and Ra-228, and can have a high degree of Sr substitution for Ba. The activity ratio of Ra-228/Ra-226 is much lower than that observed for produced waters in the Gulf Coast region.

These characterization data for the NORM vessel solids waste stream suggest several lines of attack with respect to waste volume reduction. On mass basis, the ratio of quartz to barite is approximately 2:1, but their volume ratio is 3.5:1 due to higher density of barite (4.6 g/cc) compared to quartz (2.6 g/cc). Removal of quartz alone would result in an average volume reduction of 39%. Based on their densities, the relative average volumetric abundance of fluid and solids constituents in a vessel solids waste stream is approximately 14% oil, 31% water, 48% inert solids, and 7% radium-contaminated barite. Consequently, simply removing the fluids would reduce waste volume by approximately 45%. Overall, removal of both fluids and quartz would result in an average ultimate waste volume reduction of 88%. Although fluid removal is straightforward, separation of barite from the quartz is not. Barite is brittle and mechanical handling of the vessel solids would tend to break and grind the barite present into finer fragments. Such treatment, however, would not be adequate to achieve the level of barite removal necessary to decontaminate the nonradioactive solids (to background levels). In addition to its occurrence as discrete particles, barite is also present as various precipitate geometries on quartz grains. Removal

of this barite would also be necessary. This might be accomplished mechanically or chemically.

Some of these vessel solids contain substantial concentrations of materials with environmental concerns. The average concentration of Pb is ~3,000 ppm, and the average As concentration ~150 ppm. Similar concentrations of these materials would be expected in nonradioactive vessel solids. In the past, these vessel solids have been treated like normal oilfield waste (Gray, 1993). Landfilling and landspreading have been used for their disposal. In view of the potential for land contamination by heavy metals that could results from such disposal practices, vessel solids should be analyzed for their heavy metals content prior to land disposal.

Soil Shielding

Introduction

The soil shielding experiment was conducted to determine the effectiveness of various commonly available covering agents as γ radiation shields. NORM wastes in soils present a radiological exposure risk. This radiological exposure risk is a combination of α, β and γ exposure from the decay of radium and their daughter products. One way to reduce the total radiological exposure risk is to bury the NORM material beneath soil or under commonly used materials. Such burial would provide a shield against ionizing radiation.

The most significant risk from external radiation exposure is due to high energy photons (X-rays and γ-rays). The most effective shields for photons are materials of high density and high atomic number (Chilton, Shultis and Faw, 1984). Elemental lead, for example, has a density of 11.288 g/cm^3 and an atomic number of 82, and is an excellent shielding material. Shield performance, however, is not solely a function of density or the atomic number(s) of the materials from which it is constructed. Shield performance will be degraded by the presence of voids (i.e., porosity), regions of low density (i.e., lateral

inhomogeneities), and penetrations. Shield performance is also a function of the energy of the photons interacting with the shield. Low energy photons are easily stopped; high energy photons require thicker shielding.

The ability of a material to shield against ionizing radiation is a function of its linear attenuation coefficient. Radiation traversing a layer of material is reduced in intensity by a constant fraction μ (the linear attenuation coefficient in units of 1/length). After penetrating to a depth x, the intensity of radiation is given by:

$$R = R_0 e^{-\mu x}$$

where R_0 is the intensity of radiation at the entry surface of the material. The ability of materials to shield against ionizing radiation may be expressed by a half-thickness (the thickness of material required to reduce the incoming radiation field by a factor of two) or by the linear attenuation coefficient, μ. The photon linear attenuation coefficient, μ, is the probability per unit distance of travel that a gamma photon undergoes any significant interaction (Chilton, Shultis and Faw, 1984). For photon energies in the range of 10 KeV to 10 MeV, the photoelectric effect, pair production, and Compton scattering mechanisms of interactions predominate over all others (Gollnick, 1988). Figure 11 shows the interaction of source gamma rays (Chilton, Shultis and Faw, 1984).

A sample of barite scale was tumbled to obtain a consistent, finely divided mixture that could be easily packaged in a rectangular geometry. With this geometry, the theoretical radiation field (in vacuum) should fall off as 1/r (where r is the separation distance between the detector and the source) (Gollinick, 1992). This mixture was double-bagged in plastic Ziploc^{TM} bags, and placed in a plywood box having an acrylic front. The radiation field was measured at various vertical separations from this source, both with and without shielding materials covering the source. A Ludlum Model 3-97 Survey Meter set to detect using its internal 1x1 NaI crystal was used for all radiation measurements. Shield materials investigated were: (1) marine bivalve mollusc shells typically used for location paving in

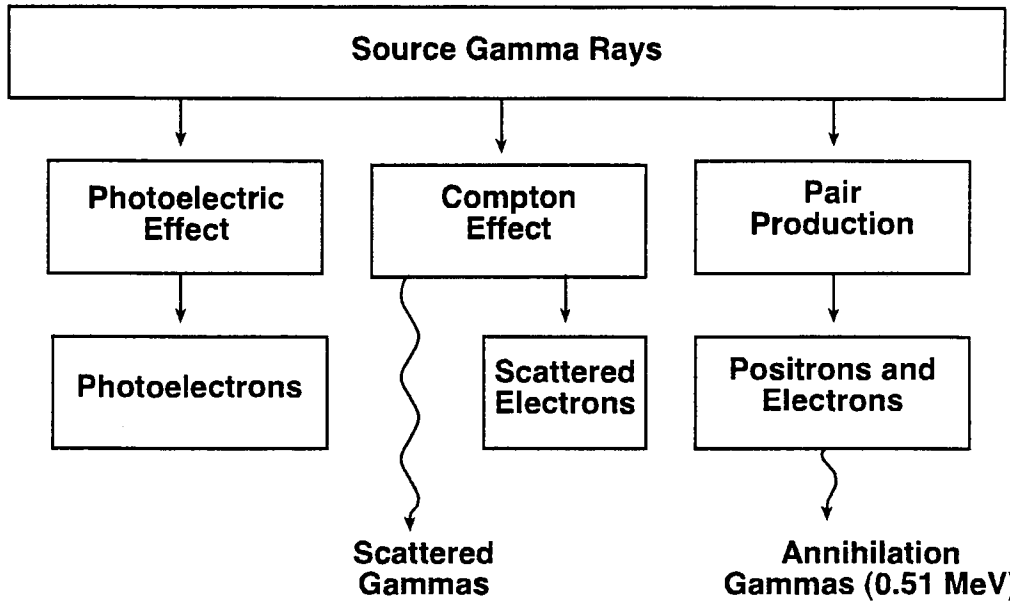

Figure 11. The interaction of source gamma rays.

the Gulf Coast area, (2) standard Ottawa sand, and (3) pelleted limestone. The mollusc shells and limestone pellets were used because of their $CaCo_3$ composition.

Porosity of the experimental shielding materials was determined by packing a tared 1,000 ml graduated cylinder to the 1,000 ml mark with shielding material, determining the mass of this volume of shielding material, and then determining the mass of water required to bring the water level in this shielding material packed container to exactly the 1,000 ml mark. Grain density of the shielding material was determined by placing a known mass of shielding material (crushed in the case of the shell material) in a 100 ml volumetric flask, and determining the mass of water required to bring the total volume of the system to exactly 100 ml. Bulk density of each shielding material was calculated by:

$$\rho_{bulk} = \rho_{grain}(1 - \phi)$$

where ρ_{bulk} is the bulk density, and ρ_{grain} is the grain density in g/cc. Porosity, ϕ, is expressed as a fraction.

Experimental Results

The radiation field measurements for the NORM source without any shielding material decreased from 165 μR/hr immediately at the surface of the NORM source to 31 μR/hr at an eight-inch (20.32 cm) separation from the source. A plot of this radiation field is given in Figure 12, and shows that the unshielded experimentally determined radiation field does decrease in proportion to 1/r. Linear attenuation coefficients for the various covering materials were calculated from radiation field measurements made with the detector immediately atop of the shielding material. All additional experimental data of shield measurements at various distances are given in Appendix B. The experimentally determined effective linear attenuation coefficients for these materials are given in Table X. Porosity and bulk density data for the various shielding materials are given in Table XI. Figure 13 shows the linear attenuation coefficient decreases with the increasing shield material's unit density. Lower linear attenuation coefficient increases the shielding efficiency.

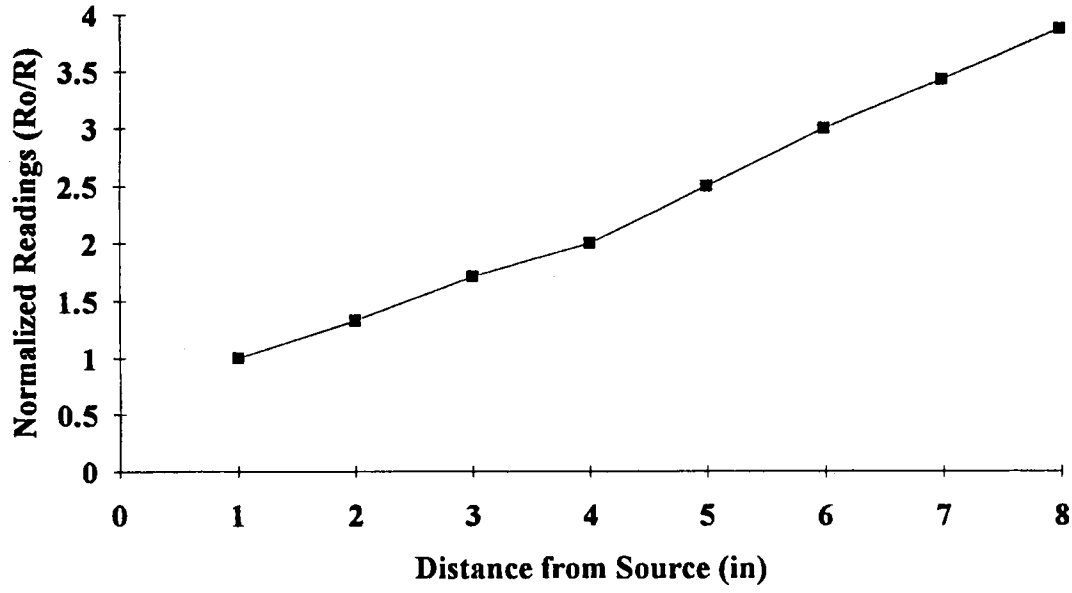

Figure 12. Exposure rate ratio of unshielded to shielded

TABLE X

Linear Attenuation Coefficients of Shielding Materials at Various Thicknesses

Shielding Material Air	Linear Attenuation Coefficient (1/cm) Thickness of Shielding Material						
	1 in.	2 in.	3 in.	4 in.	5 in.	6 in.	7 in.
Seashells	0.4773	0.2990	0.2655	0.2558	-	-	-
Limestone Pellets	0.5506	0.3490	0.3134	0.2741	0.2738	0.2375	0.2319
Ottawa Sand	0.3943	0.3376	-	-	-	-	-

TABLE XI

Porosity and Density of Shielding Materials

Shielding Material	Porosity (%)	Bulk Density (g/cc)
Seashells	64.9	.867
Limestone Pellets	44.6	1.218
Ottawa Sand	35.4	1.615

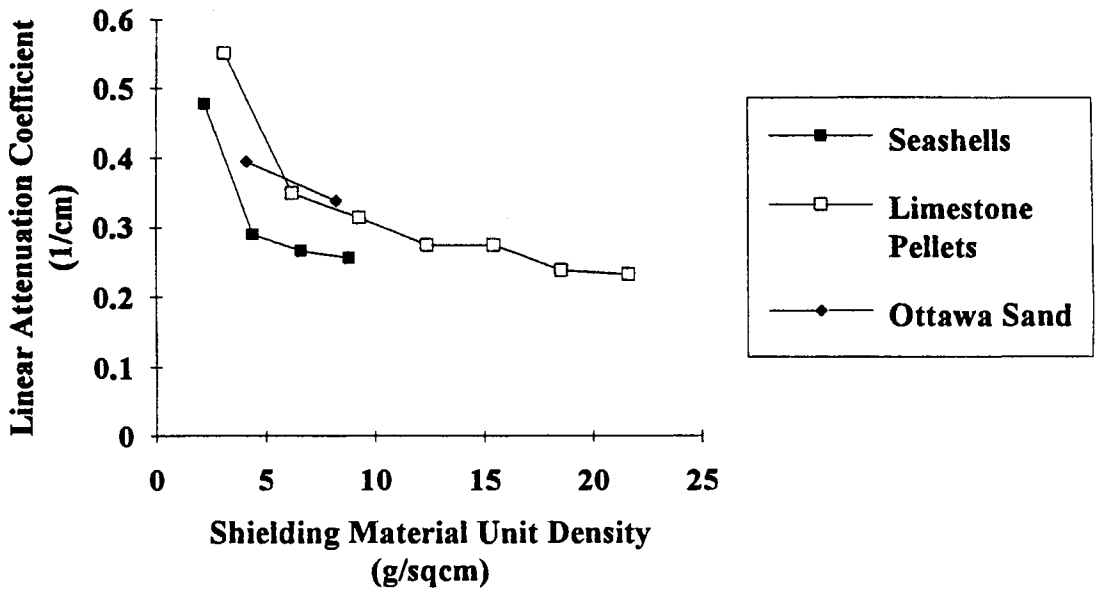

Figure 13. Linear attenuation as a function of shielding material density.

Discussion

The Ottawa sand was the most effective of the radiation shield materials examined. Although comprised of low atomic number material and has a lower grain density, the Ottawa sand had the highest bulk density. Ottawa sand had the lowest attenuation coefficients when compared to the limestone pellets and mollusc shells for the shield thickness tested. Burial of NORM-contaminated material by a layer of quartz sand 2.5 cm in thickness would reduce the radiation field by half. To achieve an equivalent reduction in radiation field, a layer of the pelletized limestone would need to be 3 cm thick, and a layer of mollusc shells would need to be 5.08 cm thick.

The mollusc shells yield a half-value layer comparable to that for concrete. This is a bit surprising, given the high porosity of the mollusc shell material. The half-value layer for concrete is approximately 4.8 cm for a similar gamma source (Gollinick, 1992). The limestone pellets and Ottawa sand had smaller half-value layers. The effectiveness of a mollusc shell burial shield could be increased by crushing. This would produce better packing, lower porosity, and greater bulk density. Although covering contaminated material with sand might be more effective, covering with mollusc shells may be more practical; mollusc shells are available, abundant and cost effective, especially in the Gulf of Mexico region.

Summary

For photons (γ and X-rays), materials with high density and high atomic number provided the most efficient shielding. Penetrations, voids, or regions of lower densities, however, reduce shield efficiency despite their high grain densities. Mollusc shells had the lowest bulk density and highest porosity, and consequently had highest (i.e., poorest) linear attenuation coefficient. In contrast, the high bulk density and gram amount of sand made it a good shielding material, even though Si and O have relative low atomic numbers.

Radiation drops off as the distance from the source increases. Shielding has a greater effect in reducing the exposure rates when closer to the source. Results obtained from this experiment indicated that mollusc shells may be an effective shielding material if the void volume can be reduced. For instance, crushing the shells would decrease the void volume. Covering the contaminated sites with shells might also be more cost effective due to their availability.

Large pieces of contaminated land could be shielded with various natural shielding materials to prevent or decrease radiation exposure.

Radon Emanation

Introduction

The radon emanation experiment was conducted to determine the effect of the presence of an activated charcoal adsorbent in mitigating radon exposure. Radium isotopes and their decay daughters, especially radon gas, can be viewed as high health hazard materials. Because it is a gas, Rn, if present in air, will be inhaled. More importantly, Rn decay yields radioactive metallic ions which may become associated with fine particles. If sufficiently fine, such particles may become lodged in deep lung tissue. In fact, inhalation of Rn-222 present in normal air is estimated to comprise the single largest radiation dose to human population at large (Nero, 1989).

Freundlich, Langmuir High and Low, and Brunauer, Emmet, Teller (BET) isotherms were generated to determine the adsorption capacity and strength of the bond of the activated charcoal to radon gas. The results also indicate that the sample highly dispersed NORM has higher emanation power than nondispersed (i.e., scale).

This experiment was performed using the accumulation method, and follows the procedure of Wilson and Scott (1992). Various mixtures of NORM-contaminated scale and sand (quartz) were sealed in one-quart paint cans (accumulation in cells), completely degassed by vacuum, returned to atmospheric pressure, and then allowed to grow in Rn for 30 days. At the end of this period, an aliquot of gas was removed from the can and assayed for total Rn activity. Pseudo adsorption isotherms were constructed to evaluate the applicability of activated coconut charcoal as the adsorbent.

Experimental Results

The addition of 8 g of activated coconut charcoal to the accumulation cells reduced Rn accumulation by 96% compared to equivalent accumulation cells without charcoal. The accumulation cell containing scale and no charcoal had an Rn-222 specific activity of 232.43 pCi/L. In contrast, in accumulation cells containing 100% scale and 8 g of charcoal the Rn-222 specific activity decreased to 9.39 pCi/L. Rn-222 emanation power decreased from 2.32×10^{-3} to 3.87×10^{-5}. Table XII lists the results from the radon emanation experiment. The samples containing 99.5% sand and .05% scale and 99% sand and 1% scale represent contaminated soil. Typical Rn-222 in the soil air are of the order of 1.5 pCi/L, indicative of Rn-222 concentrations at three meters (Wilkenang, 1990). Table XII and Figure 14 show the specific activities of Rn-222 decreased with the addition of activated coconut charcoal. Figure 15 is the same graph of Figure 14 without 100% scale line. Figure 16 is a plot of radon emanation power curve. Radon emanation power also decreased as the activated coconut charcoal was added. Finely divided and dispersed material yielded higher emanation power measurements.

TABLE XII

Rn-222 Concentration After 30 Days of Growth with Charcoal Addition

Sample			Activity Measurements		
Sand (%)	Scale (%)	Charcoal (g)	Rn-222 (pCi/L)	Ra-226 (pCi/L)	Radon Emanation Power Rn-222/Ra-226
100	0	0	0	0	0
100	0	1	0		0
100	0	2	0		0
100	0	4	0		0
100	0	8	0		0
99.5	0.5	0	1.97	0.995	3.89
99.5	0.5	1	0.92		1.82
99.5	0.5	2	0.42		8.29E-01
99.5	0.5	4	0		0
99.5	0.5	8	0		0
99	1	0	3.87	3.09	1.23
99	1	1	1.82		5.78E-01
99	1	2	0.51		1.62E-01
99	1	4	0.30		9.53E-02
99	1	8	0.43		1.37E-01
0	100	0	232.43	966.8	2.32E-03
0	100	1	67.29		6.72E-04
0	100	2	35.20		3.52E-04
0	100	4	18.82		1.88E-04
0	100	8	9.39		9.38E-05

Discussion

The activated coconut charcoal was a very effective radon scavenger. Actuated coconut charcoal is a proven adsorbent for gas. Adsorption of radon gas onto the activated coconut charcoal increased with the addition of activated charcoal. The first gram of activated charcoal decreased the specific activity by 71%. With the addition of two grams of activated charcoal, the specific activity was reduced by 85%. With each incremental addition of activated charcoal, the adsorption decreased proportionally. The decrease in radon emanation power was attributed to the increase in charcoal addition (Figure 16). The ema-

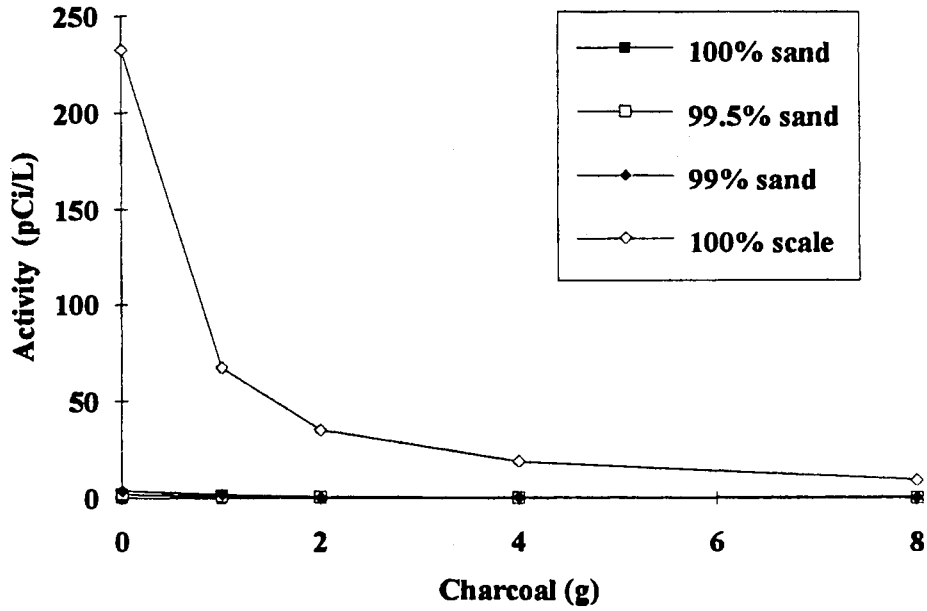

Figure 14. Radon emanation activity curve.

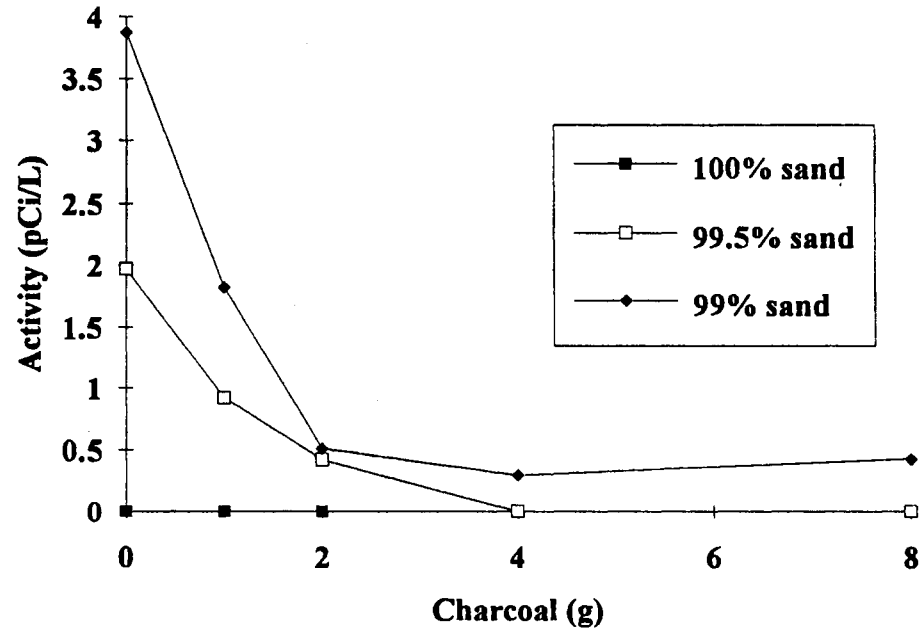

Figure 15. Radon emanation activity curve excluding 100% scale curve.

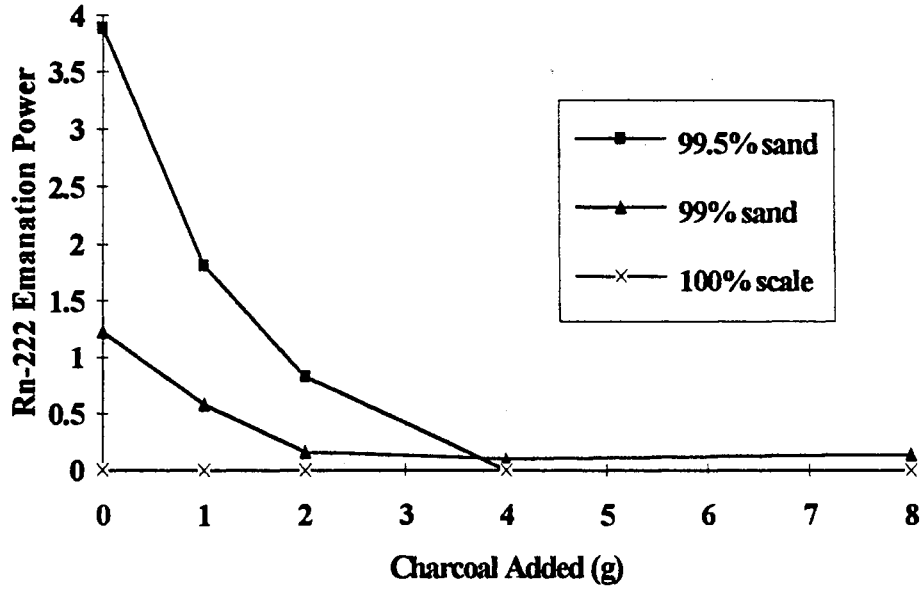

Figure 16. Effect of activated charcoal on Rn-222 emanation.

nation power data obtained from samples containing 0.5% scale were in excess over one. This may be due to low activity which can result in poor measurement. For example, the counting efficiency of the instrument was 76.2%. With a sufficient amount of activated charcoal addition, eventually all of the radon gas can be adsorbed. The results indicate that even with a modest amount of activated charcoal added, the scale will greatly reduce the Rn emanation from soils.

Isotherms

An isotherm is an equilibrium relation between the amount of solute adsorbed on the solids surface and the concentration of solute remaining in solution (Veenstra, 1993). The isotherms constructed for this experiment resulted in pseudo first order isotherms since the Freundlich, Langmuir high and low range and BET isotherms were originally developed for liquid systems. Table XIII shows the lab data used to determine the constants for each

isotherm. Table XIV shows the calculations of required constants obtained from the isotherm graphs. The actual graphs of these isotherms is shown in Appendix C. These isotherms showed a high capacity of the adsorbent for the adsorbate and a strong adsorption bond. These coefficients indicate favorable adsorption capacity for ranges emissions presented in the experiment.

TABLE XIII

Isotherms

(Freundlich, Langmuir High and Low Range, BET (Cs is assumed to be equal to Co))

Lab Data

Charcoal Doses (mg/1)	Remaining Gas (C) (pCi/L)	Co-C (pCi/L)	pCi of Adsorbed Impurities (X) (pCi)	Weight of Charcoal (M) (mg)	q (X/M) (pCi/mg)	Log X/M	Log C	1/(X/M)	1/C	C/q	C/((Cs-C)(X/M))	C/Cs
0	232.43											
1056.74	67.29	165.14	165.14	1056.7	0.1563	-0.806116	1.828	6.3991	1.49E-02	430.59	2.607439	0.289507
2113.5	35.2	197.23	197.23	2113.5	0.0933	-1.030029	1.5465	10.716	2.84E-02	377.2	1.912489	0.151443
4227	18.82	213.61	213.61	4227	0.0505	-1.296411	1.2746	19.788	5.31E-02	372.42	1.743447	0.080971
8454	9.39	223.04	223.04	8454	0.0264	-1.578679	0.9727	37.904	1.06E-01	355.91	1.595741	0.040399

TABLE XIV

Calculation of Required Constants

Freundlich Isotherm			
Slope = 1/n =	0.9108,	n =	1.097941
Intercept = Log K =	-2.458,	K =	3.48E-03
r (coefficient of correlation)		=	0.9991204
SD of points about the fitted line		=	0.0171559
Langmuir Isotherm, High			
Slope = $1/bQ_o$ =	345.47,	Q_o =	0.8491301
Intercept = $1/Q_o$ =	1.1777,	b =	3.41E-03
r (coefficient of correlation)		=	0.9998694
SD of points about the fitted line		=	0.2764353
Langmuir Isotherm, Low			
Slope = $1/Q_o$ =	1.2431,	Q_o =	0.8044229
Intercept = $1/bQ_o$ =	343.41,	b=	3.62E-03
r (coefficient of correlation		=	0.9767979
SD of points about the fitted line		=	8.4859126
BET Isotherm			
Slope = $(K_b-1)/K_bQ_o$ =	4.049,	Q_o =	0.3768696
Intercept = $1/K_bQ_o$ =	1.3956,	Kb=	1.90E+00
r (coefficient of correlation)		=	0.9894759
DS of points about the fitted line		=	0.0793153

where,

- $1/n$ = function of strength of adsorption bond
- K = Freundlich adsorption constant - related to the capacity of the adsorbent for the adsorbate
- Q_o = pCi of gas adsorbed/mass adsorbent
- b = adsorption coefficient
- K_b = constant related to energy of adsorption

Summary

Emissivity of radon gas can be significantly reduced using activated coconut charcoal. Freundlich, Langmuir High and Low, and BET pseudo isotherms showed that the activated charcoal would be an efficient adsorber for the radon gas. These pseudo isotherms also showed that the charcoal was a viable option in reducing the radon emission within the range of concentration tested. Mixing contaminated soil with activated charcoal would inhibit radon emission effectively. Massive radioactive scale with activated charcoal would inhibit radon emission effectively. Massive radioactive scale source has very low emanation power, while dispersed ground-up scale has high emanation power.

Mechanical Separation Experiment

Introduction

The mechanical separation experiment was conducted to determine if the finely divided NORM-contaminated barite in the vessel solids could be effectively separated from the nonradioactive components of the vessel solids. The underflows from the hydrocyclone carried most of the solids, the coarser grains, suspended in some liquid, and the overflows contained most of the liquid and some finer solids. The overflow of the hydrocyclone contained approximately 4:1 ratio of barite:quartz, and the underflow contained approximately 4:1 ratio of quartz:barite, shown by the mineralogy analysis. The hydrocyclone would

yield a greater separation efficiency if the flowrate of the slurry being fed through the hydrocyclone was increased. Larger volume of slurry being fed could accomplish constant rate of flow which would result in better separation.

Application of hydrocyclones in the oil industry include categories of two-phase separation with the liquid being the suspending medium (Svarosvsky, 1984). The hydrocyclone is a liquid suspension classifier of different densities. The hydrocyclone is a static separator based on centrifugal separation in a vortex generated within a cono- cylindrical body (Svarosvsky, 1984). In order for solids particles to separate under the effect of the centrifugal force, there has to be finite density difference between the solids and the liquid. Even though there were very steep velocity profiles in the flow, leading to high shearing forces which tend to break any loose flocs, or agglomerates, the shearing forces were not able to break loose barite grain coats from the silica grains. The barite grain coats from the silica grains were not broken loose with the treatments applied in this experiment.

Six sets of experiments were conducted using the hydrocyclone. The format of the tests involved mixing the composite vessel solids with water to achieve a 10% (by volume) slurry in a ten-gallon container. This slurry was fed through a hydrocyclone at a rate of 40 gpm using a 5 hp pump running at 33,520 rpm. Solids present in both the overflow and underflow streams from the hydrocyclone were collected, dried and assayed for radioactivity. First, the original untreated sample was fed through the hydrocyclone, then the samples treated with dispersator only, dispersant only, dispersator and dispersant, and ultrasonic probe. The dispersator and ultrasonic probe were additional shearing devices (aside from the hydrocyclone) used to break up the attached barite particles.

Composite vessel solids were examined by SEM to obtain visual information on grain sizes and morphologies before and after the hydrocyclone experiments. The underflows and overflows were similarly examined. The distribution and associations of barite

in these samples were investigated with SEM by obtaining barium maps with backscattered electron imaging.

X-ray diffraction, XRD, was used to determine the identity of crystalline phases present in the vessel solids. Samples were ground to 50 μm or less prior to analysis. All XRD analyses were executed on radon power mounts. The results of the XRD were interpreted by comparison of diffractograms obtained for the samples to diffractograms of pure minerals.

Experimental Results and Discussion

Radium Distribution of the Overflows and Underflows

Table XV lists the specific activity measurements obtained from the hydrocyclone experiments. The specific activity measurements of untreated samples (e.g., overflow = 1269.5 pCi/g and underflow = 1155.5 pCi/g) and samples that sheared with the dispersator (e.g., overflow = 212.6 pCi/g and underflow = 1104.85 pCi/g) showed slightly lower specific activity measurements for the underflows (coarse) than the overflows (fine). The samples treated with the dispersant (e.g., overflow = 669.32 pCi/g and underflow = 1283.6 pCi/g) and ultrasonic probe (e.g., overflow = 639.32 pCi/g and underflow = 1004.27 pCi/g) showed much lower overflow specific activities than the underflows. When both the dispersant and the dispersator was used, the underflow specific activity (1018.6 pCi/g) was much lower than the overflow specific activity (577.05 pCi/g). The overflow of the second run of the experiment ran with the dispersant and dispersator increased approximately 500 pCi/g (from 1403.75 pCi/g to 1899.2 pCi/g). The second run of the underflow collected was to simulate hydrocyclones run in series. Unfortunately, mass balance and activity balances could not be achieved due to lack of sample obtained from the underflows and overflows.

TABLE XV

Specific Activity Measurements

Hydrocyclone Experiment

		Specific Activity (pCi/g)			
Sample	Type	Ra-226	1 σ	Ac-228	1 σ
Original Untreated	-	1040.9	58.4	333.6	6.8
Untreated	Overflow	1264.5	80.7	393.4	10.6
	Underflow	1155.5	65.8	325.3	77.4
Dispersator only	Overflow	1212.6	103.4	433.5	17.33
	Underflow	1104.85	81.98	353.94	12.87
Dispersant only	Overflow	669.32	66.9	196.32	12.37
	Underflow	1283.6	90.96	477.3	14.25
Dispersator and Dispersant	Overflow	1018.6	90.7	310.7	16.14
	Underflow	577.05	49.4	170	8.98
Dispersator and Dispersant	Overflow*	1403.75	108.4	417.34	17.96
	Overflow**	1899.2	157.47	652.99	28.43
	Underflow**	1063.95	78.93	395.58	11.99
Ultrasonic Sonicator Probe	Overflow	639.32	69.15	206.3	15.72
	Underflow	1004.27	77.59	362.69	13.2

NOTE: Overflow consists of finer grains and underflow consists of coarser grains.
*First run
**Second run

SEM Analysis of the Overflows and Underflows

Figures 19 and 20 show the typical SEM photographs of solids obtained from the overflows and underflows of the hydrocyclone. Additional SEM photographs from this experiment are attached in Appendix D. These photographs indicate that the hydrocyclone did a good job of separating the smaller sized particles from the larger particles. Figure 19 shows the finer grained fraction which is rich in barite. Figure 20 shows the coarser grained material, mostly quartz, and the barite present appears to be generally present as grain coats. The overflow contained particles rich in barite, sized fine to very fine sand, angular, and as massive clasts of barite. These clasts may have originated as scale particles detached from piping and subsequently deposited in separators and tanks. The underflow contained barite-poor samples comprised of angular to subrounded quartz grains, and the barite is typically present as grain coats and isolated patches. These photographs also indicate that

barium is prevalent in smaller sized particles. The barite particles are consistently attached to the larger grains which explains the high radioactivity measurements.

XRD Analysis of the Overflows and Underflows

Table XVI shows the mineralogy data obtained from each of the hydrocyclone experiments. Mineralogy data show that the overflow of the hydrocyclone contained 70 to 83% barite and 15 to 33% quartz. The underflows of the hydrocyclone contained 14 to 25% barite and 69 to 77% quartz. The original untreated sample showed similar percentages as the underflow of the hydrocyclone which carried most of the solids. The mass transferred to the overflow was a small amount. Mineralogy data show that the hydrocyclone was efficient at separating the quartz and barite materials, since the underflow contained most of the quartz and the overflow contained most of the barite on a percent basis.

TABLE XVI

Mineralogy

Hydrocyclone Experiment

		Mineralogy		
Sample	Output	Barite (%)	Quartz (%)	Feldspar (%)
Original Untreated	-	16	76	8
Untreated	Overflow	83	16	1
	Underflow	22	77	7
Dispersator only	Overflow	83	15	2
	Underflow	18	69	13
Dispersant only	Overflow	51	33	1
	Underflow	25	70	5
Dispersator and Dispersant	Overflow*	70	27	3
	Overflow**	70	24	6
	Underflow**	18	77	5
Ultrasonic Sonicator Probe	Overflow	60	33	1
	Underflow	18	72	10

NOTE: Overflow consists of coarser grains and underflow consists of finer grains.
*First run
**Second run

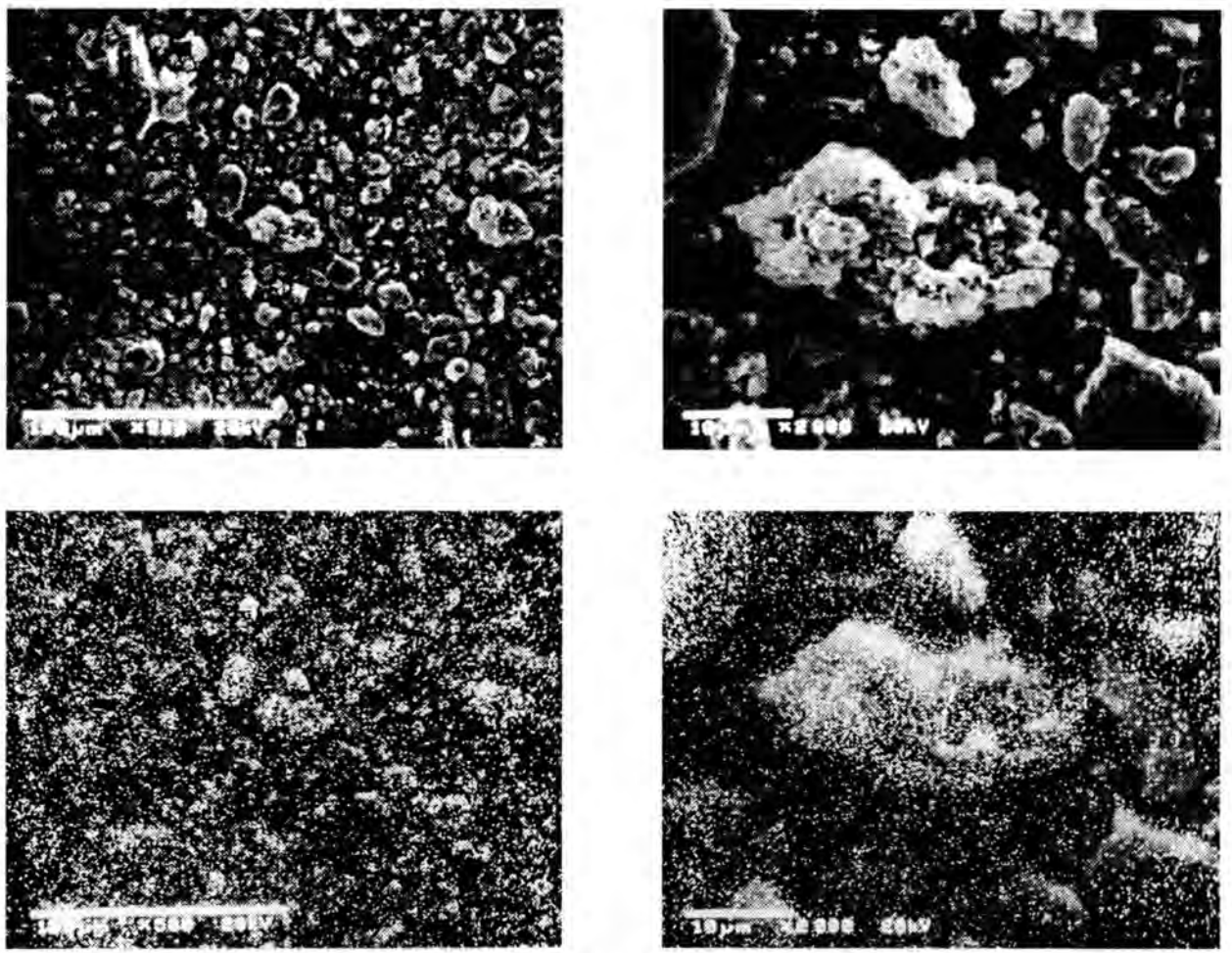

Figure 17. SEM photographs of solids obtained from the overflow of the hydrocyclone of untreated sample (11385-43). (A) x500 image showing particle morphologies. (B) x2000 image showing detailed particle morphologies. (C) x500 image showing barium X-ray map of image shown in (A). (D) x2000 image showing barium X-ray map of image shown in (B).

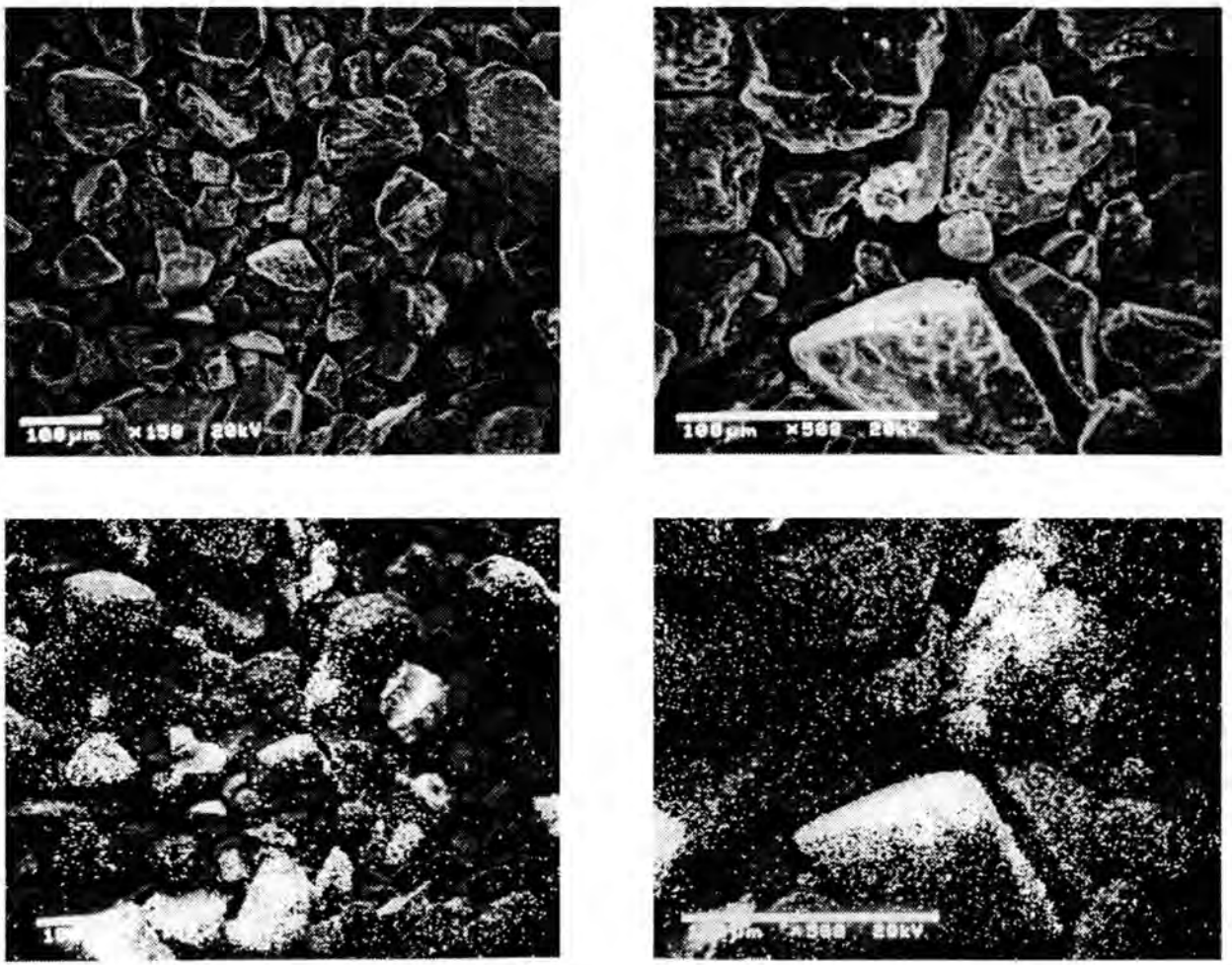

Figure 18. SEM photographs of solids obtained from the overflow of the hydrocyclone of untreated sample (11385-44). (A) x150 image showing particle morphologies. (B) x500 image showing detailed particle morphologies. (C) x150 image showing barium X-ray map of image shown in (A). (D) x500 image showing barium X-ray map of image shown in (B).

Interpretation of Barite Specific Activity

Using the specific activity measurement data of total grams of sample and mineralogy data obtained from overflows and underflows of this experiment, the barite specific activities were calculated in units of pCi of Ra-226/g of barite. These values resulted in higher specific activity for the underflows than overflows on per gram of barite basis. The specific activity of the overflows ranged from approximately 1,000 to 2,000 pCi of Ra-226/g of barite, whereas the underflows ranged from approximately 4,000 to 6,000 pCi of Ra-226/g of barite. These results suggest that barite attached onto silica grains has a higher specific activity of Ra.

TABLE XVII

Calculation of Barite Specific Activity in pCi of Ra-226/g of Barite

Sample	Overflow	Underflow
Untreated	1,523	5,252
Dispersator only	1,461	6,138
Dispersant only	1,116	5,134
Dispersator and Dispersant	1,340	4,122
Dispersator and	2,005*	-
Dispersant	2,713**	5,911**
Ultrasonic Sonicator Probe	999	5,579

NOTE: Overflow consists of coarser grains and underflow consists of finer grains.
*First run
**Second run

Summary

The specific activity measurements of underflows and overflows of each experiment were inconsistent. Despite the ability of the hydrocyclone to separate barite from quartz, the radioactivity did not necessarily follow the barite. In some instances, the underflows showed higher specific activity than the overflows and vice-versa. One explanation might be that the hydrocyclone, dispersator, or the ultrasonic probe did not provide the shearing capability to disrupt the barite particles from quartz grains.

A closer look revealed that when the specific activity of barite was calculated, the values resulted in higher specific activity for the underflows than the overflows on per gram of barite basis. These results show that the barite attached onto silica grains are more radioactive on per gram basis. This explains the high total specific activity measurements obtained for total grams of solids event through the hydrocyclone was very efficient at separating the larger particles and small particles. These barite particles that could not be sheared off from the inert silica grains were approximately four to five times more radioactive than the loose barite particles. This indicates that barite that was coated onto the silica grains are significantly more radioactive than the barite that was loosely attached.

The attempt to separate the NORM-contaminated vessel solids and non-NORM-contaminated vessel solids was not successful with the use of the hydrocyclone. Neither the dispersator nor the ultrasonic probe, along with the dispersant and the hydrocyclone, were able to disagglomerate the radiobarite particles from the sand grains.

Chemical Dissolution

Introduction

The dissolution experiment was conducted to examine the possibility of separating NORM-contaminated barite from the nonradioactive components of the vessel solids by dissolution. Commercial scale dissolvers have previously been shown to stimulate the majority of barite, calcite and mixed scales deposited was removed by dissolvers (Rhudy, 1993). Paul and Fieler (1992) have also developed a solvent for oilfield scales using an efficient chelating agent and synergist similar to chemicals used for this experiment.

Two dissolution media were used in these experiments, Calnox-271 and a DPTA (multidentate ligand material) and oxalic acid solution. Oxalate is used to suppress calcium dissolution. Ten grams of unwashed composite vessel solids were combined with 60 ml of dissolution media in a 250-ml acrylic plastic jar, and shaken for 24 hours. The samples

were then removed from the shaker and separated from the liquid by decantation, centrifugation, and filtration. Specific activity of both solids and liquids were determined by gamma spectroscopy. This experiment was performed at room and elevated temperatures.

Composite vessel solids were examined by SEM to obtain visual information on grain sizes and morphologies before and after the chemical dissolution experiments. The samples obtained from experiments running at room and elevated temperatures were examined. The distribution and associations of barite in these samples was investigated with the SEM by obtaining barium maps with backscattered electron imaging.

X-ray diffraction, XRD, was used to determine the identify of crystalline phases present in the vessel solids. Samples were ground to 50 μm or less prior to analysis. All XRD analyses were executed on random powder mounts. The results of the XRD were interpreted by comparison of diffractograms obtained for the samples to diffractograms of pure minerals.

Experimental Results and Discussion

Radium Distribution in the Vessel Solids and Solution

With both solvents at room and elevated temperatures, the specific activity measurements of the liquid concentrations are negligible compared to the specific activity measurements of the solids concentration. Composite vessel solids in Calnox-271 solution showed slightly lower specific activity measurements than the 50/50 mixture of DPTA and oxalic acid solution in the solids concentration. Paul and Fieler (1992) used a 50/50 mixture of DPTA and oxalic acid solution in their experiment. The liquid concentration from the Calnox-271 showed slightly higher specific activity measurements than the 50/50 mixture at both room temperature and elevated temperature.

Table XVIII lists the specific activity measurements for solids and liquids performed at room temperature. The dissolution experiment performed at room temperature showed

an increase in the solids, in the specific activity of Ra-226 from 1,040.9 pCi/g of untreated sample to 1,233.85 pCi/g and 1,270.45 pCi/g for samples treated with Calnox-271 and DTPA and oxalic acid, respectively. Similarly, increases in the specific activity measurements for Ac-228 are seen.

TABLE XVIII

Specific Activity Measurements

Dissolution Experiment at Room Temperature

		Specific Activity (pCi/g)			
Sample	Type	Ra-226	1 σ	Ac-228	1 σ
Untreated Sample	Soil	1040.9	58.4	333.6	6.8
Calnox-271	Liquid	16.3	2.15	4.59	0.28
	Solid	1233.85	71.9	407.6	8.64
DPTA and Oxalic Acid	Liquid	19.7	2.3	4.96	0.3
	Solid	1270.45	73.1	405.75	8.66

These results indicate that the solids became more concentrated with treatment with the scale dissolvers and negligible amounts of radium went into solution. This may attribute to dissolution of barite and not radium.

At an elevated temperature of 75°C, both the Calnox-271 and DTPA and oxalic acid showed a decrease in specific activity measurements of the solids. Increased temperature enhanced the dissolution rate and capacity, as expected for most reactions (Paul and Fieler, 1992). Despite demonstrated effectiveness of the solvent at descaling and decontaminating production tubing in a field environment under laboratory conditions tested by Harris and Fisher (1994), using Barrage^{TM} (a commercial scale dissolver), the dissolution rates were slow. This experiment also showed that the dissolution rates are shown using Calnox S-271. Field conditions (higher temperatures and pressures downhole) may be the reason for better dissolution rates shown in Paul and Fielder's (1992) study. DTPA and oxalic acid showed higher specific activity compared to the Calnox S-271. For solids in Calnox-271, the solids concentration of Ra-226, Ac-228, and Bi-214 were 801.45 pCi/g, 296.8 pCi/g, and 303.9 pCi/g, respectively. However, the specific activity in the liquid concentration

increased to 81.45 pCi/g, 23.5, and 16.59 for Ra-226, Ac-228, and Bi-214. Table XIX shows the specific activity measurements obtained from the dissolution experiment performed at elevated temperature.

TABLE XIX

Specific Activity Measurements

Dissolution Experiment at Elevated Temperature (75°C)

		Specific Activity (pCi/g)					
Sample	Type	Ra-226	±1σ	Ac-228	1 σ	Bi-214	1 σ
Untreated Sample	Soil	1040.9	58.4	333.6	6.8	445.4	8.7
Calnox-271	Liquid	81.45	4.57	23.5	0.49	16.59	0.44
	Solid	801.45	51.5	296.8	7.24	303.9	7.88
DPTA and Oxalic Acid	Liquid	61.6	3.91	15.3	0.41	13.9	0.41
	Solid	1008.25	60.38	355.65	7.85	388.9	8.9

Even though more radium went into solution at an elevated temperature, the specific activity measurements in the solids concentrations were too high for this process to be considered an effective solution to the NORM-contaminated vessel solids problem. Similar work conducted by Skeaff (1977) showed that much of the Ra-226 is dissolved from coarser material and redistributed to the finer material, indicating that it must enter the solution. If this is true, after the dissolution process, a mechanical separation technique such as a hydrocyclone may result in a waste volume reduction.

Figures 19 and 20 graphically illustrate the comparisons of Calnox-271 and DTPA and oxalic acid at room temperature and at elevated temperature for Ra-226, Ac-228 and Bi-214. These figures indicate that radium was most soluble in Calnox-271 at elevated temperature. Clearly, waste volume reduction cannot be easily achieved through simple dissolution of barite.

Mass Balance and Activity Balance

Table XX shows the mass balance and activity balance calculated from the dissolution data. The specific activity of the untreated sample was multiplied by the original

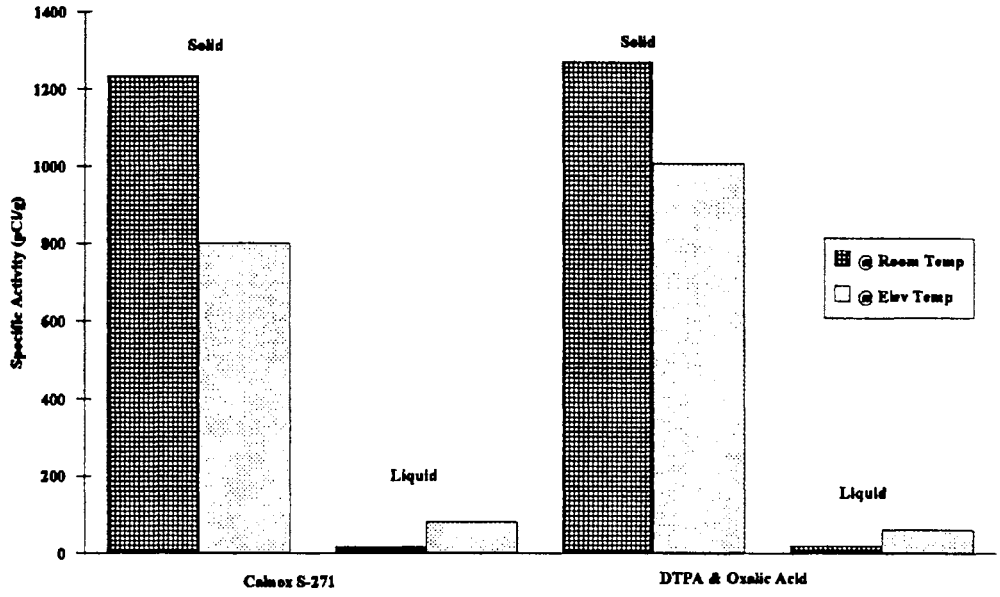

Figure 19. Ra-226 Specific Activities at Room Temperature and at Elevated Temperature

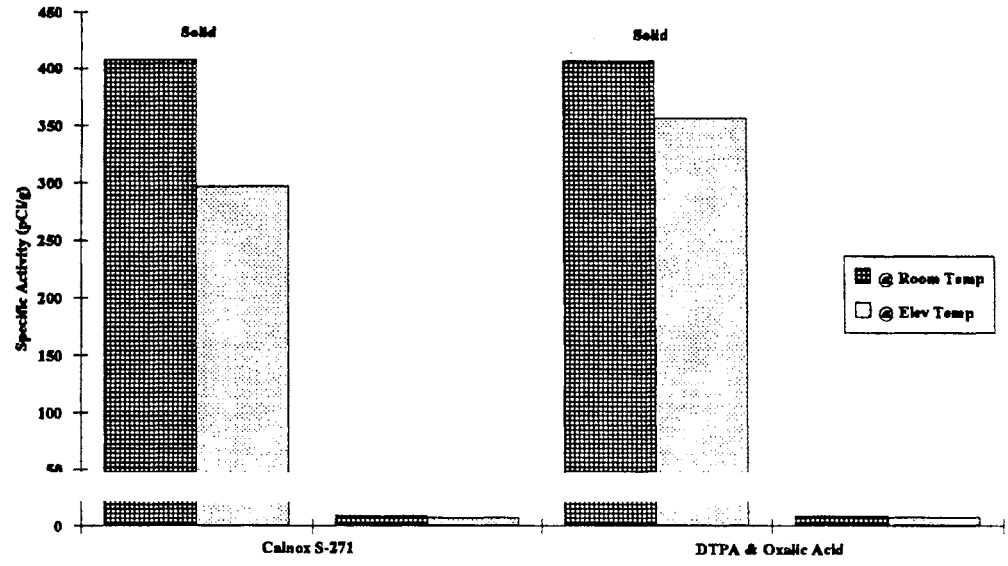

Figure 20. AC-228 Specific Activities at Room Temperature and at Elevated Temperature

amount of sample (i.e., 10 g), and the specific activity of the liquid obtained after dissolution was multiplied by the mass of the liquid (i.e., 71.82 g for Calnox S-271) to obtain the total activities. Amount of solids dissolved in the solution was determined by conservation of mass calculations. Then the specific activity of the solids was multiplied by the remaining mass to obtain the total activity of the solids after dissolution. In Calnox S-271, 11.2% of the solids were dissolved at room temperature, whereas 56.2% of the solids were dissolved at the elevated temperature. Similarly, more solids were dissolved with DTPA and oxalic acid solution at the elevated temperature. Total activity balance was not achieved. This may be the result of 20% variations in the gamma spectrometer. The higher activity resulting from the activity balance may be attributed to the fact that removing barium decreased the self-shielding capabilities within the particles.

TABLE XX

Activity and Mass Balances of Dissolution Experiment at Room Temperature

	Original Untreated		Solids Remaining		Solids Dissolved		
Sample Dissolved In	Total Activity (pCi)	Mass (g)	Total Activity (pCi)	Mass (g)	Total Activity (pCi)	Mass (g)	% Dissolved
Calnox S-271 @ room temp	10,409	10	10,956.6	8.88	18.26	1.12	11.2
Oxalic acid @ room temp	10,409	10	11,179.96	8.8	23.64	1.2	12
Calnox S-271 @ elev. temp	10,409	10	3,510.35	4.38	479.75	5.62	56.2
Oxalic acid @ elev. temp	10,409	10	6,291.48	6.24	231.56	3.76	37.6

SEM Analysis of the Vessel Solids After Dissolution

Figures 21 and 22 show the composite vessel solids before dissolution and after dissolution with Calnox-271 at elevated temperature. The barium maps indicate that solids dissolved in Calnox-271 at elevated temperature contained less barium in the solids. More

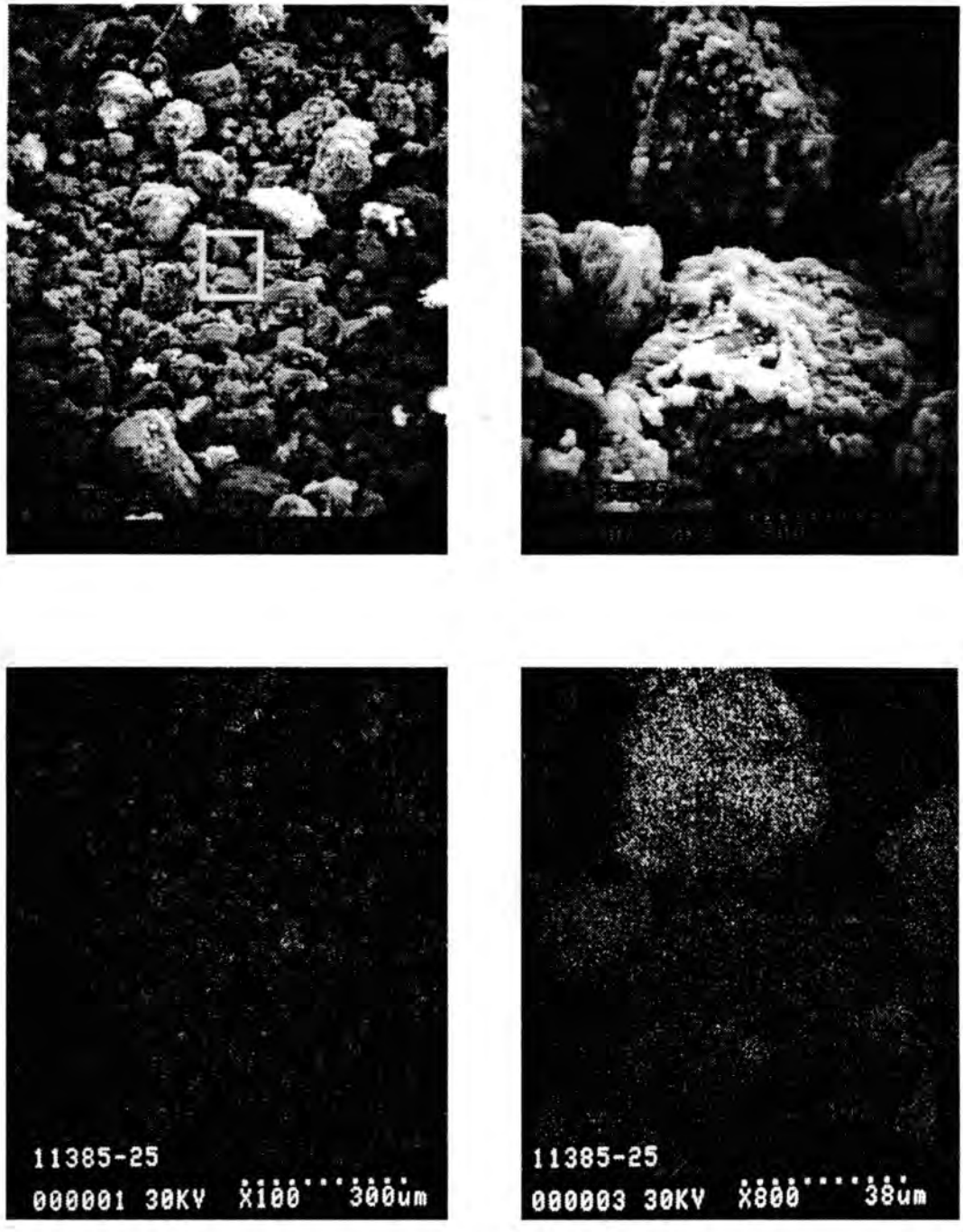

Figure 21. SEM photographs of untreated composite vessel solids (11385-25). (A) x100 image showing particle morphologies. (B) x800 image showing detailed particle morphologies. (C) x100 image showing barium X-ray map of image shown in (A). (D) x800 image showing barium X-ray map of image shown in (B).

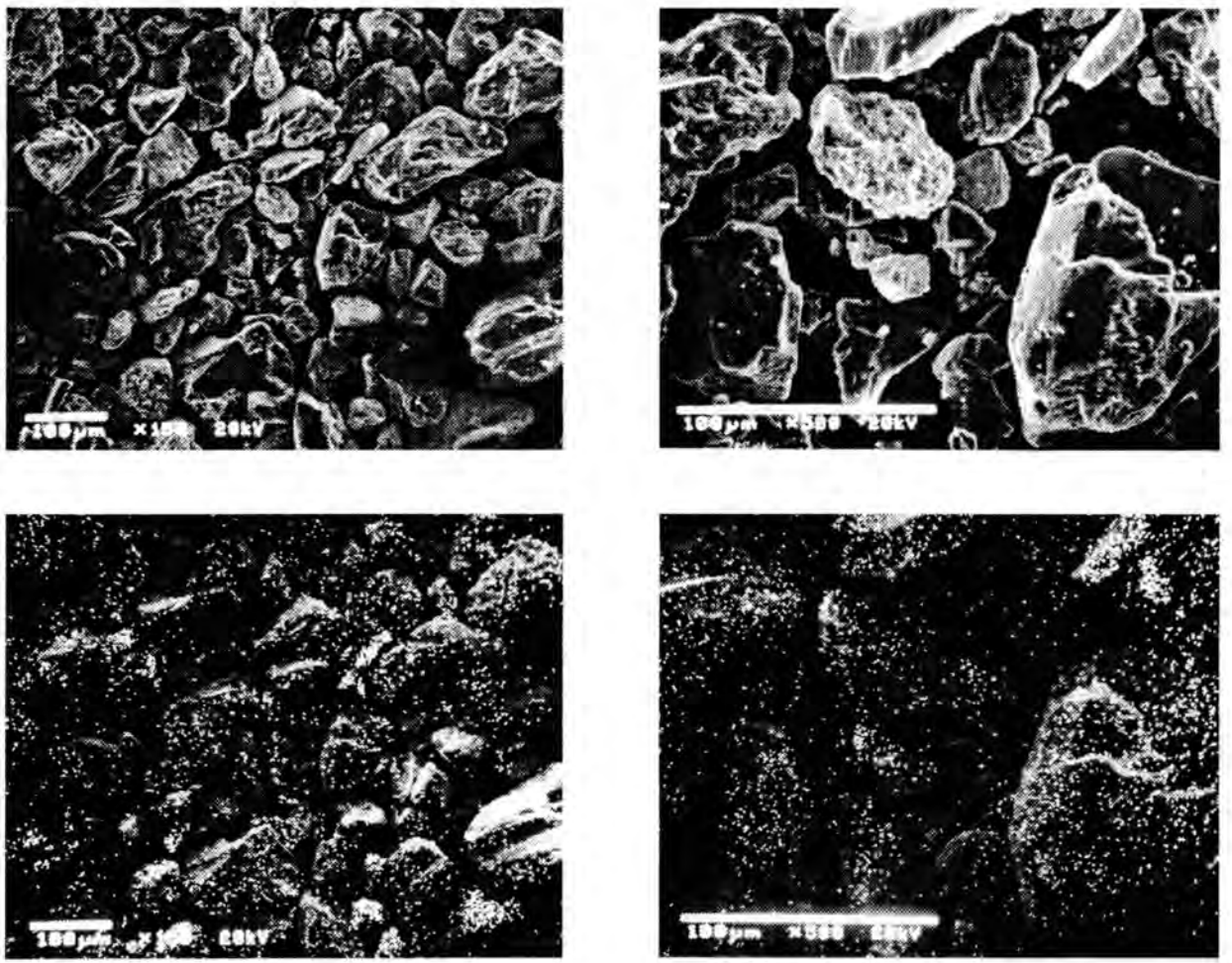

Figure 22. SEM photographs of sample from dissolution experiment performed at elevated temperature with DTPA and oxalic acid solution (11374-33F). (A) x100 image showing particle morphologies. (B) x1000 image showing detailed particle morphologies. (C) x100 image showing barium X-ray map of image shown in (A). (D) x1000 image showing barium X-ray map of image shown in (B).

barite particles were dissolved in Calnox S-271 solution overall. Additional SEM photographs of solid particles obtained from this experiment are attached in Appendix E.

XRD Analysis of the Vessel Solids After Dissolution

The mineralogy of the solids indicates that the barite percentage in the solids decreased in both cases. The untreated sample contained 16% barite, 76% quartz, and 8% feldspar. At room temperature, both Calnox-271 and DTPA and oxalic acid slightly reduced the percentage of barite. At elevated temperature, more of the barite was dissolved in Calnox-271 and DTPA and oxalic acid. Table XXI shows the resulting mineralogy data at room temperature and at elevated temperature. As the percentages of barite left in the solids decreased, the liquid radium concentration increased, as expected (Table XVII).

TABLE XXI

Mineralogy of the Solids

Dissolution Experiment

	Mineralogy					
	At Room Temperature			At Elevated Temperature		
Sample	Barite (%)	Quartz (%)	Feldspar (%)	Barite (%)	Quartz (%)	Feldspar (%)
Untreated Sample	16	76	8	16	76	8
Calnox-271	11	81	8	6	88	6
DTPA and Oxalic Acid	11	82	9	7	88	5

Summary

Overall, chemical dissolution would not be an effective method for reducing the volume of NORM waste. The liquid to solution ratio was approximately 7:1 on mass basis. Laboratory experiments suggest that at favorable conditions (Calnox S-271 at elevated temperature), 120 ml of solution would be necessary in order for 10 g of vessel solids to completely transfer of radium into solution, assuming equilibrium conditions. The commercial scale dissolver is $23.47 per gallon. In order to dissolve barite in one kilogram of

vessel solids, it would cost $533.04 at the elevated temperature, dissolving a little over 50%. To dissolve the barite completely, it would cost over $1,000 per one kilogram. The cost of the commercial scale dissolver and the amount needed to treat the radioactive scales make this process ineffective economically.

CHAPTER 5

CONCLUSIONS

Characterization

The characterization study determined that the vessel solids (tank bottoms and separator sands) are comprised of fine, very fine, and silt sized particles. These particles are a mixture of quartz, barite, and amorphous iron and manganese oxides. Barite in these materials is present as isolated precipitates on grains, grain coats, and fine to very fine sand particles. Vessel solids can be substantially radioactive due to the coprecipitation of radium with barite. Barium radium sulfate is attached onto the surface of the silica grains. These radioactive particles are usually isolated in the fine grains or as precipitates on larger grains. Both U and Th are also present in these materials. When present, U is at crustal abundance relative to Si, but Th is, on the average, present above crustal abundance levels with respect to Si. In addition to radium, vessel solids can contain substantial levels of Zn, Pb, Cu, and As.

Due to the small size, brittle, easily ground nature, and sometimes intimate association with inert materials, removal of radium-contaminated barite from these solids by simple physical means is extremely difficult. The simplest means to reduce the volume of this waste stream is fluid removal. Based on their densities, the relative average volumetric abundance of fluid and solid constituents in a vessel solids waste stream is approximately 14% oil, 31% water, 48% inert solids, and 7% radium-contaminated barite. Consequently, simply removing the fluids would reduce waste volume by approximately 45%. On a mass basis, the ratio of quartz to barite is approximately 2:1, but the volume ratio is 3.5:1 due to

the higher density of barite (4.6 g/cc) compared to quartz (2.6 g/cc). Removal of quartz alone would result in an average volume reduction of 39%. Overall, removal of both fluids and quartz would result in an average ultimate waste volume reduction of 88%. Since the fine-grained barite containing the radium is largely present as disseminated patches cemented to inert quartz grains, successful separation technology will require a means of shearing barite precipitates from these grains.

Soil Shielding

This study showed the Ottawa sand was the most effective of the radiation shield materials examined. Although the Ottawa sand was comprised of low atomic number material and had a lower grain density, it had the highest bulk density. Ottawa sand had the lowest attenuation coefficients when compared to the limestone pellets and mollusc shells. Burial of NORM-contaminated material by a layer of quartz sand 2.5 cm in thickness would reduce the radiation field by half. The unshielded material experimentally determined the radiation dropped off as distance increased.

The linear attenuation coefficient decreases with increasing the shield material's density. Mollusc shells had the lowest bulk density and highest porosity, and consequently had highest (i.e., poorest) linear attenuation coefficient. In contrast, the high bulk density and sufficient amount and thickness of sand made it a good shielding material, even though Si and O have relatively low atomic numbers. The mollusc shells yield a half-value layer comparable to concrete.

Radon Emanation

The radon emanation experiment showed that the emissivity of radon gas can be significantly reduced using activated charcoal. The addition of 8 grams of activated coconut charcoal to accumulation cells reduced Rn accumulation by 96%, compared to equivalent accumulation cells without charcoal. The decrease in radon emanation power was attrib-

uted to an increase in charcoal addition. With sufficient amounts of activated charcoal, eventually all of the radon gas can be adsorbed. The results indicated that even a modest amount of activated charcoal would greatly reduce the Rn emanation from soils.

Activated coconut charcoal used for this experiment showed very favorable pseudo isotherms. The Fruendlich, Langmuir High and Low, and BET isotherms showed high capacity of the adsorbent for the adsorbate and strong adsorption bond. These isotherms also proved that the charcoal was a viable option in reducing the radon emission. Therefore, mixing contaminated soil with activated charcoal would inhibit radon emission very effectively. This study also showed that the massive radioactive scale source has very low emanation power, while dispersed ground-up scale has high emanation power.

Mechanical Separation Experiment

The hydrocyclone experiment showed that the specific activity measurements of underflows and overflows of each experiments were inconsistent. Despite the ability of the hydrocyclone to separate barite from quartz, the radioactivity did not necessarily follow the barite. In some instances, the underflows showed higher specific activity than the overflows, and vise versa. The attempt to separate the NORM-contaminated vessel solids and non-NORM-contaminated vessel solids was not successful with the use of the hydrocyclone. Neither the dispersator nor the ultrasonic probe, along with the dispersant and the hydrocyclone, were not able to disagglomerate the radiobarite particles from the sand grains.

Mechanical separation with the hydrocyclone resulted in the overflow from the hydrocyclone containing approximately 4:1 ratio of barite:quartz, and the underflow containing approximately 4:1 ratio of quartz:barite. Solids obtained from overflows and underflows of the hydrocyclone resulted in inconsistent specific activity measurements.

The specific activity measurements reported with the hydrocyclone experiment were too high for this process to be an effective method.

A closer look revealed that when the specific activity of barite was calculated, the values resulted in higher specific activity for the overflows than the underflows on per gram of barite basis. These results indicate the barite that is attached onto silica grains is more radioactive on a per gram basis. This explains the high total specific activity measurements obtained for total grams of solids, even though the hydrocyclone was very efficient at separating the larger particles and smaller particles. These barite particles which could not be sheared off from the inert silica grains were approximately four to five times more radioactive than the loose barite particles.

Dissolution Experiment

The attempt to dissolve radiobarite particles in the scale dissolver was not very successful. While barite is effectively removed by known commercial scale dissolvers, radium sulfate is not easily dissolved. The specific activity measurements from the dissolution experiment indicate that only minute quantities of radium are dissolved into solution. Even though barium and radium dissolved more readily at elevated temperatures, the specific activity measurements of the solids concentrations remained at a high level of radioactivity.

Composite vessel solids in Calnox-271 solution showed slightly lower specific activity measurements than the 50/50 mixture of DTPA and oxalic acid solution in the solids concentration. The liquid concentration from the Calnox-271 showed slightly higher specific activity measurements than the 50/50 mixture at both room temperature (25°C) and elevated temperature (75°C). In both cases, at room and elevated temperatures, the specific activity measurements of the liquid concentrations are negligible compared to the specific activity measurements of the solids concentration.

Even though more radium went into solution at an elevated temperature, the specific activity measurements in the solids concentrations were too high for this process to be an effective solution.

The cost of the commercial scale dissolver and the amount needed to treat the radioactive scales make this process ineffective economically. The liquid-to-solution ratio was approximately 7:1 on a mass basis. Laboratory experiments suggest that, at favorable conditions (Calnox S-271 at elevated temperature), 120 ml of solution would be necessary in order for 10 grams of vessel solids to completely transfer radium into solution, assuming equilibrium conditions. The commercial scale dissolver is $23.47 per gallon. In order to dissolve barite in one kilogram of vessel solids, the cost would be $533.04 at the elevated temperature, dissolving a little over 50%. To dissolve the barite completely, it would cost over $1,000 per one kilogram.

A combination of chemical and mechanical separation techniques may yield better results at separating the NORM-contaminated vessel solids from the inert solids. Also, ion exchange may be a viable solution as a waste reduction treatment option.

BIBLIOGRAPHY

Anderson, Bob, 1990, "Dealing with radioactive scale in offshore oil production," Ocean Industry (November) 33-37, 48.

American Petroleum Institute, 1990, Management and Disposal Alternatives for NORM Wastes in Oil Production and Gas Plant Equipment, RAE-8837/2-2, Dallas, Texas, May.

American Petroleum Institute, 1991, Produced water radionuclide hazard/risk assessment - phase 1, Publication No. 4532, Health and Environmental Science Department, Dallas, Texas, June.

American Petroleum Institute, 1992, Management of Naturally Occurring Radioactive Material (NORM) in oil and gas production, API Bulletin E2, First Edition, Dallas, Texas, May.

Armburst, B. F. and Kuroda, P. K., 1956, "On the isotopic constitution of radium (Ra-224/Ra-226 and Ra-228/Ra-226) in petroleum brines," Trans. Am. Geophys. Union, 37:216-220.

Asikainen, M. and Kahlos, H., 1979, "Anomalously high concentrations of uranium, radium, and radon in water from drilled wells in the Helsinki region," Geochim. Cosmochim. Acta, 43:1681-1686.

Becquerel, H., 1896, "Sur les radiations emises par phosphorescence," Comp. rend., 122:420.

Benes, P., 1990, "Radium in (continental) surface water," *in*: The Environmental Behavior of Radium, Vol. 1, International Atomic Energy Agency, Vienna.

Bobin, P. L., 1933, "Thorium X content of water from well no. 1, in Ukhta oil field," Trav. Inst. Etat. Radium, USSR, 2:157-159 (C.A., 28:6625).

Bonotto, S., 1990, "Radium uptake by marine plants," *in*: The Environmental Behaviour of Radium, Vol. 1, Vienna, International Atomic Energy Agency.

Broecker, Wallace, S., 1964, An application of natural radon to problems in ocean circulation, Symposium on Diffusion in Oceans and Fresh Water, Lamount Geological Observator of Columbia University, Palisades, New York, p. 116-146.

Brown, E., Dairiki, J. M. and Doebler, R. E., 1978, Table of Isotopes (7th Edition), Lederer, C. M. and Shirley, V. S., eds., New York, John Wiley & Sons, Inc.

Christy, Andrew G. and Putnis, Andrew, 1993, "The kinetics of barite dissolution and precipitation in water and sodium chloride brines at 44-45°C," Geochimica et Cosmochimica Acta, Pergamon Press Ltd., Vol. 57:2161-2168.

Clifford, D. A., 1990, "Removal of Radium from Drinking Water," Radon, Radium and Uranium in Drinking Water, Lewis Publisher, Chelsea, Michigan, p. 225-248.

Conner, J. A., Clifford, D. A. and King, P. T., 1993, "In-Situ Method for Reducing the Production of Naturally Occurring Radioactive Materials (NORM) from Subsurface Reservoirs," from Proceedings of "Petro-Safe '93, Fourth Annual Environmental, Safety and Health Conference and Exhibition for the Oil, Gas and Petrochemical Industries," January 26-28, Houston, Texas.

Cothern, C. Richard and Rebers, Paul A., 1990, Radon, Radium and Uranium in Drinking Water, Lewis Publisher, Michigan.

Curie, M. Curie, P. and Bemont, G., 1898, "Sur une nouvelle substance fortement radioactive contenue dans la pechblende," Compt. rend., 127:1215.

Das, H. A., Faanhof, A. and Van Der Sloot, H. A., 1989, Radioanalysis in Geochemistry, Elsevier Publishing Company, New York, pp. 365-368.

EPA/SCA, 1991, "Diffuse NORM Waste: Waste Characterization and Risk Assessment" (DRAFT), SC and A., Inc., for Office of Radiation Programs, U.S. Environmental Protection Agency, May.

Filinov, V. A., 1964, "On the peculiar distribution of radioactive elements at the water-petroleum boundary," *in:* The Geochemistry of Oil and Oil Deposits, Tr. Inst. Geol. Razrab. Goryuch. Iskop., Akad. Nauk S.S.R. (translation), Jerusalem, Israel Programme for Scientific Translations, pp. 210-219.

Fisher, J. B. and Hammond, M., 1994, "Characterization of NORM Vessel Solids," International Petroleum Environmental Conference, March 2-4, 1994, Houston, Texas.

Friedlander, Gerhart, Kennedy, Joseph W., Macias, Edward S. and Miller, Julian Malcolm, 1981, Nuclear and Radiochemistry, Third Edition, John Wiley and Sons, New York, p. 191.

Frissel, M. J. and Köster, H. W., 1990, "Radium in soil," *in*: The Environmental Behavior of Radium, International Atomic Energy Agency, Vienna, Vol. 1.

Ganapathy, R. and Anders, E., 1974, "Bulk composition of the moon and earth, estimated from meteorites," Proc. 5th Lunar Sci. Conf., pp. 1181-1206.

Geotimes, 1993, "Disposal of NORM subject of meeting," January.

Gollnick, Daniel A., 1988, Basic Radiation Protection Technology, Second Edition, Pacific Radiation Corporation, p. 321.

Gott, G. B. and Hill, J. W., 1953, "Radioactivity in some oil fields of southeastern Kansas," Geological Survey Bulletin 988-E, U.S. Government Printing Office, Washington, DC.

Gray, Peter, 1990, "Radioactive materials could pose problems for the gas industry," Oil and Gas Journal, June 25, p. 45-48.

Gray, P. R., 1993, "NORM contamination in the petroleum industry," Journal of Petroleum Technology, January, p. 12-16.

Gutsalo, L. K., 1964, "On the distribution of radium in the ground waters of the central part of the Knieper-Donets basin," Geokhimiya, 12:1305-1312.

Gutsalo, L. K., 1967, "Geochemical connection between radium anomalies in subsurface water and oil and gas deposits," Doklady Akademii Nauk SSSR, 172:1174-1176.

Halbert, B. E., Chambers, D. B., Cassaday, V. J. and Hoffman, F. O., 1990, "Environmental assessment modeling," *in*: The Environmental Behavior of Radium, International Atomic Energy Agency, Vol. 2.

Hanor, J. F., 1969, "Barite saturation in sea water," Geochimica et cosmochimica Acta, Vol. 33, p. 898.

Hanslik, E. and Mansfeld, A., 1990, "Removal of radium from drinking water," *in*: The Environmental Behavior of Radium, International Atomic Energy Agency, Vol. 2.

He, Shiliang and Morse, John W., 1993, "Prediction of Halite, Gypsum and Anhydrite Solubility in Natural Brines Under Subsurface Conditions," Computers and Geoscience, Vol. 19, No. 1, p. 1-22.

Herczeg, Andrew L., Simpson, H. James, Anderson, Robert F., Trier, Robert M., Mathieu, Guy G. and Deck, Bruce L., 1988, "Uranium and Radium Mobility in Groundwaters and Brines Within the Delaware Basin, Southeastern New Mexico, U.S.A.," Chemical Geology (Isotope Geoscience Section), 72:181-196.

Hoover, J., 1994, "NORM Waste Technologies Used in Decontamination and Waste Handling - An Overview," International Petroleum Environmental Conference, March 2-4, 1994, Houston, Texas.

International Atomic Energy Agency, 1990, The Environmental Behavior of Radium, Volume 1, Technical Reports Series No. 310, Vienna.

International Atomic Energy Agency, 1990, The Environmental Behavior of Radium, Volume 2, Technical Reports Series No. 310, Vienna.

Iyengar, M. A. R., 1990, "The natural distribution of radium," *in*: The Environmental Behavior of Radium, Vol. 1, International Atomic Energy Agency, Vienna.

Iyengar, M. A. R. and Rao, K. N., 1990, "Uptake of radium by marine animals," *in:* The Environmental Behaviour of Radium, Vol. 1, Vienna, International Atomic Energy Agency.

Jeffree, R. A., 1990, "Radium uptake by freshwater invertebrates," *in:* The Environmental Behaviour of Radium, Vol. 1, Vienna: International Atomic Energy Agency.

John, R., Lowe, L. M. and Chambers, D. B., 1990, "Examples of dose assessment: Mining and milling in Canada," *in*: The Environmental Behavior of Radium, International Atomic Energy Agency, Vol. 2.

Johnston, A., 1990, "Examples of dose assessment: Australia," *in*: The Environmental Behavior of Radium, International Atomic Energy Agency, Vol. 2.

Justyn, J. and Havlik, B., 1990, "Radium uptake by freshwater fish," *in:* The Environmental Behavior of Radium, Vol. 1, Vienna, International Atomic Energy Agency.

Khademi, B., Alemi, A. A. and Nasseri, A., 1980, "Transfer of radium from soil to plants in an area of high natural radioactivity in Ramsar, Iran," Natural Radiation Environment III (Proc. Int. Conf., Houston, 1978) (Gesell, T. F., Lowder, W. M., eds.), Vol. 1, CONF-780422, Technical Information Center, Oak Ridge: U.S. Dept. of Energy, pp. 600-610.

Kirchmann, R. J. and DeClercq-Versele, H., 1990, "Examples of dose assessment: The Olen area in Belgium," *in*: The Environmental Behavior of Radium, International Atomic Energy Agency, Vol. 2.

Komlev, L. V., 1933, "Origin of radium in oil-field waters," Trav. Inst. Etat. Radium, USSR, 2:207-221 (C.A., 28:6626).

Kramer, T. F., 1981, "^{234}U and ^{238}U concentration in brine from geopressured aquifers of the northern Gulf of Mexico basin," Earth and Planetary Science Letters, 56:210-216.

Kramer, T. F., 1985, "Natural radioelement behavior in geopressured aquifers," Sixth U.S. Gulf Coast Geopressured Geothermal Energy Conference, Austin, Pergamon Press, pp. 126-127.

Kramer, T. F., 1986a, "Radon in unconventional natural gas from Gulf Coast geopressured-geothermal reservoirs," Environ. Sci. Technol., 20:939-942.

Kramer, T. F., 1986b, "^{234}U and ^{238}U concentration in brine from geopressured aquifers of the northern Gulf of Mexico basin," Earth and Planet. Sci. Lett., 56:210-216.

Kramer, T. F. and Reid, D. F., 1984, "The Occurrence and Behavior of Radium in Saline Formation Water of the U.S. Gulf Coast Region," Isotope Geoscience, 2, p. 153-174.

Landa, Edward R., 1987, Buried Treasure to Buried Waste: The Rise and Fall of the Radium Industry, Colorado School of Mines Quarterly No. 2, Vol. 82, Colorado School of Mines Press, Colorado.

Lucas, H. F., 1957, Improved low-level alpha scintillation counter for radon, The Review of Scientific Instruments, Vol. 28, No. 9:680.

Lucas, H. F., 1990, Markun, F. and Boulenger, R., "Methods for measuring radium isotopes: Emanometry," in: The Environmental Behavior of Radium, International Atomic Energy Agency, Vol. 1.

Mann, W. B., Rytz, A., Spernol, A. and McLaughlin, W. L., 1988, Radioactivity Measurements Principles and Practices, Pergamon Press, New York.

Mason, J. Y., Block, R. J. and Knippers, M. L., 1992, Reduction of naturally occurring radioactive material disposal by chemical and physical treatment, 67th Annual Technical Conference and Exhibition of the Society of Petroleum Engineers held in Washington, DC, October 4-7, 1992.

Makofske, William J. and Eldelstein, Michael R., 1988, Radon and the Environment, Noyes Publications, New Jersey.

Molinari, J. and Snodgrass, W. J., 1990, "The chemistry and radiochemistry of radium and the other elements of the uranium and thorium natural decay series," *in*: The Environmental Behavior of Radium, International Atomic Energy Agency, Vol. 1.

Morawska, L. and Phillips, Colin R., 1993, "Dependence of the radon emanation coefficient on radium distribution and internal structure of the material," Geochimica et Cosmochimica Acta Vol. 57: 1783-1797, Pergamon Press Ltd.

Nero, A., 1989, "Earth, air, radon and home," Physics Today, April.

Nitikin, B. A., "Radium in field waters and petroleum of Bibi-Eibat oil field," Trav. Inst. Etat. Radium, USSR, 2:160-165.

Oddo, J. E., Sitz, C. D., Ortiz, Isais, Linz, D. G., Lawrence, A. W., Kan, A. T., Thomson, M. B., 1993, "NORM Scale Formation: A Case Study of the Chemistry, Prediction, Remediation and Treatment in Wells of the Antrim Gas Field," SPE/EPA Exploration and Production Environmental Conference '93, SPE 25937, San Antonio, Texas, March 7-10.

Oddo, J. E. and Al-borno, Amal, 1993, "The Chemistry Prediction and Treatment of Scale Containing Naturally Occurring Radioactive Materials (NORM) in Antrim Gas Fields, Michigan," SPE Production Operations Symposium, Oklahoma City, Oklahoma, March 21-23.

Paul, J. M. and Fieler, E. R., 1992, "A New Solvent for Oilfield Scales," 67th Annual Technical Conference and Exhibition of the Society of Petroleum Engineers, Washington, DC, October 4-7.

Pierce, A. P., Mytton, J. W. and Gott, G. B., 1955, "Radioactive elements and their doughtier products in the Texas panhandle and other oil and gas fields in the United States," 1st U.N. Proc. Conf. on Peaceful Uses of Atomic Energy, Geneva, pp. 494-498.

Prieto, Manuel, Putnis, Andrew and Fernandez-Diaz, Lurdes, 1993, "Crystallization of solid solutions from aqueous solutions in a porous medium: zoning in (Ba,Sr)SO4," Geological Magazine, Cambridge University Press, 130(3):289-299.

Rhudy, J. S., 1993, "Removal of Mineral Scale from Reservoir Core by Scale Dissolver," SPE International Symposium on Oilfield Chemistry, New Orleans, Louisiana, March 2-5.

Rutherford, G. J. and Richardson, G. E., "Disposal of Naturally Occurring Radioactive Material from Operations on Federal Leases in the Gulf of Mexico," SPE/EPA Exploration and Production Environmental Conference '93, SPE 25940, San Antonio, Texas, March 7-10.

Satterly, J. and McLennan, J. C., 1918, "The radioactivity of natural gases of Canada," Trans. Royal Canada, 12:153.

Sawyer, Clair N. and McCarthy, Perry L., 1978, Chemistry for Environmental Engineering, Third Edition, McGraw-Hill Publishing Company, New York, p. 250.

Shannon, B. E., 1993, "An Operational Perspective on the Handling and Disposal of NORM in the Gulf of Mexico," SPE/EPA Exploration and Production Environmental Conference '93, SPE 25937, San Antonio, Texas, March 7-10.

Simon, S. L. and Ibrahim, S. A., 1990, "Biological uptake of radium by terrestrial plants," *in:* The Environmental Behaviour of Radium, Vol. 1, Vienna, International Atomic Energy Agency.

Snodgrass, W. J., 1990, "The chemistry of ^{226}Ra in the uranium milling processes," *in*: The Environmental Behavior of Radium, International Atomic Energy Agency, Vol. 2.

Sorg, T. J., 1990, "Removal of Uranium from Drinking Water by Conventional Treatment Methods," Radon, Radium and Uranium in Drinking Water, Lewis Publishers, Chelsea, Michigan, p. 173-192.

Stather, J. W., 1990, "The behavior, effects and radiation dosimetry of radium in man," *in*: The Environmental Behavior of Radium, International Atomic Energy Agency, Vienna, Vol. 2.

Svarosvsky, L., 1984, Hydrocyclones, Technomic Publishing Company, Inc., Pennsylvania, Schools of Chemical Engineering and Powder Technology, University of Bradford.

Taylor, S. R., 1964, "The abundance of chemical elements in the continental crust - a new table," Geochim. Cosmochim. Acta, 28:1273-1285.

Vdovenko, V. M. and Dubasov, Yu. V., 1990, Analytical Chemistry of Radium, John Wiley and Sons, New York.

Veenstra, J. N., 1993, Advanced Unit Operations Class Notes.

Weigel, F., 1977, "Radium Erganzungsband 2 - Element, Vebindungen Gmelin Handbuch-der Anorganischen Chemie," Berlin, Springer-Verlag.

Wilkening, M., 1990, Radon in the Environment, Studies in Environmental Science 40, Elsevier, New York, p. 29-89.

Williams, A. R., 1990, "Radium uptake by freshwater plants," in: The Environmental Behaviour of Radium, Vol. 1, Vienna, International Atomic Energy Agency.

Wilson, A. J. and Scott, Max L., 1992, Characterization of radioactive petroleum piping scale with an evaluation of subsequent land contamination, Health Physics, 63(6):681-865.

APPENDICES

APPENDIX A

ORIGINAL DATA PERTAINING TO CHARACTERIZATION OF NORM VESSEL SOLIDS


AMOCO PRODUCTION COMPANY
WD-90 TANK SCALE


AMOCO PRODUCTION COMPANY
EUGENE ISLAND 193 WELL A-7D
SEPARATOR SAND
mm 1 2 3 4 5 6 7 8


AMOCO PRODUCTION COMPANY
E. M. WATKINS
SEPARATOR SLUDGE
mm 1 2 3 4 5 6 7 8


AMOCO PRODUCTION COMPANY
OLD THORWELL FIELD
PIPE SCALE SWD
mm 1 2 3 4 5 6 7 8

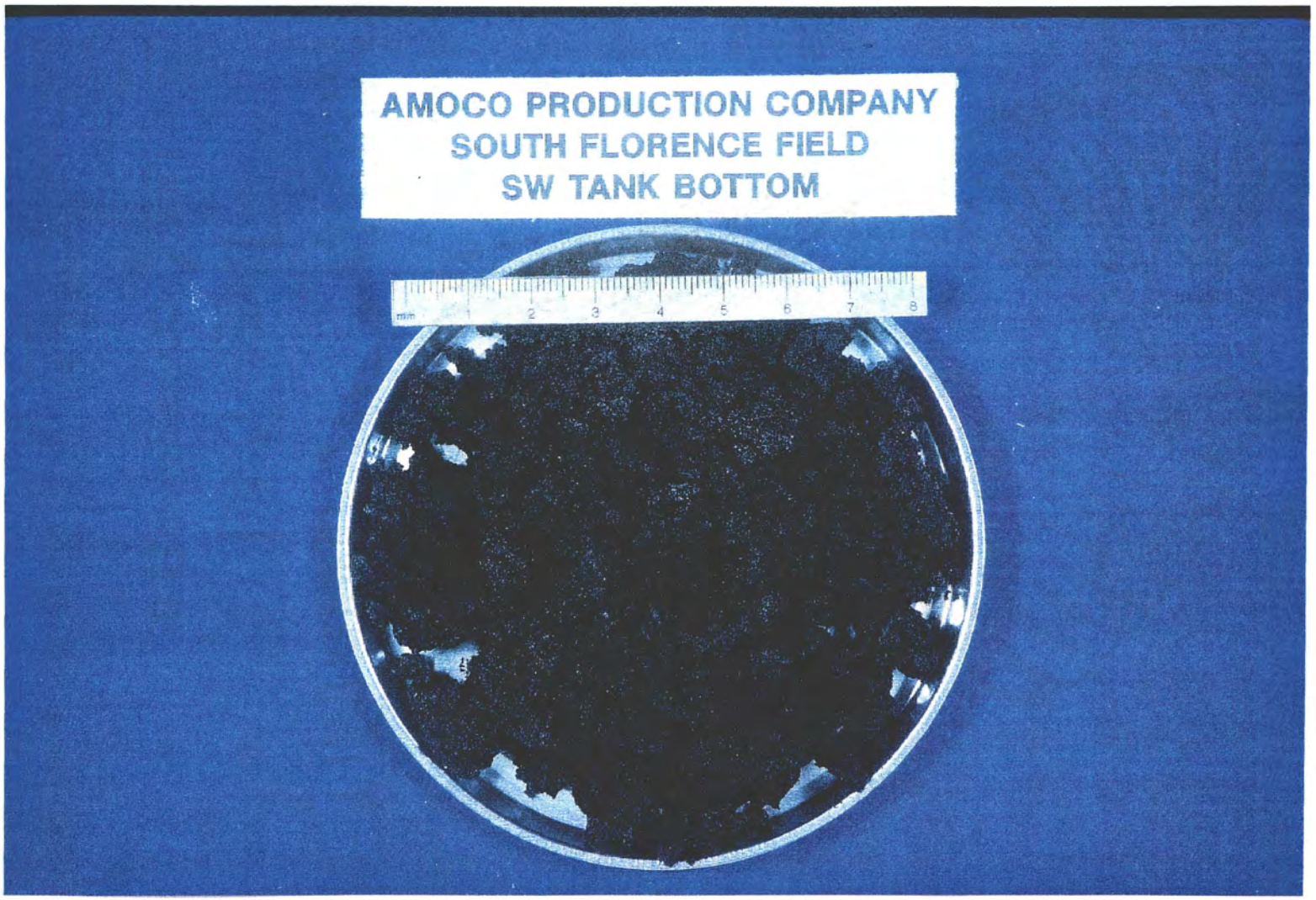
AMOCO PRODUCTION COMPANY
SOUTH FLORENCE FIELD
SW TANK BOTTOM


AMOCO PRODUCTION COMPANY
PORT HUDSON SCALE
EAST BATON ROUGE, LOUISIANA
mm 1 2 3 4 5 6 7 8


AMOCO PRODUCTION COMPANY
BICKHAM NO. 1 TREATER SAND


AMOCO PRODUCTION COMPANY
BICKHAM NO. 2 TREATER SAND

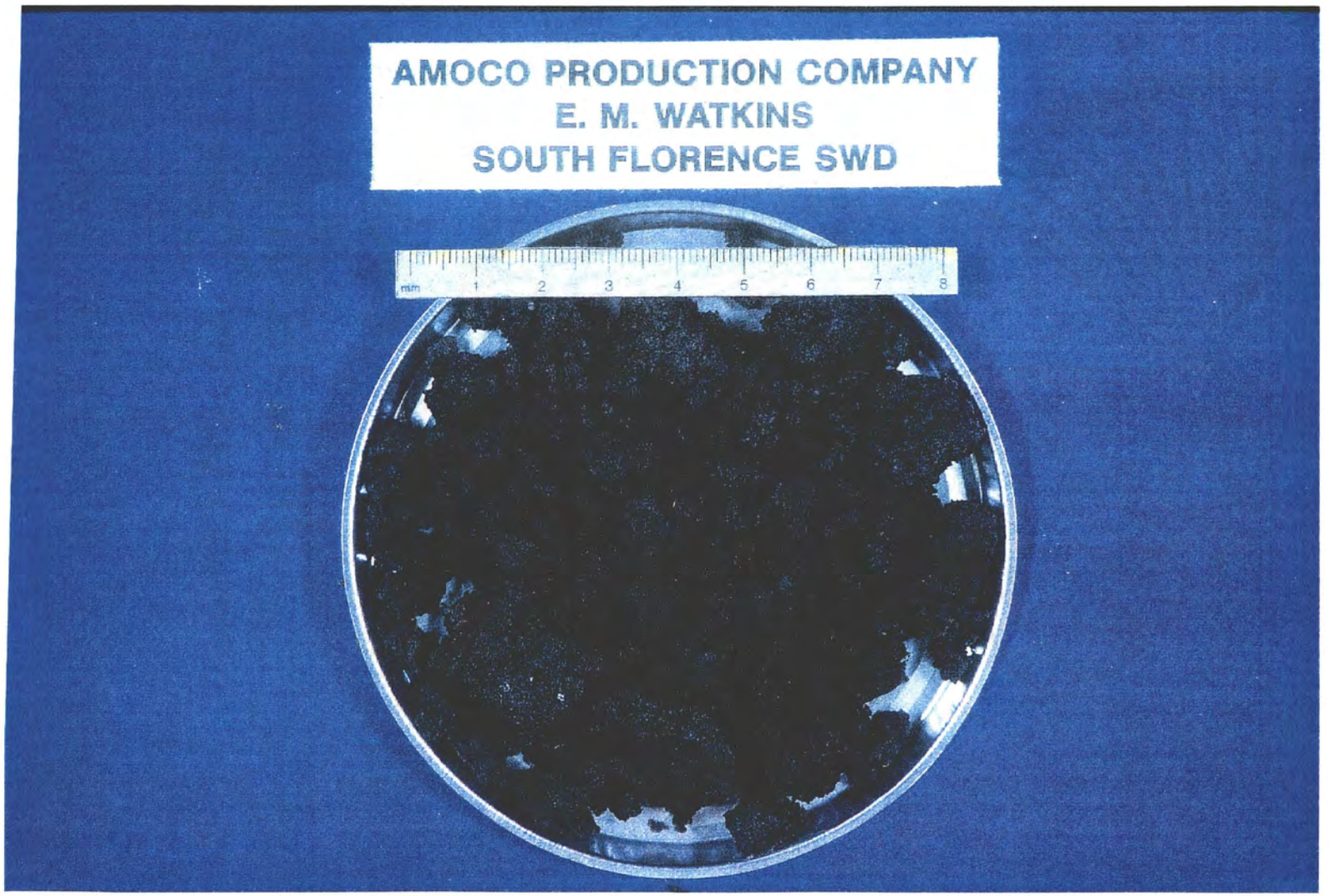
AMOCO PRODUCTION COMPANY
E. M. WATKINS
SOUTH FLORENCE SWD

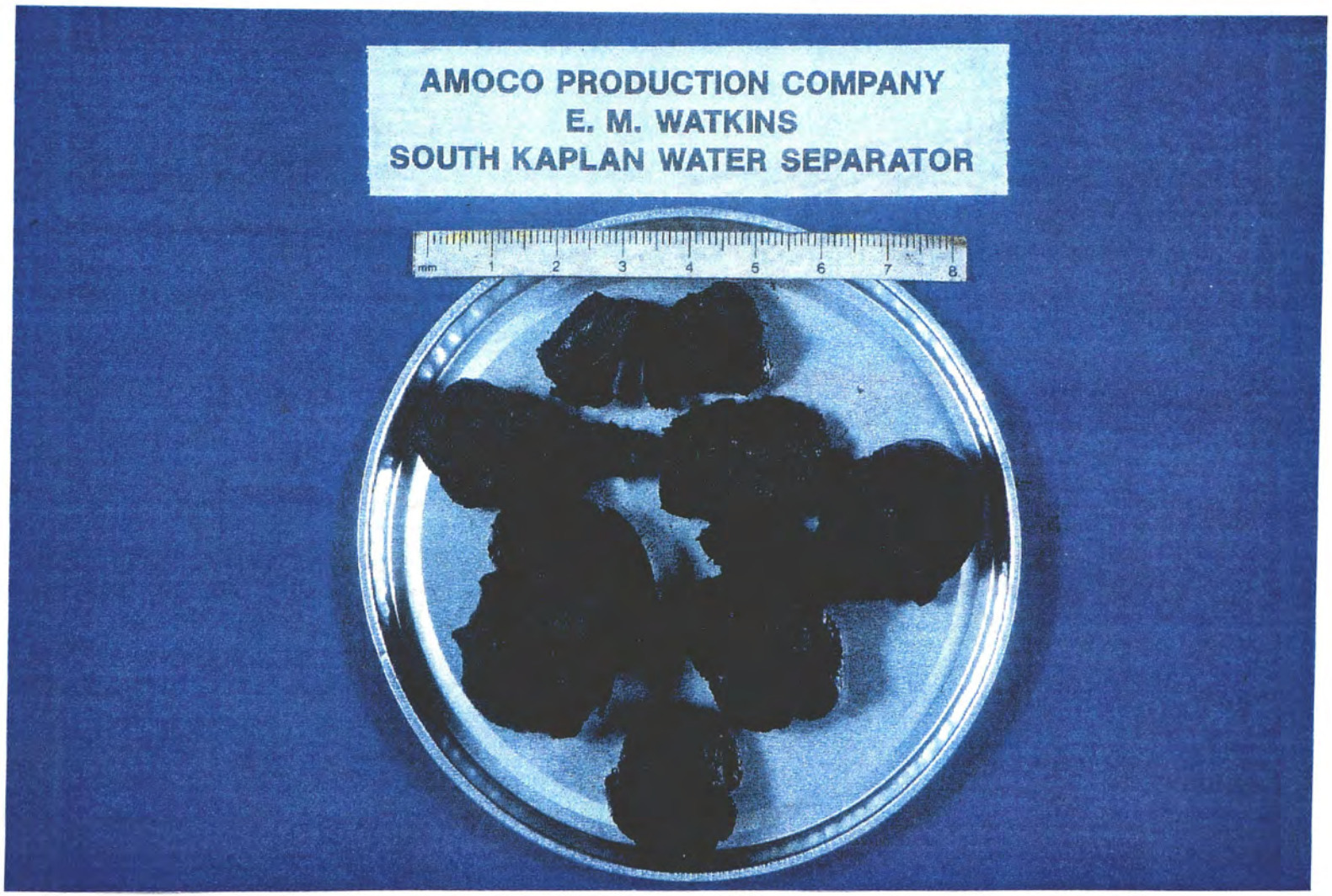
AMOCO PRODUCTION COMPANY
E. M. WATKINS
SOUTH KAPLAN WATER SEPARATOR
mm 1 2 3 4 5 6 7 8

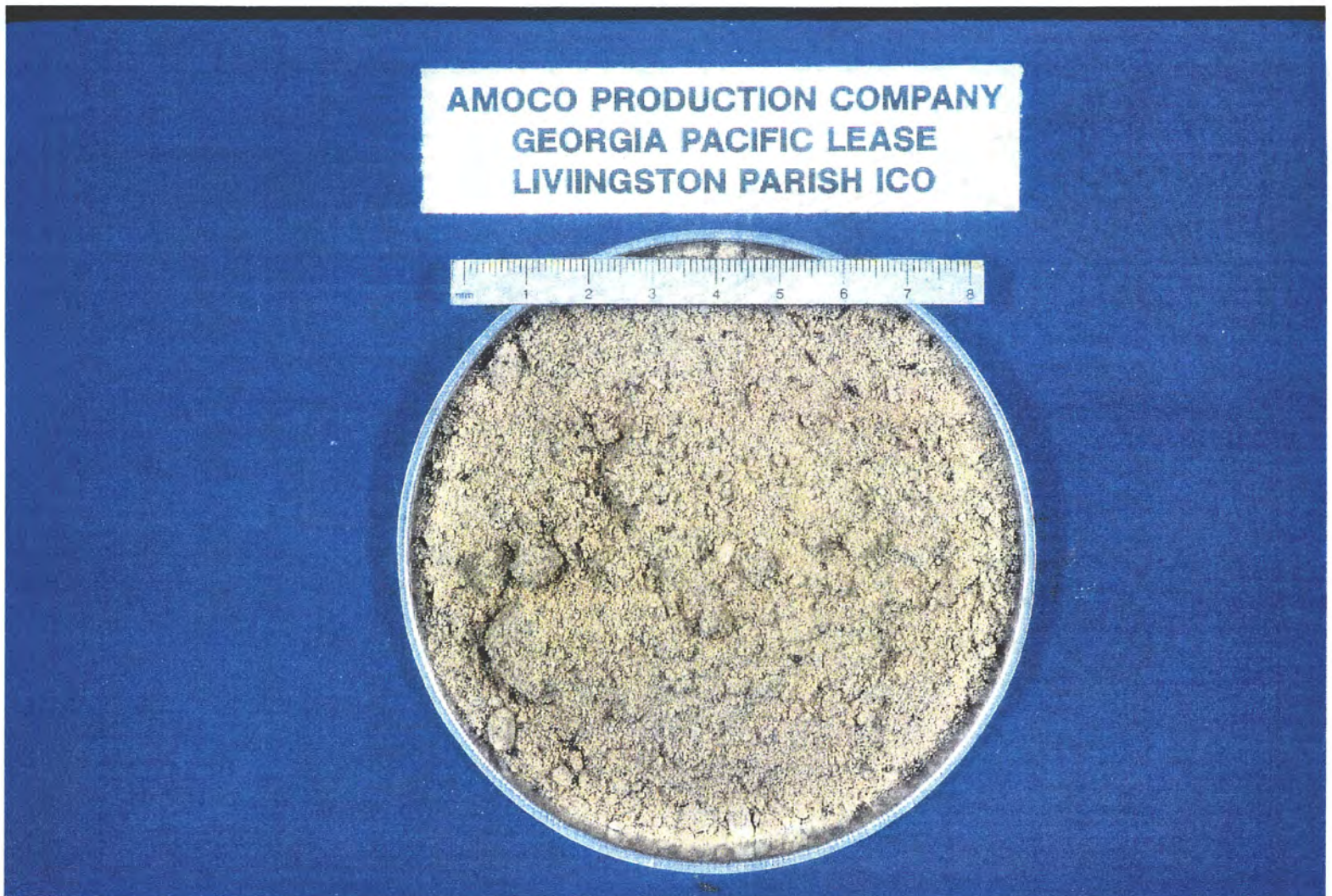
AMOCO PRODUCTION COMPANY
GEORGIA PACIFIC LEASE
LIVIINGSTON PARISH ICO
mm 1 2 3 4 5 6 7 8


AMOCO PRODUCTION COMPANY
GEORGIA PACIFIC NO. 3 TREATER SAND

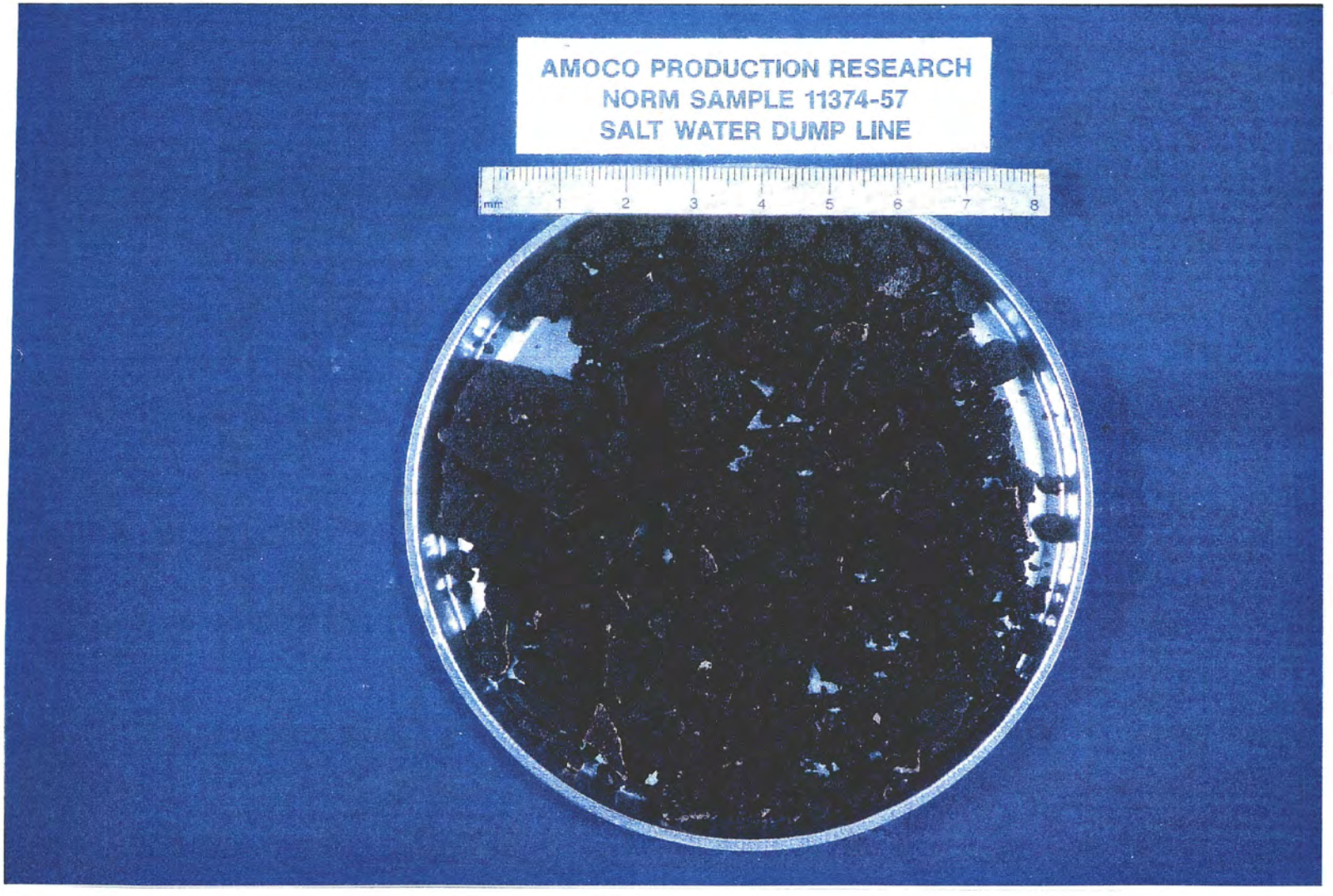
AMOCO PRODUCTION RESEARCH
NORM SAMPLE 11374-57
SALT WATER DUMP LINE
mm 1 2 3 4 5 6 7 8

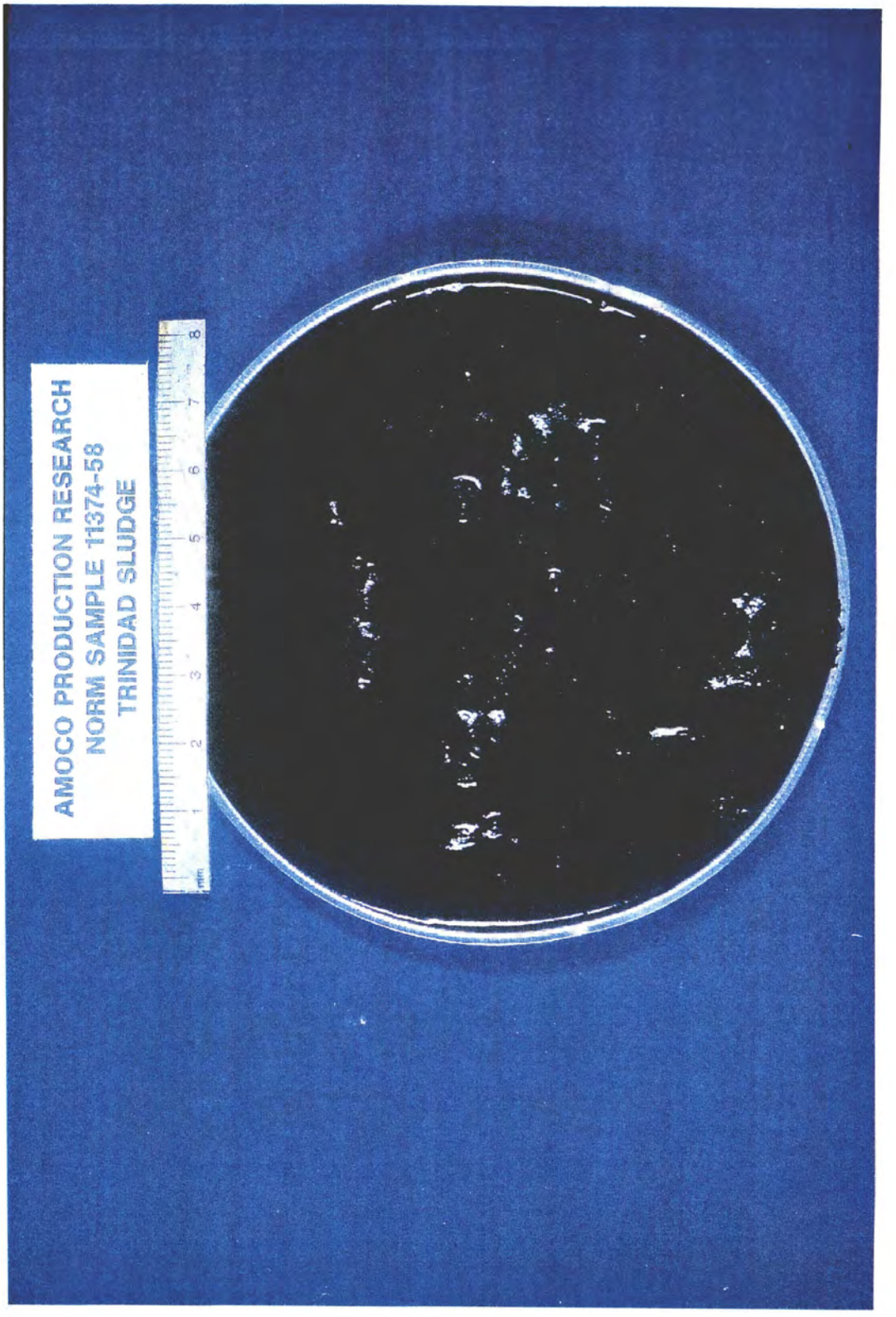
AMOCO PRODUCTION RESEARCH
NORM SAMPLE 11374-58
TRINIDAD SLUDGE

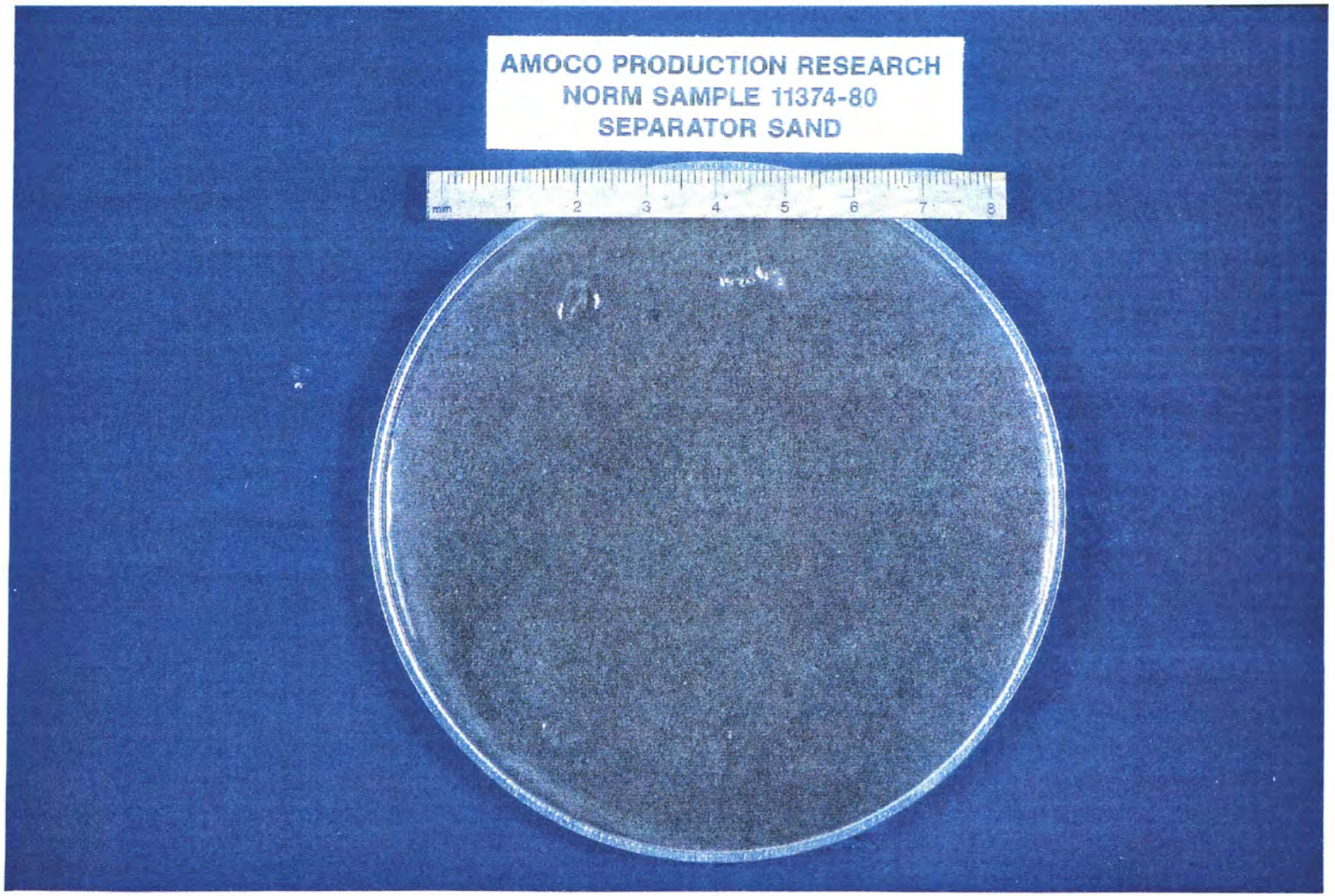
AMOCO PRODUCTION RESEARCH
NORM SAMPLE 11374-80
SEPARATOR SAND

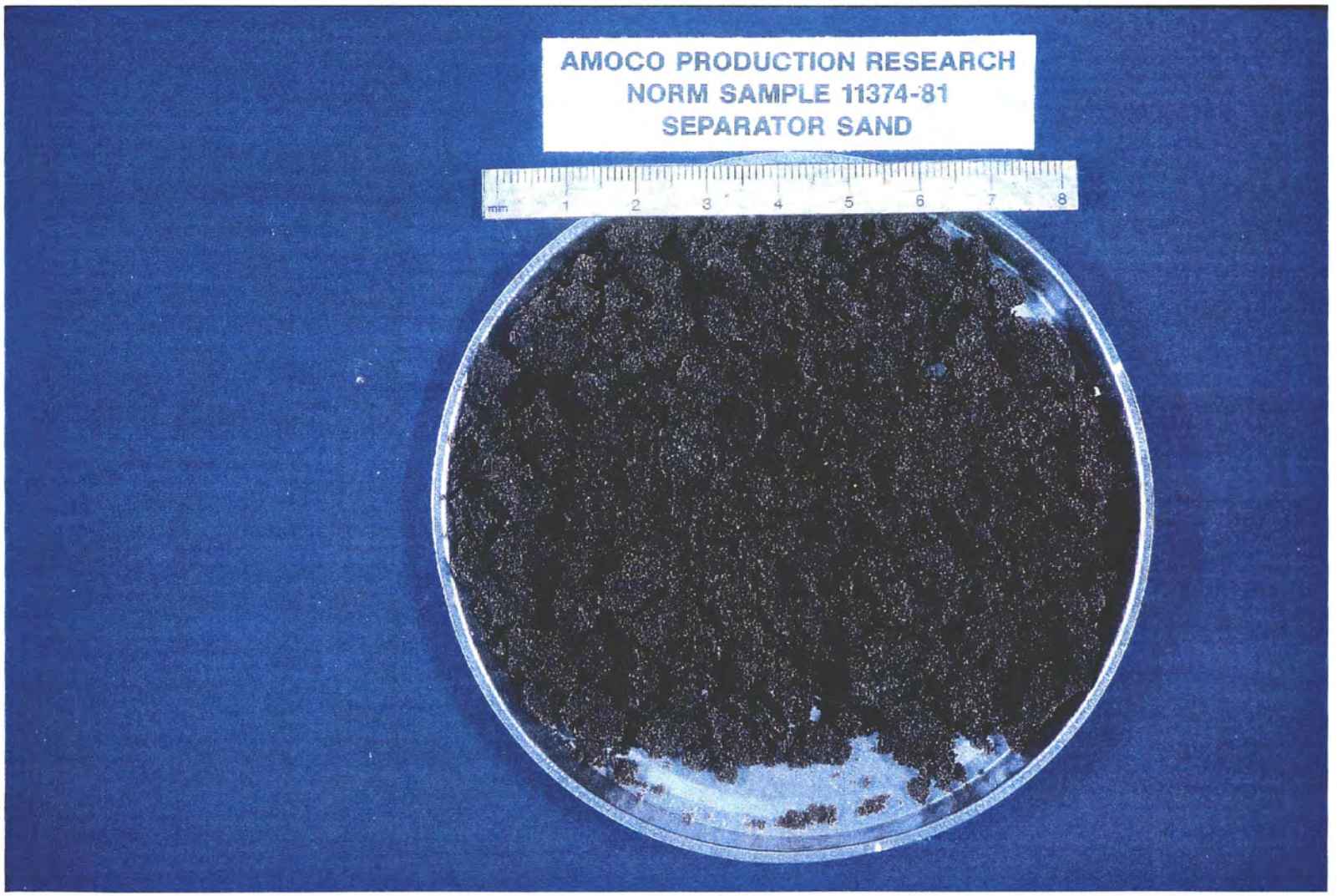
AMOCO PRODUCTION RESEARCH
NORM SAMPLE 11374-81
SEPARATOR SAND
mm 1 2 3 4 5 6 7 8

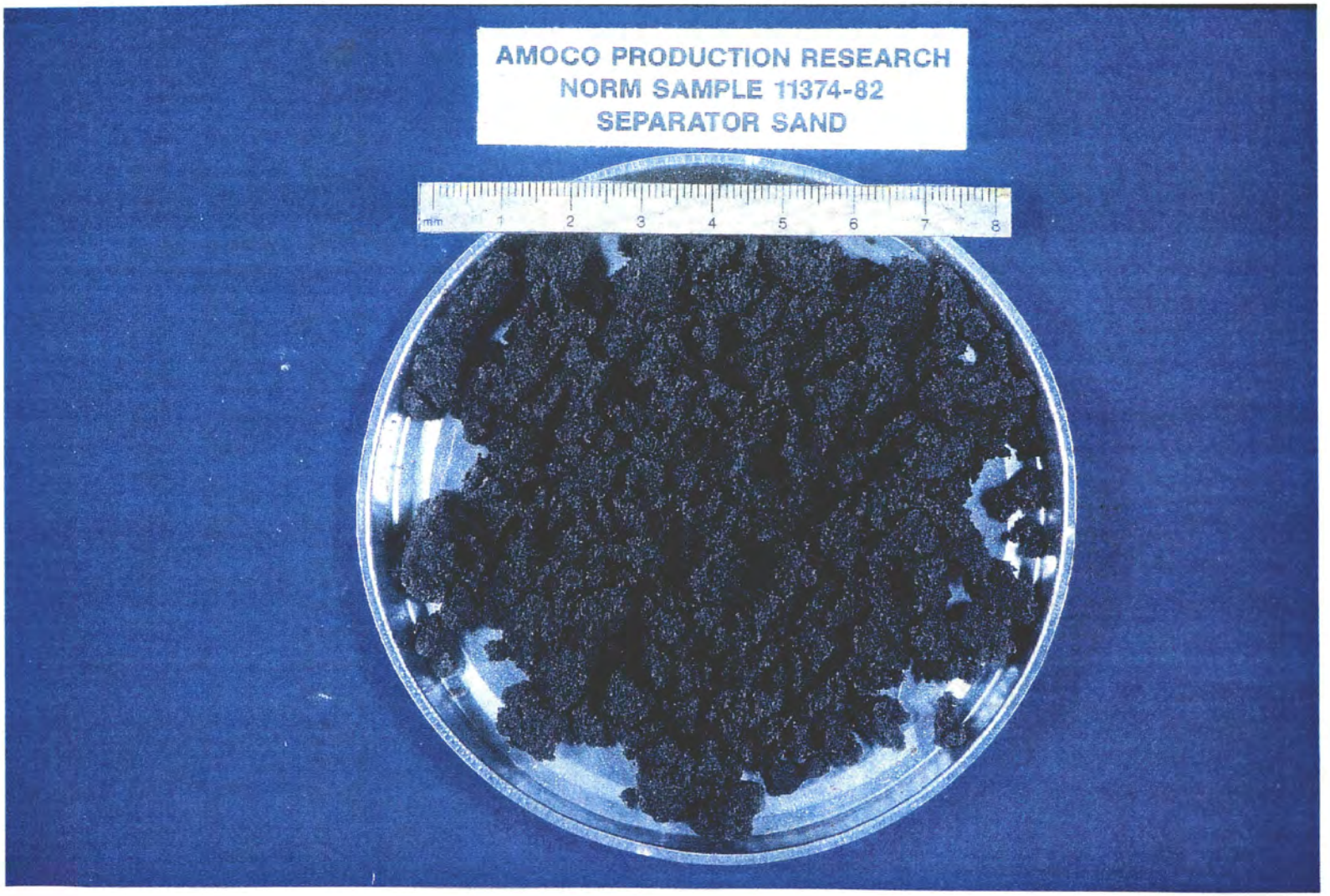
AMOCO PRODUCTION RESEARCH
NORM SAMPLE 11374-82
SEPARATOR SAND
mm 1 2 3 4 5 6 7 8

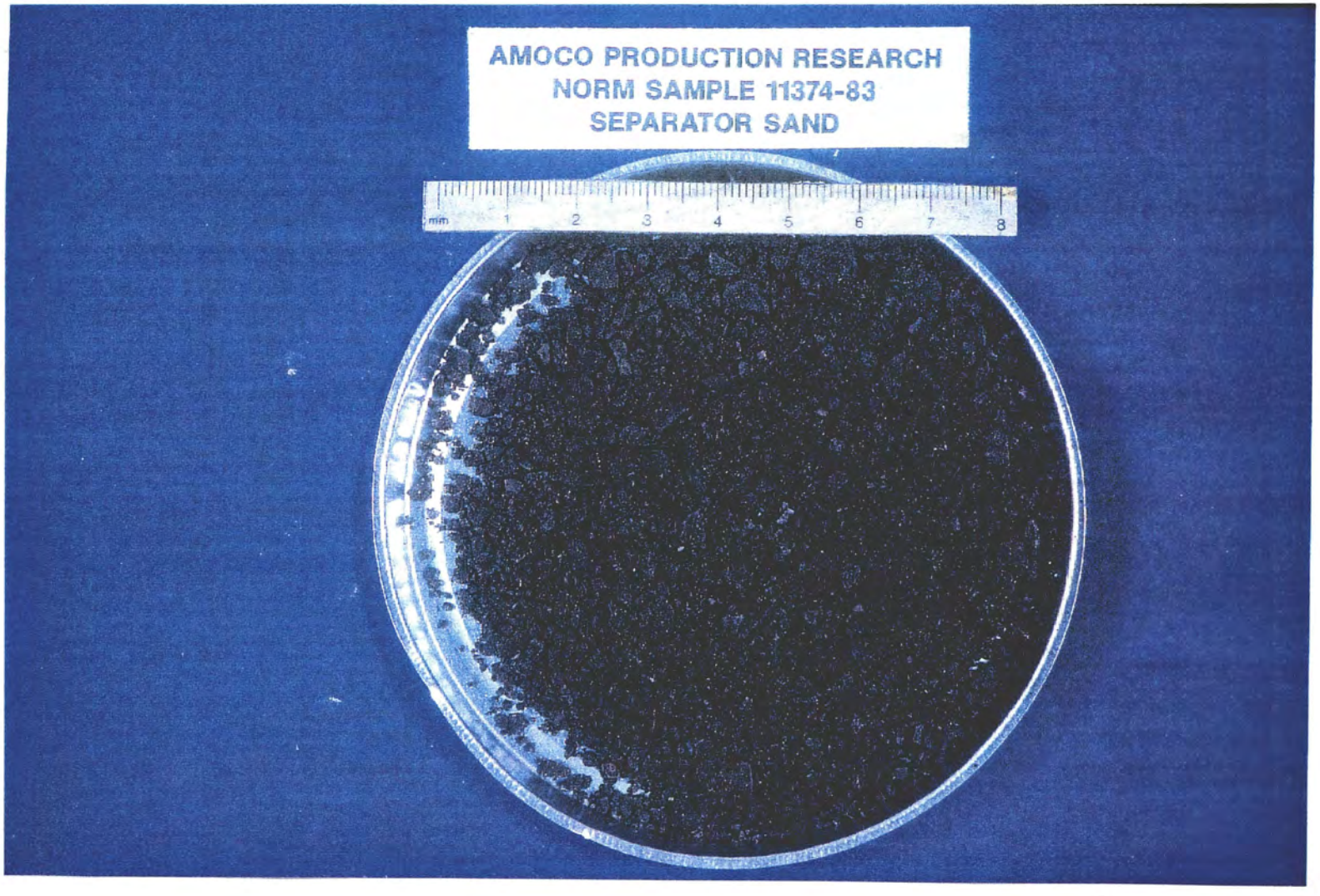
AMOCO PRODUCTION RESEARCH
NORM SAMPLE 11374-83
SEPARATOR SAND

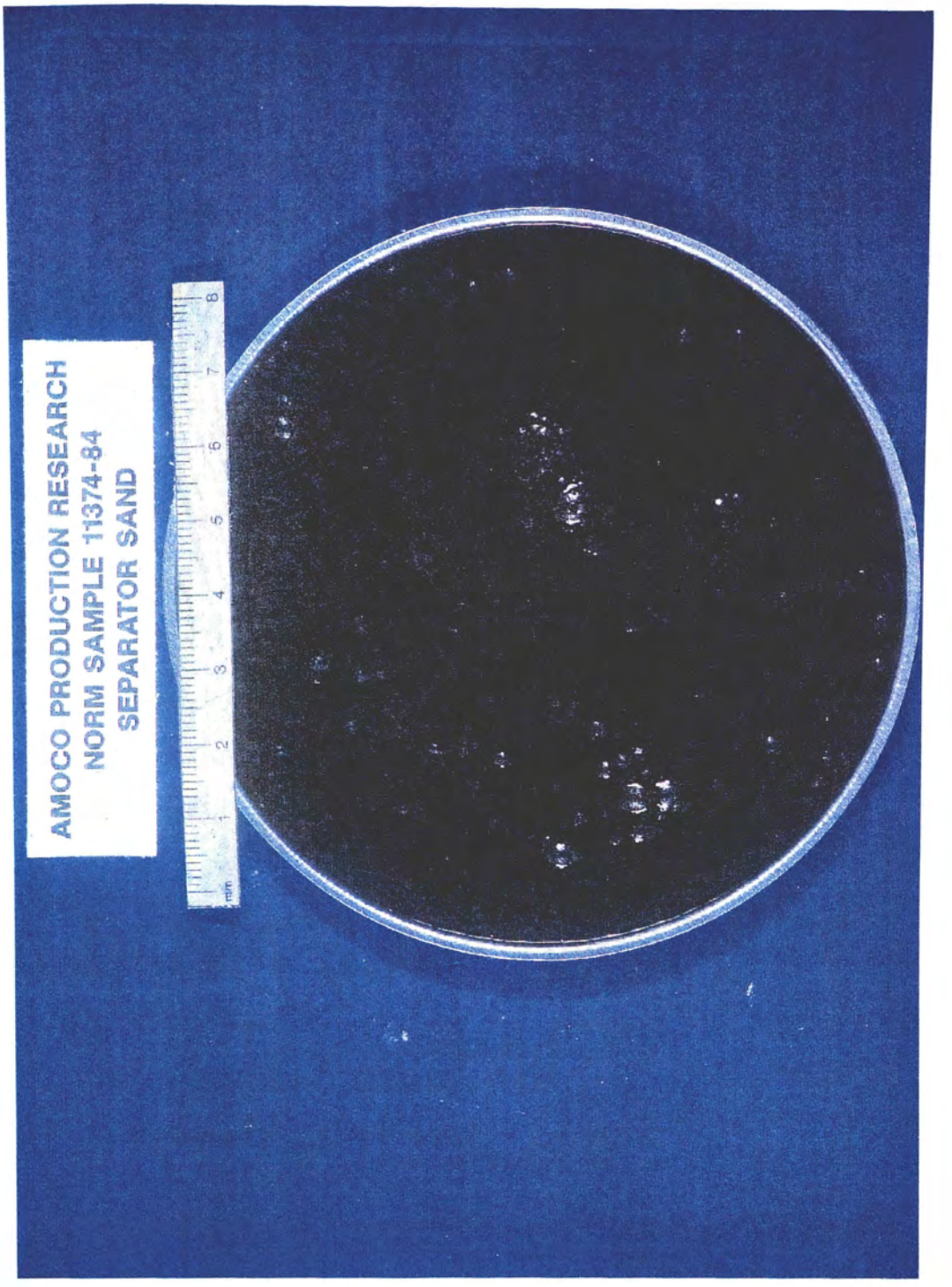
AMOCO PRODUCTION RESEARCH
NORM SAMPLE 11374-84
SEPARATOR SAND


AMOCO PRODUCTION RESEARCH
Sample 11385-25
Composit Vessel Solids

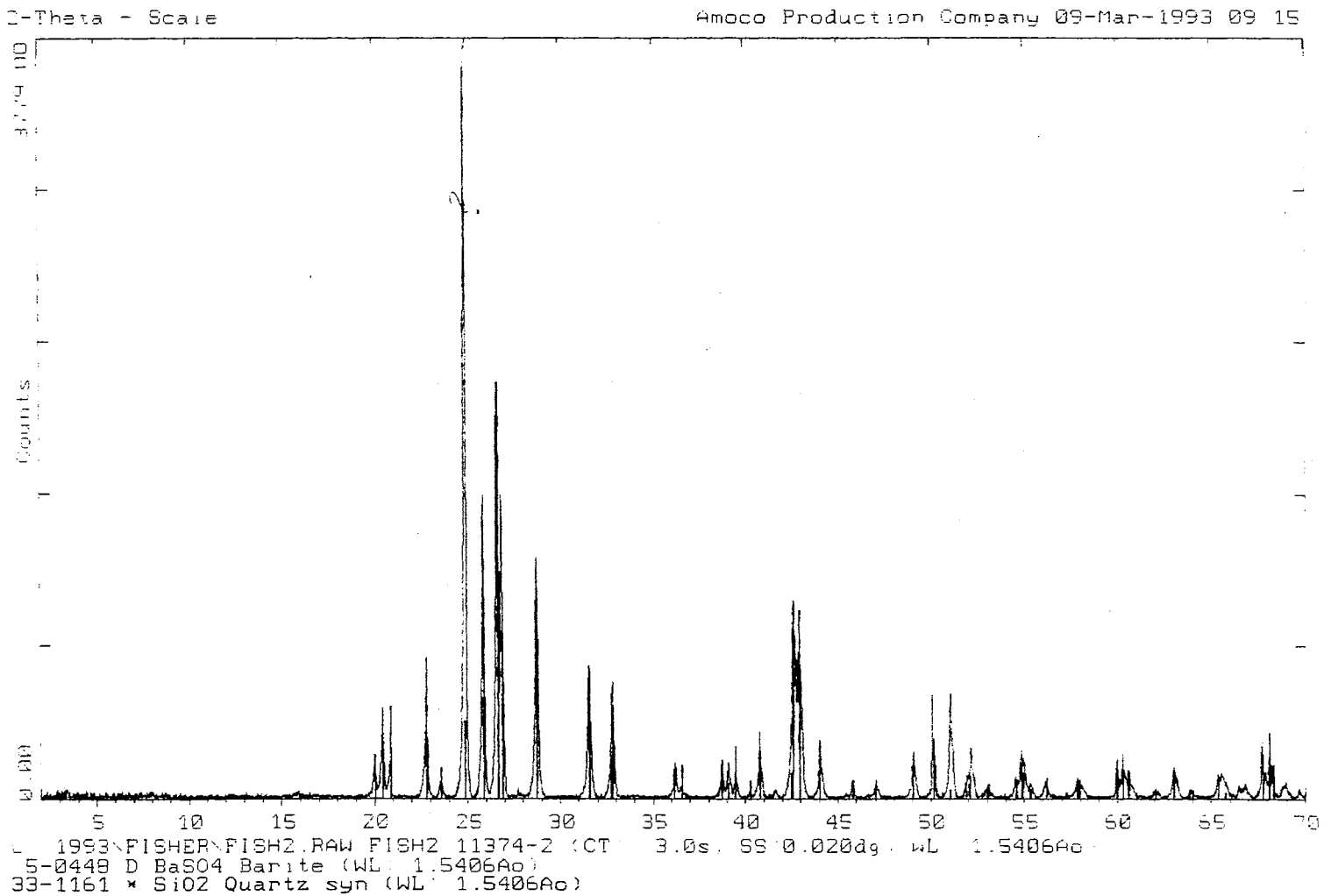
2-Theta - Scale
Amoco Production Company 09-Mar-1993 09 15
Counts
0.00
5
10
15
20
25
30
35
40
45
50
55
60
65
70
1993\FISHER\FISH2.RAW FISH2 11374-2 (CT 3.0s, SS 0.020dg, WL 1.5406Ao
5-0448 D BaSO4 Barite (WL: 1.5406Ao)
33-1161 * SiO2 Quartz syn (WL: 1.5406Ao)

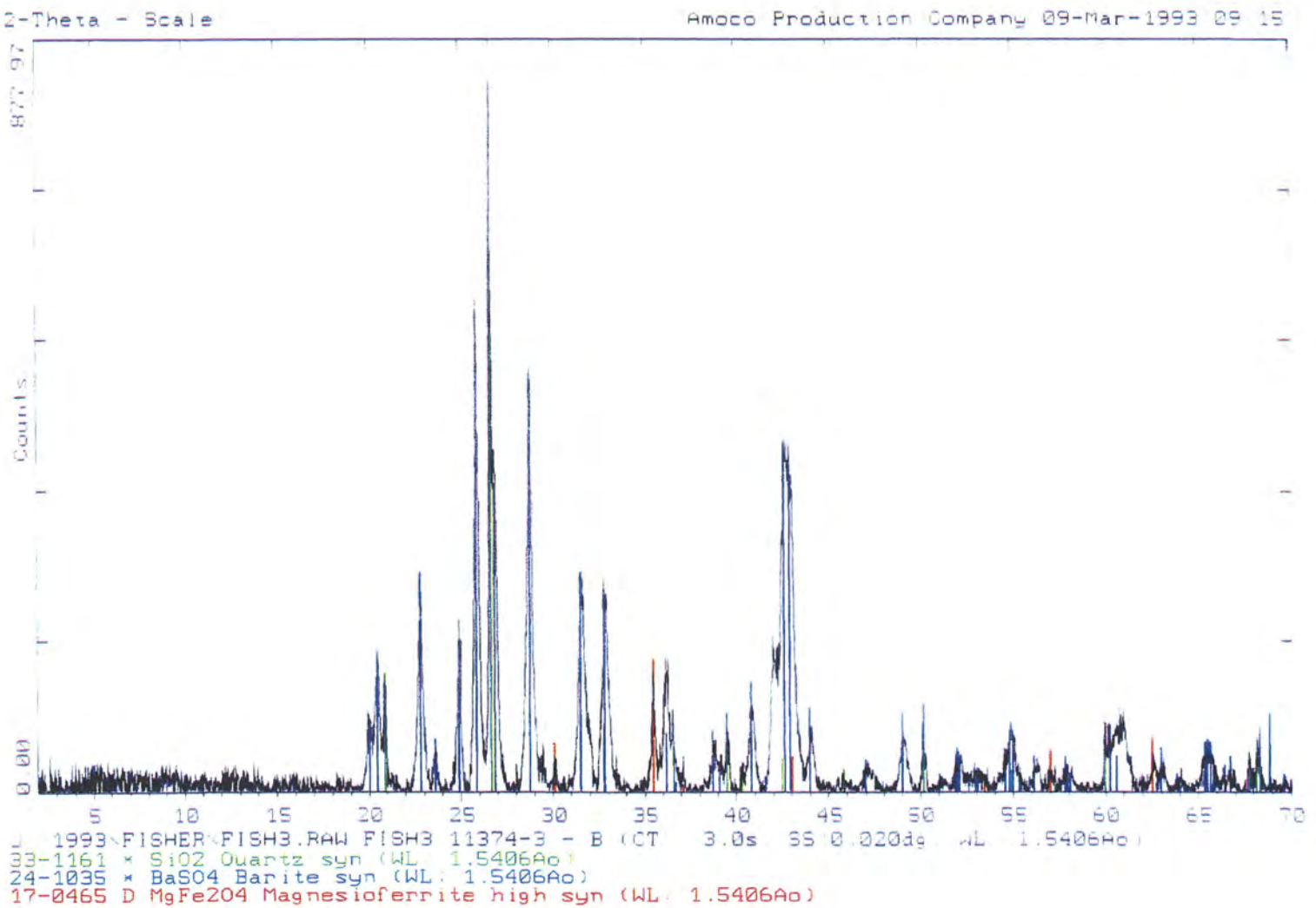
2-Theta - Scale
Amoco Production Company 09-Mar-1993 09:15
877.97
Counts
0.00
5
10
15
20
25
30
35
40
45
50
55
60
65
70
1993\FISHER\FISH3.RAW FISH3 11374-3 - B (CT 3.0s SS 0.020deg WL 1.5406Ao)
33-1161 * SiO2 Quartz syn (WL: 1.5406Ao)
24-1035 * BaSO4 Barite syn (WL: 1.5406Ao)
17-0465 D MgFe2O4 Magnesioferrite high syn (WL: 1.5406Ao)

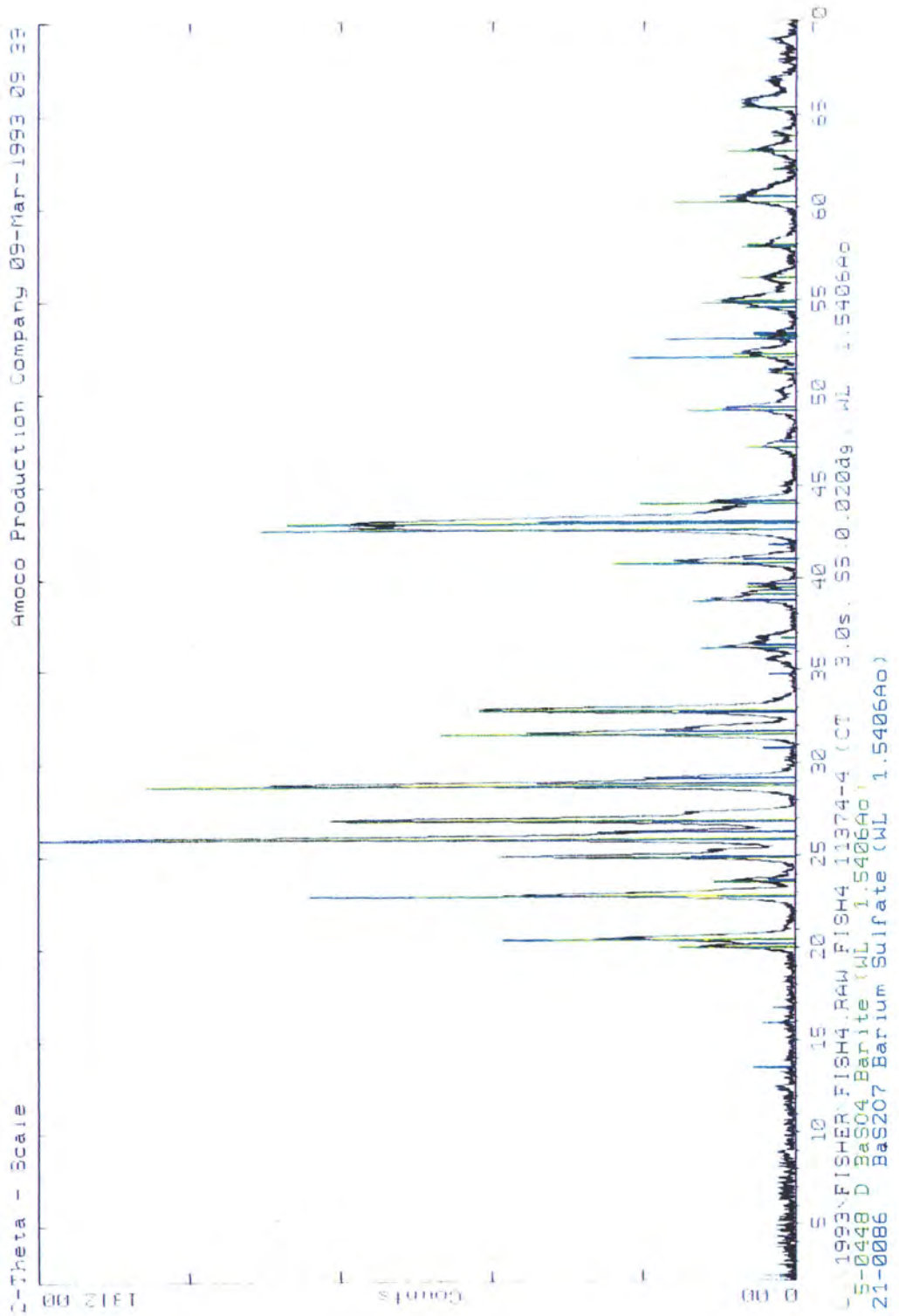
Amoco Production Company 09-Mar-1993 09:33
2-Theta - Scale
Counts
1312.00
0.00
5
10
15
20
25
30
35
40
45
50
55
60
65
70
1993 FISHER FISH4.RAW FISH4 11374-4 (CT 3.0s, SS 0.020d, WL 1.5406Ao)
5-0448 D BaSO4 Barite (WL 1.5406Ao)
21-0086 BaS2O7 Barium Sulfate (WL 1.5406Ao)

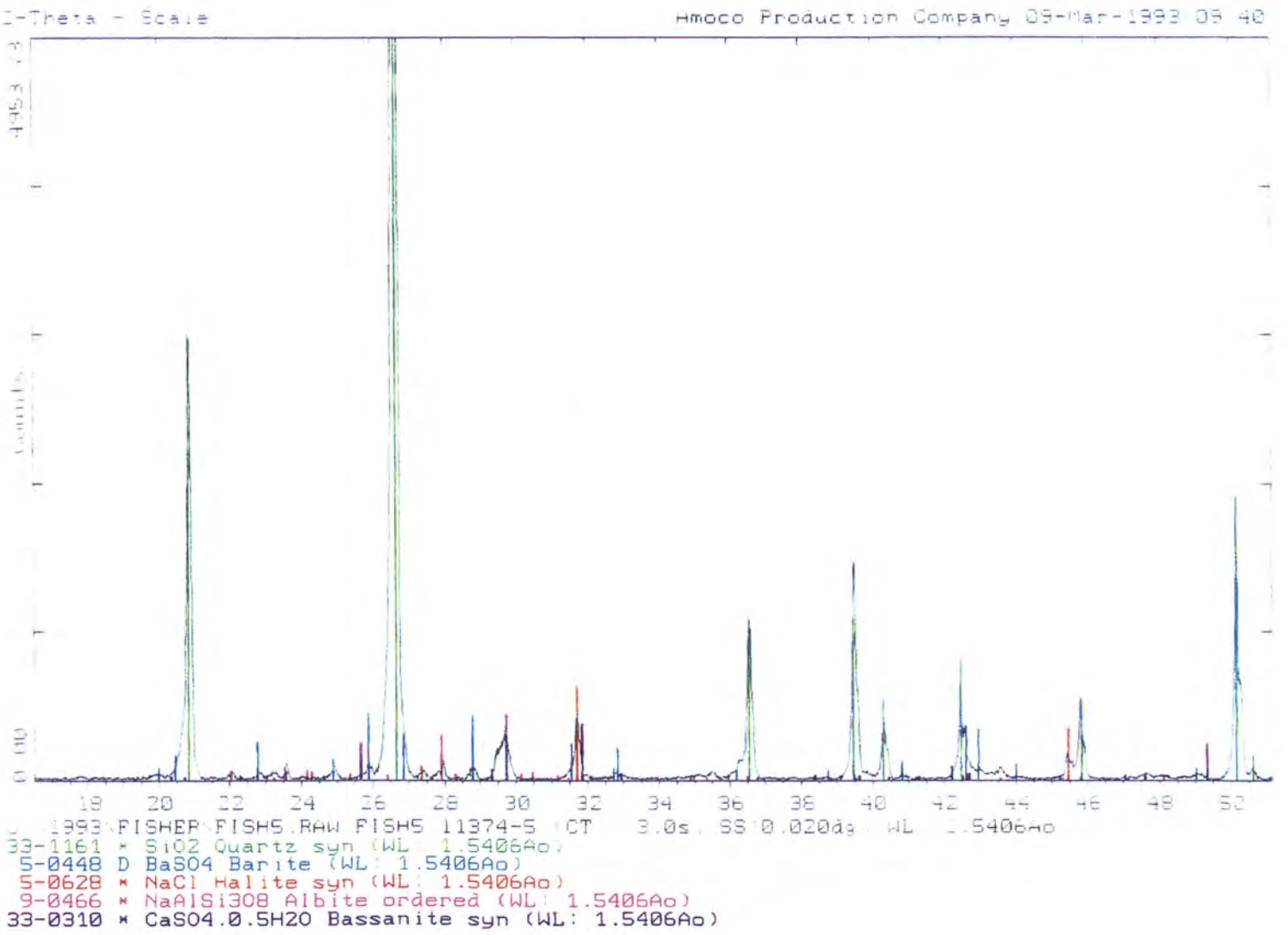
2-Theta - Scale
Amoco Production Company 05-Mar-1993 09:40
18 20 22 24 26 28 30 32 34 36 38 40 42 44 46 48 50
C:\1993\FISHER\FISH5.RAW FISH5 11374-5 CT 3.0s SS 0.020deg WL 1.5406Ao
33-1161 * SiO2 Quartz syn (WL: 1.5406Ao)
5-0448 D BaSO4 Barite (WL: 1.5406Ao)
5-0628 * NaCl Halite syn (WL: 1.5406Ao)
9-0466 * NaAlSi3O8 Albite ordered (WL: 1.5406Ao)
33-0310 * CaSO4.0.5H2O Bassanite syn (WL: 1.5406Ao)

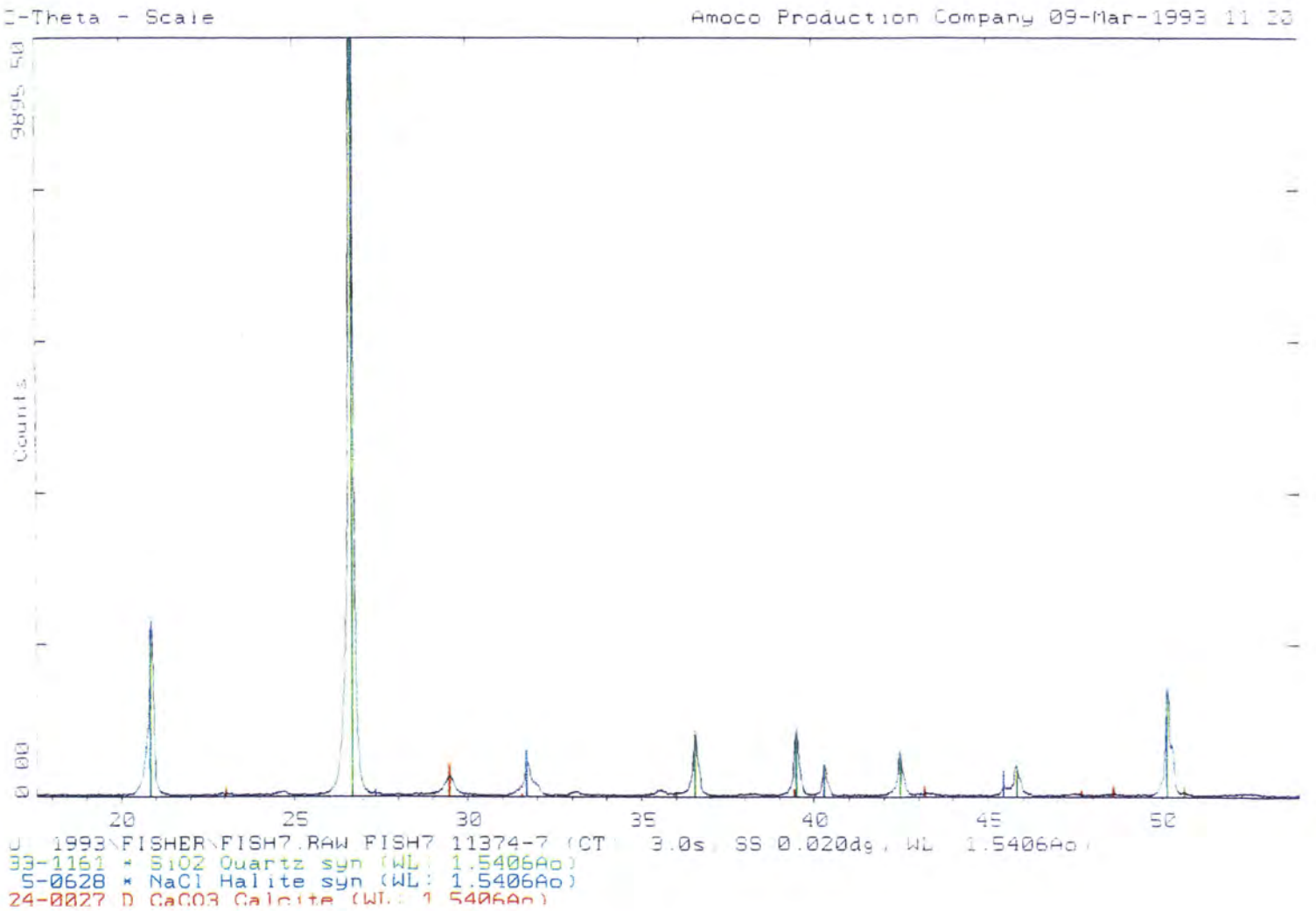
I-Theta - Scale
Amoco Production Company 09-Mar-1993 11 20
9895.50
Counts
0.00
20
25
30
35
40
45
50
1993\FISHER\FISH7.RAW FISH7 11374-7 (CT 3.0s, SS 0.020dg, WL 1.5406Ao)
33-1161 * SiO2 Quartz syn (WL: 1.5406Ao)
5-0628 * NaCl Halite syn (WL: 1.5406Ao)
24-0027 D CaCO3 Calcite (WL: 1.5406Ao)

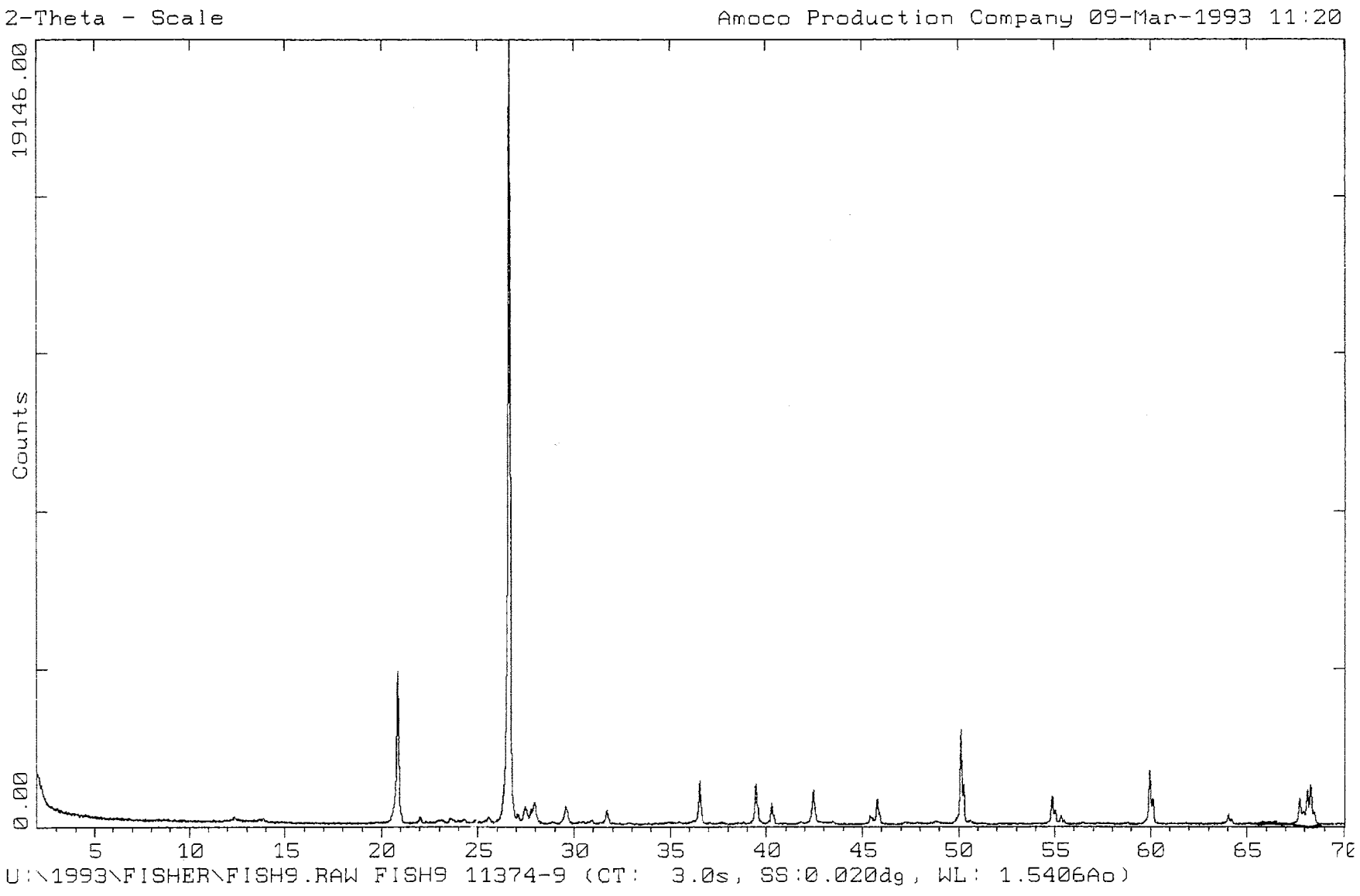
2-Theta - Scale
Amoco Production Company 09-Mar-1993 11:20
19146.00
Counts
0.00
5
10
15
20
25
30
35
40
45
50
55
60
65
U:\1993\FISHER\FISH9.RAW FISH9 11374-9 (CT: 3.0s, SS:0.020dg, WL: 1.5406Ao)

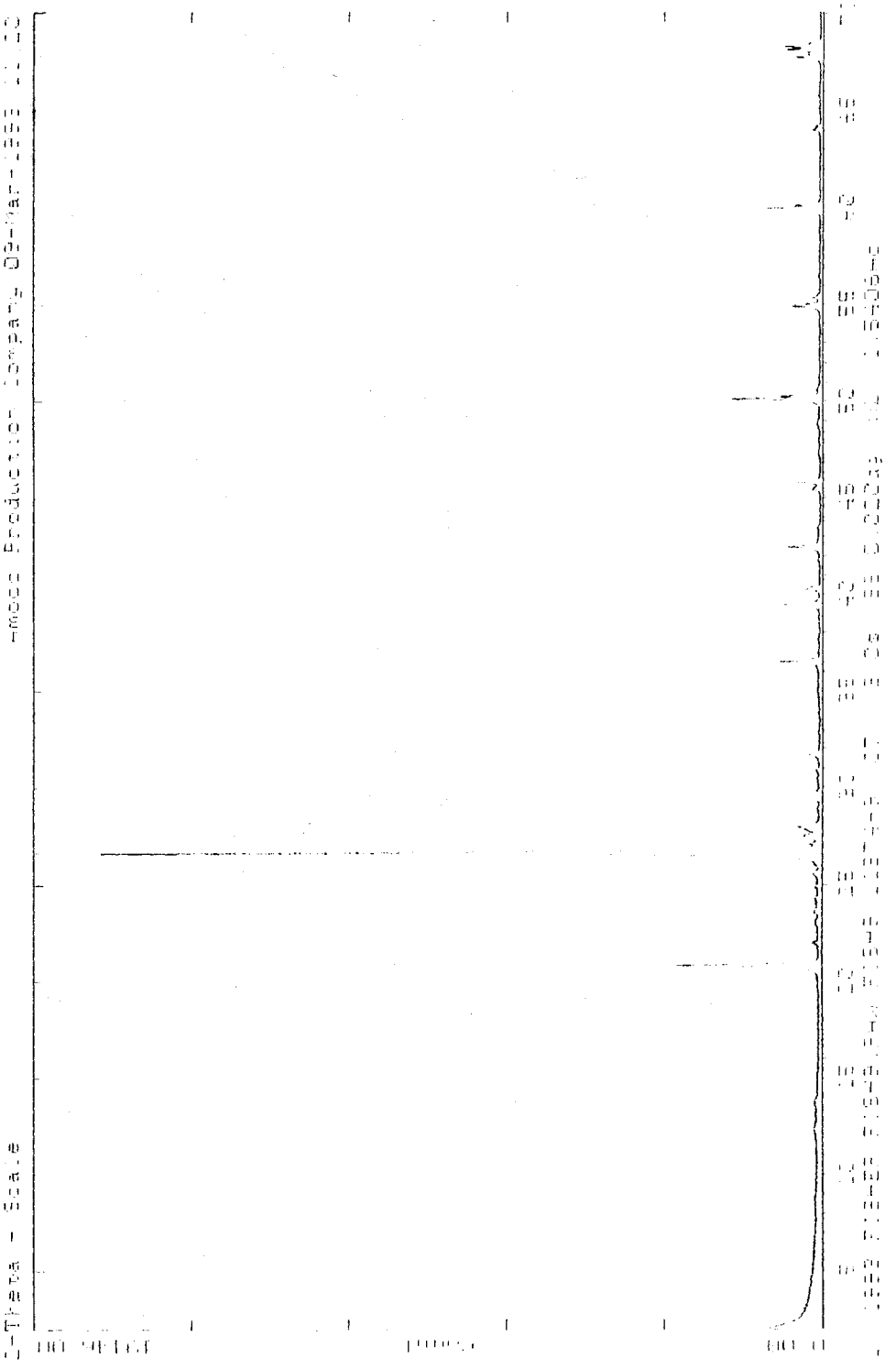

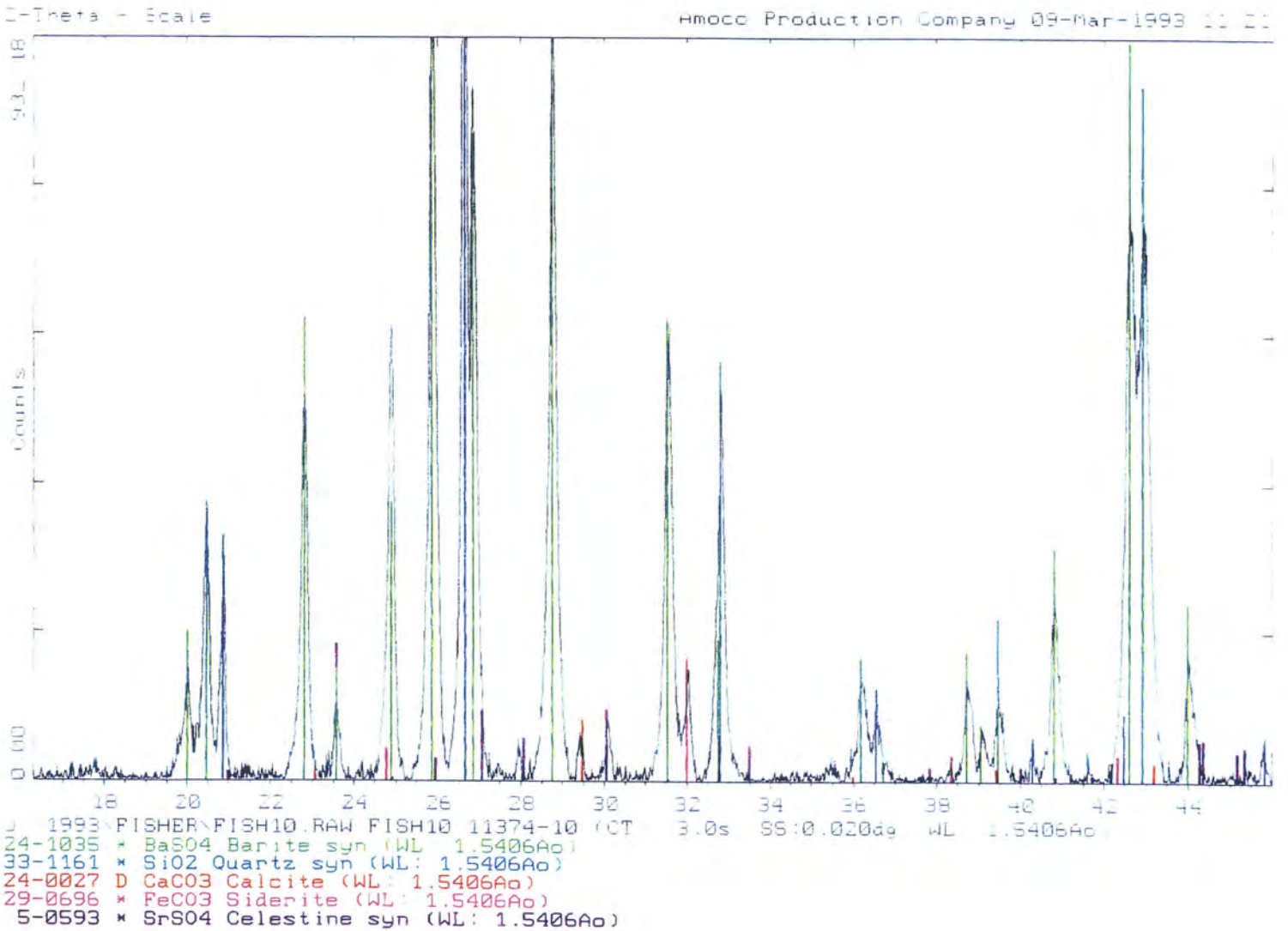
2-Theta - Scale
Amoco Production Company 09-Mar-1993
Counts
18
20
22
24
26
28
30
32
34
36
38
40
42
44
1993\FISHER\FISH10.RAW FISH10 11374-10 (CT 3.0s SS:0.020dg WL 1.5406Ao
24-1035 * BaSO4 Barite syn (WL 1.5406Ao)
33-1161 * SiO2 Quartz syn (WL: 1.5406Ao)
24-0027 D CaCO3 Calcite (WL: 1.5406Ao)
29-0696 * FeCO3 Siderite (WL: 1.5406Ao)
5-0593 * SrSO4 Celestine syn (WL: 1.5406Ao)

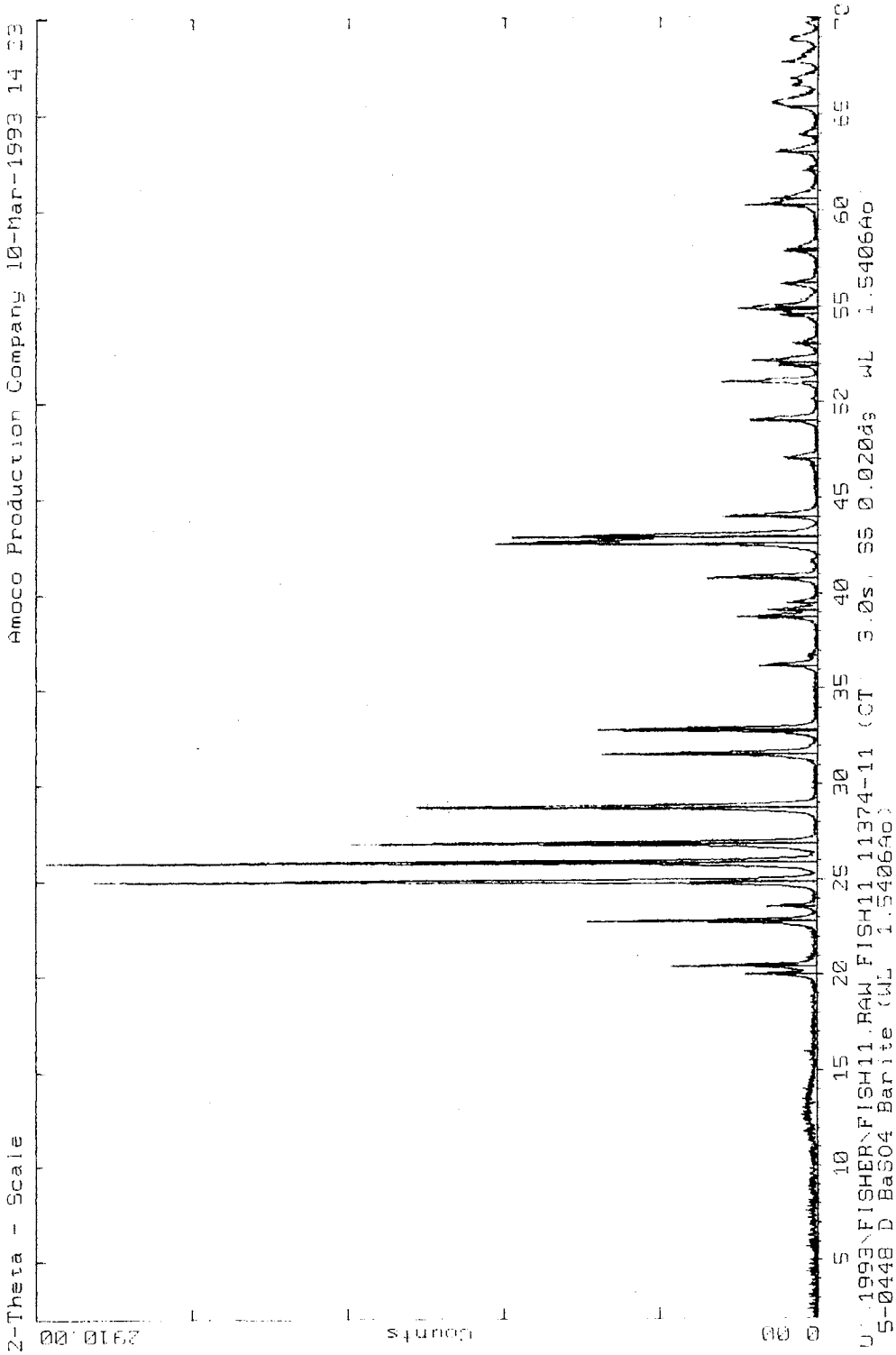
Amoco Production Company 10-Mar-1993 14:23
2-Theta - Scale
Counts
2910.00
00.0
0
5
10
15
20
25
30
35
40
45
50
55
60
65
70
D:\1993\FISHER\FISH11.RAW FISH11 11374-11 (CT 3.0s, SS 0.020° WL 1.540600
5-0448 D BaSO4 Barite (WL 1.540600)

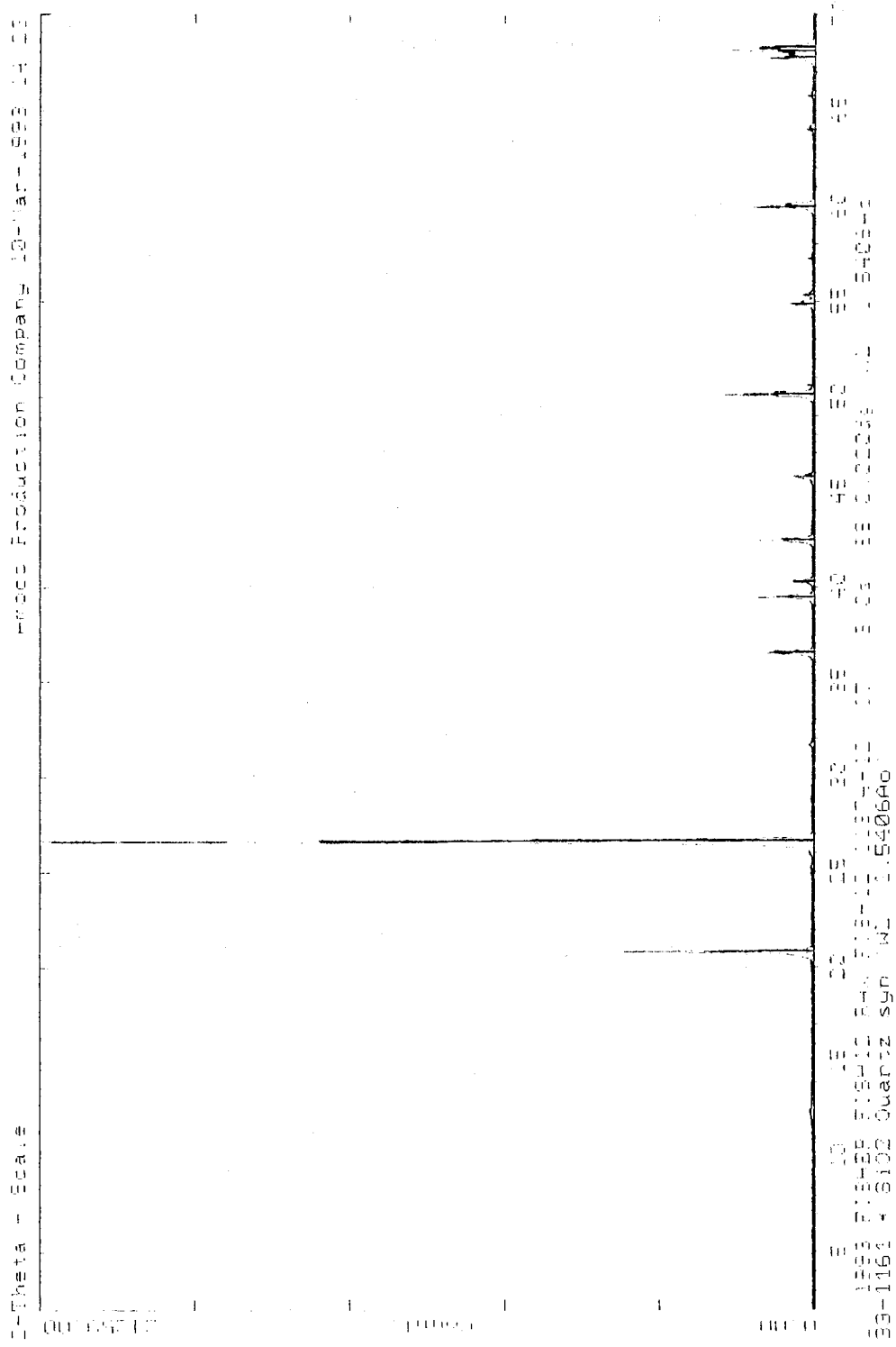
Phase Production Company 10-Mar-1998 17:22
C-Theta - Scale
33-1161 * SiO2 Quartz syn WL: 1.540640

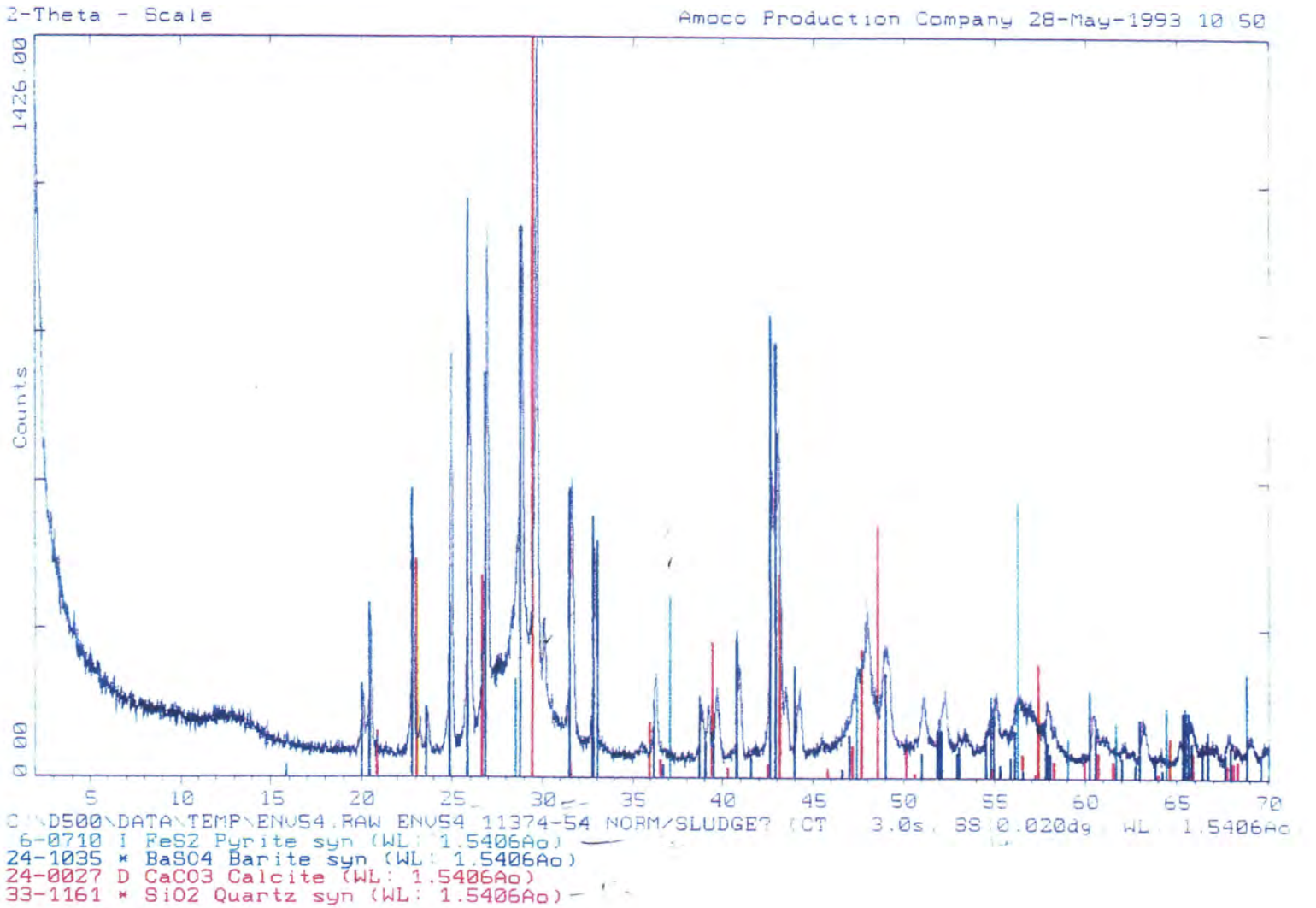
2-Theta - Scale
Amoco Production Company 28-May-1993 10 50
1426.00
Counts
0.00
5
10
15
20
25
30
35
40
45
50
55
60
65
70
C:\D500\DATA\TEMP\ENV54.RAW ENV54 11374-54 NORM/SLUDGE? (CT 3.0s, SS 0.020dg, WL: 1.5406Ao
6-0710 I FeS2 Pyrite syn (WL: 1.5406Ao)
24-1035 * BaSO4 Barite syn (WL: 1.5406Ao)
24-0027 D CaCO3 Calcite (WL: 1.5406Ao)
33-1161 * SiO2 Quartz syn (WL: 1.5406Ao)

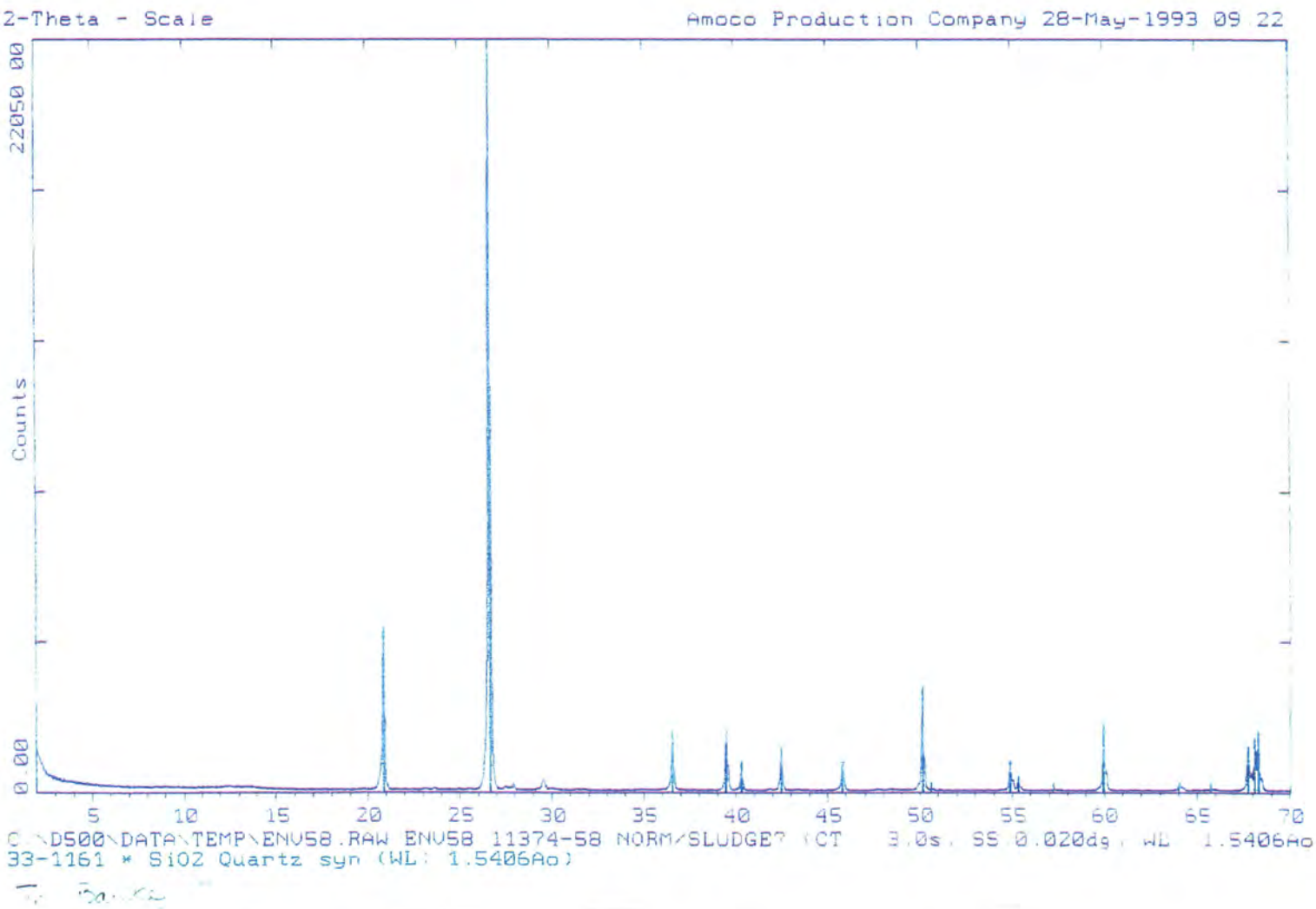
2-Theta - Scale
Amoco Production Company 28-May-1993 09 22
22050.00
Counts
0.00
5
10
15
20
25
30
35
40
45
50
55
60
65
70
C:\D500\DATA\TEMP\ENV58.RAW ENV58 11374-58 NORM/SLUDGE? (CT 3.0s, SS 0.020dg, WL 1.5406Ao)
33-1161 * SiO2 Quartz syn (WL: 1.5406Ao)

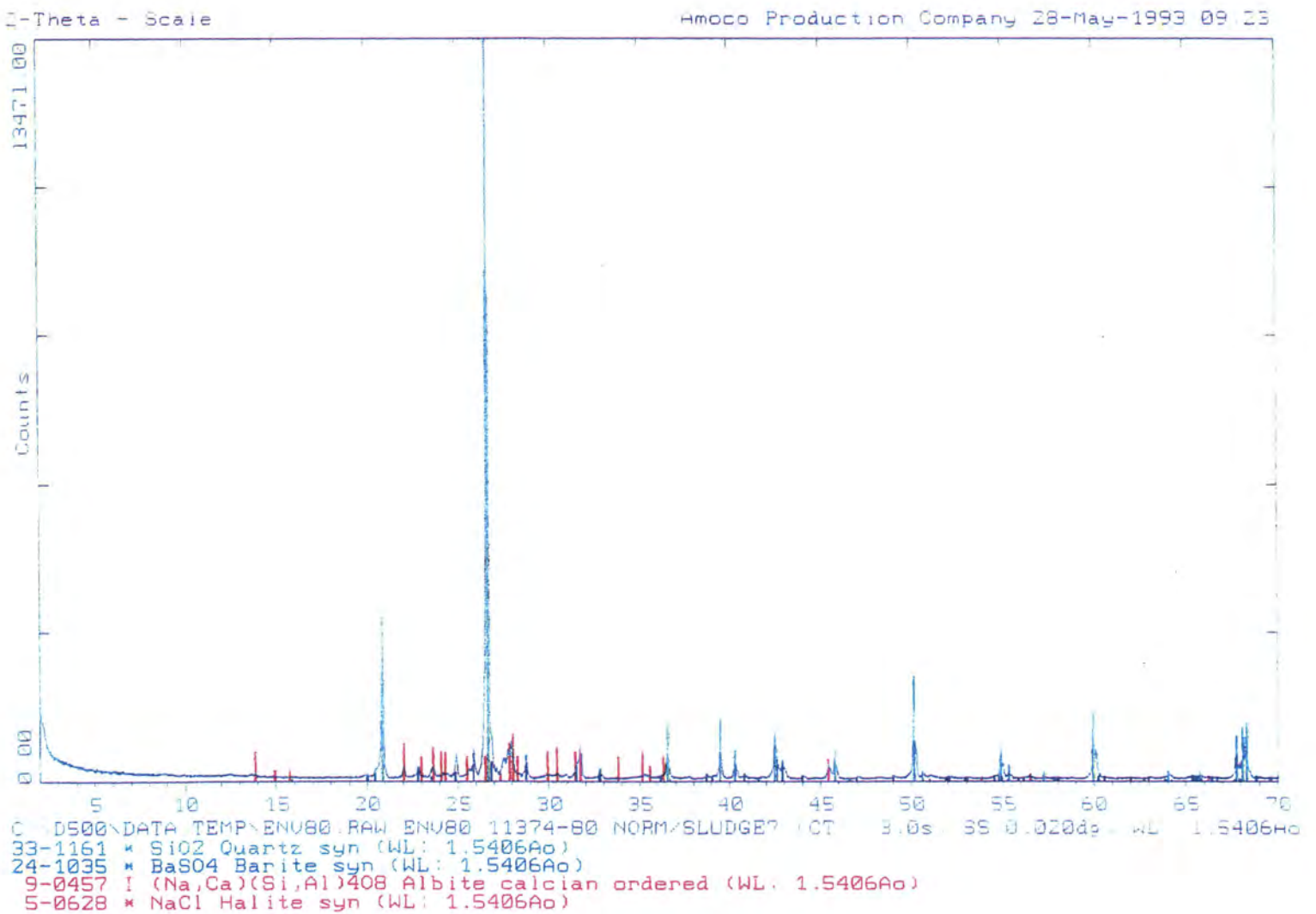
2-Theta - Scale
Amoco Production Company 28-May-1993 09:23
13471.00
Counts
0.00
5
10
15
20
25
30
35
40
45
50
55
60
65
70
C:\D500\DATA\TEMP\ENV80.RAW ENV80 11374-80 NORM/SLUDGE? /CT 3.0s 3S 0.020d WL: 1.5406Ao
33-1161 * SiO2 Quartz syn (WL: 1.5406Ao)
24-1035 * BaSO4 Barite syn (WL: 1.5406Ao)
9-0457 I (Na,Ca)(Si,Al)4O8 Albite calcian ordered (WL: 1.5406Ao)
5-0628 * NaCl Halite syn (WL: 1.5406Ao)

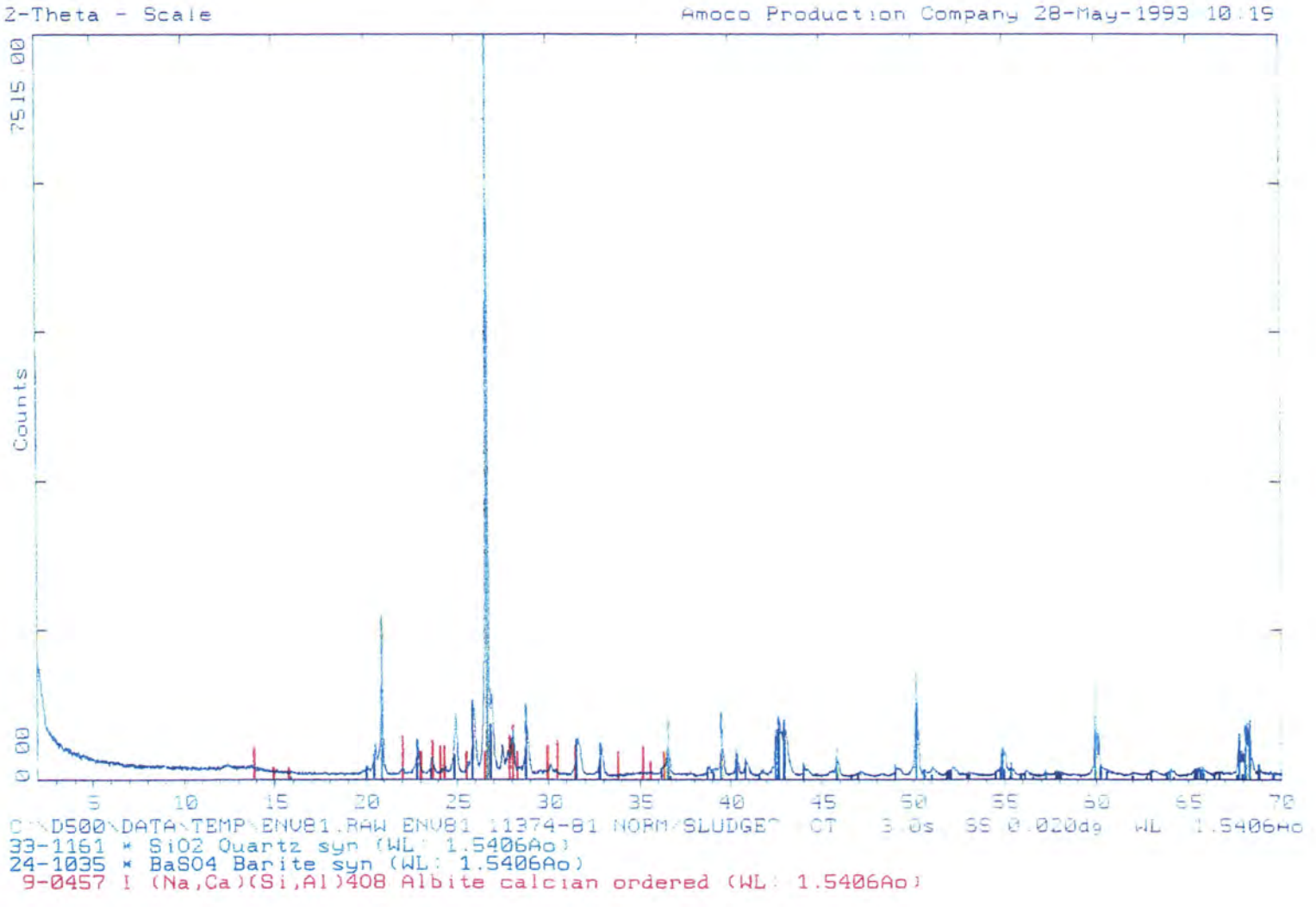
2-Theta - Scale
Amoco Production Company 28-May-1993 10:19
7515.00
Counts
0.00
5
10
15
20
25
30
35
40
45
50
55
60
65
70
C:\D500\DATA\TEMP\ENV81.RAW ENV81 11374-81 NORM/SLUDGE CT 3.0s SS 0.020deg WL 1.5406Ao
33-1161 * SiO2 Quartz syn (WL: 1.5406Ao)
24-1035 * BaSO4 Barite syn (WL: 1.5406Ao)
9-0457 I (Na,Ca)(Si,Al)4O8 Albite calcian ordered (WL: 1.5406Ao)

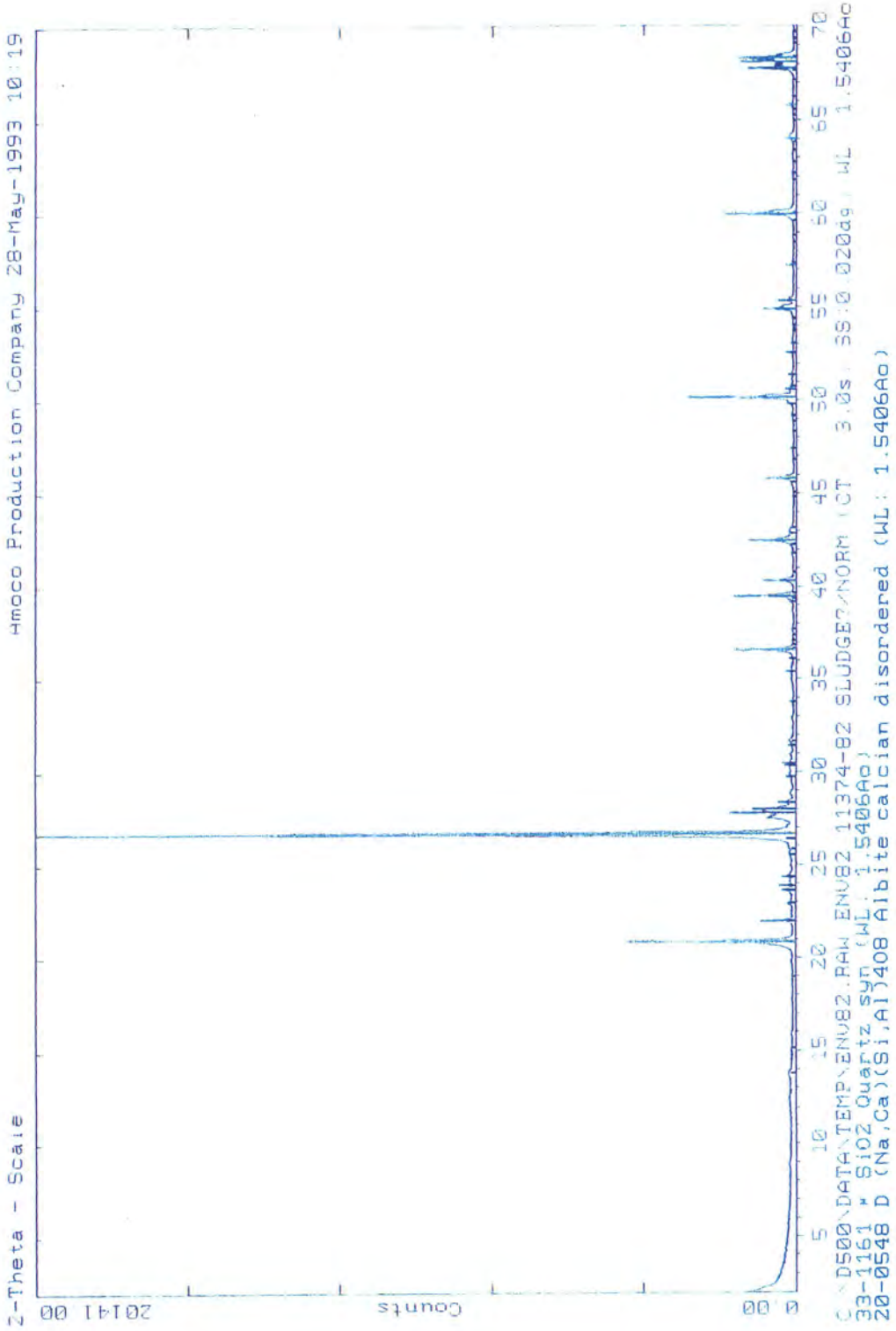
Amoco Production Company 28-May-1993 10:19
2-Theta - Scale
Counts
20141.00
0.00
C:\D500\DATA\TEMP\ENV82.RAW ENV82 11374-82 SLUDGE?/NORM (CT 3.0s, 38:0.020dg, WL 1.54064o
33-1161 * SiO2 Quartz syn (WL: 1.5406Ao)
20-0548 D (Na,Ca)(Si,Al)4O8 Albite calcian disordered (WL: 1.5406Ao)

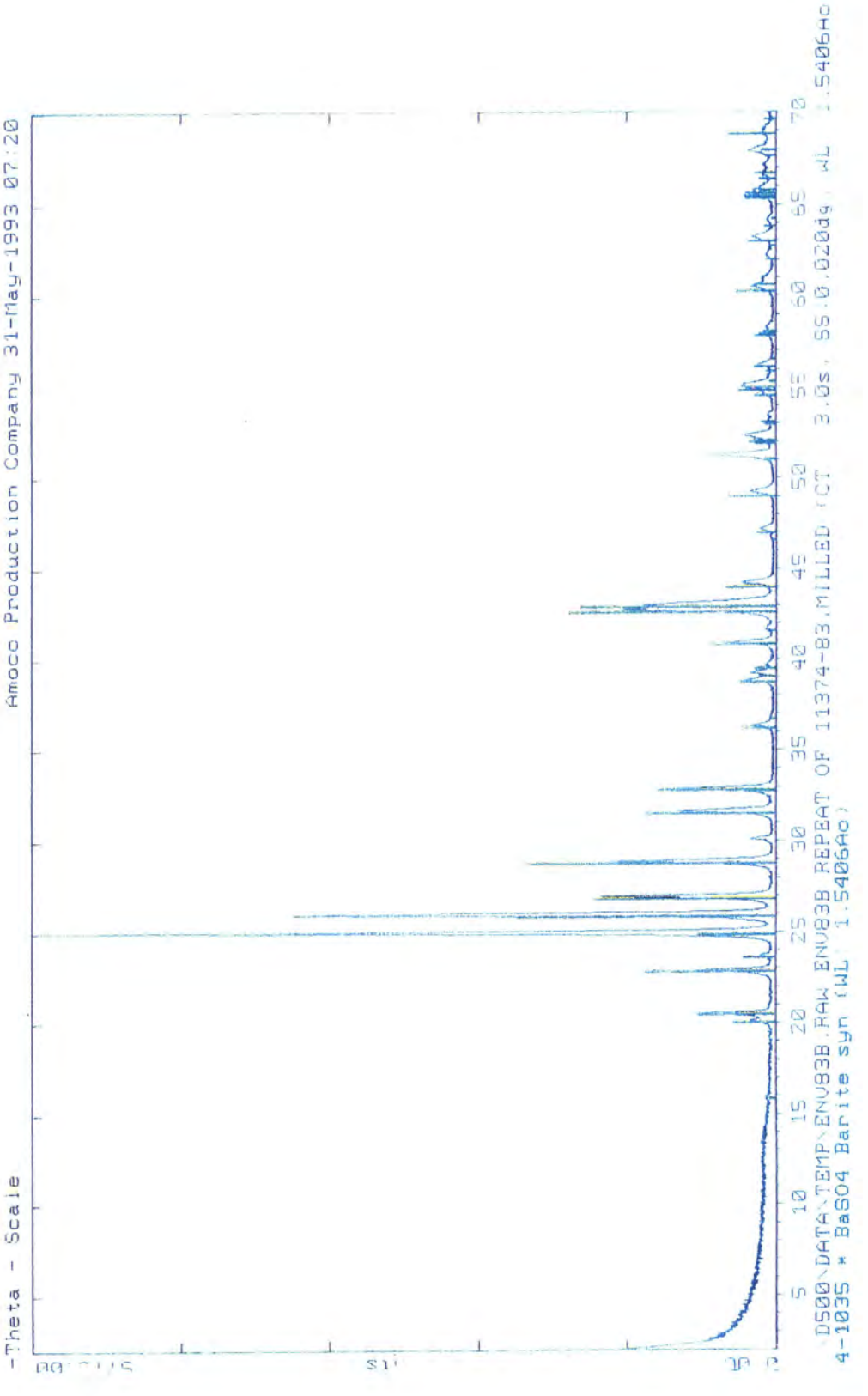
Amoco Production Company 31-May-1993 07:20
-Theta - Scale
5 10 15 20 25 30 35 40 45 50 55 60 65 70
D500\DATA\TEMP\ENV83B.RAW ENV83B REPEAT OF 11374-83,MILLED (CT 3.0s, 55.0,0.020d9, WL 1.5406Ho
4-1035 * BaSO4 Barite syn (WL 1.540640)

Particle Size Analysis

Sample # 11374-2

Total Weight 1.89 grams

grain sizes > 180 um 1.1 grams

size, um	weight (g)
> 850	0.042
> 600	0.061
> 425	0.098
> 300	0.171
> 250	0.232
> 180	0.487
sum	1.091

grain sizes < 180 um 0.79 grams

size, um	% under	%	weight (g)	size, um	% under	%	weight (g)
< 188	100	0	0.0000	< 17.7	56.7	5.5	0.0435
< 162	100	0	0.0000	< 15.3	51.2	3.4	0.0269
< 140	100	0	0.0000	< 13.2	47.8	3.2	0.0253
< 120	100	0	0.0000	< 11.4	44.6	3.9	0.0308
< 104	100	0	0.0000	< 9.8	40.7	4.5	0.0356
< 89.9	100	0.5	0.0040	< 8.5	36.2	4.1	0.0324
< 77.5	99.5	1.6	0.0126	< 7.3	32.1	3.9	0.0308
< 66.9	97.9	2.7	0.0213	< 6.3	28.2	4.5	0.0356
< 57.7	95.2	3.7	0.0292	< 5.4	23.7	4	0.0316
< 49.8	91.5	4.5	0.0356	< 4.7	19.7	2.7	0.0213
< 42.9	87	4.6	0.0363	< 4.1	17	1.8	0.0142
< 37.1	82.4	4.6	0.0363	< 3.5	15.2	1.7	0.0134
< 32	77.8	4.1	0.0324	< 3.0	13.5	2.4	0.0190
< 27.6	73.7	3.9	0.0308	< 2.6	11.1	2.5	0.0198
< 23.8	69.8	5.8	0.0458	< 2.2	8.6	2.2	0.0174
< 20.5	64	7.3	0.0577	< 1.9	6.4	6.4	0.0506
						Total	0.79

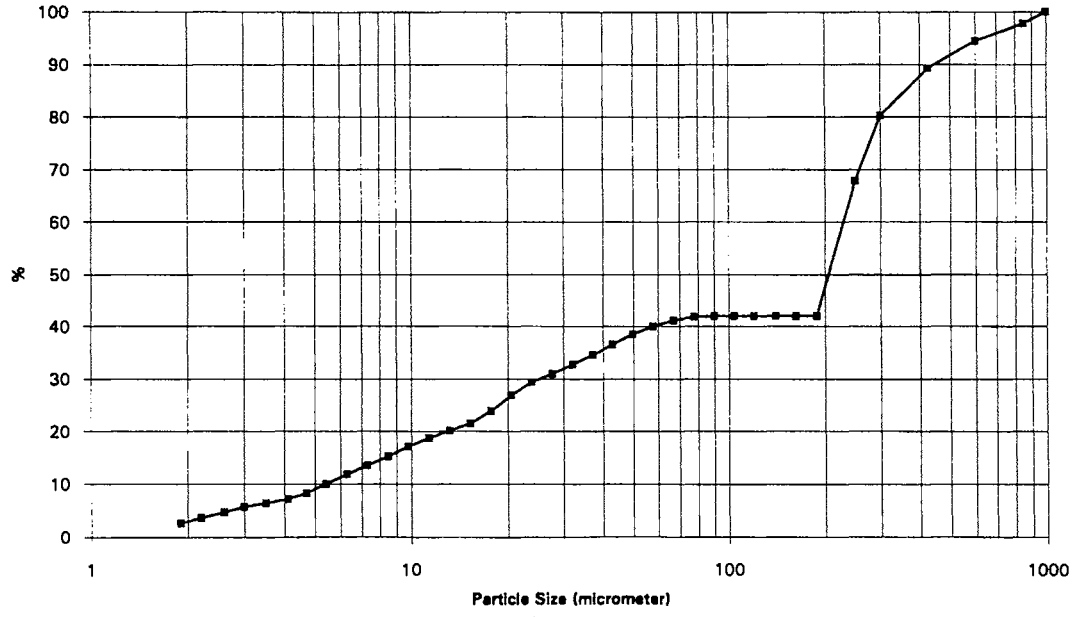

Particle Size Analysis

Sample # 11374-3

Total Weight 5.92 grams

grain sizes > 180 um 1.85 grams

size, um	weight (g)
> 850	0.936
> 600	0.137
> 425	0.149
> 300	0.166
> 250	0.139
> 180	0.191
sum	1.718

grain sizes < 180 um 4.07 grams

size, um	% under	%	weight (g)	size, um	% under	%	weight (g)
< 188	100	0	0.0000	< 17.7	62.1	6.9	0.2808
< 162	100	0	0.0000	< 15.3	55.2	5.3	0.2157
< 140	100	0	0.0000	< 13.2	49.9	4.8	0.1954
< 120	100	0	0.0000	< 11.4	45.1	5.1	0.2076
< 104	100	0	0.0000	< 9.8	40	5	0.2035
< 89.9	100	0.3	0.0122	< 8.5	35	4.6	0.1872
< 77.5	99.7	0.4	0.0163	< 7.3	30.4	4.2	0.1709
< 66.9	99.3	0.5	0.0204	< 6.3	26.2	4.4	0.1791
< 57.7	98.8	0.7	0.0285	< 5.4	21.8	3.9	0.1587
< 49.8	98.1	2.6	0.1058	< 4.7	17.9	3.1	0.1262
< 42.9	95.5	3.6	0.1465	< 4.1	14.8	2.4	0.0977
< 37.1	91.9	3.9	0.1587	< 3.5	12.4	2.1	0.0855
< 32	88	4.4	0.1791	< 3.0	10.3	2	0.0814
< 27.6	83.6	5.6	0.2279	< 2.6	8.3	2	0.0814
< 23.8	78	7.4	0.3012	< 2.2	6.3	1.8	0.0733
< 20.5	70.6	8.5	0.3459	< 1.9	4.5	4.5	0.1832
						Total	4.07

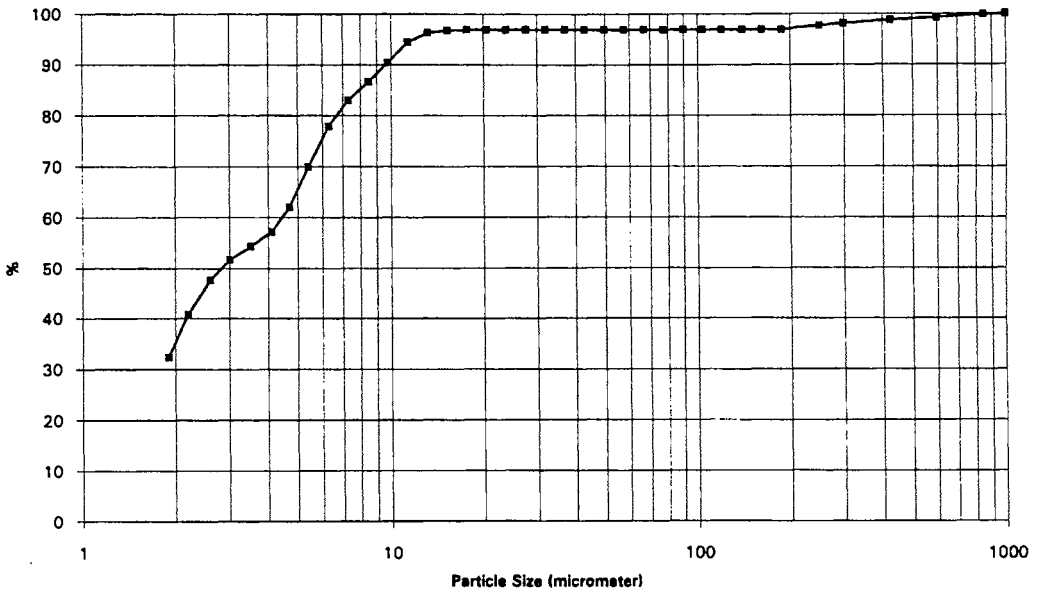

Particle Size Analysis

Sample # 11374-4

Total Weight 5.46 grams

grain sizes > 180 um 0.17 grams

size, um	weight (g)
> 850	0.007
> 600	0.034
> 425	0.026
> 300	0.04
> 250	0.019
> 180	0.042
sum > 180 um	0.168

grain sizes < 180 um 5.29 grams

size, um	% under	%	weight (g	size, um	% under	%	weight (g)
< 188	100	0	0.0000	< 17.7	100	0.2	0.0106
< 162	100	0	0.0000	< 15.3	99.8	0.5	0.0265
< 140	100	0	0.0000	< 13.2	99.3	1.9	0.1005
< 120	100	0	0.0000	< 11.4	97.4	4.1	0.2169
< 104	100	0	0.0000	< 9.8	93.3	3.9	0.2063
< 89.9	100	0	0.0000	< 8.5	89.4	3.8	0.2010
< 77.5	100	0	0.0000	< 7.3	85.6	5.2	0.2751
< 66.9	100	0	0.0000	< 6.3	80.4	8.3	0.4391
< 57.7	100	0	0.0000	< 5.4	72.1	8.1	0.4285
< 49.8	100	0	0.0000	< 4.7	64	5	0.2645
< 42.9	100	0	0.0000	< 4.1	59	2.9	0.1534
< 37.1	100	0	0.0000	< 3.5	56.1	2.8	0.1481
< 32	100	0	0.0000	< 3.0	53.3	4.2	0.2222
< 27.6	100	0	0.0000	< 2.6	49.1	7	0.3703
< 23.8	100	0	0.0000	< 2.2	42.1	8.7	0.4602
< 20.5	100	0	0.0000	< 1.9	33.4	33.4	1.7669
						Total	5.29

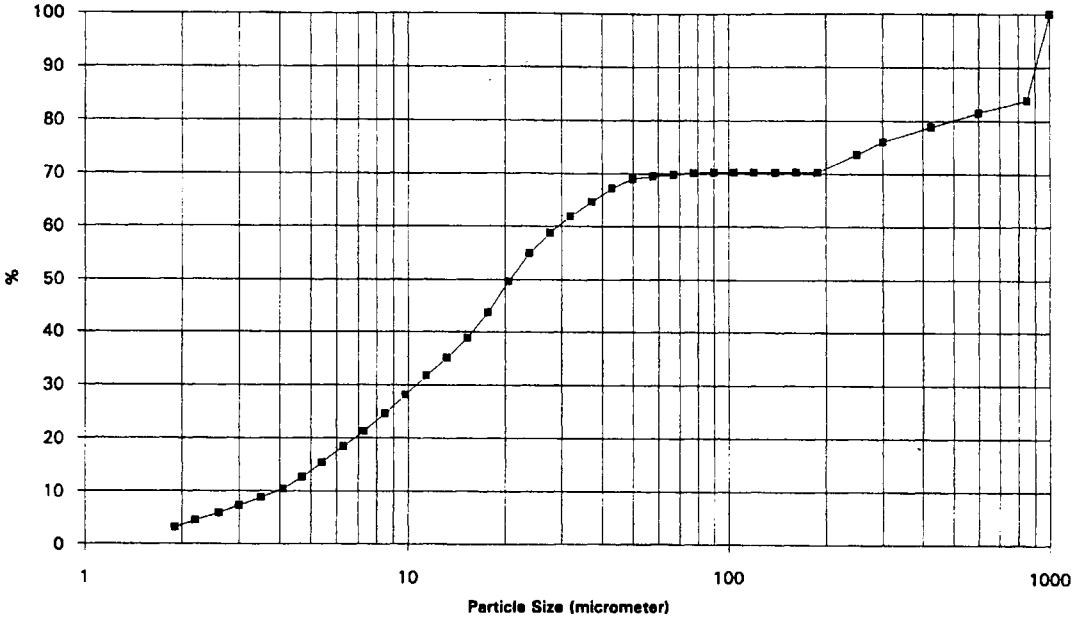

Particle Size Analysis

Sample # 11374-5

Total Weight 3.98 grams

grain sizes > 180 um 0.77 grams

size, um	weight (g)
> 850	0.028
> 600	0.034
> 425	0.035
> 300	0.086
> 250	0.093
> 180	0.473
sum	0.749

grain sizes < 180 um 3.21 grams

size, um	% under	%	weight (g)	size, um	% under	%	weight (g)
< 188	100	0	0.0000	< 17.7	39.8	5.4	0.1733
< 162	100	0	0.0000	< 15.3	34.4	3.9	0.1252
< 140	100	0	0.0000	< 13.2	30.5	3.3	0.1059
< 120	100	0.6	0.0193	< 11.4	27.2	3.5	0.1124
< 104	99.4	2.3	0.0738	< 9.8	23.7	3.5	0.1124
< 89.9	97.1	4.1	0.1316	< 8.5	20.2	2.9	0.0931
< 77.5	93	5.3	0.1701	< 7.3	17.3	2.3	0.0738
< 66.9	87.7	5.4	0.1733	< 6.3	15	2.5	0.0803
< 57.7	82.3	4.5	0.1445	< 5.4	12.5	2.3	0.0738
< 49.8	77.8	3.9	0.1252	< 4.7	10.2	1.6	0.0514
< 42.9	73.9	4.6	0.1477	< 4.1	8.6	1	0.0321
< 37.1	69.3	6.2	0.1990	< 3.5	7.6	0.9	0.0289
< 32	63.1	6.2	0.1990	< 3.0	6.7	1.2	0.0385
< 27.6	56.9	5	0.1605	< 2.6	5.5	1.2	0.0385
< 23.8	51.9	5.6	0.1798	< 2.2	4.3	1.1	0.0353
< 20.5	46.3	6.5	0.2087	< 1.9	3.2	3.2	0.1027
						Total	3.21

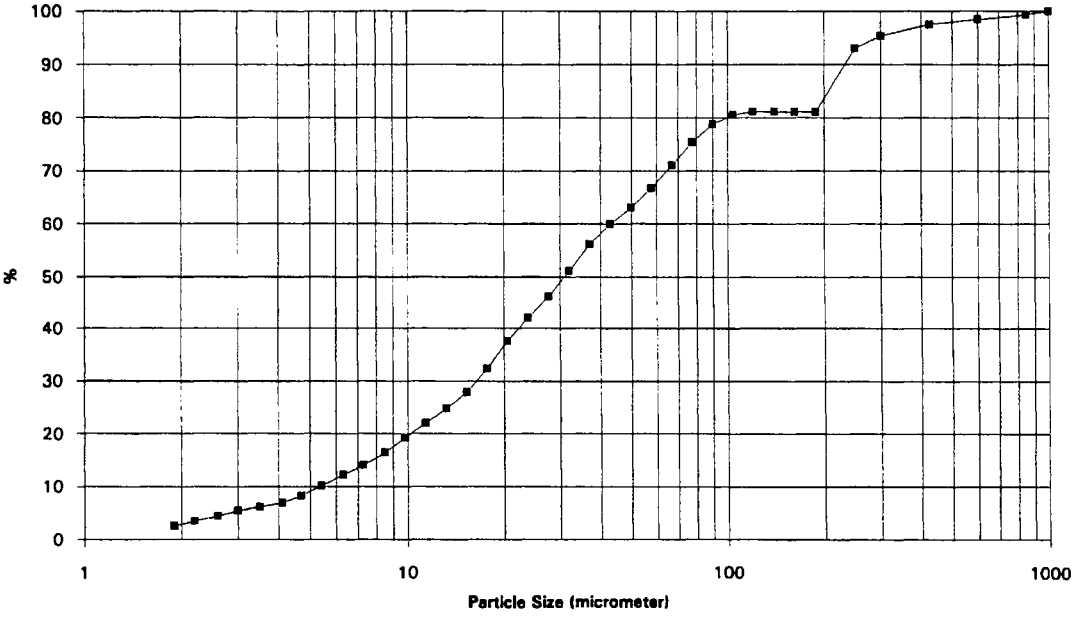

Particle Size Analysis

Sample # 11374-7

Total Weight 1.49 grams

grain sizes > 180 um 0.02 grams

size, um	weight (g)
> 850	
> 600	
> 425	
> 300	
> 250	
> 180	0.02
sum	0.02

grain sizes < 180 um 1.47 grams

size, um	% under	%	weight (g)	size, um	% under	%	weight (g)
< 188	100	0	0.0000	< 17.7	74.8	5.4	0.0794
< 162	100	0	0.0000	< 15.3	69.4	4	0.0588
< 140	100	0	0.0000	< 13.2	65.4	4.4	0.0647
< 120	100	0	0.0000	< 11.4	61	4.9	0.0720
< 104	100	0	0.0000	< 9.8	56.1	4.3	0.0632
< 89.9	100	0.1	0.0015	< 8.5	51.8	3.9	0.0573
< 77.5	99.9	0.1	0.0015	< 7.3	47.9	4.2	0.0617
< 66.9	99.8	0.1	0.0015	< 6.3	43.7	5.8	0.0853
< 57.7	99.7	0.4	0.0059	< 5.4	37.9	5.5	0.0809
< 49.8	99.3	1.9	0.0279	< 4.7	32.4	3.4	0.0500
< 42.9	97.4	2.5	0.0368	< 4.1	29	2.3	0.0338
< 37.1	94.9	2.3	0.0338	< 3.5	26.7	2.2	0.0323
< 32	92.6	3	0.0441	< 3.0	24.5	3.2	0.0470
< 27.6	89.6	4.3	0.0632	< 2.6	21.3	3.9	0.0573
< 23.8	85.3	5.5	0.0809	< 2.2	17.4	4.1	0.0603
< 20.5	79.8	5	0.0735	< 1.9	13.3	13.3	0.1955
						Total	1.47

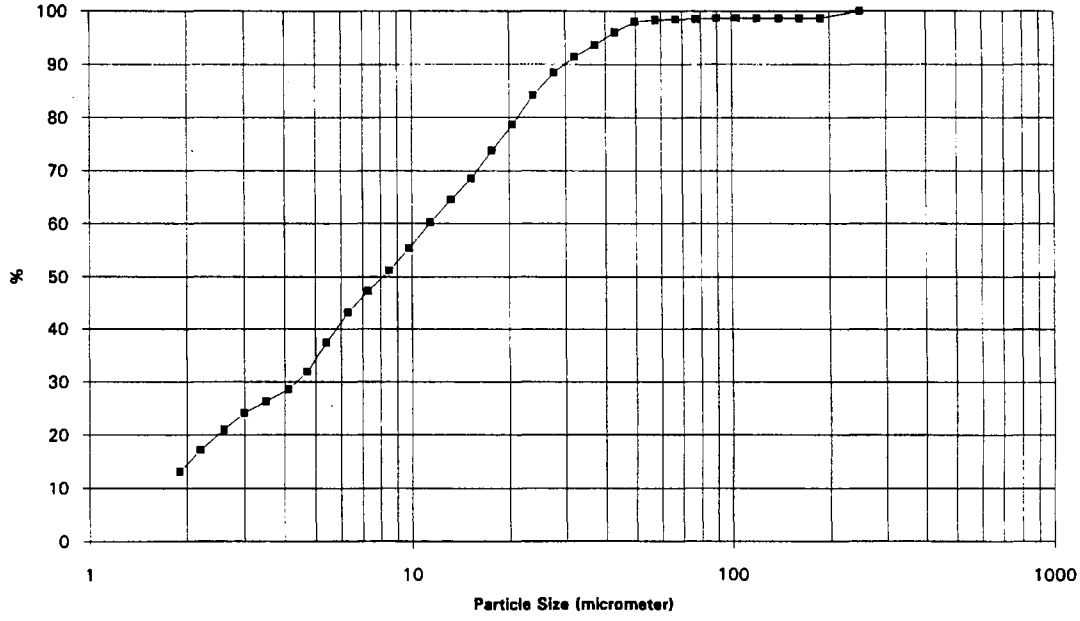

Particle Size Analysis

Sample # 11374-8

Total Weight 5.02 grams

grain sizes > 180 um 1.59 grams

size, um	weight (g)
> 850	0.004
> 600	0.011
> 425	0.016
> 300	0.393
> 250	0.488
> 180	0.632
sum	1.544

grain sizes < 180 um 3.43 grams

size, um	% under	%	weight (g)	size, um	% under	%	weight (g)
< 188	100	0	0.0000	< 17.7	89.9	3.1	0.1063
< 162	100	0	0.0000	< 15.3	86.8	2.6	0.0892
< 140	100	0	0.0000	< 13.2	84.2	2.7	0.0926
< 120	100	0	0.0000	< 11.4	81.5	3.1	0.1063
< 104	100	0	0.0000	< 9.8	78.4	3.2	0.1098
< 89.9	100	0	0.0000	< 8.5	75.2	2.9	0.0995
< 77.5	100	0	0.0000	< 7.3	72.3	4	0.1372
< 66.9	100	0	0.0000	< 6.3	68.3	7.1	0.2435
< 57.7	100	0.1	0.0034	< 5.4	61.2	7.4	0.2538
< 49.8	99.9	0.4	0.0137	< 4.7	53.8	4.7	0.1612
< 42.9	99.5	0.6	0.0206	< 4.1	49.1	3.2	0.1098
< 37.1	98.9	0.7	0.0240	< 3.5	45.9	3.7	0.1269
< 32	98.2	0.8	0.0274	< 3.0	42.2	6.2	0.2127
< 27.6	97.4	1.2	0.0412	< 2.6	36	7.2	0.2470
< 23.8	96.2	2.6	0.0892	< 2.2	28.8	6.8	0.2332
< 20.5	93.6	3.7	0.1269	< 1.9	22	22	0.7546
						Total	3.43

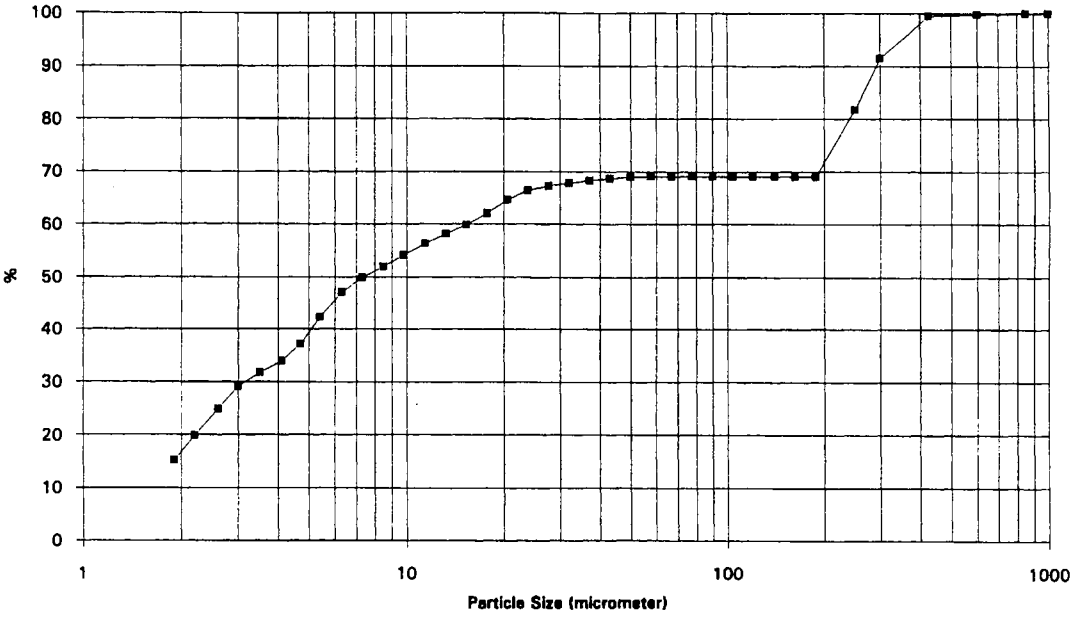

Particle Size Analysis

Sample # 11374-9

Total Weight 5.76 grams

grain sizes > 180 um 0.22 grams

size, um	weight (g)
> 850	0
> 600	0.031
> 425	0.065
> 300	0.026
> 250	0.032
> 180	0.059
sum	0.213

grain sizes < 180 um 5.54 grams

size, um	% under	%	weight	size, um	% under	%	weight
< 188	100	0	0.0000	< 17.7	61.8	4.2	0.2327
< 162	100	0.1	0.0055	< 15.3	57.6	3	0.1662
< 140	99.9	0	0.0000	< 13.2	54.6	3.1	0.1717
< 120	99.9	0	0.0000	< 11.4	51.5	3.7	0.2050
< 104	99.9	0	0.0000	< 9.8	47.8	4.4	0.2438
< 89.9	99.9	1.2	0.0665	< 8.5	43.4	4.1	0.2271
< 77.5	98.7	3.6	0.1994	< 7.3	39.3	4.4	0.2438
< 66.9	95.1	4.5	0.2493	< 6.3	34.9	6.2	0.3435
< 57.7	90.6	4.3	0.2382	< 5.4	28.7	5.8	0.3213
< 49.8	86.3	3.5	0.1939	< 4.7	22.9	3.7	0.2050
< 42.9	82.8	2.9	0.1607	< 4.1	19.2	2.5	0.1385
< 37.1	79.9	2.8	0.1551	< 3.5	16.7	2.5	0.1385
< 32	77.1	2.8	0.1551	< 3.0	14.2	3.3	0.1828
< 27.6	74.3	3.1	0.1717	< 2.6	10.9	3.1	0.1717
< 23.8	71.2	4.3	0.2382	< 2.2	7.8	2.2	0.1219
< 20.5	66.9	5.1	0.2825	< 1.9	5.6	5.6	0.3102
						Total	5.54

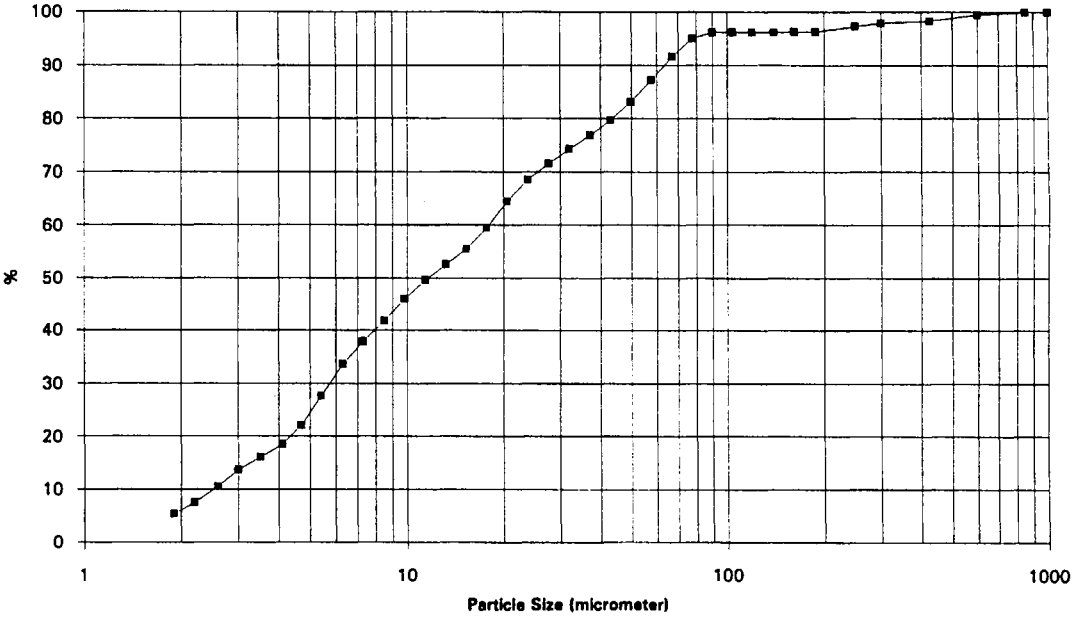

Particle Size Analysis

Sample # 11374-10

Total Weight 4.99 grams

grain sizes > 180 um 0.33 grams

size, um	weight (g)
> 850	0.036
> 600	0.012
> 425	0.01
> 300	0.024
> 250	0.126
> 180	0.103
sum	0.311

grain sizes < 180 um 4.66 grams

size, um	% under	%	weight	size, um	% under	%	weight
< 188	100	0	0.0000	< 17.7	79.3	2.5	0.1165
< 162	100	0.1	0.0047	< 15.3	76.8	2.7	0.1258
< 140	99.9	0.1	0.0047	< 13.2	74.1	3	0.1398
< 120	99.8	0	0.0000	< 11.4	71.1	3.5	0.1631
< 104	99.8	0	0.0000	< 9.8	67.6	3.7	0.1724
< 89.9	99.8	1.8	0.0839	< 8.5	63.9	3.9	0.1817
< 77.5	98	4.7	0.2190	< 7.3	60	4.7	0.2190
< 66.9	93.3	4.5	0.2097	< 6.3	55.3	6.8	0.3169
< 57.7	88.8	1.4	0.0652	< 5.4	48.5	6.9	0.3215
< 49.8	87.4	0.7	0.0326	< 4.7	41.6	5.3	0.2470
< 42.9	86.7	0.7	0.0326	< 4.1	36.3	3.9	0.1817
< 37.1	86	0.7	0.0326	< 3.5	32.4	3.6	0.1678
< 32	85.3	0.6	0.0280	< 3.0	28.8	4.4	0.2050
< 27.6	84.7	1.2	0.0559	< 2.6	24.4	5	0.2330
< 23.8	83.5	1.9	0.0885	< 2.2	19.4	4.8	0.2237
< 20.5	81.6	2.3	0.1072	< 1.9	14.6	14.6	0.6804
						Total	4.66

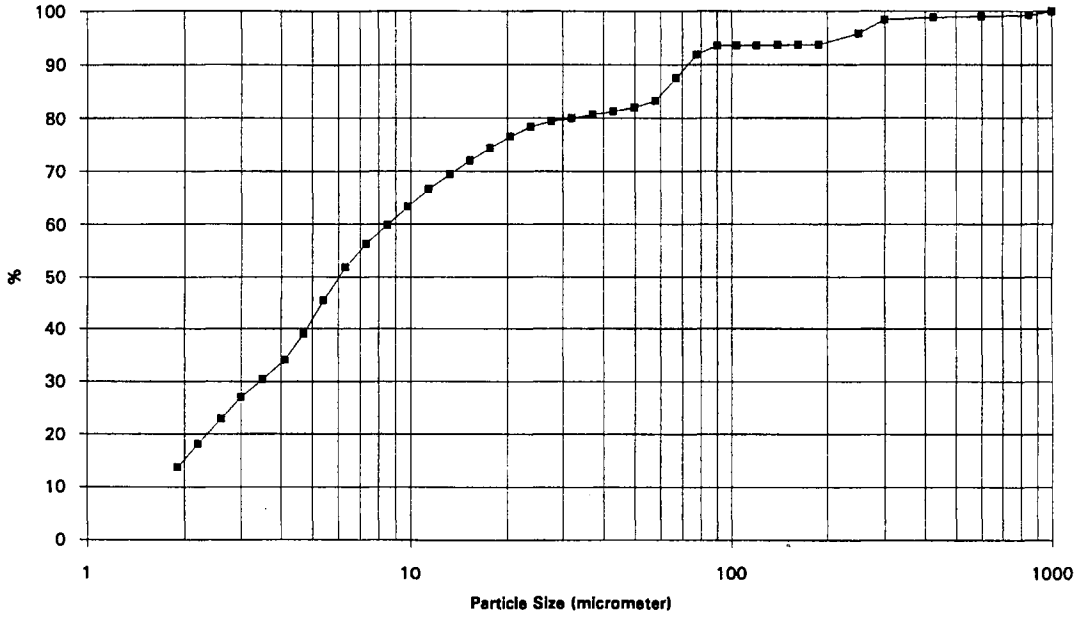

Particle Size Analysis

Sample # 11374-11

Total Weight 6.32 grams

grain sizes > 180 um 2.12 grams

size, um	weight (g)
> 850	0.801
> 600	0.122
> 425	0.105
> 300	0.211
> 250	0.242
> 180	0.573
sum	2.054

grain sizes < 180 um 4.2 grams

size, um	% under	%	weight	size, um	% under	%	weight
< 188	100	0	0.0000	< 17.7	49.2	5.6	0.2352
< 162	100	0	0.0000	< 15.3	43.6	4.1	0.1722
< 140	100	0	0.0000	< 13.2	39.5	4	0.1680
< 120	100	0	0.0000	< 11.4	35.5	4.2	0.1764
< 104	100	0	0.0000	< 9.8	31.3	3.9	0.1638
< 89.9	100	0.1	0.0042	< 8.5	27.4	3.2	0.1344
< 77.5	99.9	0.9	0.0378	< 7.3	24.2	2.7	0.1134
< 66.9	99	2	0.0840	< 6.3	21.5	3	0.1260
< 57.7	97	3.8	0.1596	< 5.4	18.5	2.7	0.1134
< 49.8	93.2	5.3	0.2226	< 4.7	15.8	2.2	0.0924
< 42.9	87.9	5.6	0.2352	< 4.1	13.6	1.5	0.0630
< 37.1	82.3	5.4	0.2268	< 3.5	12.1	1.3	0.0546
< 32	76.9	5.9	0.2478	< 3.0	10.8	1.5	0.0630
< 27.6	71	6.8	0.2856	< 2.6	9.3	1.8	0.0756
< 23.8	64.2	7.7	0.3234	< 2.2	7.5	1.8	0.0756
< 20.5	56.5	7.3	0.3066	< 1.9	5.7	5.7	0.2394
						Total	4.2

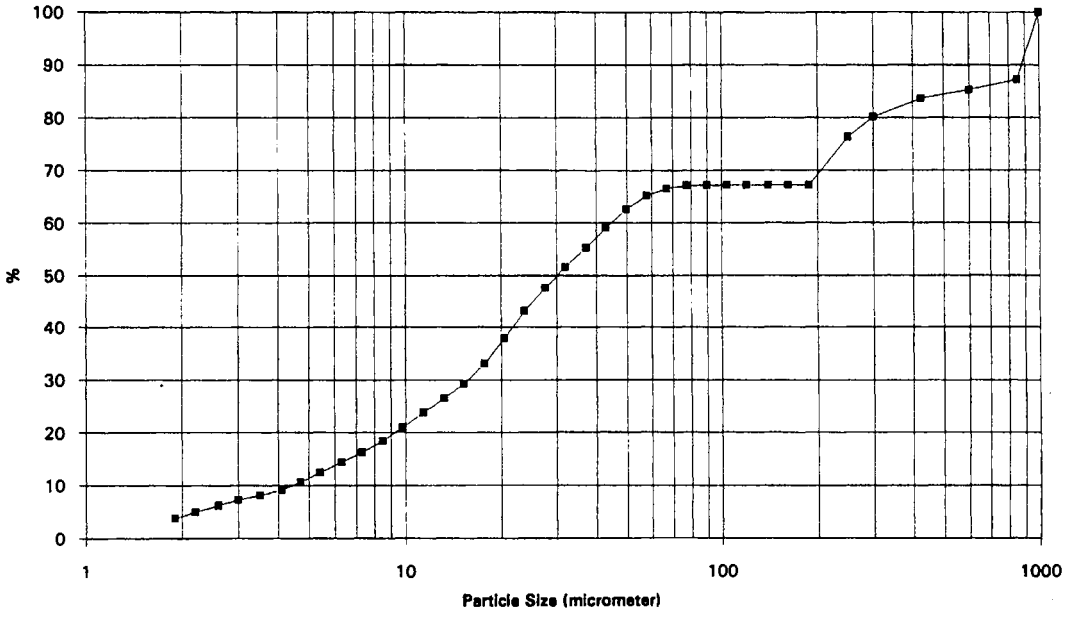

Particle Size Analysis

Sample # 11374-12

Total Weight 5.66 grams

grain sizes > 180 um 1.36 grams

size, um	weight (g)
> 850	0.016
> 600	0.023
> 425	0.052
> 300	0.061
> 250	0.127
> 180	1.007
sum	1.286

grain sizes < 180 um 4.3 grams

size, um	% under	%	weight (g)	size, um	% under	%	weight (g)
< 188	100	0	0.0000	< 17.7	35.6	3.4	0.1462
< 162	100	0	0.0000	< 15.3	32.2	2.6	0.1118
< 140	100	0	0.0000	< 13.2	29.6	2.4	0.1032
< 120	100	1.1	0.0473	< 11.4	27.2	2.4	0.1032
< 104	98.9	3.3	0.1419	< 9.8	24.8	2.3	0.0989
< 89.9	95.6	5.8	0.2494	< 8.5	22.5	2	0.0860
< 77.5	89.8	7.2	0.3096	< 7.3	20.5	2.2	0.0946
< 66.9	82.6	7.4	0.3182	< 6.3	18.3	2.7	0.1161
< 57.7	75.2	6.1	0.2623	< 5.4	15.6	2.7	0.1161
< 49.8	69.1	4.7	0.2021	< 4.7	12.9	2	0.0860
< 42.9	64.4	4.6	0.1978	< 4.1	10.9	1.6	0.0688
< 37.1	59.8	5.4	0.2322	< 3.5	9.3	1.4	0.0602
< 32	54.4	5.5	0.2365	< 3.0	7.9	1.5	0.0645
< 27.6	48.9	4.6	0.1978	< 2.6	6.4	1.4	0.0602
< 23.8	44.3	4.5	0.1935	< 2.2	5	1.4	0.0602
< 20.5	39.8	4.2	0.1806	< 1.9	3.6	3.6	0.1548
						Total	4.3

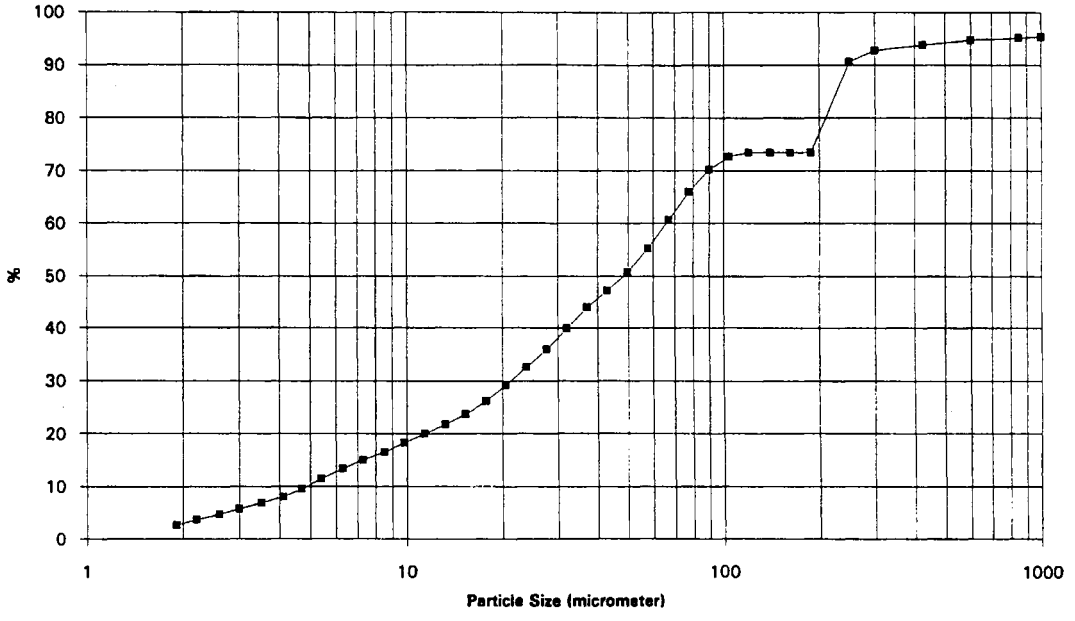

Particle Size Analysis

Sample # 11374-57

Total Weight 5.3 grams

grain sizes > 180 um 0.46 grams

size, um	weight (g)
> 850	0.084
> 600	0.056
> 425	0.028
> 300	0.082
> 250	0.056
> 180	0.103
sum	0.409

grain sizes < 180 um 4.84 grams

size, um	% under	%	weight	size, um	% under	%	weight
< 188	100	0	0.0000	< 17.7	53.7	3.1	0.1500
< 162	100	0	0.0000	< 15.3	50.6	2.6	0.1258
< 140	100	0	0.0000	< 13.2	48	2.6	0.1258
< 120	100	0.7	0.0339	< 11.4	45.4	2.9	0.1404
< 104	99.3	2.8	0.1355	< 9.8	42.5	2.7	0.1307
< 89.9	96.5	4.9	0.2372	< 8.5	39.8	2.9	0.1404
< 77.5	91.6	6.1	0.2952	< 7.3	36.9	3.3	0.1597
< 66.9	85.5	5.9	0.2856	< 6.3	33.6	4.3	0.2081
< 57.7	79.6	4.2	0.2033	< 5.4	29.3	4.1	0.1984
< 49.8	75.4	2.6	0.1258	< 4.7	25.2	3	0.1452
< 42.9	72.8	2.5	0.1210	< 4.1	22.2	2.2	0.1065
< 37.1	70.3	3.4	0.1646	< 3.5	20	2	0.0968
< 32	66.9	3.6	0.1742	< 3.0	18	2.6	0.1258
< 27.6	63.3	3	0.1452	< 2.6	15.4	3	0.1452
< 23.8	60.3	3.2	0.1549	< 2.2	12.4	3	0.1452
< 20.5	57.1	3.4	0.1646	< 1.9	9.4	9.4	0.4550
						Total	4.84

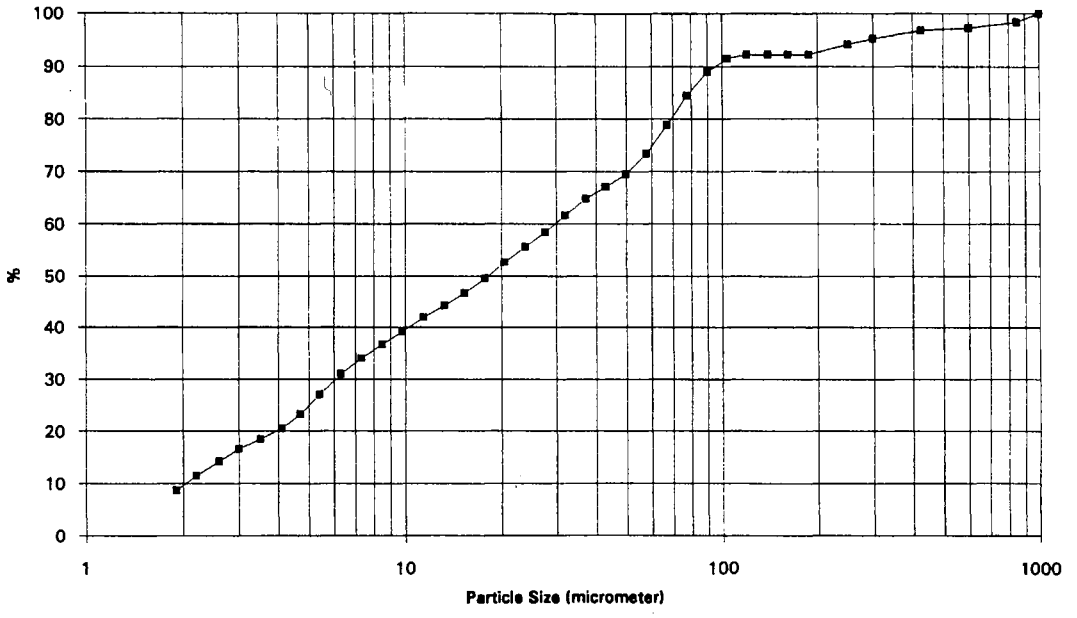

Particle Size Analysis

Sample # 11374-58

Total Weight 5.38 grams

grain sizes > 180 um 2.05 grams

size, um	weight (g)
> 850	0.785
> 600	0.199
> 425	0.171
> 300	0.217
> 250	0.235
> 180	0.357
sum	1.964

grain sizes < 180 um 3.33 grams

size, um	% under	%	weight	size, um	% under	%	weight
< 188	100	0	0.0000	< 17.7	97.4	3.3	0.1099
< 162	100	0	0.0000	< 15.3	94.1	3.6	0.1199
< 140	100	0	0.0000	< 13.2	90.5	3.5	0.1166
< 120	100	0	0.0000	< 11.4	87	4.7	0.1565
< 104	100	0	0.0000	< 9.8	82.3	4	0.1332
< 89.9	100	0	0.0000	< 8.5	78.3	5.5	0.1832
< 77.5	100	0	0.0000	< 7.3	72.8	7.1	0.2364
< 66.9	100	0	0.0000	< 6.3	65.7	9.5	0.3164
< 57.7	100	0	0.0000	< 5.4	56.2	8.6	0.2864
< 49.8	100	0	0.0000	< 4.7	47.6	5.7	0.1898
< 42.9	100	0	0.0000	< 4.1	41.9	3.9	0.1299
< 37.1	100	0	0.0000	< 3.5	38	3.8	0.1265
< 32	100	0	0.0000	< 3.0	34.2	5.2	0.1732
< 27.6	100	0.1	0.0033	< 2.6	29	5.9	0.1965
< 23.8	99.9	0.3	0.0100	< 2.2	23.1	5.6	0.1865
< 20.5	99.6	2.2	0.0733	< 1.9	17.5	17.5	0.5828
						Total	3.33

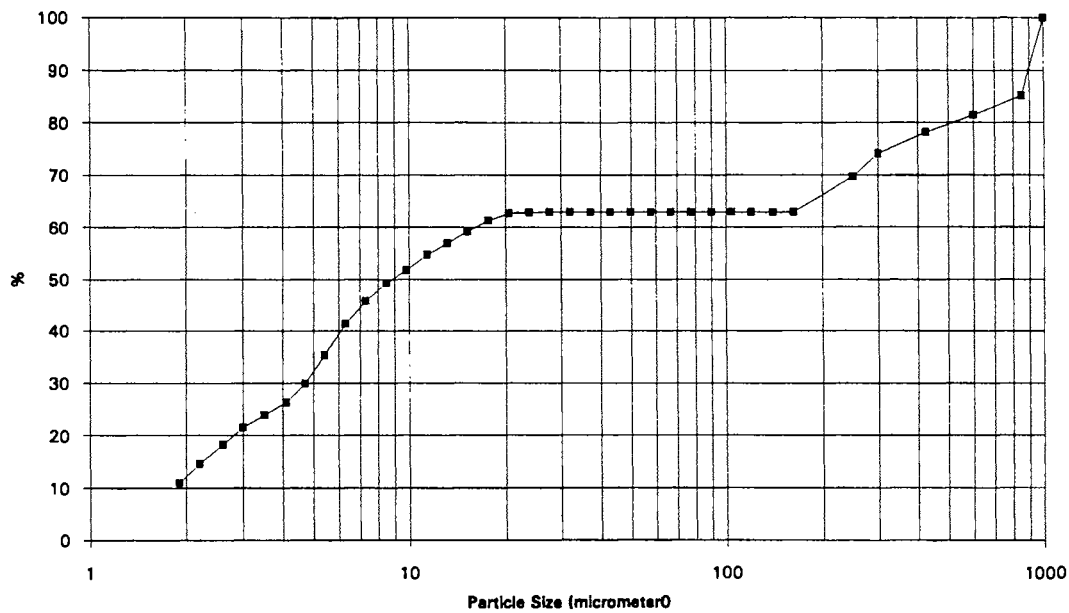

Particle Size Analysis

Sample # 11374-80

Total Weight 5.92 grams

grain sizes > 180 um 0.74 grams

size, um	weight (g)
> 850	0.006
> 600	0.059
> 425	0.097
> 300	0.155
> 250	0.092
> 180	0.326
sum	0.735

grain sizes < 180 um 5.18 grams

size, um	% under	%	weight (g)	size, um	% under	%	weight (g)
< 188	100	0.5	0.0259	< 17.7	11.5	2.1	0.1088
< 162	99.5	1.8	0.0932	< 15.3	9.4	1.5	0.0777
< 140	97.7	3.3	0.1709	< 13.2	7.9	1	0.0518
< 120	94.4	5.4	0.2797	< 11.4	6.9	1	0.0518
< 104	89	7.6	0.3937	< 9.8	5.9	0.7	0.0363
< 89.9	81.4	10.1	0.5232	< 8.5	5.2	0.7	0.0363
< 77.5	71.3	11.2	0.5802	< 7.3	4.5	0.6	0.0311
< 66.9	60.1	10.5	0.5439	< 6.3	3.9	0.7	0.0363
< 57.7	49.6	7.9	0.4092	< 5.4	3.2	0.6	0.0311
< 49.8	41.7	5.4	0.2797	< 4.7	2.6	0.4	0.0207
< 42.9	36.3	4.9	0.2538	< 4.1	2.2	0.4	0.0207
< 37.1	31.4	6	0.3108	< 3.5	1.8	0.3	0.0155
< 32	25.4	5.5	0.2849	< 3.0	1.5	0.3	0.0155
< 27.6	19.9	3.5	0.1813	< 2.6	1.2	0.3	0.0155
< 23.8	16.4	2.5	0.1295	< 2.2	0.9	0.3	0.0155
< 20.5	13.9	2.4	0.1243	< 1.9	0.6	0.6	0.0311
						Total	5.18

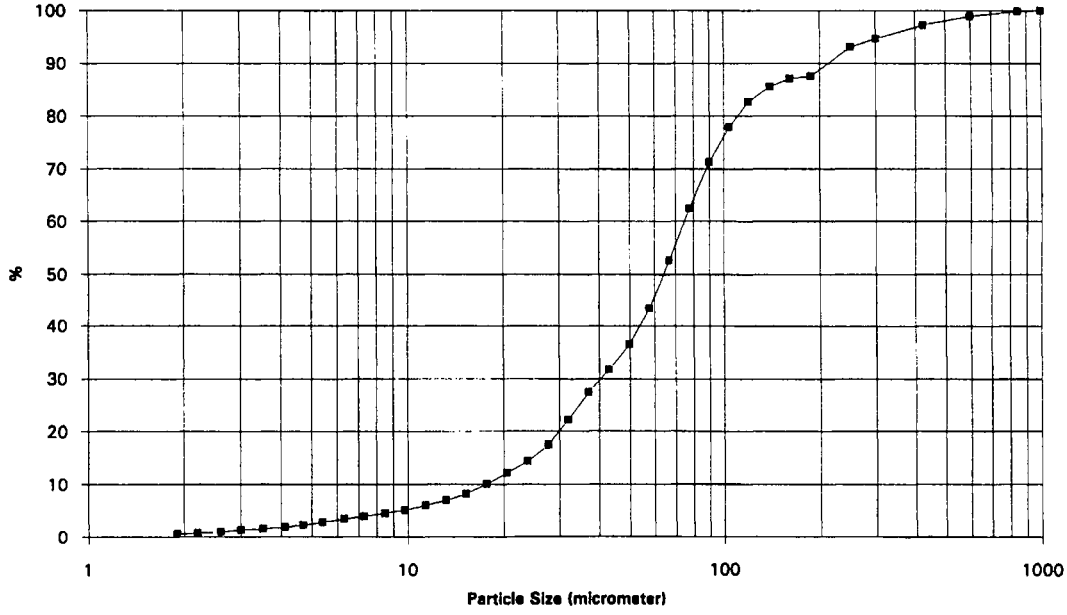

Particle Size Analysis

Sample # 11374-81

Total Weight 6.3 grams

grain sizes > 180 um 0.75 grams

size, um	weight (g)
> 850	0.158
> 600	0.031
> 425	0.038
> 300	0.081
> 250	0.108
> 180	0.316
sum	0.732

grain sizes < 180 um 5.55 grams

size, um	% under	%	weight (g)	size, um	% under	%	weight (g)
< 188	100	0	0.0000	< 17.7	31.4	3.3	0.1831
< 162	100	0.3	0.0166	< 15.3	28.1	2.6	0.1443
< 140	99.7	1.1	0.0611	< 13.2	25.5	2.3	0.1277
< 120	98.6	2.7	0.1498	< 11.4	23.2	2.1	0.1165
< 104	95.9	4.5	0.2498	< 9.8	21.1	2.1	0.1166
< 89.9	91.4	7	0.3885	< 8.5	19	2.1	0.1166
< 77.5	84.4	8.3	0.4607	< 7.3	16.9	2.2	0.1221
< 66.9	76.1	8.1	0.4495	< 6.3	14.7	2.3	0.1276
< 57.7	68	6.2	0.3441	< 5.4	12.4	2.2	0.1221
< 49.8	61.8	4.5	0.2498	< 4.7	10.2	1.6	0.0888
< 42.9	57.3	4.4	0.2442	< 4.1	8.6	1.3	0.0722
< 37.1	52.9	5.3	0.2941	< 3.5	7.3	1.2	0.0666
< 32	47.6	5	0.2775	< 3.0	6.1	1.2	0.0666
< 27.6	42.6	3.9	0.2164	< 2.6	4.9	1.1	0.0611
< 23.8	38.7	3.6	0.1998	< 2.2	3.8	1	0.0555
< 20.5	35.1	3.7	0.2054	< 1.9	2.8	2.8	0.1554
						Total	5.55

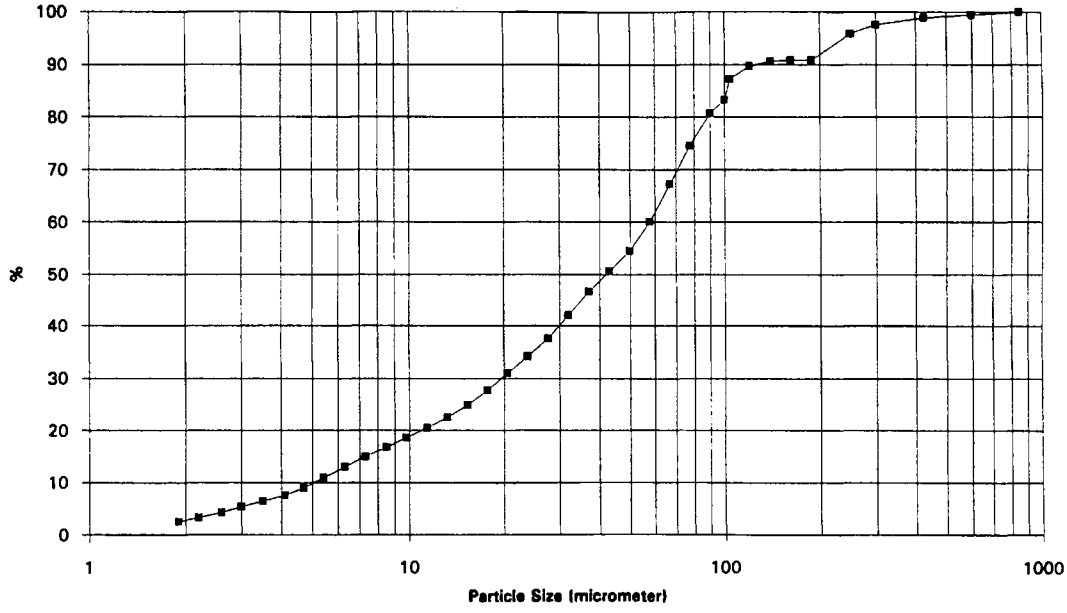

Particle Size Analysis

Sample # 11374-82

Total Weight 5.79 grams

grain sizes > 180 um 1.45 grams

size, um	weight (g)
> 850	0.062
> 600	0.01
> 425	0.016
> 300	0.045
> 250	0.09
> 180	1.126
sum	1.349

grain sizes < 180 um 4.34 grams

size, um	% under	%	weight (g)	size, um	% under	%	weight (g)
< 188	100	2.2	0.0955	< 17.7	14.1	1.7	0.0738
< 162	97.8	5.8	0.2517	< 15.3	12.4	1.4	0.0608
< 140	92	8.3	0.3602	< 13.2	11	1.3	0.0564
< 120	83.7	10.1	0.4383	< 11.4	9.7	1.1	0.0477
< 104	73.6	9.9	0.4297	< 9.8	8.6	1.1	0.0477
< 89.9	63.7	9.5	0.4123	< 8.5	7.5	1	0.0434
< 77.5	54.2	8.1	0.3515	< 7.3	6.5	1	0.0434
< 66.9	46.1	6.6	0.2864	< 6.3	5.5	1	0.0434
< 57.7	39.5	4.9	0.2127	< 5.4	4.5	0.9	0.0391
< 49.8	34.6	3.6	0.1562	< 4.7	3.6	0.8	0.0347
< 42.9	31	3.1	0.1345	< 4.1	2.8	0.5	0.0217
< 37.1	27.9	3.4	0.1476	< 3.5	2.3	0.5	0.0217
< 32	24.5	3.3	0.1432	< 3.0	1.8	0.4	0.0174
< 27.6	21.2	2.8	0.1215	< 2.6	1.4	0.4	0.0174
< 23.8	18.4	2.3	0.0998	< 2.2	1	0.3	0.0130
< 20.5	16.1	2	0.0868	< 1.9	0.7	0.7	0.0304
						Total	4.34

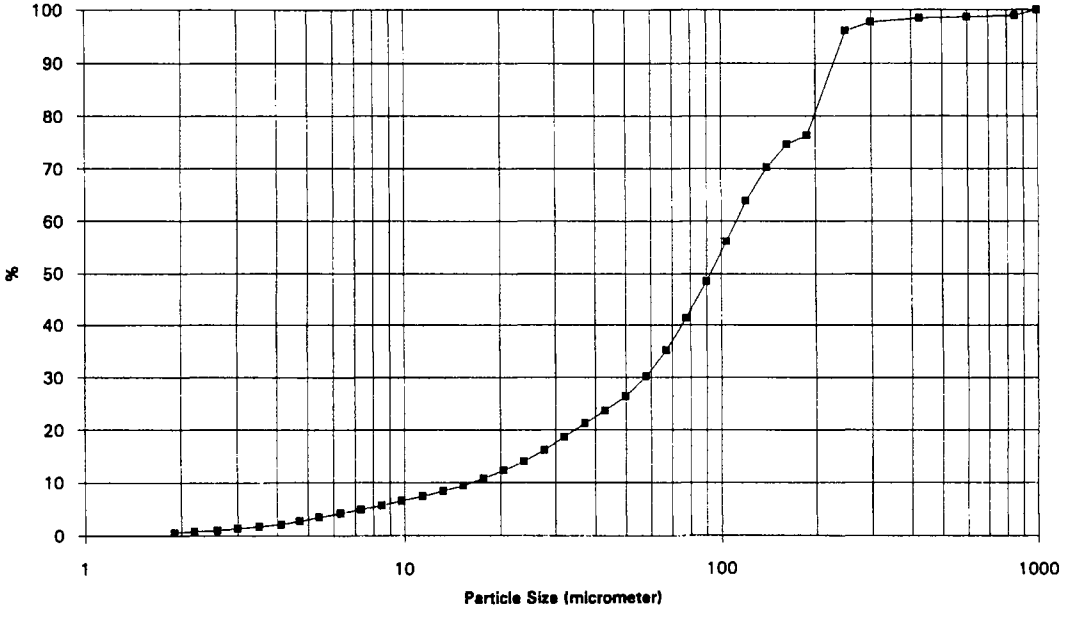

Particle Size Analysis

Sample # 11374-83

Total Weight 7.421 grams

grain sizes > 180 um 6.35 grams

size, um	weight (g)
> 850	5.311
> 600	0.422
> 425	0.194
> 300	0.157
> 250	0.088
> 180	0.142
sum	6.314

grain sizes < 180 um 1.071 grams

size, um	% under	%	weight (g)	size, um	% under	%	weight (g)
< 188	100	0.8	0.0086	< 17.7	39.4	3.3	0.0353
< 162	99.2	2.2	0.0236	< 15.3	36.1	2.4	0.0257
< 140	97	3.4	0.0364	< 13.2	33.7	2.3	0.0246
< 120	93.6	4.4	0.0471	< 11.4	31.4	2.7	0.0289
< 104	89.2	4.8	0.0514	< 9.8	28.7	2.9	0.0311
< 89.9	84.4	5.2	0.0557	< 8.5	25.8	2.6	0.0278
< 77.5	79.2	5.3	0.0568	< 7.3	23.2	2.6	0.0278
< 66.9	73.9	4.9	0.0525	< 6.3	20.6	3	0.0321
< 57.7	69	4.4	0.0471	< 5.4	17.6	2.7	0.0289
< 49.8	64.6	3.9	0.0418	< 4.7	14.9	2	0.0214
< 42.9	60.7	3.4	0.0364	< 4.1	12.9	1.4	0.0150
< 37.1	57.3	3.4	0.0364	< 3.5	11.5	1.2	0.0129
< 32	53.9	3.2	0.0343	< 3.0	10.3	1.6	0.0171
< 27.6	50.7	3.2	0.0343	< 2.6	8.7	1.8	0.0193
< 23.8	47.5	3.8	0.0407	< 2.2	6.9	1.7	0.0182
< 20.5	43.7	4.3	0.0461	< 1.9	5.2	5.2	0.0557
						Total	1.071

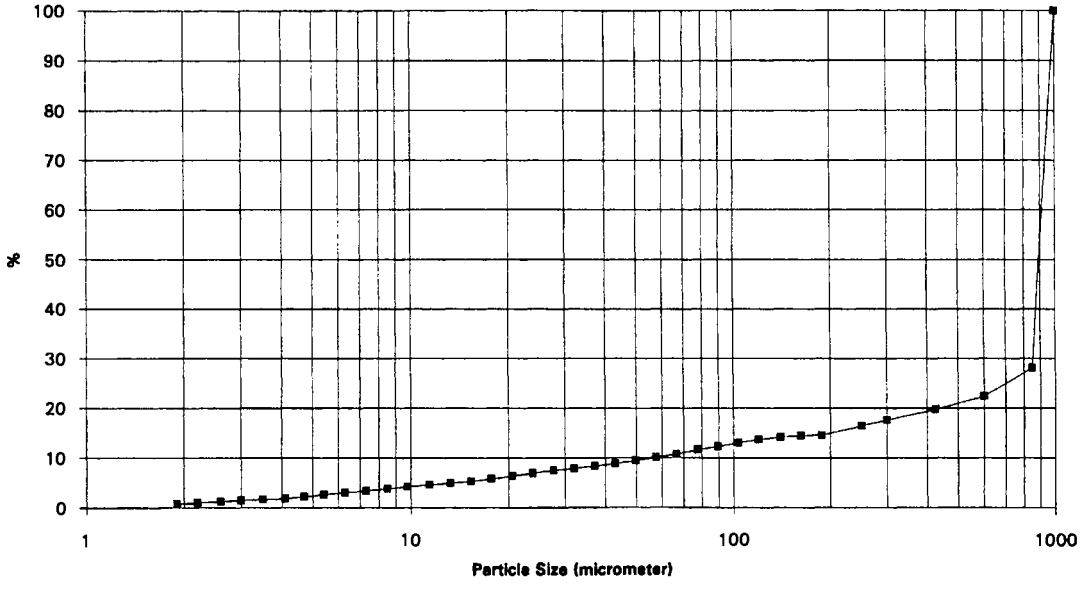

Particle Size Analysis

Sample # 11374-84

Total Weight 2.94 grams

grain sizes > 180 um 0.042 grams

size, um	weight (g)
> 850	0.007
> 600	0.005
> 425	0.006
> 300	0.004
> 250	0.005
> 180	0.013
sum	0.04

grain sizes < 180 um 2.898 grams

size, um	% under	%	weight (g)	size, um	% under	%	weight (g)
< 188	100	0	0.0000	< 17.7	44.6	5.8	0.1681
< 162	100	0	0.0000	< 15.3	38.8	4.2	0.1217
< 140	100	0	0.0000	< 13.2	34.6	4.3	0.1246
< 120	100	0	0.0000	< 11.4	30.3	4.7	0.1362
< 104	100	0	0.0000	< 9.8	25.6	4.2	0.1217
< 89.9	100	0.3	0.0087	< 8.5	21.4	3.3	0.0956
< 77.5	99.7	0.4	0.0116	< 7.3	18.1	3	0.0869
< 66.9	99.3	0.4	0.0116	< 6.3	15.1	3.4	0.0985
< 57.7	98.9	1.4	0.0406	< 5.4	11.7	3.3	0.0956
< 49.8	97.5	6.5	0.1884	< 4.7	8.4	2.3	0.0667
< 42.9	91	8.4	0.2434	< 4.1	6.1	1.4	0.0406
< 37.1	82.6	7.8	0.2260	< 3.5	4.7	1.2	0.0348
< 32	74.8	7.3	0.2116	< 3.0	3.5	1.1	0.0319
< 27.6	67.5	7.3	0.2116	< 2.6	2.4	0.8	0.0232
< 23.8	60.2	8	0.2318	< 2.2	1.6	0.5	0.0145
< 20.5	52.2	7.6	0.2202	< 1.9	1.1	1.1	0.0319
						Total	2.898

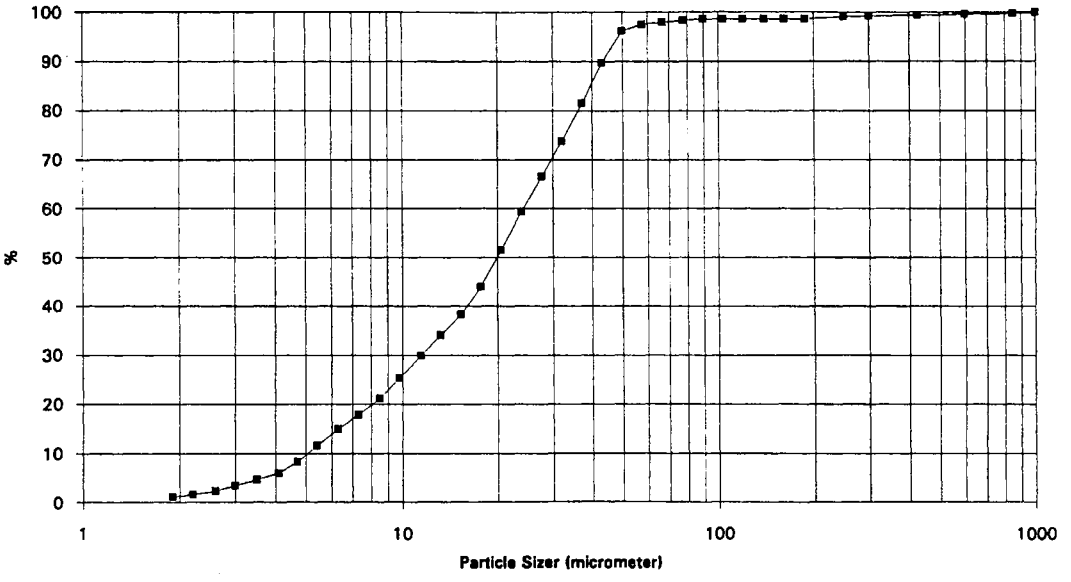

Particle Size Analysis

Sample # 11385-25

Total Weight 6 grams

grain sizes > 180 um 1.889 grams

size, um	weight (g)
> 850	0.678
> 600	0.092
> 425	0.112
> 300	0.099
> 250	0.185
> 180	0.723
sum	1.889

grain sizes < 180 um 4.111 grams

size, um	% under	%	weight (g)	size, um	% under	%	weight (g)
< 188	100	1.6	0.0658	< 17.7	26.3	2.8	0.1151
< 162	98.4	4.2	0.1727	< 15.3	23.5	2.3	0.0946
< 140	94.2	6	0.2467	< 13.2	21.2	1.9	0.0781
< 120	88.2	7.4	0.3042	< 11.4	19.3	1.9	0.0781
< 104	80.8	7.6	0.3124	< 9.8	17.4	1.8	0.0740
< 89.9	73.2	7.4	0.3042	< 8.5	15.6	1.8	0.0740
< 77.5	65.8	6.6	0.2713	< 7.3	13.8	1.9	0.0781
< 66.9	59.2	5.5	0.2261	< 6.3	11.9	2.1	0.0863
< 57.7	53.7	4	0.1644	< 5.4	9.8	2	0.0822
< 49.8	49.7	3	0.1233	< 4.7	7.8	1.6	0.0658
< 42.9	46.7	3.2	0.1316	< 4.1	6.2	1	0.0411
< 37.1	43.5	4	0.1644	< 3.5	5.2	0.9	0.0370
< 32	39.5	4	0.1644	< 3.0	4.3	0.8	0.0329
< 27.6	35.5	3.2	0.1316	< 2.6	3.5	0.8	0.0329
< 23.8	32.3	2.9	0.1192	< 2.2	2.7	0.7	0.0288
< 20.5	29.4	3.1	0.1274	< 1.9	2	2	0.0822
						Total	4.111

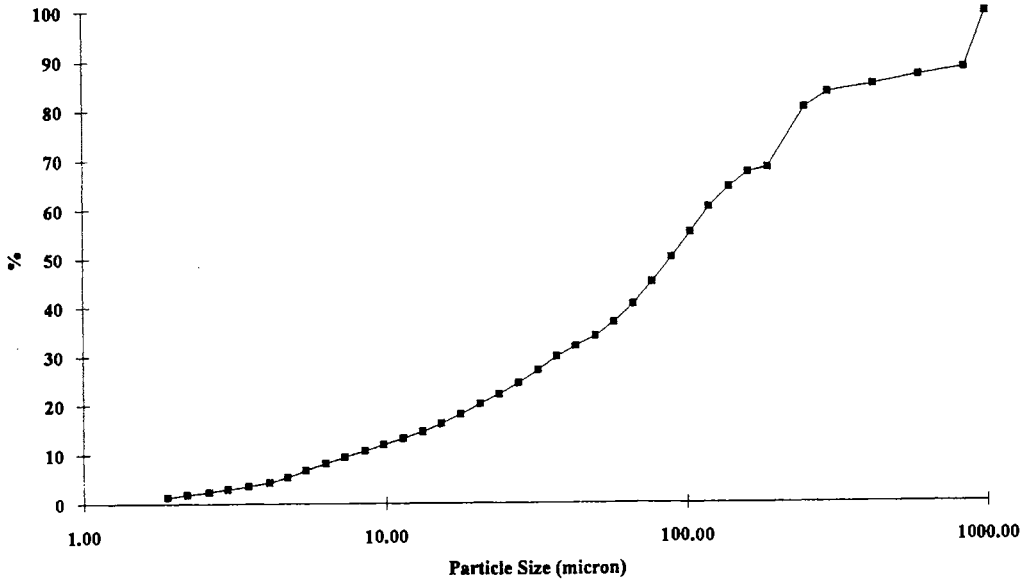

Retort Data

Sample No. 11374-2

Before Retort:

Tare 1589.5 g
Content 118.8 g

Weight of cylinder = 73.17 g
Weight of stopper = 4.09 g

After Retort:

Weight of cylinder, content and stopper = 85.4 g
Weight of content in cylinder = 8.14 g

Volume of water = 5.6 ml
Volume of oil = 2.7 ml

Weight of solids content after cooled = 110.1 g

Content	Weight (g)	Weight Percent (%)
Water	5.6	4.71
Oil	3.1	2.61
Solids	110.1	92.68

WOR: 2.07

Retort Data

Sample No. 11374-3

Before Retort:

Tare 1548 g
Content 95.5 g

Weight of cylinder = 73.17 g
Weight of stopper = 4.09 g

After Retort:

Weight of cylinder, content and stopper = 94.27 g
Weight of content in cylinder = 17.01 g

Volume of water = 14.4 ml
Volume of oil = 2.2 ml

Weight of solids content after cooled = 76.9 g

Content	Weight (g)	Weight Percent (%)
Water	14.4	15.08
Oil	4.2	4.4
Solids	76.9	80.52

WOR: 6.55

Retort Data

Sample No. 11374-4

Before Retort:

Tare 1589.1 g
Content 83.8 g

Weight of cylinder = 72.2 g
Weight of stopper = 4.09 g

After Retort:

Weight of cylinder, content and stopper = 81.55 g
Weight of content in cylinder = 5.26 g

Volume of water = 4.3 ml
Volume of oil = 0.7 ml

Weight of solids content after cooled = 78.5 g

Content	Weight (g)	Weight Percent (%)
Water	4.3	5.13
Oil	1	1.19
Solids	78.5	93.68

WOR: 6.14

Retort Data

Sample No. 11374-5

Before Retort:

Tare 1550.2 g
Content 74.9 g

Weight of cylinder = 72.2 g
Weight of stopper = 4.09 g

After Retort:

Weight of cylinder, content and stopper = 89 g
Weight of content in cylinder = 12.71 g

Volume of water = 5.8 ml
Volume of oil = 6.5 ml

Weight of solids content after cooled = 63.3 g

Content	Weight (g)	Weight Percent (%)
Water	5.8	7.75
Oil	5.8	7.75
Solids	63.3	84.5

WOR: .89

Retort Data

Sample No. 11374-8

Before Retort:

Tare 1590.1 g
Content 81.7 g

Weight of cylinder = 72.2 g
Weight of stopper = 4.09 g

After Retort:

Weight of cylinder, content and stopper = 87.65 g
Weight of content in cylinder = 11.36 g

Volume of water = 9.5 ml
Volume of oil = 2.1 ml

Weight of solids content after cooled = 70.4 g

Content	Weight (g)	Weight Percent (%)
Water	9.5	11.63
Oil	1.8	2.2
Solids	70.4	86.17

WOR: 4.52

Retort Data

Sample No. 11374-9

Before Retort:

Tare 1589.6 g
Content 82.7 g

Weight of cylinder = 73.17 g
Weight of stopper = 4.09 g

After Retort:

Weight of cylinder, content and stopper = 91.1 g
Weight of content in cylinder = 13.84 g

Volume of water = 8.3 ml
Volume of oil = 6.7 ml

Weight of solids content after cooled = 68.8 g

Content	Weight (g)	Weight Percent (%)
Water	8.3	10.04
Oil	5.6	6.77
Solids	68.8	83.19

WOR: 1.24

Retort Data

Sample No. 11374-10

Before Retort:

Tare 1551.9 g
Content 87.6 g

Weight of cylinder = 73.17 g
Weight of stopper = 4.09 g

After Retort:

Weight of cylinder, content and stopper = 105.8 g
Weight of content in cylinder = 28.54 g

Volume of water = 24.7 ml
Volume of oil = 4.7 ml

Weight of solids content after cooled = 52.6 g

Content	Weight (g)	Weight Percent (%)
Water	24.7	28.13
Oil	10.5	11.96
Solids	52.6	59.91

WOR: 5.26

Retort Data

Sample No. 11374-11

Before Retort:

Tare 1550 g
Content 93.8 g

Weight of cylinder = 72.2 g
Weight of stopper = 4.09 g

After Retort:

Weight of cylinder, content and stopper = 77.96 g
Weight of content in cylinder = 1.67 g

Volume of water = .7 ml
Volume of oil = .3 ml

Weight of solids content after cooled = 92 g

Content	Weight (g)	Weight Percent (%)
Water	.7	.75
Oil	1.1	1.17
Solids	92	98.08

WOR: 2.33

Retort Data

Sample No. 11374-12

Before Retort:

Tare 1587.5 g
Content 76.5 g

Weight of cylinder = 73.17 g
Weight of stopper = 4.09 g

After Retort:

Weight of cylinder, content and stopper = 89.68 g
Weight of content in cylinder = 12.42 g

Volume of water = 11.9 ml
Volume of oil = .6 ml

Weight of solids content after cooled = 64.1 g

Content	Weight (g)	Weight Percent (%)
Water	11.9	15.56
Oil	.5	.65
Solids	64.1	83.79

WOR:

Retort Data

Sample No. 11374-57

Before Retort:

Tare 1603.2 g
Content 72 g

Weight of cylinder = 73.17 g
Weight of stopper = 4.09 g

After Retort:

Weight of cylinder, content and stopper = ____ g
Weight of content in cylinder = ____ g

Volume of water = 10.9 ml
Volume of oil = 11.1 ml

Weight of solids content after cooled = 54.1 g

Content	Weight (g)	Weight Percent (%)
Water	10.9	15.14
Oil	7	9.72
Solids	54.1	75.14

WOR: .982

Retort Data

Sample No. 11374-58

Before Retort:

Tare 1584.7 g
Content 86.5 g

Weight of cylinder = 72.2 g
Weight of stopper = 4.09 g

After Retort:

Weight of cylinder, content and stopper = 97.47 g
Weight of content in cylinder = 21.18 g

Volume of water = 17.8 ml
Volume of oil = 3.7 ml

Weight of solids content after cooled = 65.6 g

Content	Weight (g)	Weight Percent (%)
Water	17.8	20.58
Oil	3.1	3.58
Solids	65.6	75.84

WOR: 4.81

Retort Data

Sample No. 11374-80

Before Retort:

Tare 1549.8 g
Content 98.5 g

Weight of cylinder = 73.09 g
Weight of stopper = 4.09 g

After Retort:

Weight of cylinder, content and stopper = 101.17 g
Weight of content in cylinder = ____ g

Volume of water = 24 ml
Volume of oil = .5 ml

Weight of solids content after cooled = 74.3 g

Content	Weight (g)	Weight Percent (%)
Water	24	24.37
Oil	1.53	1.55
Solids	72.97	74.08

WOR: 15.7

Retort Data

Sample No. 11374-81

Before Retort:

Tare 1613.9 g
Content 80 g

Weight of cylinder = 72.01 g
Weight of stopper = 4.09 g

After Retort:

Weight of cylinder, content and stopper = 87.81 g
Weight of content in cylinder = 11.71 g

Volume of water = 8.6 ml
Volume of oil = 4.1 ml

Weight of solids content after cooled = 66.61 g

Content	Weight (g)	Weight Percent (%)
Water	8.6	10.75
Oil	4.79	5.99
Solids	66.61	83.26

WOR:

Retort Data

Sample No. 11374-82

Before Retort:

Tare 1549.7 g
Content 81.31 g

Weight of cylinder = 73.09 g
Weight of stopper = 4.09 g

After Retort:

Weight of cylinder, content and stopper = 91.46 g
Weight of content in cylinder = 14.2 g

Volume of water = 12.7 ml
Volume of oil = 2.1 ml

Weight of solids content after cooled = 66.93 g

Content	Weight (g)	Weight Percent (%)
Water	12.9	15.87
Oil	1.48	1.82
Solids	66.93	82.31

WOR: 8.72

Retort Data

Sample No. 11374-83

Before Retort:

Tare 1615.1 g
Content 64.7 g

Weight of cylinder = 72.01 g
Weight of stopper = 4.09 g

After Retort:

Weight of cylinder, content and stopper = 76.57 g
Weight of content in cylinder = .47 g

Volume of water = 1 ml
Volume of oil = 1 ml

Weight of solids content after cooled = 62.7 g

Content	Weight (g)	Weight Percent (%)
Water	1	1
Oil	1	1
Solids	62.7	98

WOR: 1

Retort Data

Sample No. 11374-84

Before Retort:

Tare 1549.9 g
Content 47.5 g

Weight of cylinder = 72.04 g
Weight of stopper = 4.09 g

After Retort:

Weight of cylinder, content and stopper = 122.5 g
Weight of content in cylinder = 47.9 g

Volume of water = 32.5 ml
Volume of oil = 15.4 ml

Weight of solids content after cooled = 2.9 g

Content	Weight (g)	Weight Percent (%)
Water	32.5	68.42
Oil	12.1	25.47
Solids	2.9	6.11

WOR: 2.69

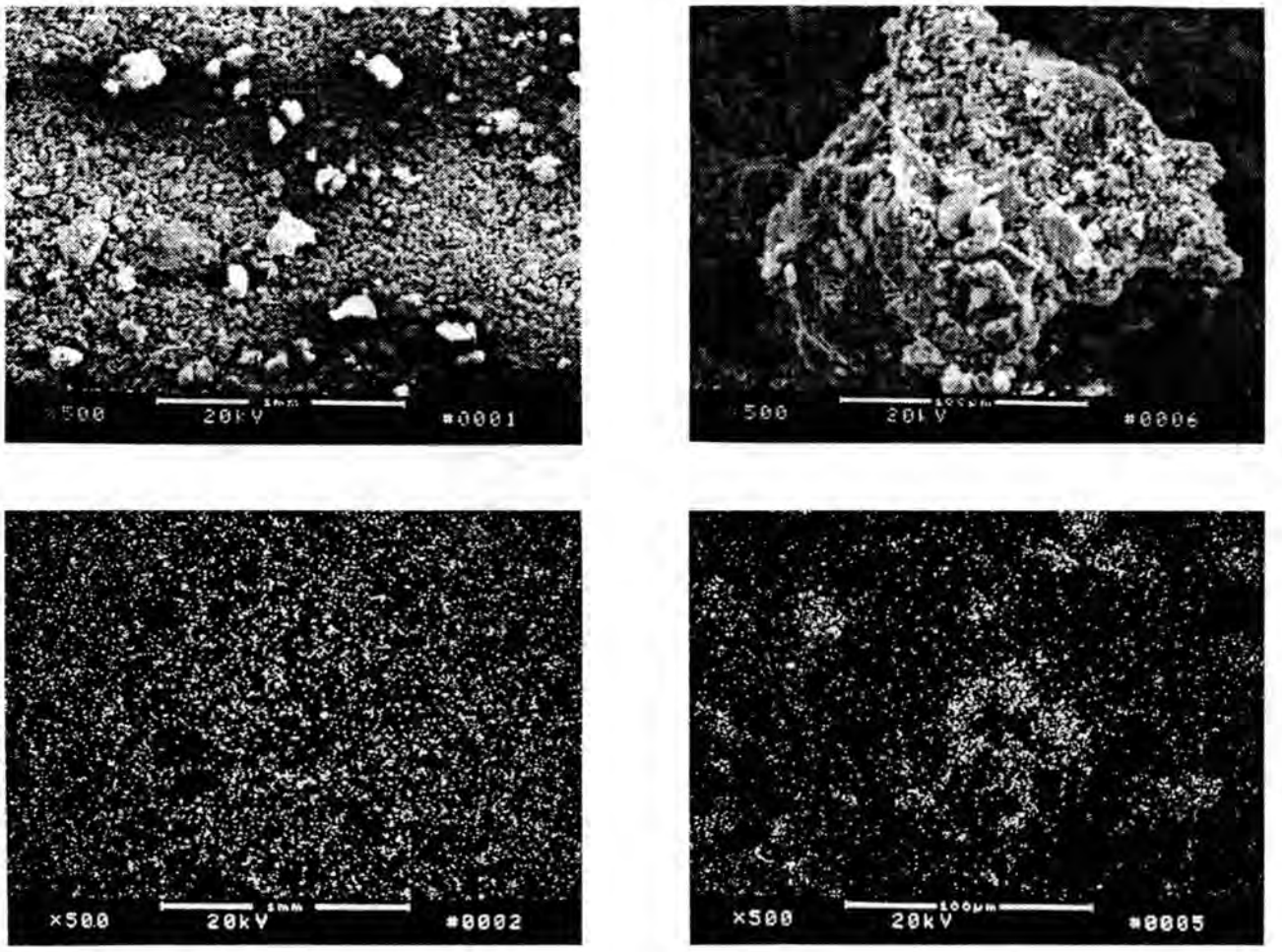

SEM photographs of sample 11374-3. (A) x50 image showing particle morphologies. (B) x500 image showing detailed particle morphologies. (C) x50 image showing barium X-ray map of image shown in (A). (D) x500 image showing barium X-ray map of image shown in (B).

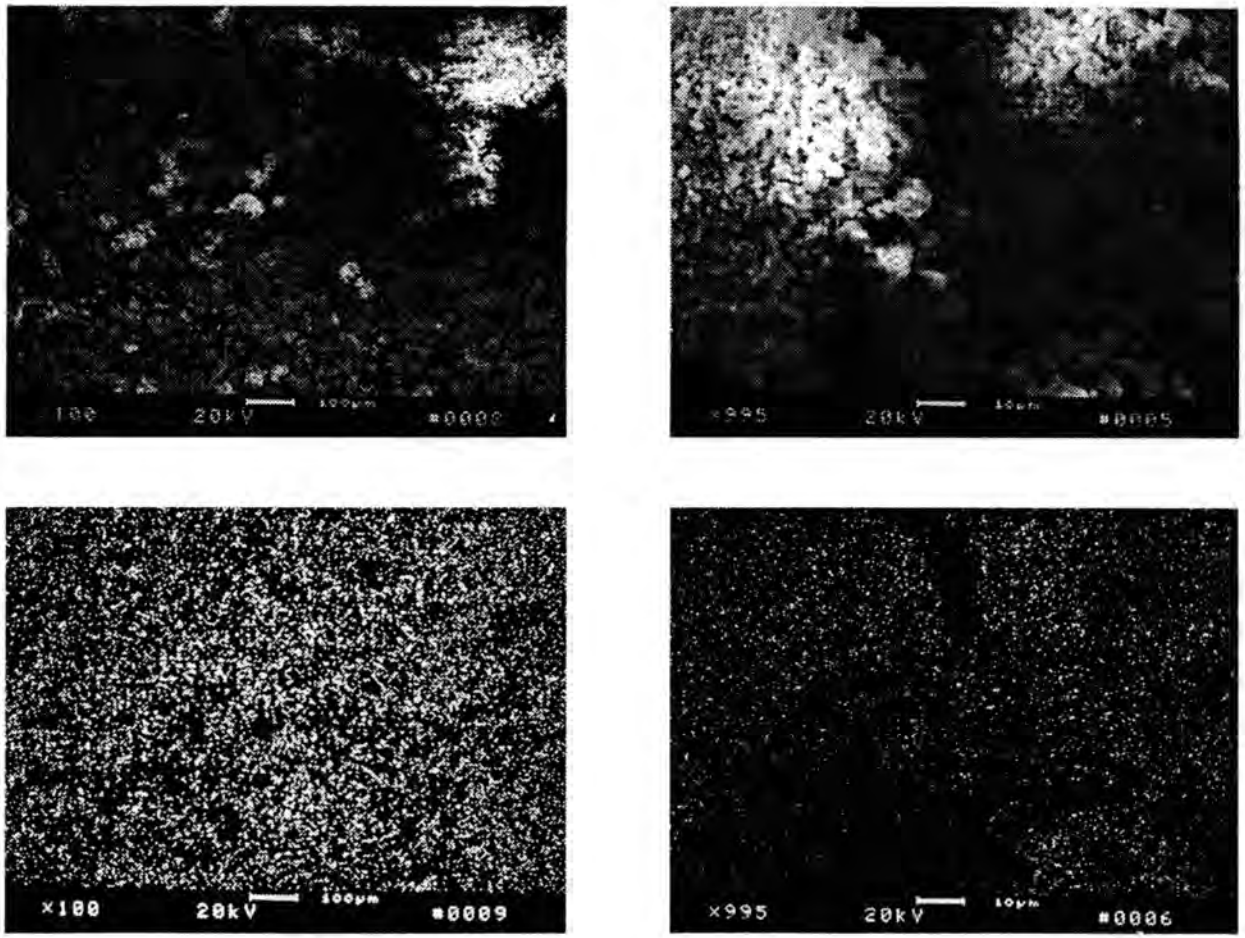

SEM photographs of sample 11374-4. (A) x100 image showing particle morphologies. (B) x1000 image showing detailed particle morphologies. (C) x100 image showing barium X-ray map of image shown in (A). (D) x1000 image showing barium X-ray map of image shown in (B).

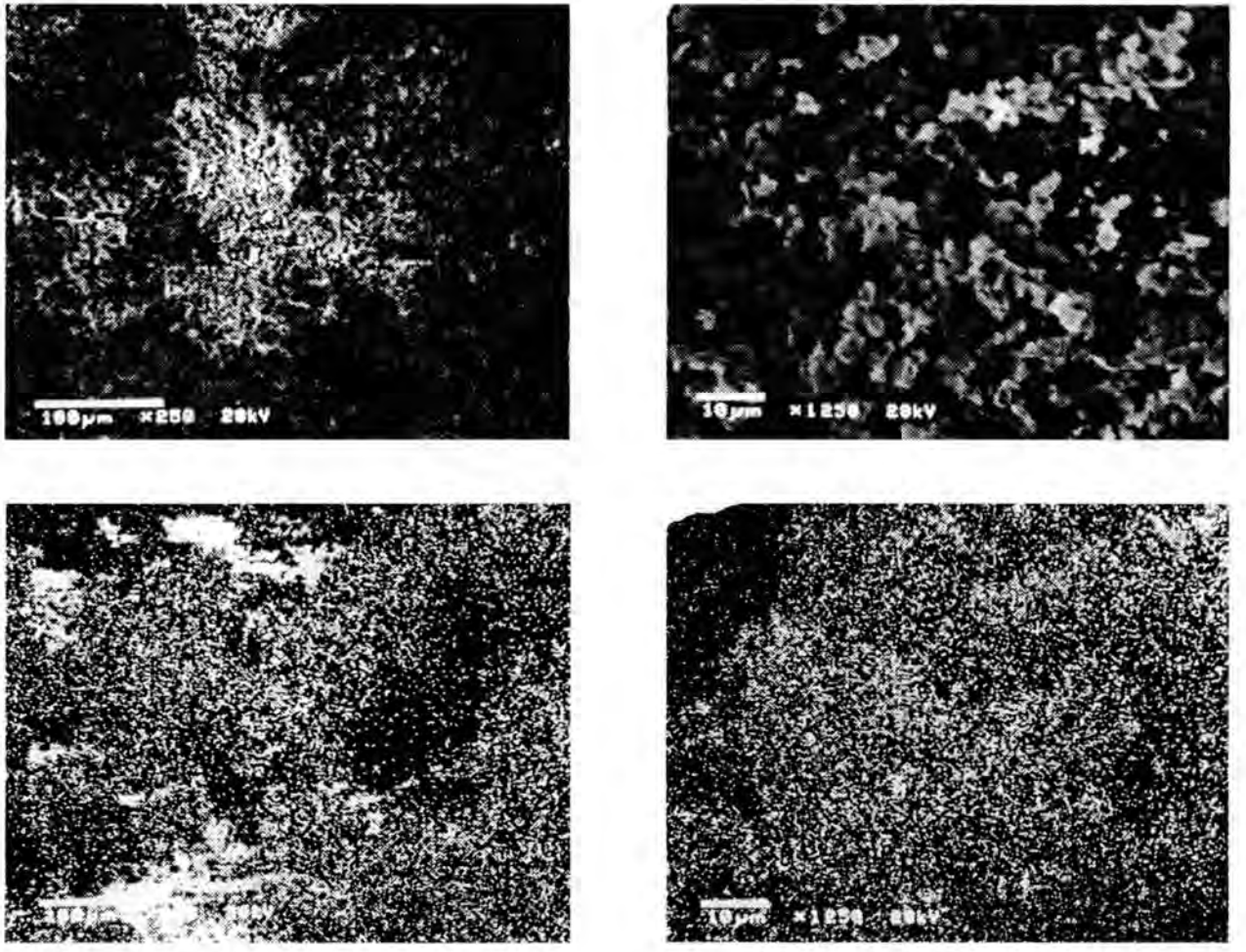

SEM photographs of sample 11374-5. (A) x100 image showing particle morphologies. (B) x1250 image showing detailed particle morphologies. (C) x100 image showing barium X-ray map of image shown in (A). (D) x1250 image showing barium X-ray map of image shown in (B).

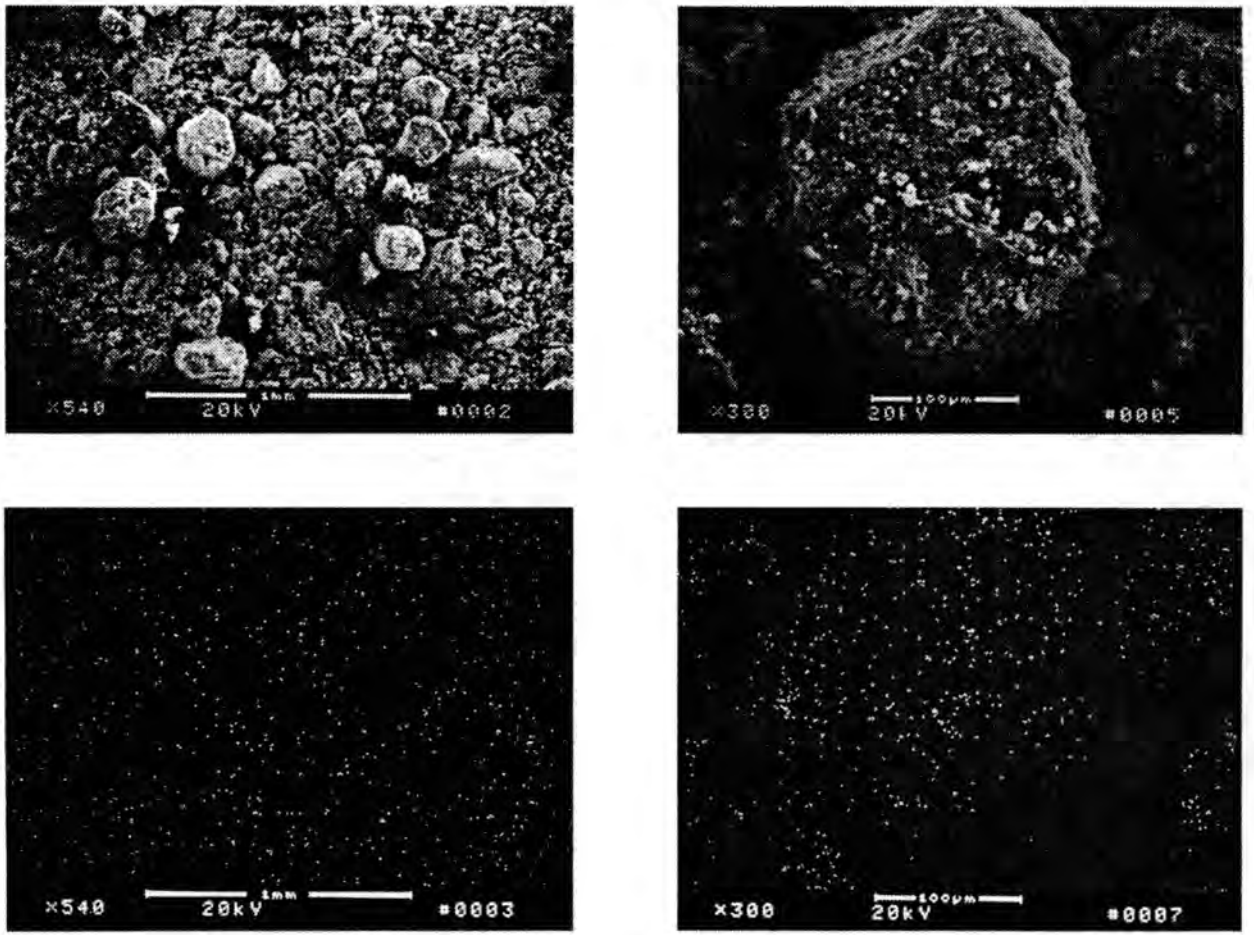

SEM photographs of sample 11374-8. (A) x50 image showing particle morphologies. (B) x300 image showing detailed particle morphologies. (C) x50 image showing barium X-ray map of image shown in (A). (D) x300 image showing barium X-ray map of image shown in (B).

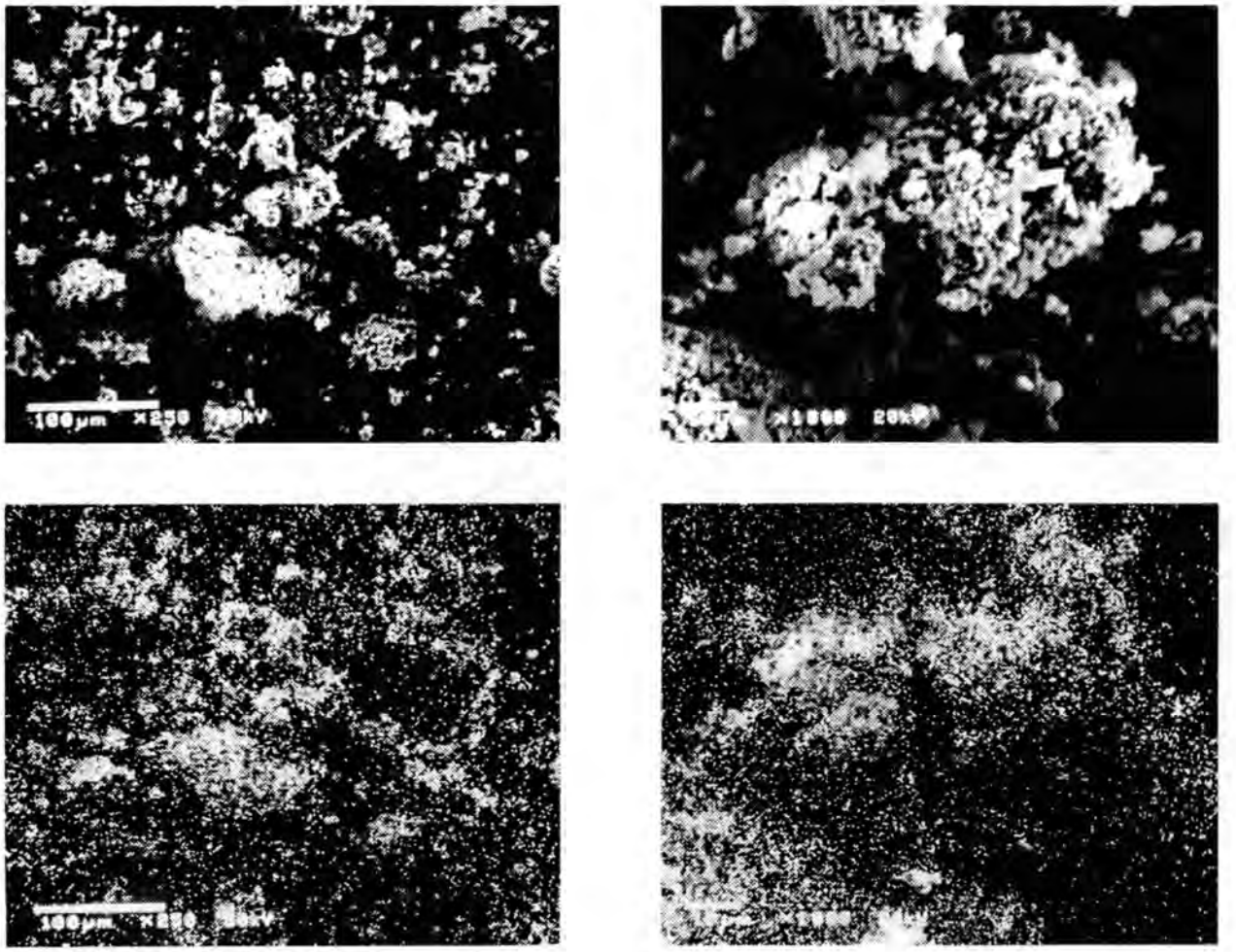

SEM photographs of sample 11374-10. (A) x250 image showing particle morphologies. (B) x1000 image showing detailed particle morphologies. (C) x250 image showing barium X-ray map of image shown in (A). (D) x1000 image showing barium X-ray map of image shown in (B).

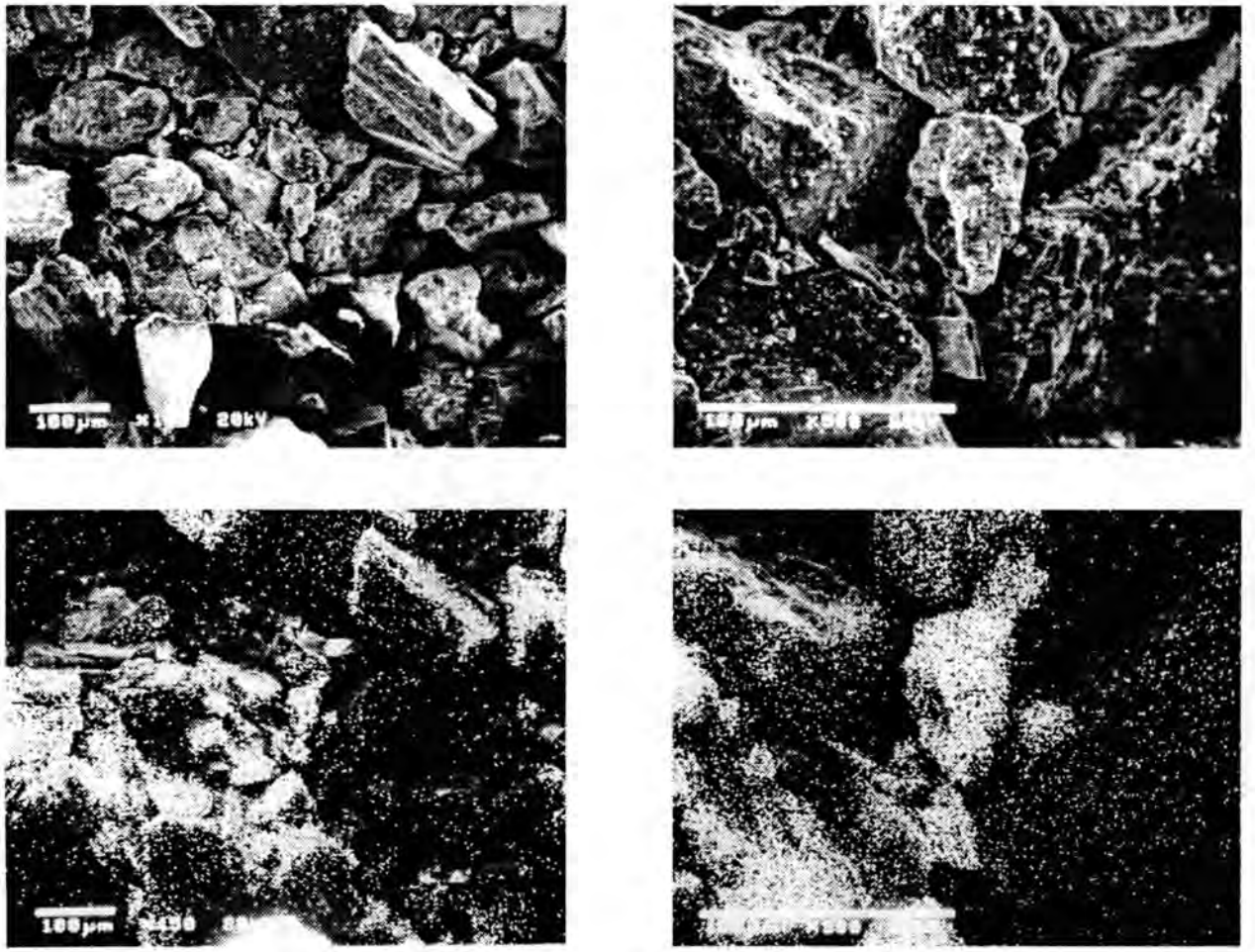

SEM photographs of sample 11374-11. (A) x100 image showing particle morphologies. (B) x500 image showing detailed particle morphologies. (C) x100 image showing barium X-ray map of image shown in (A). (D) x500 image showing barium X-ray map of image shown in (B).

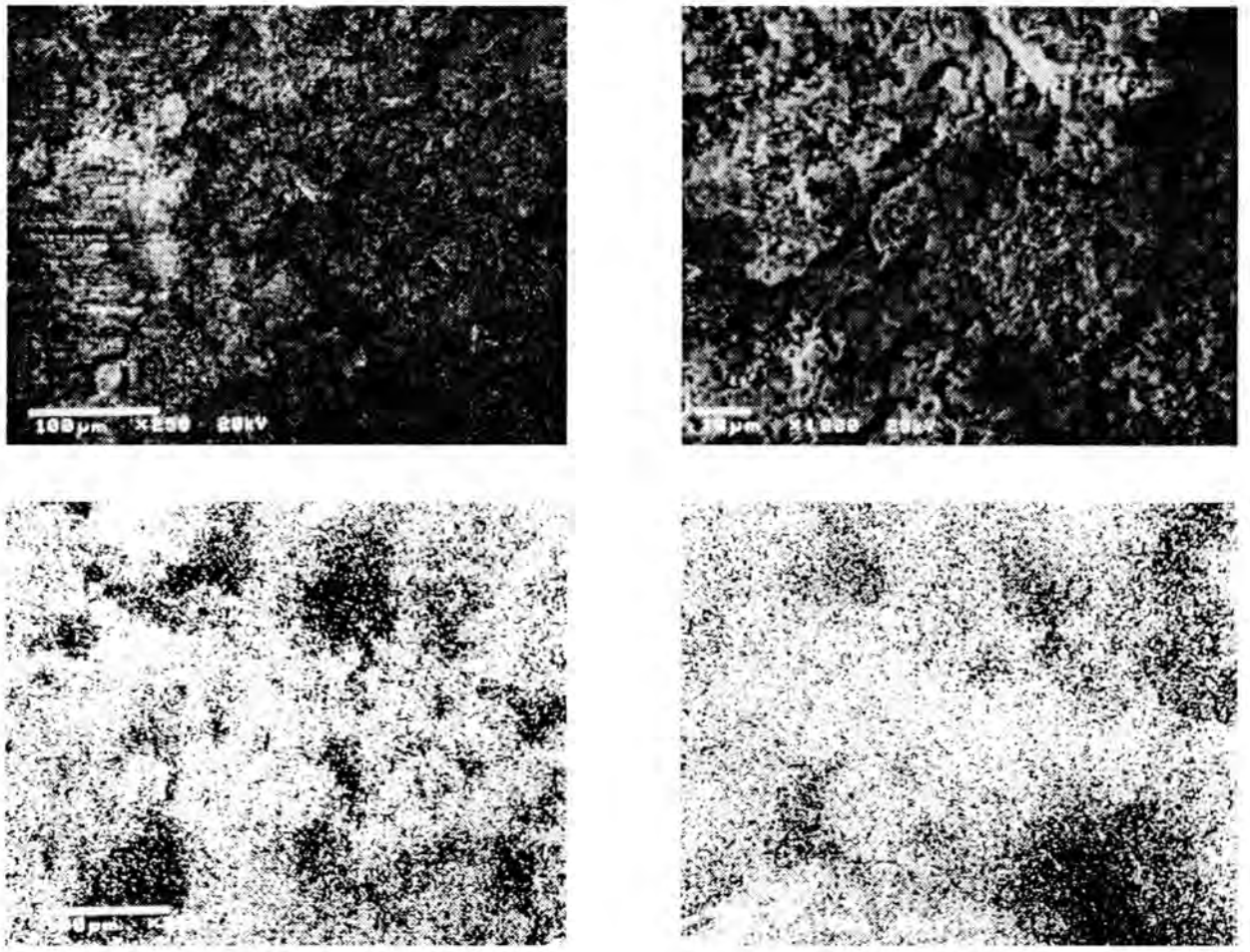

SEM photographs of sample 11374-12. (A) x100 image showing particle morphologies. (B) x1000 image showing detailed particle morphologies. (C) x100 image showing barium X-ray map of image shown in (A). (D) x1000 image showing barium X-ray map of image shown in (B).

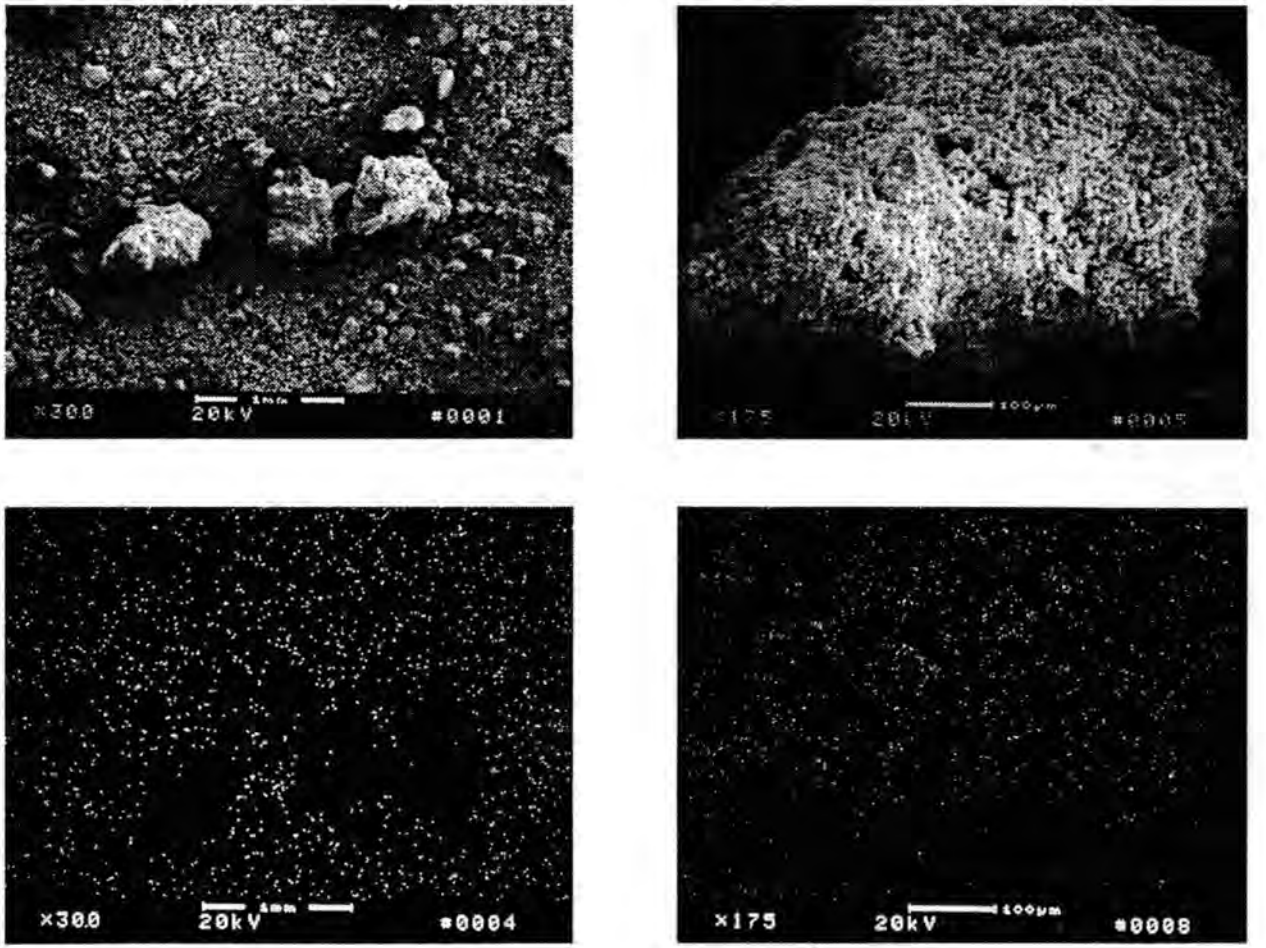

SEM photographs of sample 11374-58. (A) x30 image showing particle morphologies. (B) x175 image showing detailed particle morphologies. (C) x30 image showing barium X-ray map of image shown in (A). (D) x175 image showing barium X-ray map of image shown in (B).

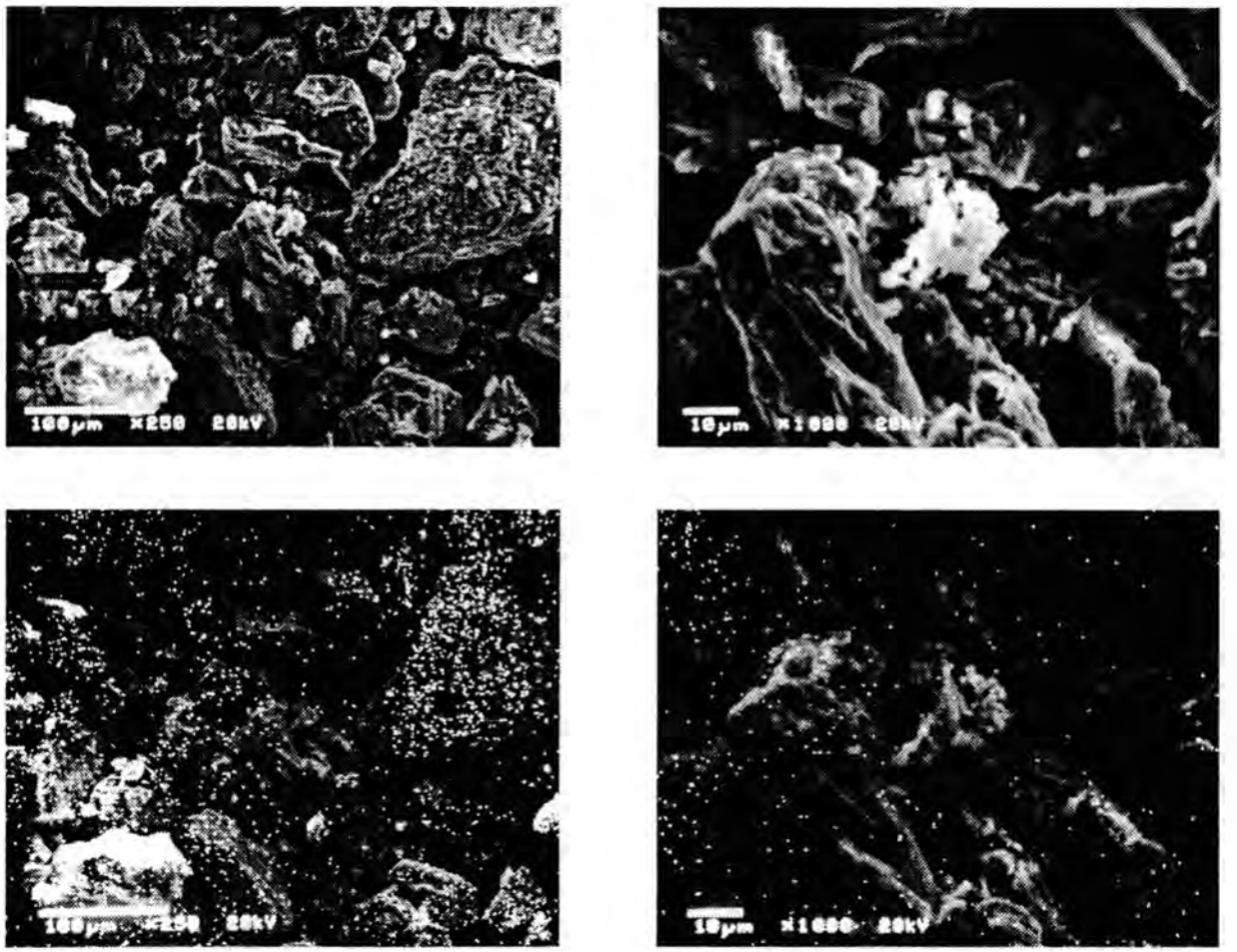

SEM photographs of sample 11374-80. (A) x250 image showing particle morphologies. (B) x1000 image showing detailed particle morphologies. (C) x250 image showing barium X-ray map of image shown in (A). (D) x1000 image showing barium X-ray map of image shown in (B).

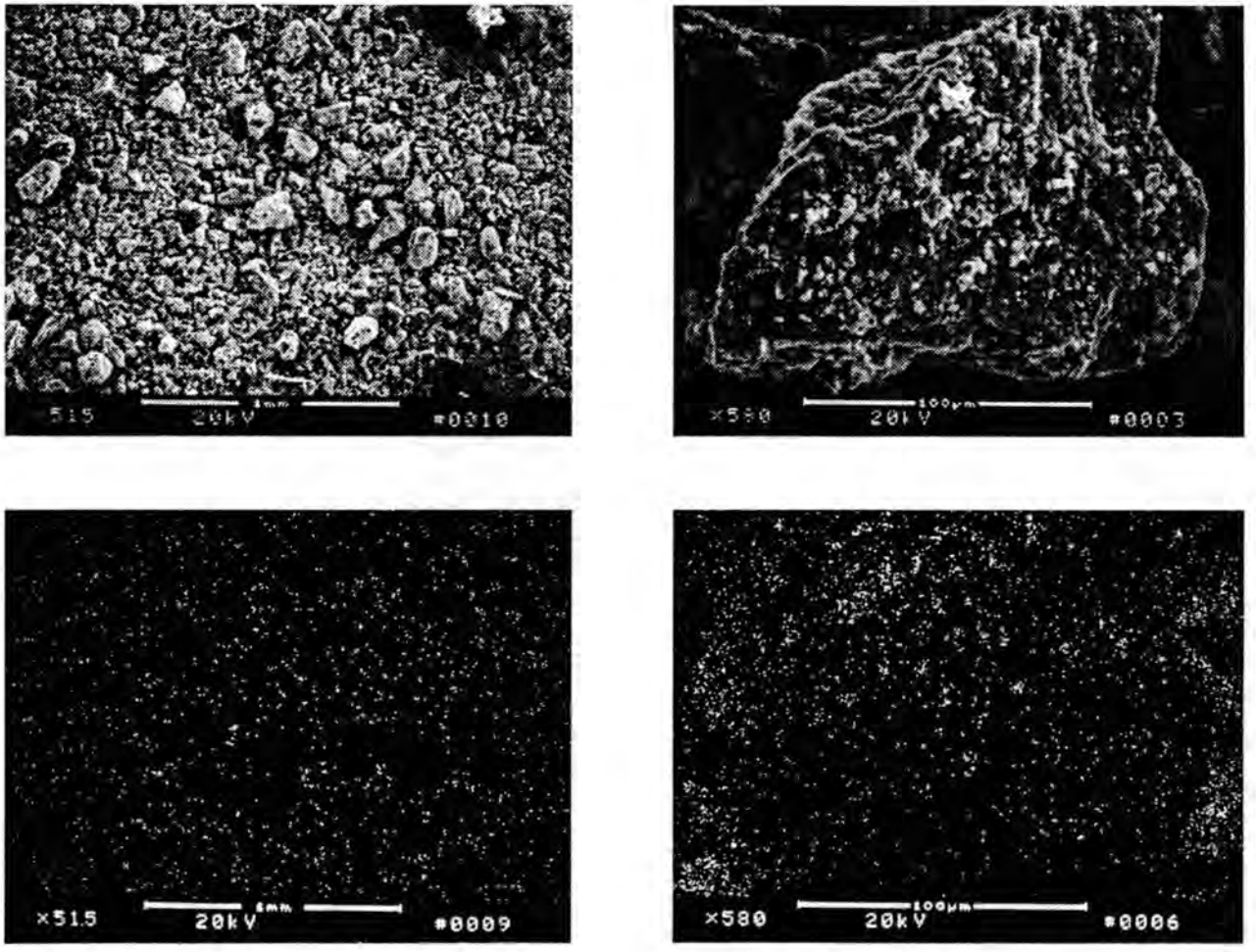

SEM photographs of sample 11374-81. (A) x50 image showing particle morphologies. (B) x1500 image showing detailed particle morphologies. (C) x50 image showing barium X-ray map of image shown in (A). (D) x500 image showing barium X-ray map of image shown in (B).

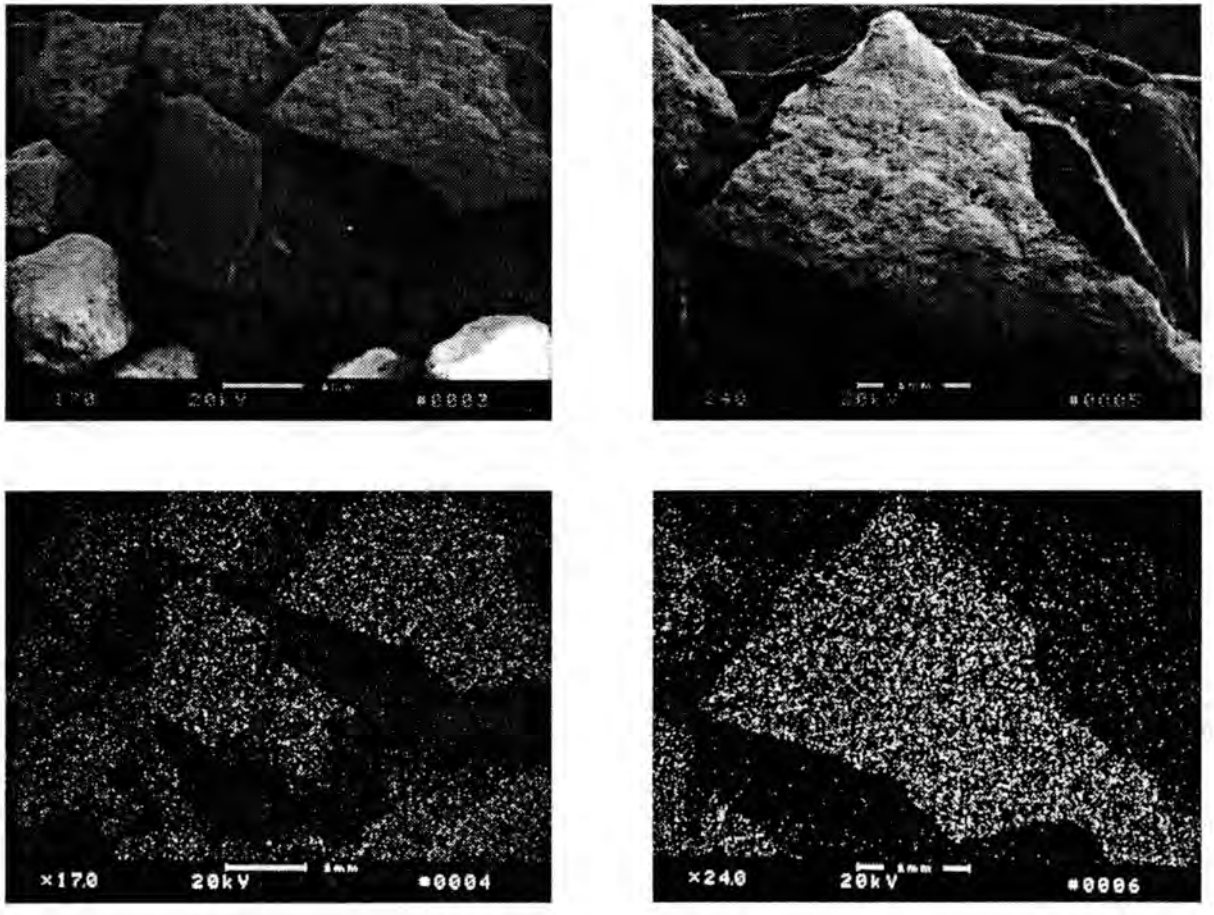

SEM photographs of sample 11374-83. (A) x17 image showing particle morphologies. (B) x24 image showing detailed particle morphologies. (C) x17 image showing barium X-ray map of image shown in (A). (D) x24 image showing barium X-ray map of image shown in (B).

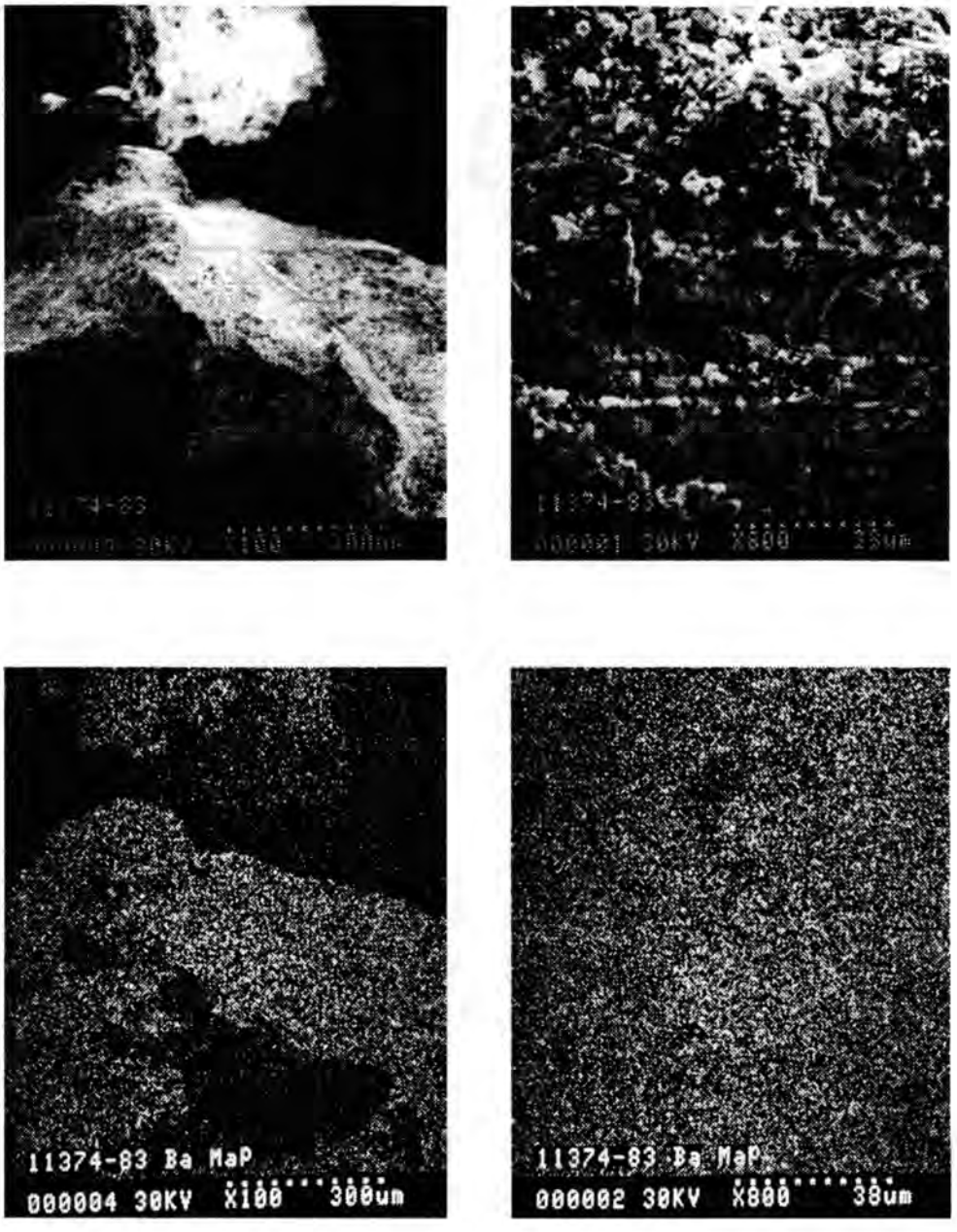

SEM photographs of sample 11374-83. (A) x100 image showing particle morphologies. (B) x300 image showing detailed particle morphologies. (C) x100 image showing barium X-ray map of image shown in (A). (D) x300 image showing barium X-ray map of image shown in (B).

KEVEX Results

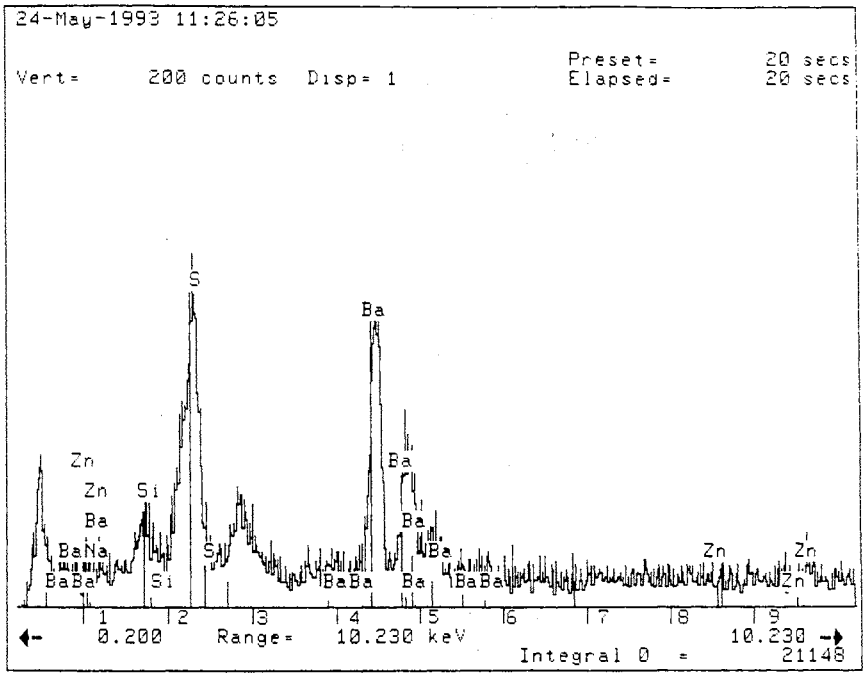

11374-2

SPECTRA ON WHITE MATERIAL

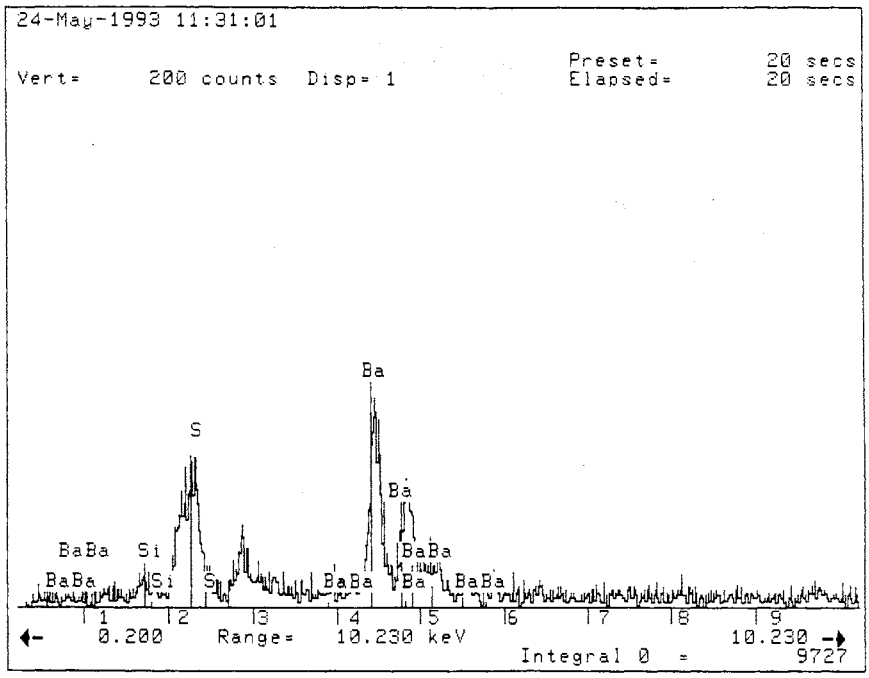

11374-2

SPECTRA ON DARK MATERIAL

KEVEX Results

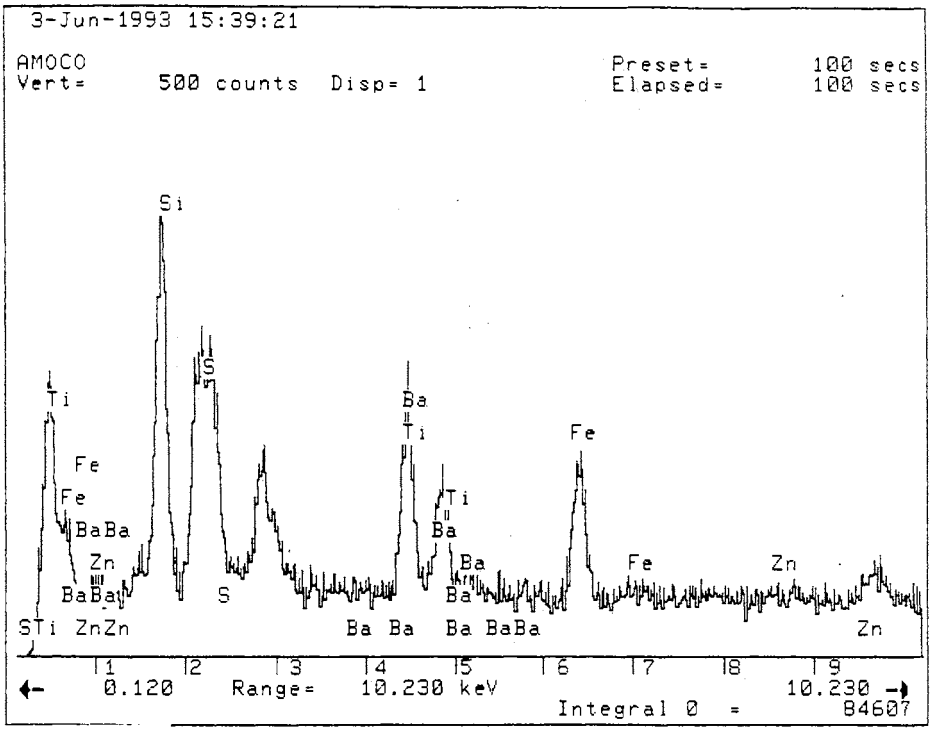

11374-3

SPECTRA ON WHITE MATERIAL

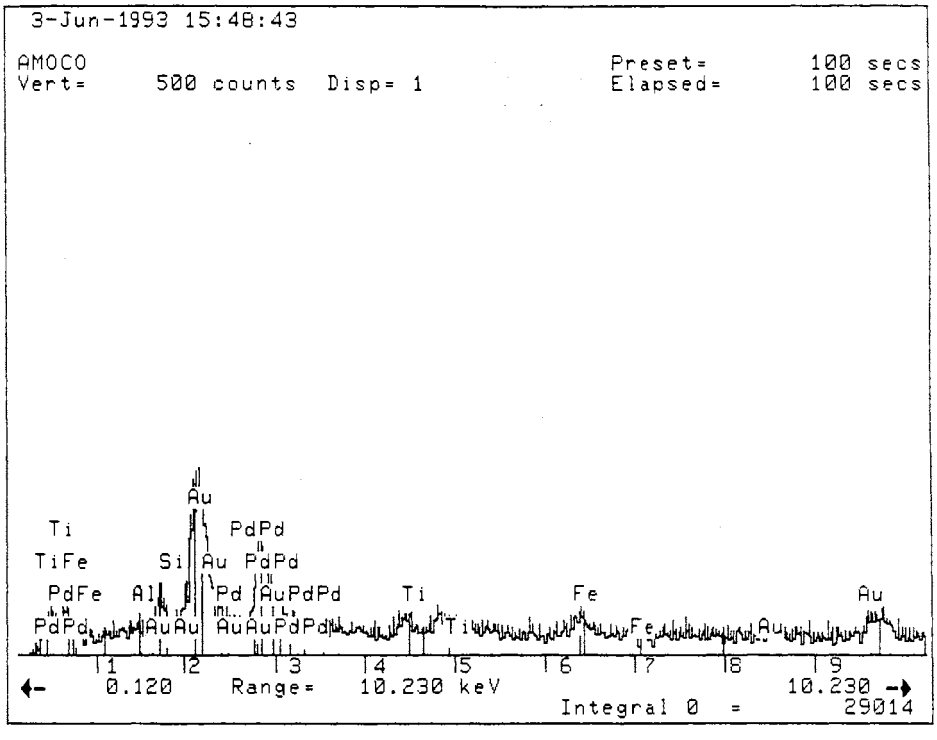

11374-3

SPECTRA ON DARK MATERIAL

KEVEX Results

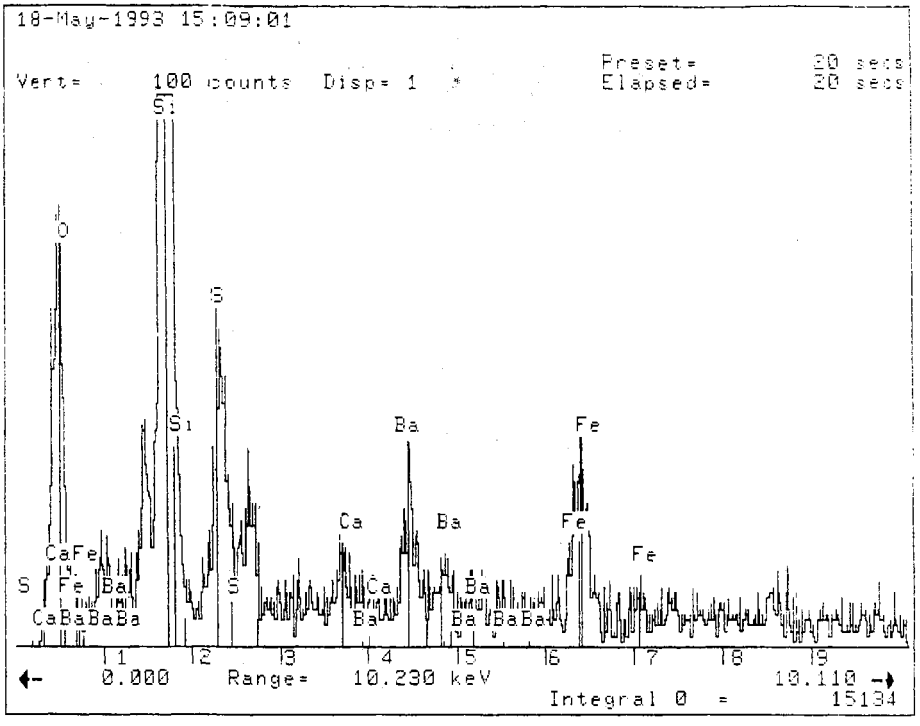

11374-5

SPECTRA ON WHITE MATERIAL

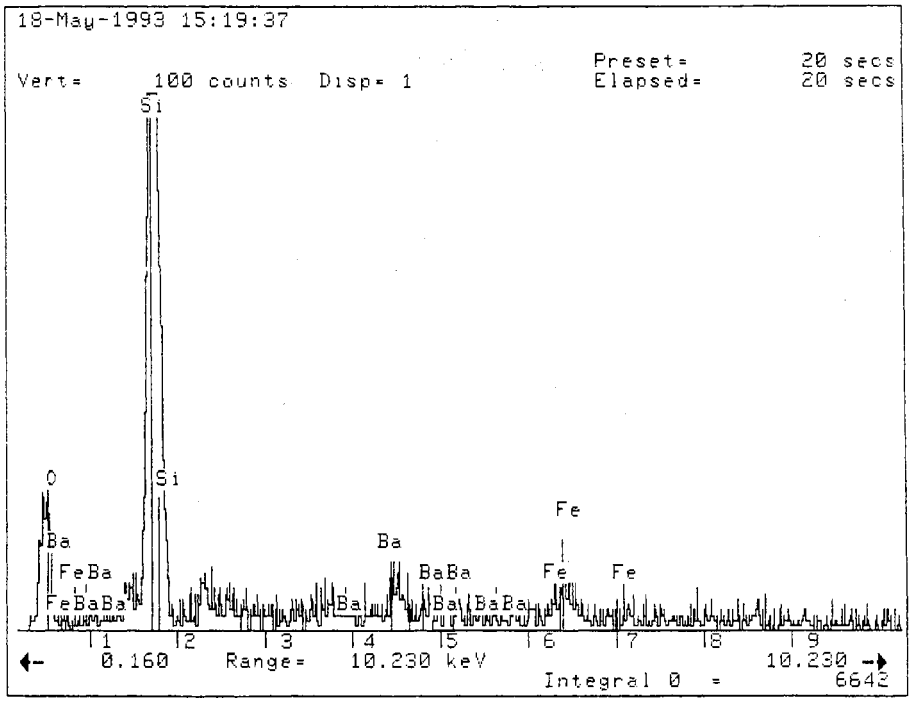

11374-5

SPECTRA ON DARK MATERIAL

KEVEX Results

11374-7

SPECTRA ON WHITE MATERIAL

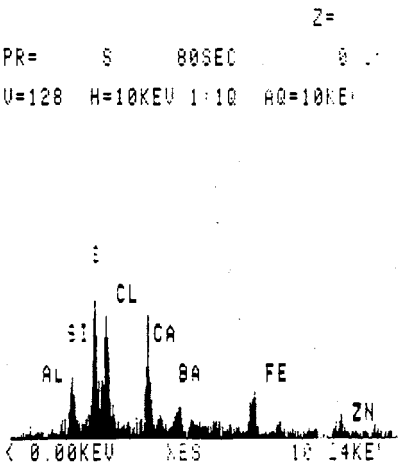

11374-7

SPECTRA ON DARK MATERIAL

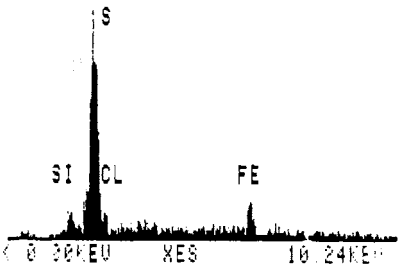

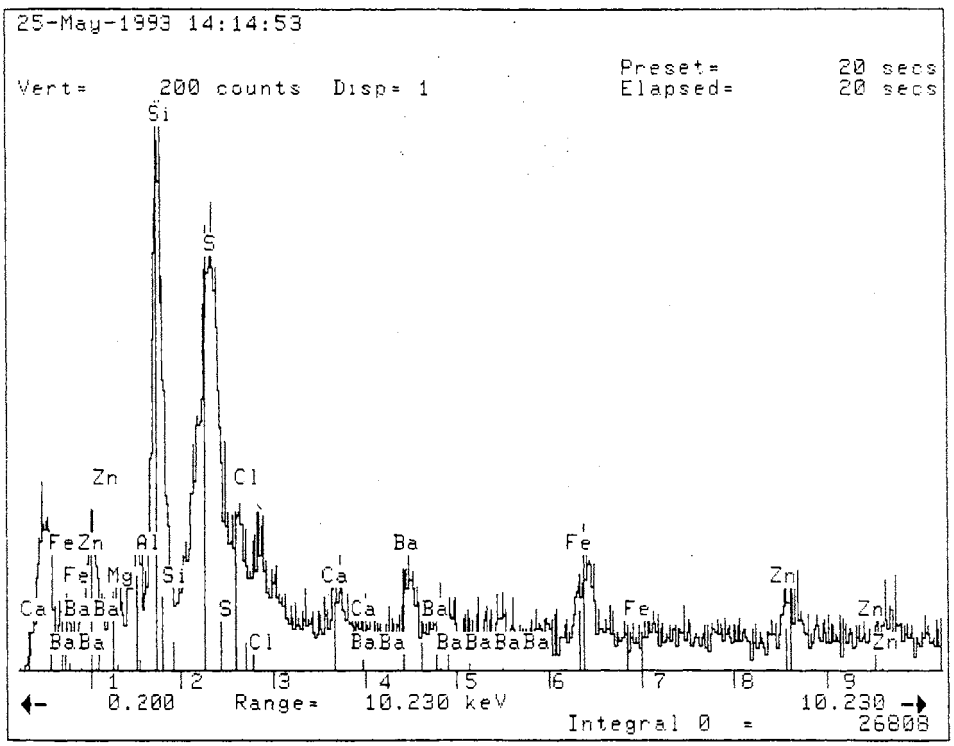

11374-8

SPECTRA ON WHITE MATERIAL

KEVEX Results

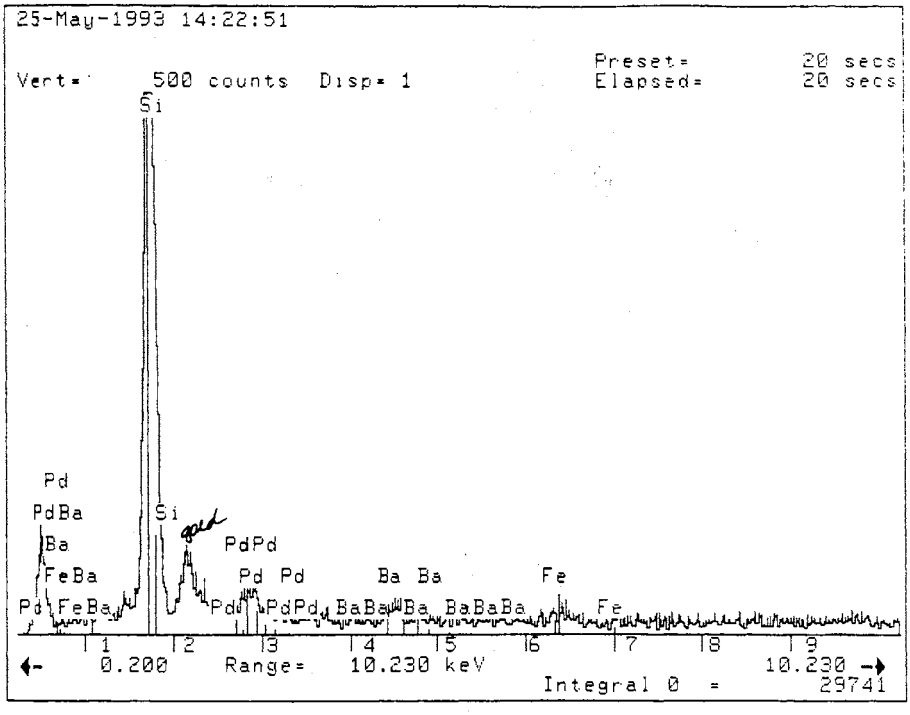

11374-8

SPECTRA ON DARK MATERIAL

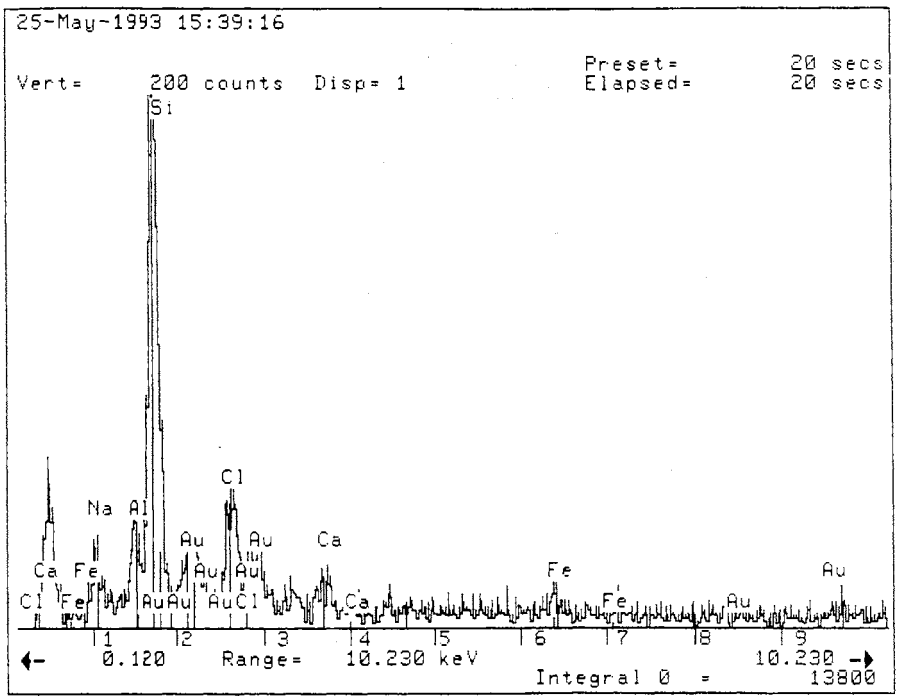

11374-9

SPECTRA ON WHITE MATERIAL

KEVEX Results

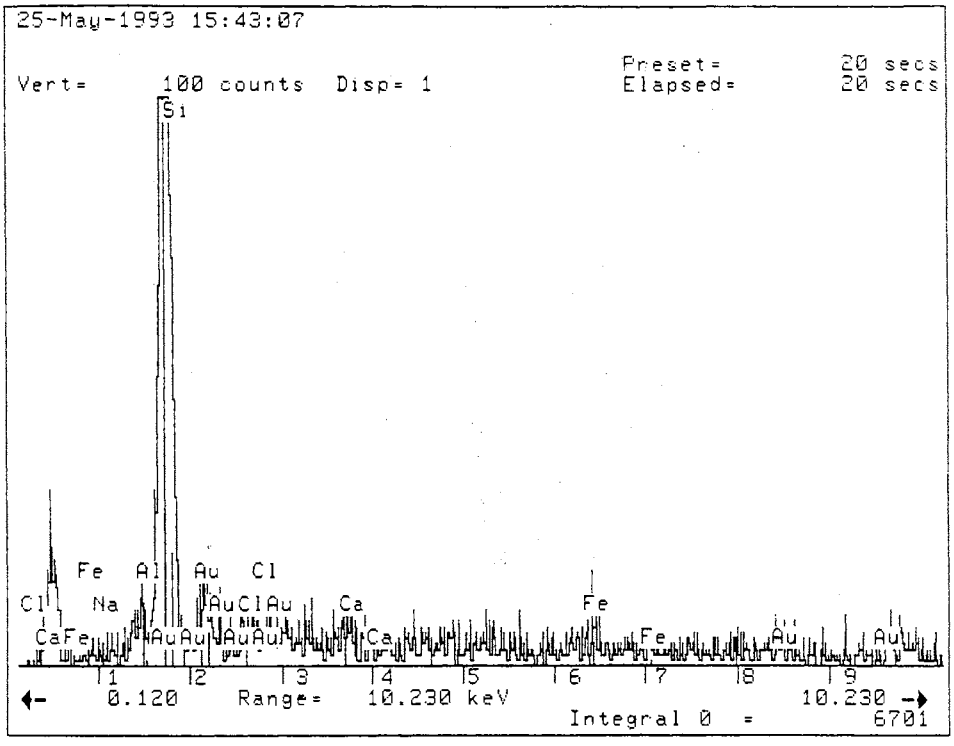

11374-9

SPECTRA ON DARK MATERIAL

11374-11

SPECTRA ON WHITE MATERIAL

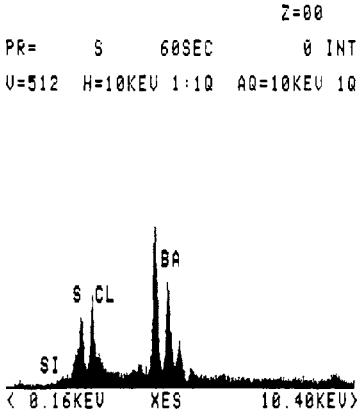

11374-11

SPECTRA ON DARK MATERIAL

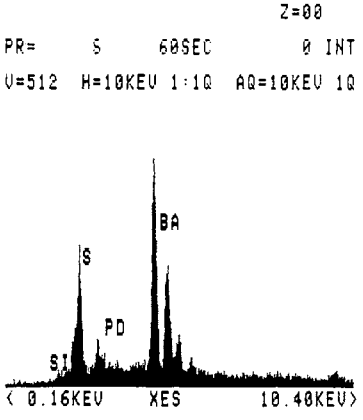

KEVEX Results

11374-12

SPECTRA ON WHITE MATERIAL

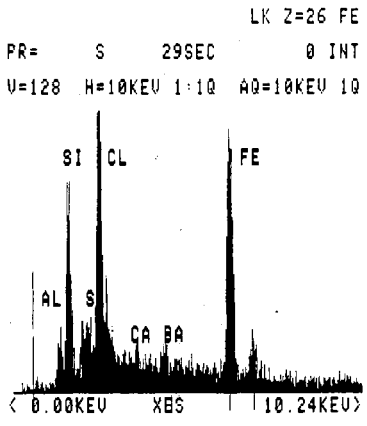

11374-12

SPECTRA ON DARK MATERIAL

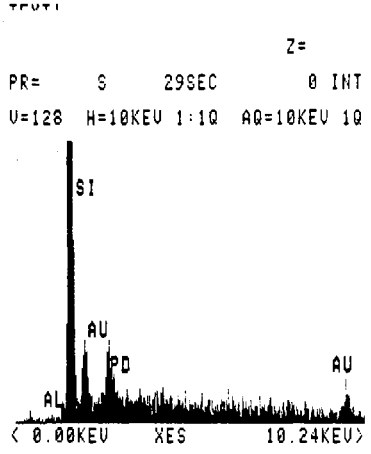

11374-57

SPECTRA ON WHITE MATERIAL

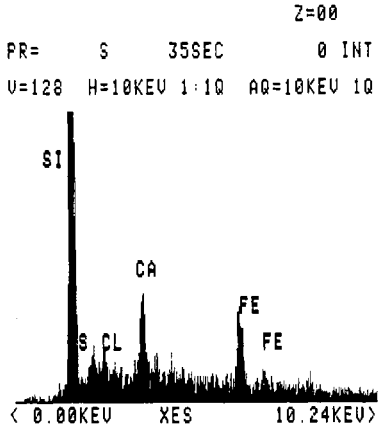

11374-57

SPECTRA ON DARK MATERIAL

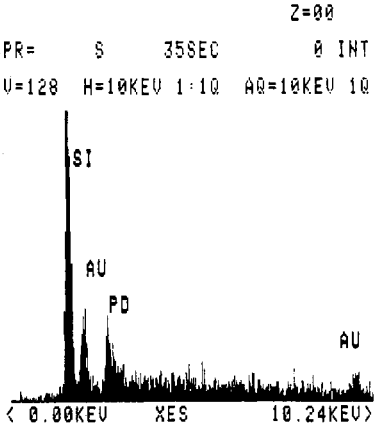

KEVEX Results

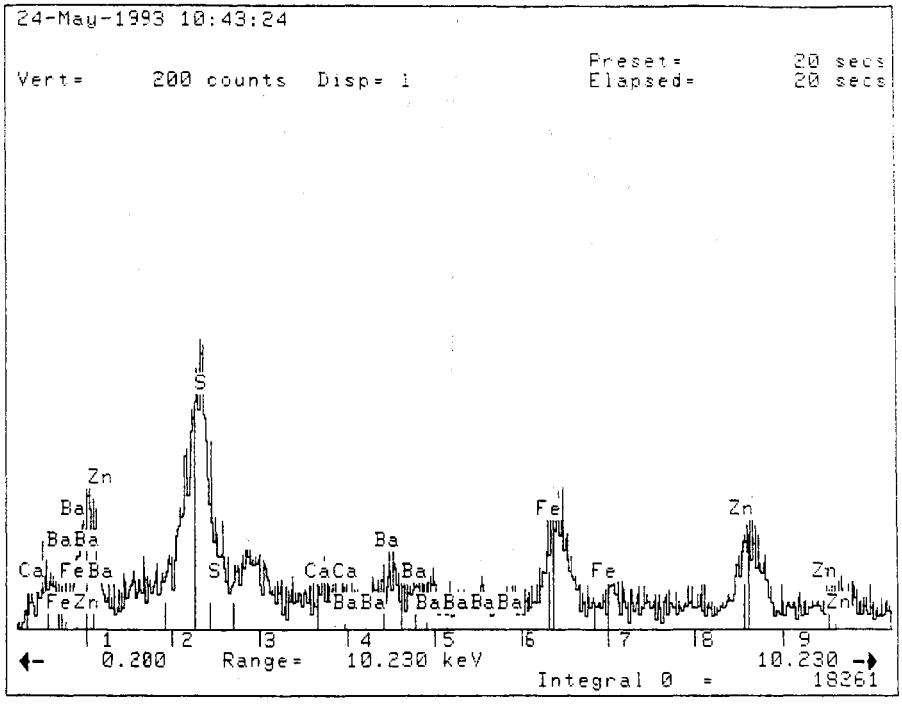

11374-58

SPECTRA ON WHITE MATERIAL

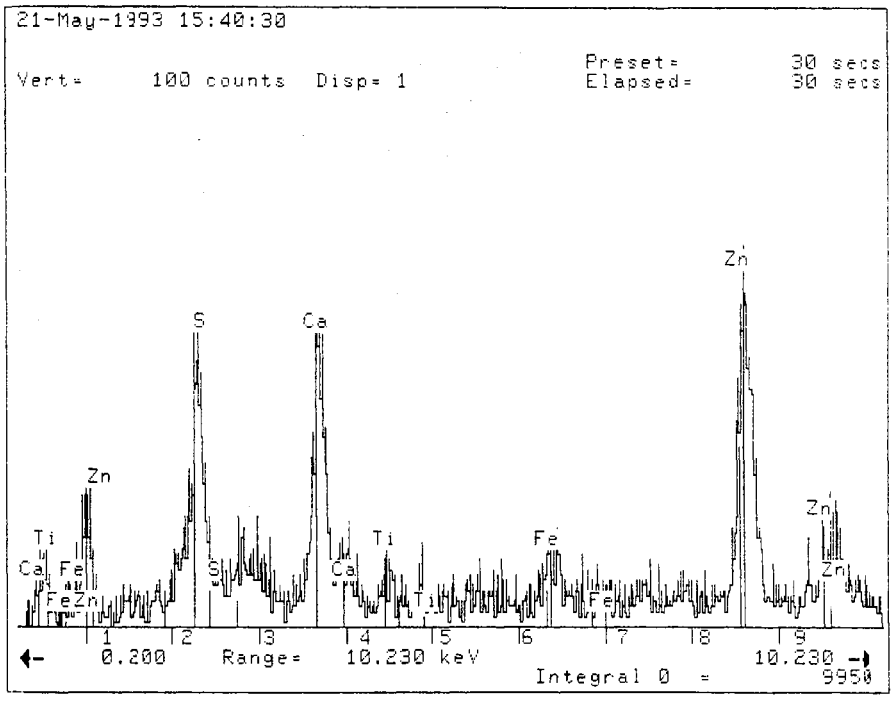

11374-58

SPECTRA ON WHITE MATERIAL

KEVEX Results

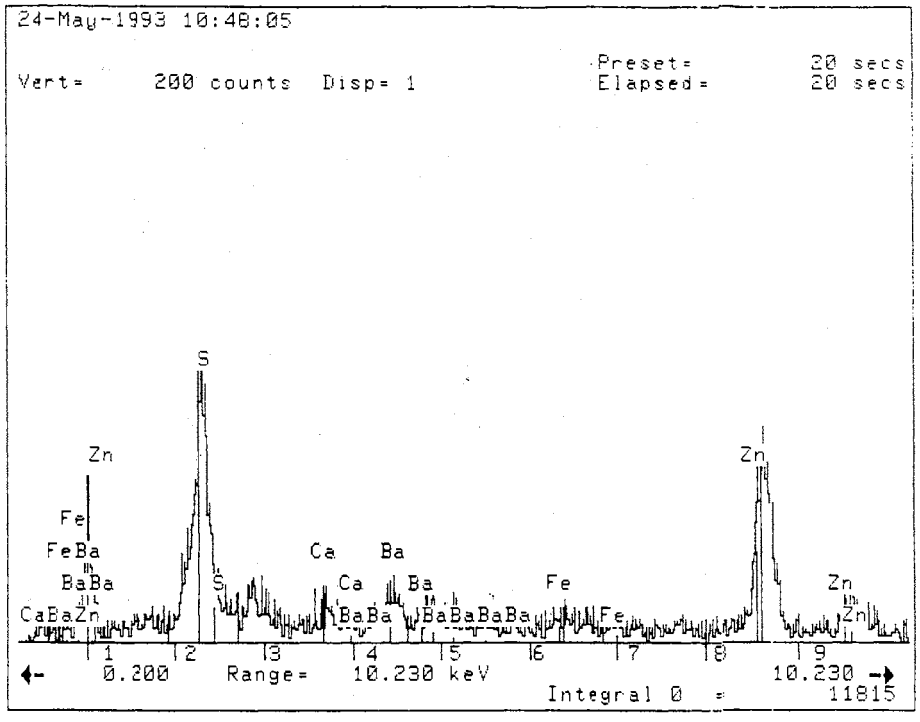

11374-58

SPECTRA ON DARK MATERIAL

113874-80

SPECTRA ON WHITE MATERIAL

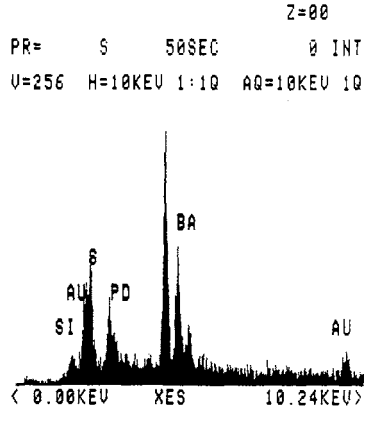

113874-80

SPECTRA ON DARK MATERIAL

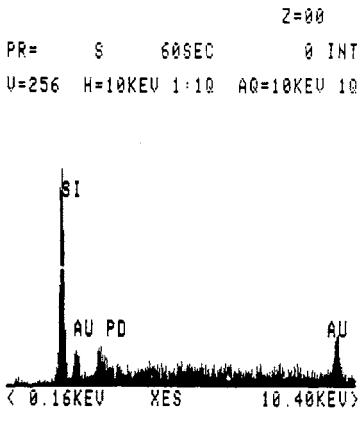

KEVEX Results

113874-81

SPECTRA ON WHITE MATERIAL

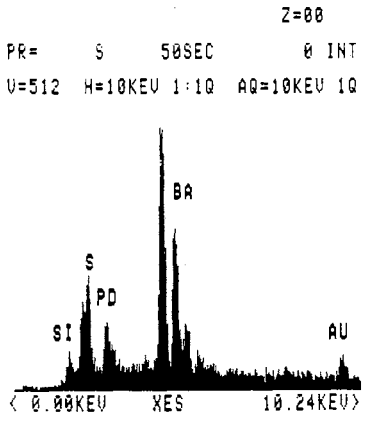

113874-81

SPECTRA ON DARK MATERIAL

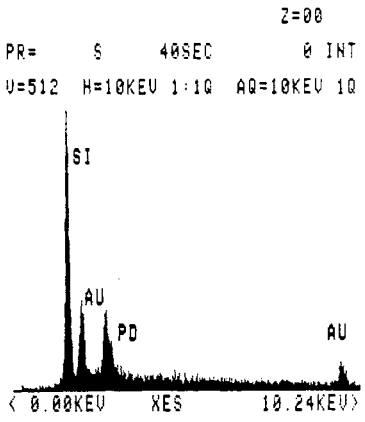

XRAL Data

XRAL

X-RAY ASSAY LABORATORIES

A DIVISION OF SGS CANADA INC.

1885 LESLIE STREET • DON MILLS, ONTARIO M3B 3J4 • CANADA

TEL: (416)445-5755 TELEX: 06-986947 FAX: (416)445-4152

CERTIFICATE OF ANALYSIS

REPORT 23006

TO: AMOCO PRODUCTION COMPANY, RESEARCH CENTRE
ATTN: MIYOUNG HAMMOND
P.O. BOX 3385
4502 EAST 41ST STREET
TULSA, OKLAHOMA 74102

CUSTOMER No. 816

DATE SUBMITTED
10-May-93

REF. FILE 14859-S6

Total Pages 1

5 S. SEDIMENT Proj. SEDIMENT/SCALE

	METHOD	DETECTION LIMIT
C %	LECO	.01
CO2 %	COULOM	.01
C ORG %	COULOM	.05
WRMAJ %	WR	.01
S PPM	XRF	50.
S %	LECO	.01
CL PPM	XRF	50.
TI PPM	XRF	5.
FE PPM	XRF	3.
FEO %	WET	.1
CO PPM	XRF	2.
NI PPM	XRF	2.
CU PPM	XRF	2.
ZN PPM	XRF	2.
GA PPM	XRF	3.
AS PPM	XRF	3.
SE PPM	XRF	3.

	METHOD	DETECTION LIMIT
RB PPM	XRF	2.
SR PPM	XRF	2.
Y PPM	XRF	2.
ZR PPM	XRF	3.
NB PPM	XRF	2.
MO PPM	XRF	2.
SN PPM	XRF	5.
SB PPM	XRF	3.
BA PPM	XRF	20.
TA PPM	XRF	2.
W PPM	XRF	5.
TL PPM	XRF	5.
PB PPM	XRF	2.
BI PPM	XRF	3.
TH PPM	XRF	2.
U PPM	XRF	2.

DATE 10-JUN-93

CERTIFIED BY .....
Jean H.L. Opdebeeck, General Manager

XRAL Data

X-RAY ASSAY LABORATORIES 01-APR-93 REPORT ----- REF. 14338 PAGE 1

SAMPLE	C % LECO	CO2 % COULOM	C ORG % COULOM	NA2O % WR	MGO % WR	AL2O3 % WR	SIO2 % WR	P2O5 % WR	S PPM XRF	S % LECO	CL PPM XRF
11374-1	8.44	30.4	.76	39.0	.08	.65	21.0	.07	<50	.03	27800
11374-2	.52	.89	3.79	.30	<.01	.21	22.3	.02	103000	9.77	3650
11374-3	1.83	1.39	5.13	.60	.06	1.21	14.2	.07	76600	7.60	4910
11374-4	.82	.41	1.05	.28	<.01	.56	2.07	.05	105000	10.3	5690
11374-5	1.67	2.60	9.84	.81	.10	1.66	77.4	.05	14400	.87	14700
11374-6	.30	.13	.50	<.01	<.01	<.01	.84	.02	119000	12.8	1910
11374-7	1.09	2.92	.85	.49	.08	.42	72.0	.03	21900	1.22	39000
11374-8	.61	.55	2.23	.52	.17	.43	87.0	.05	11300	.73	18800
11374-9	1.07	1.91	6.23	1.23	.19	3.85	82.8	.05	4260	.31	12900
11374-10	4.30	2.34	5.74	.67	.35	2.66	24.2	.26	80600	6.98	2070
11374-11	.25	.17	.12	<.01	<.01	.32	1.99	.02	116000	12.6	1720
11374-12	.15	.17	.73	.20	.14	.45	85.5	.03	17100	1.05	7270
D 11374-1	8.42	30.4	.60	38.4	.08	.66	21.0	.03	<50	.04	28000
D 11374-12	--	--	--	.20	.13	.43	87.3	.03	--	--	--

SAMPLE	K2O % WR	CAO % WR	TI PPM XRF	TIO2 % WR	CR2O3 % WR	MNO % WR	FE PPM XRF	FEO % WET	FE2O3 % WR	CO PPM XRF	NI PPM XRF
11374-1	.20	.39	347	.051	<.01	.02	1950	.1	.61	34	16
11374-2	.28	.13	369	.263	<.01	.02	449	.1	.17	12	31
11374-3	.28	1.72	925	.344	.02	.22	169000	18.7	28.1	45	146
11374-4	.13	.92	579	.287	<.01	.11	106000	1.9	13.7	20	216
11374-5	.62	3.01	2110	.451	<.01	.05	15200	1.1	2.78	47	25
11374-6	.11	.38	275	.259	<.01	.01	<3	<.1	<.01	12	11
11374-7	.25	4.39	1050	.232	.01	.06	43900	2.9	7.93	38	71
11374-8	.26	.61	2230	.426	.02	.02	7190	1.1	1.50	78	35
11374-9	1.05	2.93	1910	.380	<.01	.07	4280	.4	.84	77	17
11374-10	.44	2.88	1030	.351	.03	.13	75000	5.9	10.7	34	115
11374-11	.18	.12	288	.269	<.01	.04	14900	.9	2.44	18	25
11374-12	.21	.31	1240	.234	<.01	.01	1540	.2	.40	70	15
D 11374-1	.20	.31	342	.062	<.01	.02	1970	.1	.58	34	17
D 11374-12	.22	.32	--	.245	<.01	.01	--	--	.42	--	--

SAMPLE	CU PPM XRF	ZN PPM XRF	GA PPM XRF	AS PPM XRF	SE PPM XRF	RB PPM XRF	RB PPM WR	SR PPM XRF	SR PPM WR	Y PPM XRF	Y PPM WR
11374-1	3	38	13	7	18	7	<10	73	122	<2	<10
11374-2	295	103	<3	6	6	12	<10	7490	3490	<2	<10
11374-3	528	3750	<3	50	10	11	<10	4470	1850	<2	<10
11374-4	591	1170	<3	41	<3	11	<10	29000	10400	<2	<10
11374-5	105	1670	10	64	22	16	<10	1270	1460	<2	18
11374-6	297	138	<3	<3	<3	<2	<10	28200	10200	<2	<10
11374-7	754	108	7	11	54	<2	18	2470	2410	<2	<10
11374-8	64	2700	14	540	42	5	<10	1140	1440	<2	15
11374-9	28	247	16	25	43	31	22	513	642	<2	17
11374-10	713	10900	<3	234	7	7	<10	4820	2590	<2	<10
11374-11	292	520	<3	6	<3	<2	<10	10600	3940	<2	<10
11374-12	15	421	10	37	40	<2	<10	907	1050	<2	<10
D 11374-1	4	41	14	5	19	6	31	75	96	<2	<10
D 11374-12	--	--	--	--	--	--	<10	--	1080	--	<10

SAMPLE	ZR PPM XRF	ZR PPM WR	NB PPM XRF	NB PPM WR	MO PPM XRF	SN PPM XRF	SB PPM XRF	BA PPM XRF	BA PPM WR	TA PPM XRF	W PPM XRF
11374-1	37	26	3	<10	18	8	12	913	468	14	242
11374-2	<3	<10	<2	<10	5	<5	41	228000	409000	3	79
11374-3	<3	41	<2	<10	69	<5	27	182000	230000	<2	107
11374-4	<3	<10	<2	<10	43	<5	64	231000	367000	36	<5
11374-5	696	790	12	<10	<2	<5	15	26800	30600	4	302
11374-6	<3	<10	<2	<10	9	<5	10	256000	503000	64	47
11374-7	80	133	5	<10	30	141	47	40700	47900	<2	768
11374-8	156	161	20	29	16	<5	25	18000	24100	25	597
11374-9	578	684	11	23	<2	9	23	5730	6840	14	603
11374-10	<3	16	<2	<10	54	<5	73	162000	254000	<2	77
11374-11	<3	<10	<2	<10	53	<5	39	260000	512000	38	64
11374-12	<3	41	7	<10	<2	<5	<3	39100	46800	19	537
D 11374-1	35	32	4	<10	19	7	12	537	689	14	235
D 11374-12	--	50	--	11	--	--	--	--	47300	--	--

SAMPLE	TL PPM XRF	PB PPM XRF	BI PPM XRF	TH PPM XRF	U PPM XRF	LOI % WR	SUM % WR
11374-1	5	4	<3	<2	<2	29.5	91.6
11374-2	9	145	22	24	<2	1.77	71.5

XRAL Data

* APR 01 '93 16:29 X-RAY ASSAY LAB 416 445 4152

X-RAY ASSAY LABORATORIES 01-APR-93 REPORT ----- REF. 14338 PAGE 2

	SAMPLE	TL PPM XRF	PB PPM XRF	BI PPM XRF	TH PPM XRF	U PPM XRF	LOI % WR	SUM % WR
	11374-3	14	572	9	<2	<2	4.95	77.7
	11374-4	<3	1080	<3	16	<2	2.70	62.8
	11374-5	<3	531	7	9	3	5.65	96.3
	11374-6	4	61	<3	<2	<2	1.54	60.5
	11374-7	<3	76	6	<2	2	6.62	98.2
	11374-8	<3	4500	7	47	<2	3.85	97.7
	11374-9	6	160	10	4	4	4.50	98.8
	11374-10	57	3950	<3	46	<2	18.8	90.1
	11374-11	8	193	15	<2	<2	1.23	64.2
	11374-12	<3	306	<3	8	<2	1.45	97.3
D	11374-1	<3	6	<3	<2	<2	27.4	88.8
D	11374-12	--	--	--	--	--	1.45	96.2

XRAL Data

XRAL

10-JUN-93 REPORT Z3005 REF.FILE 14858-86 PAGE 1 OF 1

ELEMENT	METHOD	11374-57	11374-57-D	11374-58
CO2 %	COULOM	9.43	9.40	2.57
S PPM	XRF	151000	150000	6770
S %	LECO	13.7	13.9	.50
CL PPM	XRF	6210	6220	4740
TI PPM	XRF	295	292	1240
FE PPM	XRF	38800	39200	7160
FEO %	WET	2.6	2.5	.8
CO PPM	XRF	31	35	70
NI PPM	XRF	90	92	19
CU PPM	XRF	353	351	18
ZN PPM	XRF	219000	221000	2310
GA PPM	XRF	<3	<3	12
AS PPM	XRF	429	430	35
SE PPM	XRF	<3	<3	15
RB PPM	XRF	8	9	12
SR PPM	XRF	6560	6660	382
Y PPM	XRF	<2	<2	<2
ZR PPM	XRF	<3	<3	276
NB PPM	XRF	<2	<2	9
MO PPM	XRF	33	31	<2
SN PPM	XRF	<5	<5	<5
SB PPM	XRF	<3	<3	17
BA PPM	XRF	106000	105000	3520
TA PPM	XRF	<2	<2	12
W PPM	XRF	<5	<5	578
TL PPM	XRF	74	75	<5
PB PPM	XRF	12200	12300	236
BI PPM	XRF	12	11	<3
TH PPM	XRF	141	138	3
U PPM	XRF	<2	<2	3
SIO2 %	WR	2.62	2.58	87.0
AL2O3 %	WR	.11	.10	1.54
CAO %	WR	11.4	11.1	3.39
MGO %	WR	.07	.07	.36
NA2O %	WR	2.90	2.86	.40
K2O %	WR	.06	.05	.36
FE2O3 %	WR	3.66	3.61	1.59
MNO %	WR	.48	.47	.03
TIO2 %	WR	.114	.109	.227
P2O5 %	WR	.50	.49	.05
CR2O3 %	WR	<.01	<.01	<.01
LOI %	WR	7.70	7.54	4.30
SUM %	WR	29.6	29.0	99.3

D - QUALITY CONTROL DUPLICATE

X-RAY ASSAY LABORATORIES 1885 Leslie Street Don Mills Ontario M3B 3J4 (416)445-5755 Fax (416)445-4152 Tlx 06-986947
Member of the SGS Group (Société Générale de Surveillance)

XRAL Data

XRAL

10-JUN-93 REPORT 23006 REF.FILE 14859-86 PAGE 1 OF 1

ELEMENT	METHOD	11374-80	11374-80-D	11374-81	11374-82	11374-83	11374-84
C %	LECO	.18	.17	.46	.56	.26	13.0
CO2 %	COULOM	.34	.34	.34	.21	.09	.42
C ORG %	COULOM	.29	.33	2.83	1.49	2.03	14.6
S PPM	XRF	43300	43600	48400	5530	121000	63100
S %	LECO	3.20	3.07	3.88	.39	13.7	6.60
CL PPM	XRF	34200	34000	7020	6090	621	355000
TI PPM	XRF	909	916	841	1240	287	550
FE PPM	XRF	2020	1920	3890	4930	1950	46200
FEO %	WET	.3	.3	.5	.6	.2	2.0
CO PPM	XRF	34	36	35	86	15	28
NI PPM	XRF	11	14	29	32	52	56
CU PPM	XRF	72	73	731	91	404	82
ZN PPM	XRF	115	109	271	204	291	11800
GA PPM	XRF	3	4	<3	16	<3	<3
AS PPM	XRF	67	68	253	125	444	192
SE PPM	XRF	8	8	14	18	<3	10
RB PPM	XRF	28	28	25	32	14	<2
SR PPM	XRF	1070	1080	4380	650	30900	535
Y PPM	XRF	<2	<2	<2	<2	<2	<2
ZR PPM	XRF	<3	<3	<3	213	<3	17
NB PPM	XRF	4	3	<2	7	<2	6
MO PPM	XRF	<2	<2	<2	<2	14	2
SN PPM	XRF	<5	<5	<5	8	<5	<5
SB PPM	XRF	36	38	30	13	48	3
BA PPM	XRF	101000	101000	110000	12900	247000	17800
TA PPM	XRF	17	17	14	12	79	<2
W PPM	XRF	259	266	494	661	55	117
TL PPM	XRF	<5	<5	<5	<5	<5	38
PB PPM	XRF	872	863	3480	919	16200	2150
BI PPM	XRF	6	4	<3	<3	26	<3
TH PPM	XRF	12	13	38	13	178	20
U PPM	XRF	<2	<2	<2	<2	<2	<2
SIO2 %	WR	62.9	62.9	62.0	84.7	1.27	24.7
AL2O3 %	WR	4.48	4.52	3.53	4.54	.59	3.12
CAO %	WR	.93	.96	1.35	.82	.36	1.01
MGO %	WR	.25	.27	.56	.22	<.01	1.31
NA2O %	WR	2.44	2.43	1.18	1.29	.56	7.22
K2O %	WR	1.04	1.05	.86	1.10	.04	.67
FE2O3 %	WR	.75	.77	.83	1.24	.50	2.22
MNO %	WR	.03	.03	.03	.03	.01	.04
TIO2 %	WR	.242	.273	.226	.236	.262	.269
P2O5 %	WR	.04	.04	.04	.05	.14	.09
CR2O3 %	WR	<.01	<.01	<.01	<.01	<.01	<.01
LOI %	WR	2.70	2.47	2.16	2.08	.62	34.6
SUM %	WR	75.8	75.7	72.8	96.3	4.4	75.3

D - QUALITY CONTROL DUPLICATE

X-RAY ASSAY LABORATORIES 1885 Leslie Street Don Mills Ontario M3B 3J4 (416)445-6755 Fax (416)445-4152 Tlx 06-98894
Member of the SGS Group (Société Générale de Surveillance)

APPENDIX B

ORIGINAL DATA PERTAINING TO SOIL SHIELDING EXPERIMENT

Dose Rate in μrem/hr From the Shielding Experiment

Distance from Source	Depth of Seashells					Depth of Ottawa Sand			Depth of Limestone Pellets								Thickness of Lead		
	0	1"	2"	3"	4"	0	1"	2"	0	1"	2"	3"	4"	5"	6"	7"	0	1/8"	1/4"
1"	120	-	-	-	-	120	-	-	120	82	-	-	-	-	-	-	120	25	19
2"	90	85	-	-	-	89	75	-	89	73	68	-	-	-	-	-	89	25	19
3"	70	70	60	-	-	70	70	55	70	63	61	50	-	-	-	-	70	22	18
4"	60	60	50	47	-	58	53	50	58	55	53	46	41	-	-	-	58	21	19
5"	48	47	45	40	35	50	48	44	50	48	45	41	39	29	-	-	50	19	18
6"	40	40	38	35	31	42	42	39	42	41	40	38	35	28	27	-	38	19	15
7"	35	35	34	30	30	38	36	35	38	35	37	32	31	27	27	21	38	19	15
8"	31	31	30	30	30	32	31	31	32	34	33	30	28	25	25	22	32	18	14

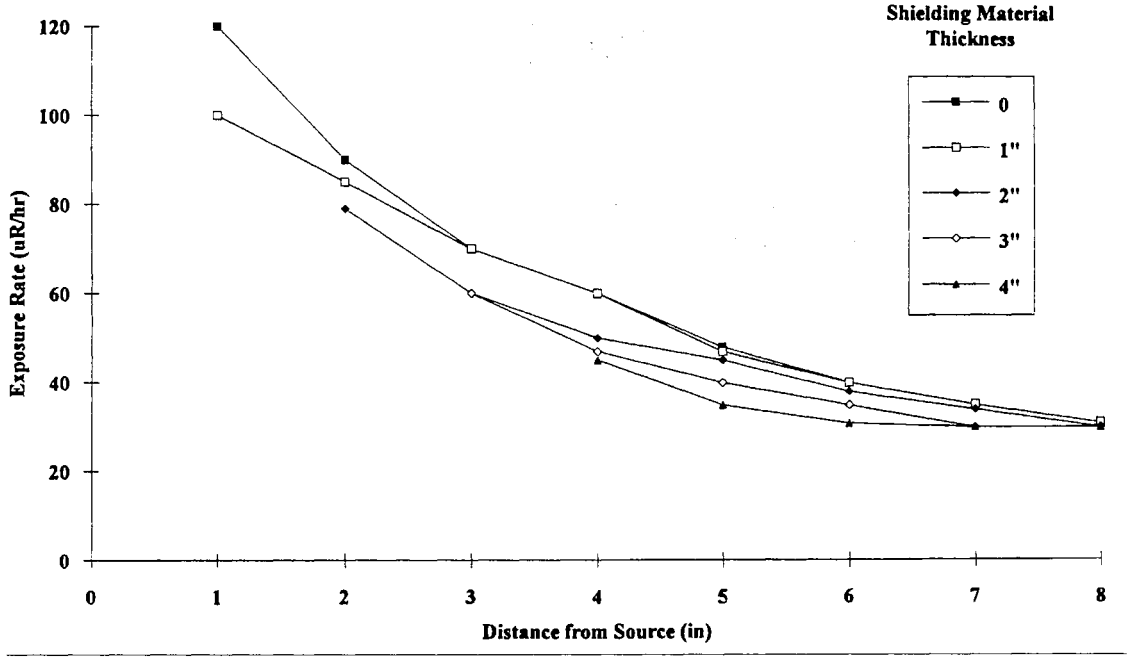

Exposure rate curve using mollusc shells as shielding material.

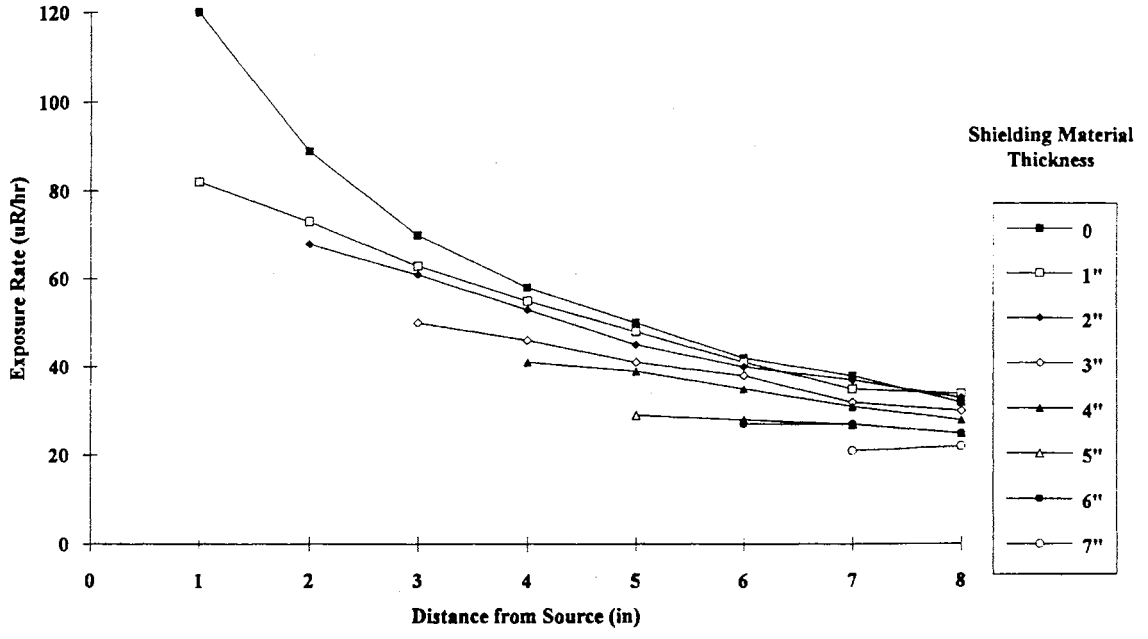

Exposure rate curve using limestone pellets as shielding material.

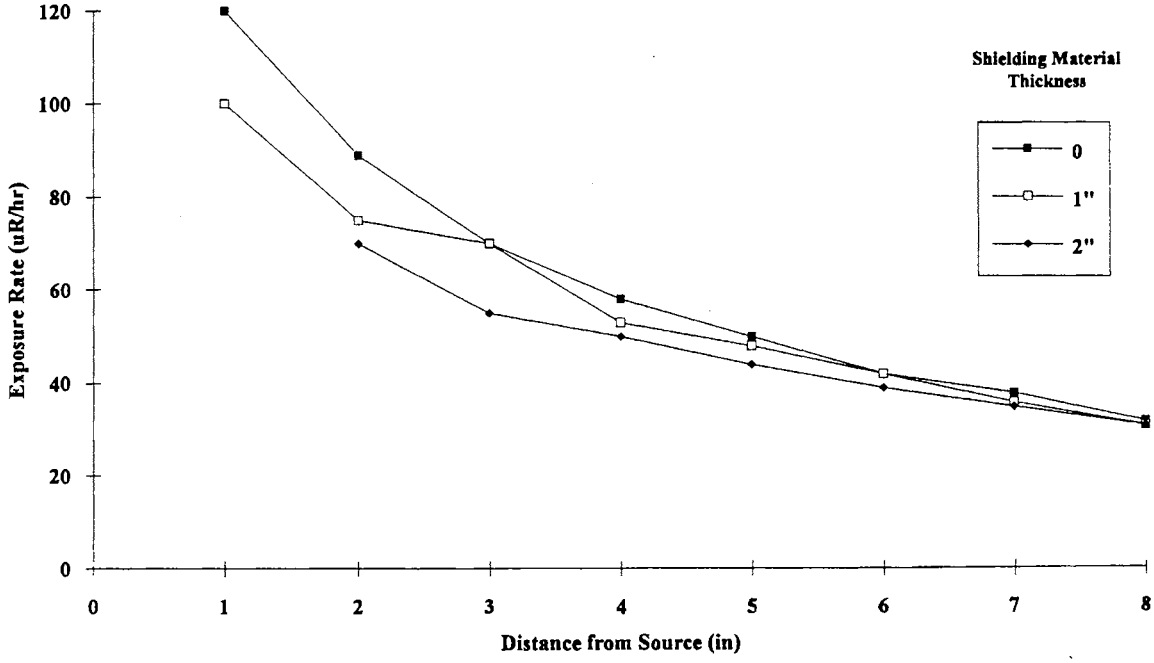

Exposure rate curve using Ottawa sand as shielding material.

```
*****************************************************************************
*****        G A M M A   S P E C T R U M   A N A L Y S I S          *****
*****************************************************************************

Report Generated On                 :  2-08-94 10:35:56 PM

Sample Title                        : NORMCO scale
Sample Identification               : 94020701        11385-60
Sample Type                         : soil
Sample Geometry                     : 3

Peak Locate Threshold               :  5.00
Peak Locate Range (in channels)     :     1 -  4096
Identification Energy Tolerance     :  1.00

Sample Size                         :  5.900E+000 grams

Sample Taken On                     :  1-13-94 12:00:00 PM
Acquisition Started                 :  2-08-94 10:23:25 PM

Live Time                           :      600.0 seconds
Real Time                           :      602.0 seconds


          Energy Calibration Used Done On       :  6-16-93
          Efficiency Calibration Used Done On   :  6-16-93
```

Nuclide Identification Report 2-08-94 10:36:15 PM Page 2

****
***** N U C L I D E I D E N T I F I C A T I O N R E P O R T *****
****

Sample Title: NORMCO scale
Nuclide Library Used: C:\GENIEPC\CAMFILES\STDLIB.NLB

IDENTIFIED NUCLIDES

Nuclide Name	Id Confidence	Energy (keV)	Yield (%)	Activity (uCi/gram)	Activity Uncertainty
SC-46	0.196	889.25	99.98		
		1120.51*	99.99	1.077E-003	6.128E-005
CD-109	0.876	88.03*	3.72	9.352E-003	7.439E-004
BI-211	0.190	72.87	1.20		
		351.10*	12.20	3.195E-002	1.346E-003
		404.80	4.10		
		426.90	1.90		
		831.80	3.30		
BI-212	0.425	39.86	1.10		
		727.17*	11.80	9.858E-004	2.166E-004
		785.42	2.00		
		1620.56	2.75		
PB-212	0.923	74.81*	9.60	6.224E-003	5.549E-004
		77.11*	17.50	5.921E-003	4.485E-004
		87.20*	6.30	5.309E-003	4.222E-004
		89.80*	1.75	6.912E-003	7.126E-004
		115.19	0.60		
		238.63*	44.60	2.883E-003	1.286E-004
		300.09	3.41		
BI-214	0.768	609.31*	46.30	5.759E-003	1.803E-004
		768.36*	5.04	4.965E-003	6.123E-004
		806.17	1.23		
		934.06*	3.21	5.891E-003	1.112E-003
		1120.29*	15.10	5.733E-003	3.261E-004
		1155.19	1.69		
		1238.11*	5.94	5.449E-003	6.473E-004
		1280.96	1.47		
		1377.67*	4.11	9.322E-003	1.194E-003
		1385.31	0.78		
		1401.50	1.39		
		1407.98	2.48		
		1509.19	2.19		
		1661.28	1.15		
		1729.60*	3.05	1.299E-002	1.407E-003
		1764.49*	15.80	8.769E-003	4.821E-004
		1847.44	2.12		
		2118.54	1.21		
PB-214	0.978	74.81*	6.33	9.439E-003	8.416E-004
		77.11*	10.70	9.684E-003	7.335E-004
		87.20*	3.70	9.039E-003	7.190E-004
		89.80*	1.03	1.174E-002	1.211E-003
		241.98*	7.49	1.199E-002	5.823E-004

Nuclide Identification Report 2-08-94 10:36:15 PM Page 3

Nuclide Name	Id Confidence	Energy (keV)	Yield (%)	Activity (uCi/gram)	Activity Uncertainty
PB-214	0.978	295.21*	19.20	1.083E-002	4.922E-004
		351.92*	37.20	1.048E-002	4.413E-004
		785.91	1.10		
RA-226	0.999	186.21*	3.28	1.364E-002	7.634E-004
AC-228	0.368	89.95*	2.10	5.760E-003	5.939E-004
		93.35	3.50		
		129.08	2.80		
		209.28	4.40		
		270.23	3.60		
		327.64	3.20		
		338.32*	11.40	1.749E-003	2.036E-004
		409.51	2.13		
		463.00	4.40		
		794.70	4.60		
		911.60*	27.70	1.607E-003	1.552E-004
		964.60	5.20		
		969.11*	16.60	8.015E-004	2.218E-004
		1587.90	3.71		
U-235	0.470	89.96*	1.50	8.064E-003	8.314E-004
		93.35	2.50		
		105.00	1.00		
		109.14	1.50		
		143.76	10.50		
		163.35	4.70		
		185.71*	54.00	8.283E-004	4.637E-005
		202.12	1.00		
		205.31	4.70		

* = Energy line found in the spectrum.
Energy tolerance used was 1.000
Nuclide confidence index threshold = 0.01
Errors quoted at 1.000 sigma

Nuclide Identification Report 2-08-94 10:36:15 PM Page 4

********** U N I D E N T I F I E D P E A K S **********

Peak Locate Performed on: 2-08-94 10:35:59 PM
Peak Locate From Channel: 1
Peak Locate To Channel: 4096

Peak No.	Energy (keV)	Peak Size in Counts per Second	Peak CPS % Uncertainty
1	31.96	1.8225E+000	4.89
12	583.39	8.3771E-001	7.23

M = First peak in a multiplet region
m = Other peak in a multiplet region

Errors quoted at 1.000 sigma

****
***** N U C L I D E M D A R E P O R T *****
****

Detector Name: NORMCO soil shield exp
Sample Geometry: 3
Spectrum Title: NORMCO scale
Nuclide Library Used: C:\GENIEPC\CAMFILES\STDLIB.NLB

	Nuclide Name	Energy (keV)	Yield (%)	Line MDA (uCi/gram)	Nuclide MDA (uCi/gram)
	K-40	1460.81	10.67	1.18E-003	1.18E-003
+	SC-46	889.25	99.98	1.30E-004	1.19E-004
		1120.51*	99.99	1.19E-004	
	CO-57	122.06	85.51	5.71E-005	5.71E-005
		136.48	10.60	4.81E-004	
	CO-60	1173.22	100.00	1.18E-004	1.18E-004
		1332.49	100.00	1.21E-004	
	SE-75	96.73	3.41	1.75E-003	9.36E-005
		121.11	16.70	3.22E-004	
		136.00	59.20	9.36E-005	
		198.60	1.45	4.33E-003	
		264.65	59.80	1.00E-004	
		279.53	25.20	2.64E-004	
		303.91	1.32	5.46E-003	
		400.65	11.40	7.12E-004	
	KR-85	513.99	0.43	1.99E-002	1.99E-002
@	KR-85M	151.18	75.30	1.00E+020	1.00E+020
@		304.87	14.00	1.00E+020	
	SR-85	513.99	99.27	1.14E-004	1.14E-004
	Y-88	898.02	93.40	1.32E-004	1.05E-004
		1836.01	99.38	1.05E-004	
+	CD-109	88.03*	3.72	1.70E-003	1.70E-003
	SN-113	255.12	1.93	3.19E-003	1.31E-004
		391.69	64.90	1.31E-004	
	CS-134	475.35	1.46	5.12E-003	1.25E-004
		563.23	8.38	8.85E-004	
		569.32	15.43	5.06E-004	
		604.70	97.60	1.68E-004	
		795.84	85.40	1.25E-004	
		801.93	8.73	1.25E-003	
		1038.57	1.00	1.18E-002	
		1167.94	1.80	6.72E-003	
		1365.15	3.04	3.99E-003	
	CS-136	66.91	12.50	2.24E-003	4.00E-004
		86.29	6.30	5.30E-003	
		153.22	7.46	2.68E-003	
		163.89	4.61	4.21E-003	
		176.55	13.56	1.43E-003	
		273.65	12.66	1.94E-003	
		340.57	48.50	7.15E-004	
		818.50	99.70	4.00E-004	
		1048.07	79.60	5.97E-004	

Nuclide MDA Report 2-08-94 10:36:29 PM Page 6

	Nuclide Name	Energy (keV)	Yield (%)	Line MDA (uCi/gram)	Nuclide MDA (uCi/gram)
	CS-136	1235.34	19.70	3.38E-003	4.00E-004
	CS-137	661.65	85.12	1.02E-004	1.02E-004
@	CS-138	138.10	1.49	1.00E+020	1.00E+020
@		227.76	1.51	1.00E+020	
@		408.98	4.66	1.00E+020	
@		462.79	30.70	1.00E+020	
@		546.94	10.80	1.00E+020	
@		871.80	5.11	1.00E+020	
@		1009.78	29.80	1.00E+020	
@		1147.22	1.24	1.00E+020	
@		1343.59	1.14	1.00E+020	
@		1435.86	76.30	1.00E+020	
	CE-139	165.85	80.35	6.73E-005	6.73E-005
	HG-203	279.19	77.30	1.09E-004	1.09E-004
+	BI-214	609.31*	46.30	1.75E-004	1.75E-004
		768.36*	5.04	1.67E-003	
		806.17	1.23	8.66E-003	
		934.06*	3.21	3.33E-003	
		1120.29*	15.10	6.32E-004	
		1155.19	1.69	7.83E-003	
		1238.11*	5.94	1.69E-003	
		1280.96	1.47	8.82E-003	
		1377.67*	4.11	3.30E-003	
		1385.31	0.78	1.98E-002	
		1401.50	1.39	9.80E-003	
		1407.98	2.48	5.88E-003	
		1509.19	2.19	6.90E-003	
		1661.28	1.15	1.10E-002	
		1729.60*	3.05	3.15E-003	
		1764.49*	15.80	6.33E-004	
		1847.44	2.12	7.24E-003	
>		2118.54	1.21	0.00E+000	
+	PB-214	74.81*	6.33	1.04E-003	1.98E-004
		77.11*	10.70	6.13E-004	
		87.20*	3.70	1.64E-003	
		89.80*	1.03	5.41E-003	
		241.98*	7.49	6.57E-004	
		295.21*	19.20	3.31E-004	
		351.92*	37.20	1.98E-004	
		785.91	1.10	1.03E-002	

+ = Nuclide identified during the nuclide identification
* = Energy line found in the spectrum
> = MDA value not calculated
@ = Half-life too short to be able to perform the decay correction

Interference Corrected Activity Report 2-08-94 10:36:44 PM Page 7

****
***** N U C L I D E I D E N T I F I C A T I O N R E P O R T *****
****

Sample Title: NORMCO scale
Nuclide Library Used: C:\GENIEPC\CAMFILES\STDLIB.NLB

..... IDENTIFIED NUCLIDES .....

Nuclide Name	Id Confidence	Energy (keV)	Yield (%)	Activity (uCi/gram)	Activity Uncertainty
BI-211	0.190	72.87	1.20		
		351.10*	12.20	3.195E-002	1.346E-003
		404.80	4.10		
		426.90	1.90		
		831.80	3.30		
BI-212	0.425	39.86	1.10		
		727.17*	11.80	9.858E-004	2.166E-004
		785.42	2.00		
		1620.56	2.75		
PB-212	0.923	74.81*	9.60	6.224E-003	5.549E-004
		77.11*	17.50	5.921E-003	4.485E-004
		87.20*	6.30	5.309E-003	4.222E-004
		89.80*	1.75	6.912E-003	7.126E-004
		115.19	0.60		
		238.63*	44.60	2.883E-003	1.286E-004
		300.09	3.41		
BI-214	0.768	609.31*	46.30	5.759E-003	1.803E-004
		768.36*	5.04	4.965E-003	6.123E-004
		806.17	1.23		
		934.06*	3.21	5.891E-003	1.112E-003
		1120.29*	15.10	5.733E-003	3.261E-004
		1155.19	1.69		
		1238.11*	5.94	5.449E-003	6.473E-004
		1280.96	1.47		
		1377.67*	4.11	9.322E-003	1.194E-003
		1385.31	0.78		
		1401.50	1.39		
		1407.98	2.48		
		1509.19	2.19		
		1661.28	1.15		
		1729.60*	3.05	1.299E-002	1.407E-003
		1764.49*	15.80	8.769E-003	4.821E-004
		1847.44	2.12		
		2118.54	1.21		
PB-214	0.978	74.81*	6.33	9.439E-003	8.416E-004
		77.11*	10.70	9.684E-003	7.335E-004
		87.20*	3.70	9.039E-003	7.190E-004
		89.80*	1.03	1.174E-002	1.211E-003
		241.98*	7.49	1.199E-002	5.823E-004
		295.21*	19.20	1.083E-002	4.922E-004
		351.92*	37.20	1.048E-002	4.413E-004
		785.91	1.10		

Interference Corrected Activity Report 2-08-94 10:36:44 PM Page 8

Nuclide Name	Id Confidence	Energy (keV)	Yield (%)	Activity (uCi/gram)	Activity Uncertainty
RA-226	0.999	186.21*	3.28	1.364E-002	7.634E-004
AC-228	0.368	89.95*	2.10	5.760E-003	5.939E-004
		93.35	3.50		
		129.08	2.80		
		209.28	4.40		
		270.23	3.60		
		327.64	3.20		
		338.32*	11.40	1.749E-003	2.036E-004
		409.51	2.13		
		463.00	4.40		
		794.70	4.60		
		911.60*	27.70	1.607E-003	1.552E-004
		964.60	5.20		
		969.11*	16.60	8.015E-004	2.218E-004
		1587.90	3.71		

* = Energy line found in the spectrum.
Energy tolerance used was 1.000
Nuclide confidence index threshold = 0.01
Errors quoted at 1.000 sigma

Interference Corrected Activity Report 2-08-94 10:36:44 PM Page 9

****
***** I N T E R F E R E N C E C O R R E C T E D R E P O R T *****
****

	Nuclide Name	Nuclide Id Confidence	Wt mean Activity (uCi/gram)	Wt mean Activity Uncertainty
X	SC-46	0.196		
X	CD-109	0.876		
	BI-211	0.190	5.5855E-003	1.6133E-003
	BI-212	0.425	9.8582E-004	2.1661E-004
	PB-212	0.923	2.3703E-003	1.2034E-004
	BI-214	0.768	6.0718E-003	1.3932E-004
	PB-214	0.978	8.6466E-003	2.9193E-004
	RA-226	0.999	1.3637E-002	7.6335E-004
	AC-228	0.368	1.3955E-003	1.0621E-004
X	U-235	0.470		

X = nuclide rejected by the interference analysis

Errors quoted at 1.000 sigma

Interference Corrected Activity Report 2-08-94 10:36:44 PM Page 10

********** U N I D E N T I F I E D P E A K S **********

Peak Locate Performed on: 2-08-94 10:35:59 PM
Peak Locate From Channel: 1
Peak Locate To Channel: 4096

Peak No.	Energy (keV)	Peak Size in Counts per Second	Peak CPS % Uncertainty
1	31.96	1.8225E+000	4.89
12	583.39	8.3771E-001	7.23

M = First peak in a multiplet region
m = Other peak in a multiplet region

Errors quoted at 1.000 sigma

****
***** N U C L I D E M D A R E P O R T *****
****

Detector Name: NORMCO soil shield exp
Sample Geometry: 3
Spectrum Title: NORMCO scale
Nuclide Library Used: C:\GENIEPC\CAMFILES\STDLIB.NLB

	Nuclide Name	Energy (keV)	Yield (%)	Line MDA (uCi/gram)	Nuclide MDA (uCi/gram)
	K-40	1460.81	10.67	1.18E-003	1.18E-003
	SC-46	889.25	99.98	1.30E-004	1.19E-004
		1120.51*	99.99	1.19E-004	
	CO-57	122.06	85.51	5.71E-005	5.71E-005
		136.48	10.60	4.81E-004	
	CO-60	1173.22	100.00	1.18E-004	1.18E-004
		1332.49	100.00	1.21E-004	
	SE-75	96.73	3.41	1.75E-003	9.36E-005
		121.11	16.70	3.22E-004	
		136.00	59.20	9.36E-005	
		198.60	1.45	4.33E-003	
		264.65	59.80	1.00E-004	
		279.53	25.20	2.64E-004	
		303.91	1.32	5.46E-003	
		400.65	11.40	7.12E-004	
	KR-85	513.99	0.43	1.99E-002	1.99E-002
@	KR-85M	151.18	75.30	1.00E+020	1.00E+020
@		304.87	14.00	1.00E+020	
	SR-85	513.99	99.27	1.14E-004	1.14E-004
	Y-88	898.02	93.40	1.32E-004	1.05E-004
		1836.01	99.38	1.05E-004	
	CD-109	88.03*	3.72	1.70E-003	1.70E-003
	SN-113	255.12	1.93	3.19E-003	1.31E-004
		391.69	64.90	1.31E-004	
	CS-134	475.35	1.46	5.12E-003	1.25E-004
		563.23	8.38	8.85E-004	
		569.32	15.43	5.06E-004	
		604.70	97.60	1.68E-004	
		795.84	85.40	1.25E-004	
		801.93	8.73	1.25E-003	
		1038.57	1.00	1.18E-002	
		1167.94	1.80	6.72E-003	
		1365.15	3.04	3.99E-003	
	CS-136	66.91	12.50	2.24E-003	4.00E-004
		86.29	6.30	5.30E-003	
		153.22	7.46	2.68E-003	
		163.89	4.61	4.21E-003	
		176.55	13.56	1.43E-003	
		273.65	12.66	1.94E-003	
		340.57	48.50	7.15E-004	
		818.50	99.70	4.00E-004	
		1048.07	79.60	5.97E-004	

Nuclide MDA Report 2-08-94 10:36:58 PM Page 12

	Nuclide Name	Energy (keV)	Yield (%)	Line MDA (uCi/gram)	Nuclide MDA (uCi/gram)
	CS-136	1235.34	19.70	3.38E-003	4.00E-004
	CS-137	661.65	85.12	1.02E-004	1.02E-004
@	CS-138	138.10	1.49	1.00E+020	1.00E+020
@		227.76	1.51	1.00E+020	
@		408.98	4.66	1.00E+020	
@		462.79	30.70	1.00E+020	
@		546.94	10.80	1.00E+020	
@		871.80	5.11	1.00E+020	
@		1009.78	29.80	1.00E+020	
@		1147.22	1.24	1.00E+020	
@		1343.59	1.14	1.00E+020	
@		1435.86	76.30	1.00E+020	
	CE-139	165.85	80.35	6.73E-005	6.73E-005
	HG-203	279.19	77.30	1.09E-004	1.09E-004
+	BI-214	609.31*	46.30	1.75E-004	1.75E-004
		768.36*	5.04	1.67E-003	
		806.17	1.23	8.66E-003	
		934.06*	3.21	3.33E-003	
		1120.29*	15.10	6.32E-004	
		1155.19	1.69	7.83E-003	
		1238.11*	5.94	1.69E-003	
		1280.96	1.47	8.82E-003	
		1377.67*	4.11	3.30E-003	
		1385.31	0.78	1.98E-002	
		1401.50	1.39	9.80E-003	
		1407.98	2.48	5.88E-003	
		1509.19	2.19	6.90E-003	
		1661.28	1.15	1.10E-002	
		1729.60*	3.05	3.15E-003	
		1764.49*	15.80	6.33E-004	
		1847.44	2.12	7.24E-003	
>		2118.54	1.21	0.00E+000	
+	PB-214	74.81*	6.33	1.04E-003	1.98E-004
		77.11*	10.70	6.13E-004	
		87.20*	3.70	1.64E-003	
		89.80*	1.03	5.41E-003	
		241.98*	7.49	6.57E-004	
		295.21*	19.20	3.31E-004	
		351.92*	37.20	1.98E-004	
		785.91	1.10	1.03E-002	

+ = Nuclide identified during the nuclide identification
* = Energy line found in the spectrum
> = MDA value not calculated
@ = Half-life too short to be able to perform the decay correction

APPENDIX C

ORIGINAL DATA PERTAINING TO RADON EMANATION EXPERIMENT

1 100% sand 0 g. charcoal	2 100% sand 0 g. charcoal	3 100% sand 0 g. charcoal	4 .5% scale mixture 0 g. charcoal	5 .5% scale mixture 0 g. charcoal	6 .5% scale mixture 0 g. charcoal	7 1% scale mixture 0 g. charcoal	8 1% scale mixture 0 g. charcoal	9 1% scale mixture 0 g. charcoal	10 100% scale 0 g. charcoal
11 100% scale 0 g. charcoal	12 100% scale 0 g. charcoal	13 100% sand 1 g. charcoal	14 100% sand 1 g. charcoal	15 100% sand 1 g. charcoal	16 .5% scale mixture 1 g. charcoal	17 .5% scale mixture 1 g. charcoal	18 .5% scale mixture 1 g. charcoal	19 1% scale mixture 1 g. charcoal	20 1% scale mixture 1 g. charcoal
21 1% scale mixture 1 g. charcoal	22 100% scale 1 g. charcoal	23 100% scale 1 g. charcoal	24 100% scale 1 g. charcoal	25 100% sand 2 g. charcoal	26 100% sand 2 g. charcoal	27 100% sand 2 g. charcoal	28 .5% scale mixture 2 g. charcoal	29 5% scale mixture 2 g. charcoal	30 .5% scale mixture 2 g. charcoal
31 1% scale mixture 2 g. charcoal	32 1% scale mixture 2 g. charcoal	33 1% scale mixture 2 g. charcoal	34 100% scale 2 g. charcoal	35 100% scale 2 g. charcoal	36 100% scale 2 g. charcoal	37 100% sand 4 g. charcoal	38 100% sand 4 g. charcoal	39 100% sand 4 g. charcoal	40 .5% scale mixture 4 g. charcoal
41 .5% scale mixture 4 g. charcoal	42 .5% scale mixture 4 g. charcoal	43 1% scale mixture 4 g. charcoal	44 1% scale mixture 4 g. charcoal	45 1% scale mixture 4 g. charcoal	46 100% scale 4 g. charcoal	47 100% scale 4 g. charcoal	48 100% scale 4 g. charcoal	49 100% sand 8 g. charcoal	50 100% sand 8 g. charcoal
51 100% sand 8 g. charcoal	52 .5% scale mixture 8 g. charcoal	53 .5% scale mixture 8 g. charcoal	54 .5% scale mixture 8 g. charcoal	55 1% scale mixture 8 g. charcoal	56 1% scale mixture 8 g. charcoal	57 1% scale mixture 8 g. charcoal	58 100% scale 8 g. charcoal	59 100% scale 8 g. charcoal	60 100% scale 8 g. charcoal

Data Obtained from Radon Emanation Experiment

		Background				Count				Time in	NCPM	A	Activity
cell #	sample #	#1	#2	#3	#4	#1	#2	#3	#4	Cell (min)	count/min		(pCi/L)
295	1	4	8	3	1	5	2	4	3	283.2	-0.1	0.965001	-0.13558
296	2	8	5	5	7	0	9	2	1	313.2	-0.65	0.961366	-0.88463
299	3	4	4	0	1	4	3	2	1	282	0.05	0.965146	0.067782
300	13	1	1	2	2	2	4	2	4	304.2	0.3	0.962455	0.407827
302	14	4	0	1	0	0	2	0	1	321	-0.1	0.960423	-0.13623
303	15	1	2	1	2	0	1	3	1	336	-0.05	0.958612	-0.06824
301	25	3	1	1	1	2	1	0	1	1114.2	-0.1	0.869214	-0.15053
304	26	2	5	3	3	1	2	2	2	1135.2	-0.3	0.86692	-0.45277
295	37	5	2	3	4	2	1	4	1	262.8	-0.3	0.96748	-0.40571
299	38	2	1	4	1	3	0	2	1	250.8	-0.1	0.968942	-0.13503
296	39	1	3	1	3	3	2	2	2	244.8	0.05	0.969674	0.067465
300	49	2	1	0	3	1	4	2	3	256.8	0.2	0.968211	0.270268
302	50	0	1	3	0	2	1	0	1	253.8	0	0.968576	0
303	51	6	3	1	2	1	3	2	1	251	-0.25	0.968918	-0.33759
297	52	3	3	4	0	4	5	6	6	248	0.55	0.969283	0.742416
304	53	5	1	3	2	4	1	1	2	1066.2	-0.15	0.874478	-0.22443
301	54	1	2	1	2	2	0	2	1	1078.2	-0.05	0.873159	-0.07492
295	40	2	3	5	2	2	0	1	0	295	-0.45	0.963569	-0.61103
296	41	3	0	3	2	0	1	2	0	310	-0.25	0.961753	-0.3401
299	42	3	2	2	4	2	0	2	1	481	-0.3	0.941285	-0.417
300	28	0	1	3	2	1	2	0	3	478	0	0.94164	0
301	29	0	1	3	2	3	6	1	3	549	0.35	0.933267	0.490679
304	30	3	1	1	1	5	3	0	3	537	0.25	0.934677	0.349956
297	16	6	0	1	0	5	5	7	2	550	0.6	0.933149	0.84127
303	17	2	2	1	3	3	5	5	2	320	0.35	0.960544	0.476745
296	18	1	2	1	4	6	7	10	6	315	1.05	0.961148	1.429336
299	4	2	3	1	2	13	10	12	9	318	1.8	0.960785	2.451215
302	5	2	4	0	2	9	10	9	10	314	1.5	0.961269	2.041652
300	6	3	1	4	1	9	3	9	3	308	0.75	0.961995	1.020056
304	55	0	1	0	2	2	0	2	4	304	0.25	0.962479	0.339847
297	56	4	5	0	1	3	2	8	9	296	0.6	0.963448	0.814814
301	57	2	1	3	4	3	3	4	2	292	0.1	0.963933	0.135734
295	43	5	1	0	2	2	1	4	0	288	-0.05	0.964418	-0.06783
303	44	0	4	3	2	2	3	6	1	235	0.15	0.97087	0.202146
296	45	1	3	4	2	5	2	8	1	236	0.3	0.970748	0.404343
299	31	1	1	3	0	2	3	4	4	243	0.4	0.969893	0.539599
297	32	2	0	4	1	5	6	0	3	245	0.35	0.969649	0.472268
300	33	0	2	4	3	3	2	2	3	255	0.05	0.96843	0.067552
304	19	5	0	1	3	40	19	12	11	250	3.65	0.969039	4.928181
302	20	7	0	0	1	4	2	5	4	230	0.35	0.971481	0.471378
301	21	9	1	3	1	2	5	5	3	241	0.05	0.970137	0.067433
295	7	5	2	3	2	17	14	18	15	265	2.6	0.967213	3.517116
296	8	5	2	4	2	23	19	18	21	289	3.4	0.964297	4.613212
303	9	0	3	2	0	15	12	13	16	321	2.55	0.960423	3.473866
299	58	2	2	1	3	47	31	36	53	364	7.95	0.955241	10.88903
300	59	2	9	1	5	31	43	36	23	372	5.8	0.954281	7.952198
297	60	10	4	2	1	39	41	32	41	385	6.8	0.952721	9.338526
304	46	3	1	2	0	80	86	80	89	390	16.45	0.952122	22.60521
302	47	8	0	3	1	60	61	57	58	242	11.2	0.970015	15.10688
301	48	4	3	2	1	77	78	71	62	239	13.9	0.970381	18.74164
295	34	3	7	1	1	135	128	132	124	251	25.35	0.968918	34.23154
296	35	2	2	1	1	137	120	119	109	247	23.95	0.969405	32.32477
303	36	8	2	3	0	157	141	152	144	212	29.05	0.973683	39.03587
299	22	4	0	1	1	265	287	261	269	210	53.8	0.973928	72.27543
304	23	5	3	3	2	263	240	253	257	260	50	0.967821	67.59431
300	24	1	0	0	0	213	243	223	238	272	45.8	0.966361	62.00993
302	10	4	1	1	2	862	833	817	800	284	165.2	0.964903	224.0069
303	11	4	1	7	1	843	923	939	922	291	180.7	0.964054	245.2404
296	12	7	0	1	0	825	832	858	851	297	167.9	0.963327	228.0407

Freundlich Isotherm for 100% scale sample in Radon Emanation Experiment

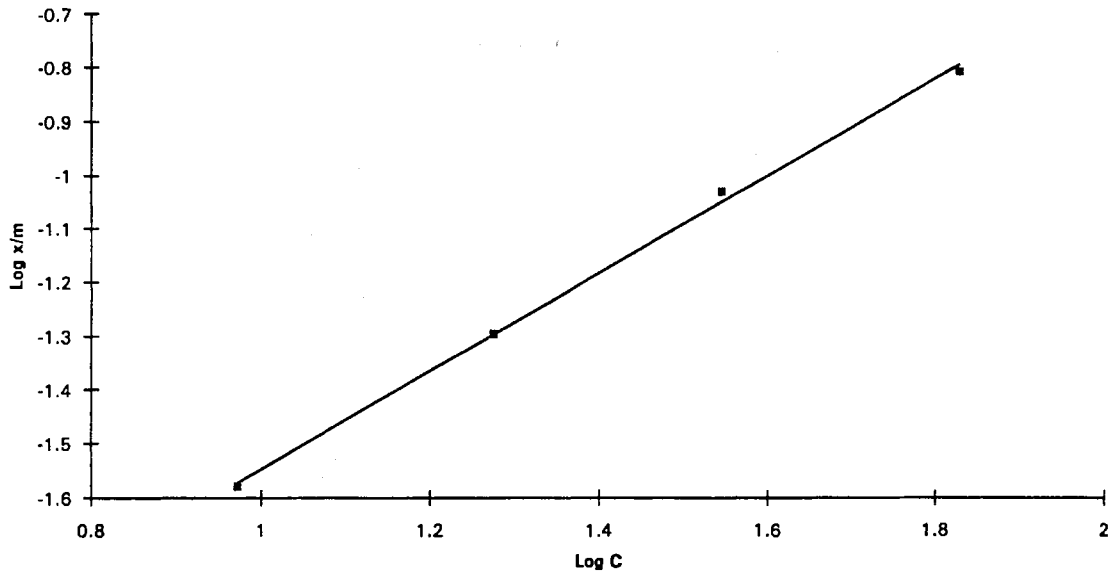

Langmuir High Plot for 100% scale sample in Radon Emanation Experiment

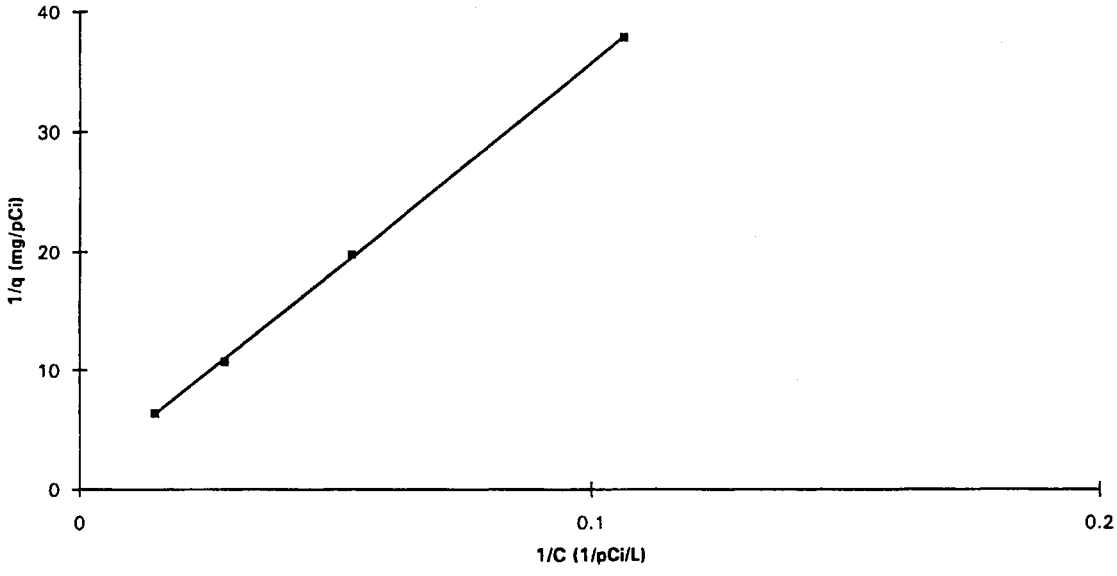

Langmuir Low Plot for 100% scale sample in Radon Emanation Experiment

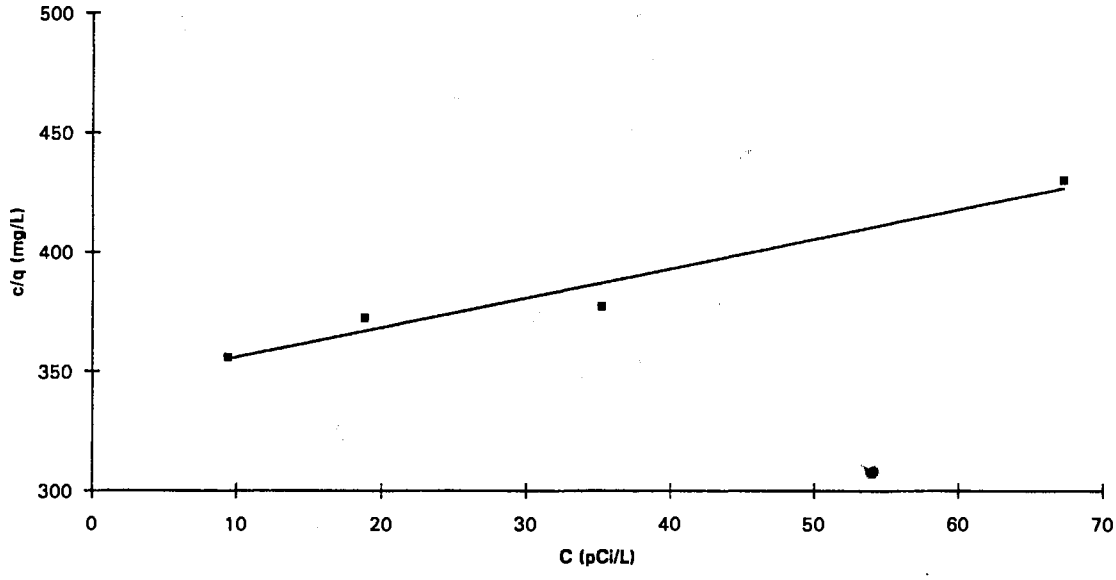

BET Isotherm for 100% scale sample in Radon Emanation Experiment

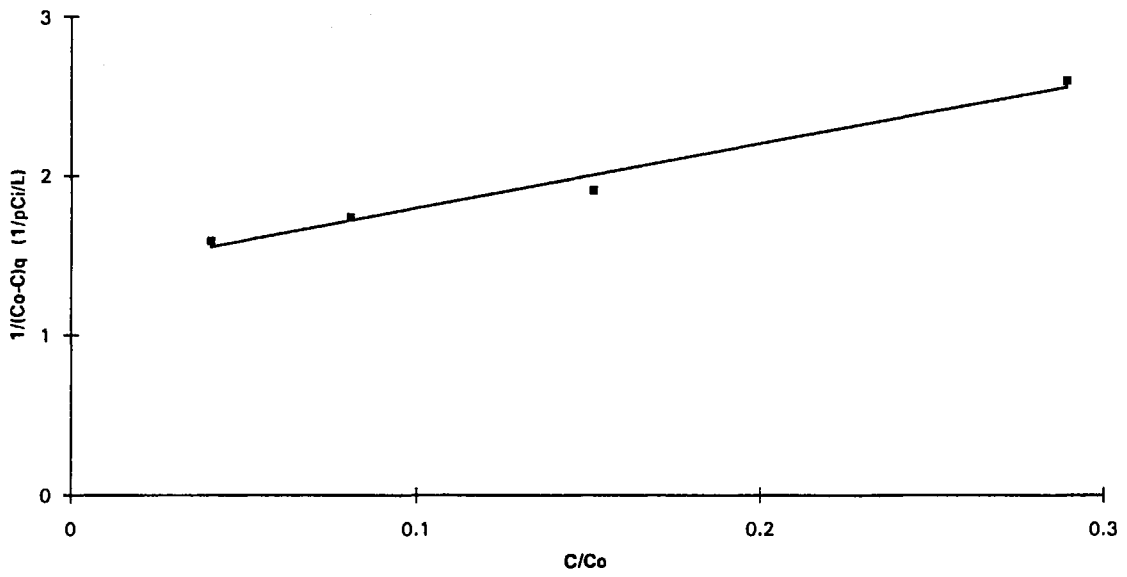

APPENDIX D

ORIGINAL DATA PERTAINING TO MECHANICAL SEPARATION EXPERIMENT

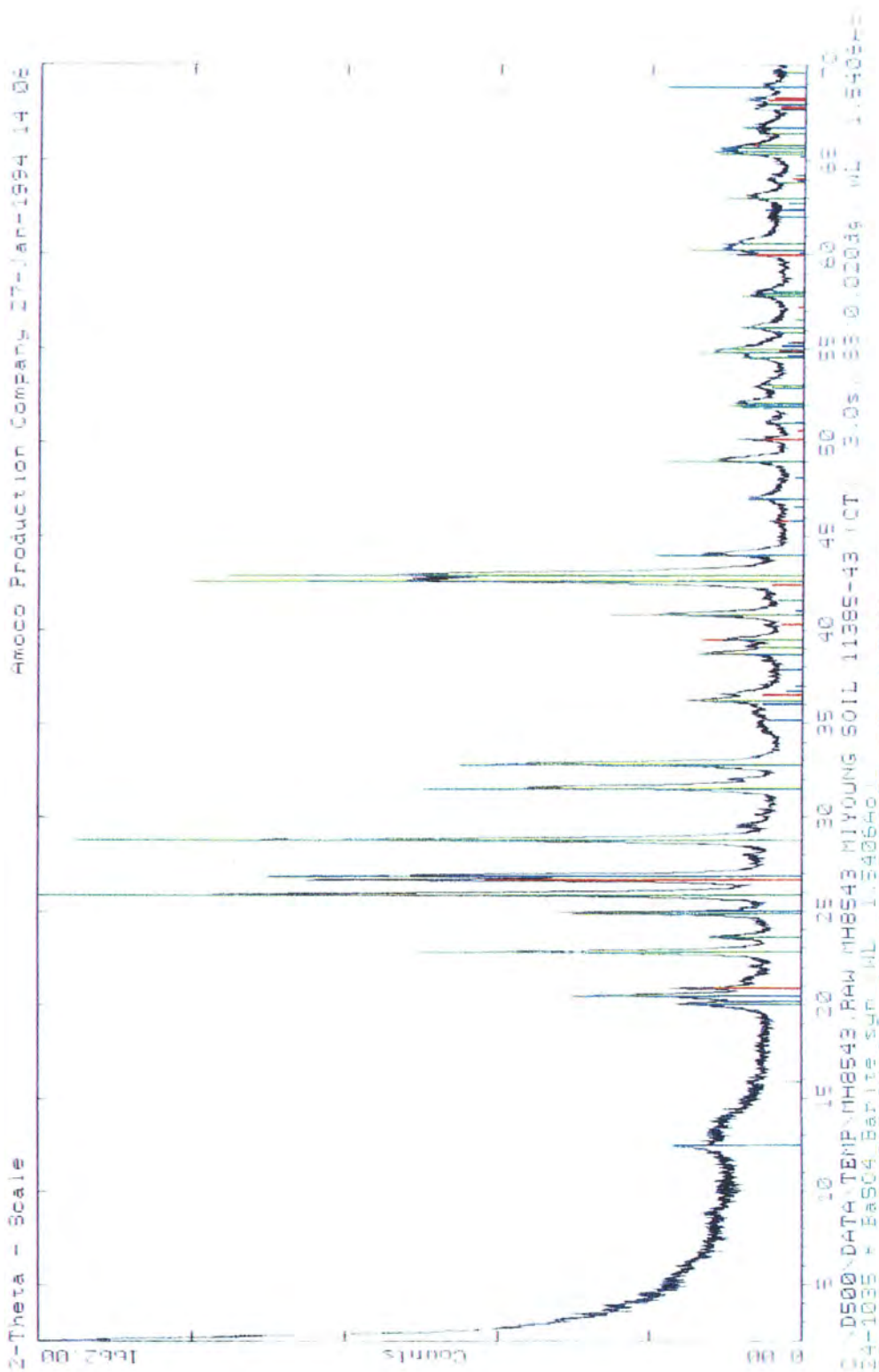
Amoco Production Company 27-Jan-1994 14:08
2-Theta - Scale
Counts
C:\D500\DATA\TEMP\MH8543.RAW MH8543 MIYOUNG SOIL 11395-43 (CT 3.0s, 33 0.02deg WL 1.5406Ao)
24-1035 * BaSO4 Barite syn WL 1.5406Ao
29-1488 Al2Si2O5(OH)4 Kaolinite 1T Md RG (WL 1.5406Ao)
5-0490 D SiO2 Quartz low (WL 1.5406Ao)

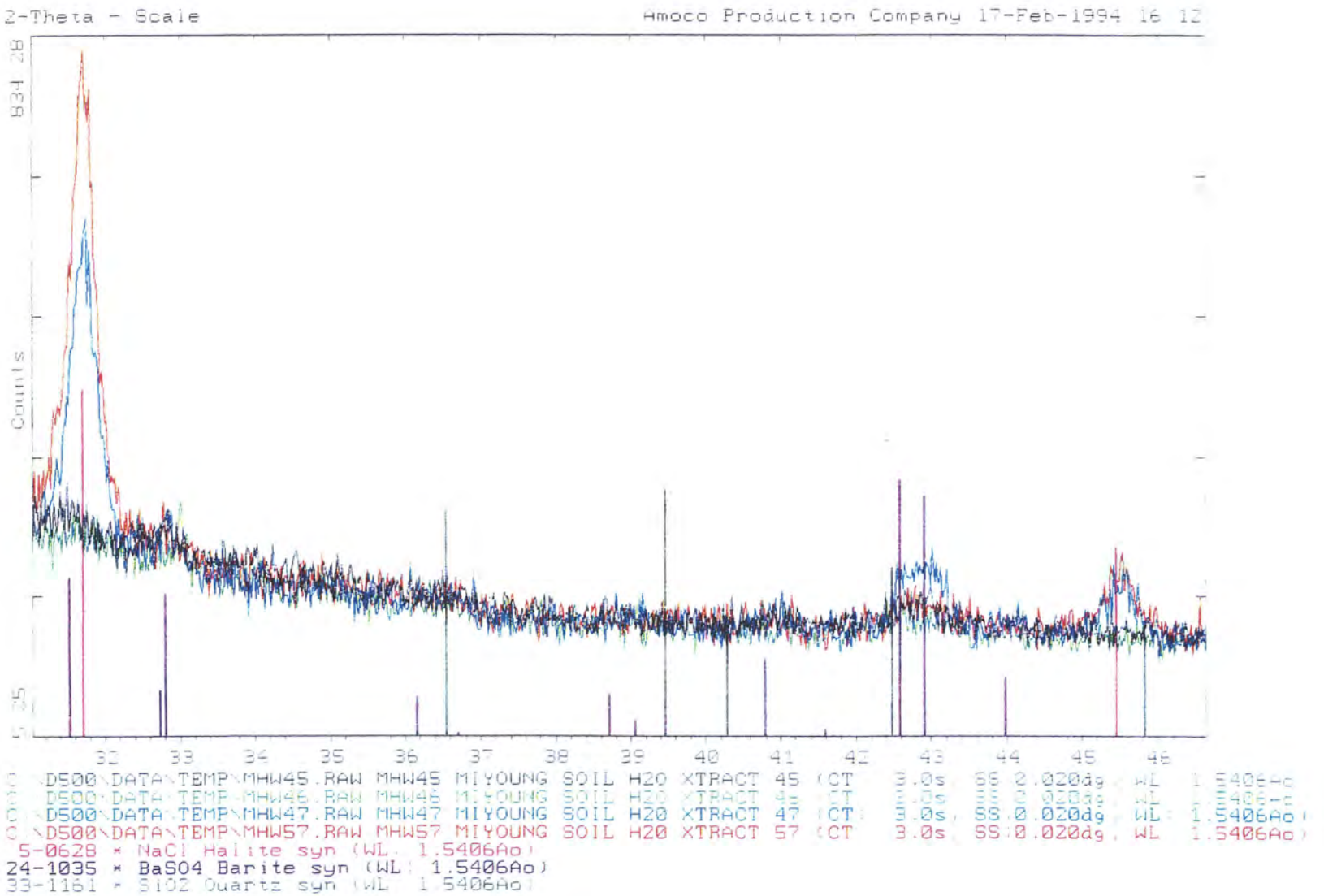
2-Theta - Scale
Amoco Production Company 17-Feb-1994 16:12
Counts
834.28
5.35
30
31
32
33
34
35
36
37
38
39
40
41
42
43
44
45
46
D:\D500\DATA\TEMP\MHW45.RAW MHW45 MIYOUNG SOIL H20 XTRACT 45 (CT: 3.0s, SS:2.020dg, WL: 1.5406Ao)
D:\D500\DATA\TEMP\MHW46.RAW MHW46 MIYOUNG SOIL H20 XTRACT 46 (CT: 3.0s, SS:2.020dg, WL: 1.5406Ao)
D:\D500\DATA\TEMP\MHW47.RAW MHW47 MIYOUNG SOIL H20 XTRACT 47 (CT: 3.0s, SS:2.020dg, WL: 1.5406Ao)
D:\D500\DATA\TEMP\MHW57.RAW MHW57 MIYOUNG SOIL H20 XTRACT 57 (CT: 3.0s, SS:2.020dg, WL: 1.5406Ao)
5-0628 * NaCl Halite syn (WL: 1.5406Ao)
24-1035 * BaSO4 Barite syn (WL: 1.5406Ao)
33-1161 * SiO2 Quartz syn (WL: 1.5406Ao)

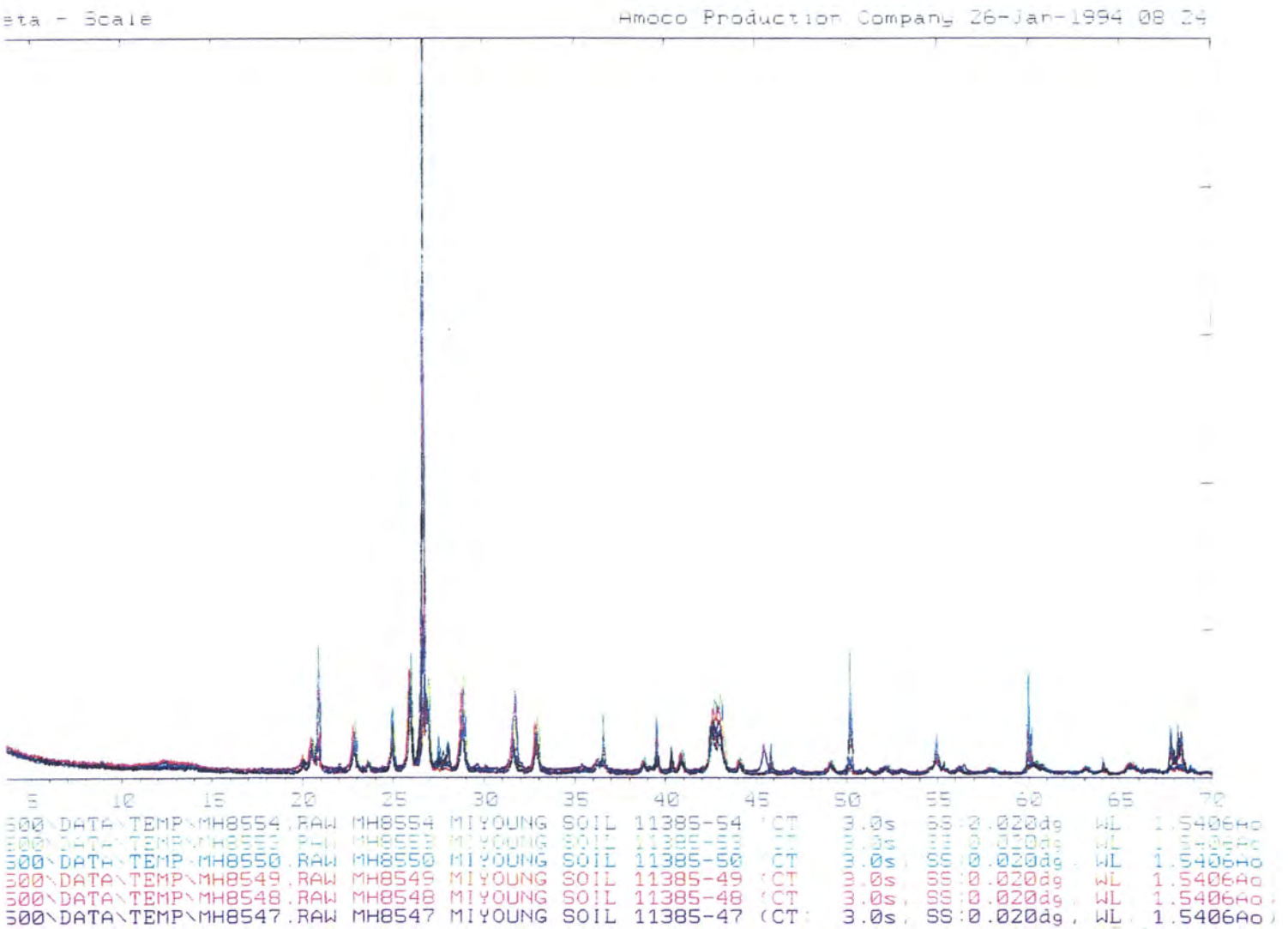
eta - Scale
Amoco Production Company 26-Jan-1994 08:24
5 10 15 20 25 30 35 40 45 50 55 60 65 70
500\DATA\TEMP\MH8554.RAW MH8554 MIYOUNG SOIL 11385-54 (CT 3.0s, SS:0.020dg, WL 1.5406Ao
500\DATA\TEMP\MH8550.RAW MH8550 MIYOUNG SOIL 11385-50 (CT 3.0s, SS:0.020dg, WL 1.5406Ao
500\DATA\TEMP\MH8549.RAW MH8549 MIYOUNG SOIL 11385-49 (CT 3.0s, SS:0.020dg, WL 1.5406Ao
500\DATA\TEMP\MH8548.RAW MH8548 MIYOUNG SOIL 11385-48 (CT 3.0s, SS:0.020dg, WL 1.5406Ao
500\DATA\TEMP\MH8547.RAW MH8547 MIYOUNG SOIL 11385-47 (CT 3.0s, SS:0.020dg, WL 1.5406Ao

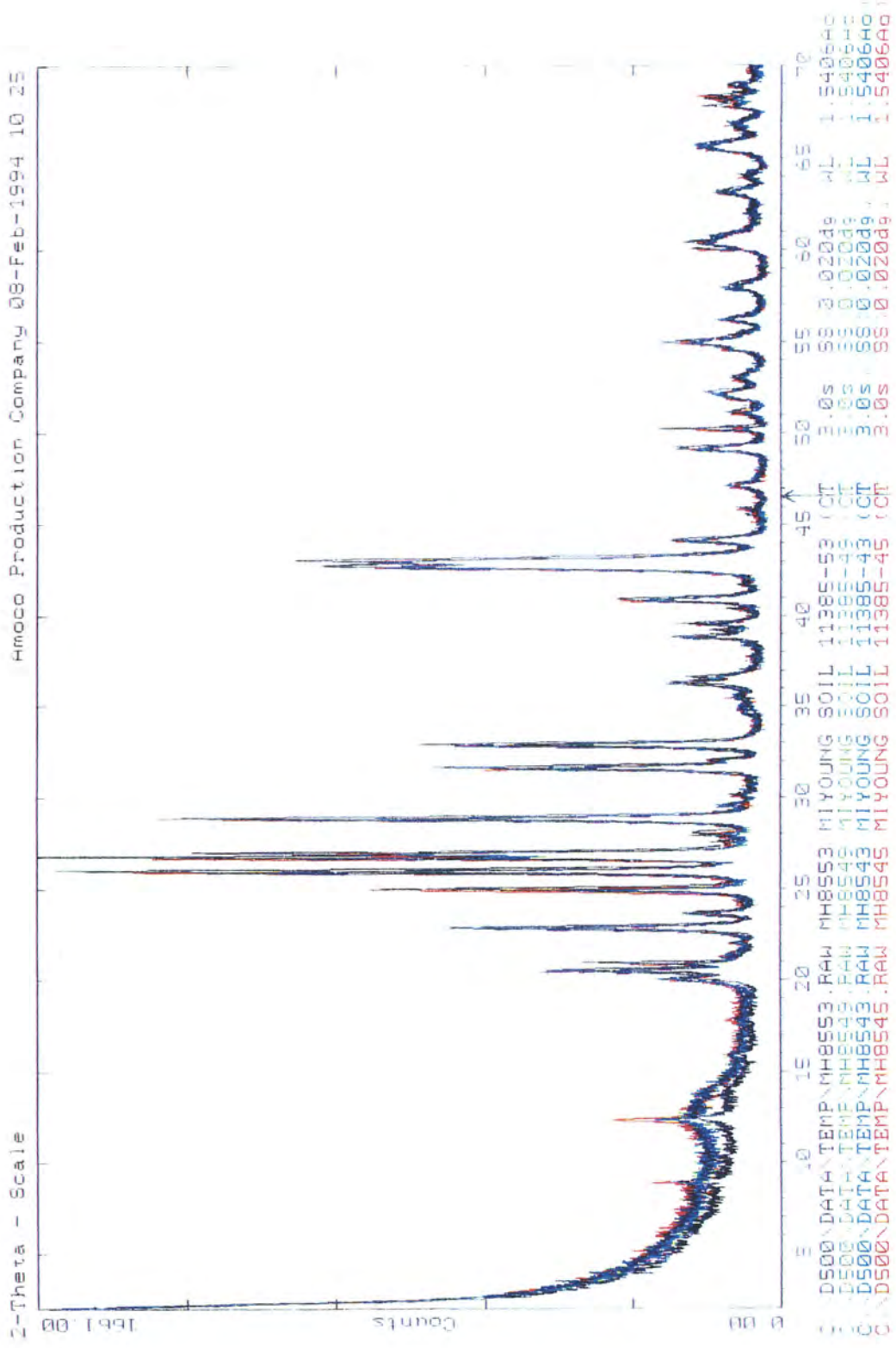
Amoco Production Company 08-Feb-1994 10:25
2-Theta - Scale
Counts
1661.00
0.00
5 10 15 20 25 30 35 40 45 50 55 60 65 70
C:\D500\DATA\TEMP\MH8553.RAW MH8553 MIYOUNG SOIL 11385-53 (CT 3.0s 58 0.020d9 WL 1.54060
C:\D500\DATA\TEMP\MH8546.RAW MH8546 MIYOUNG SOIL 11385-46 (CT 3.0s 58 0.020d9 WL 1.54060
C:\D500\DATA\TEMP\MH8543.RAW MH8543 MIYOUNG SOIL 11385-43 (CT 3.0s 58 0.020d9 WL 1.5406Ho
C:\D500\DATA\TEMP\MH8545.RAW MH8545 MIYOUNG SOIL 11385-45 (CT 3.0s 58 0.020d9 WL 1.5406Ao

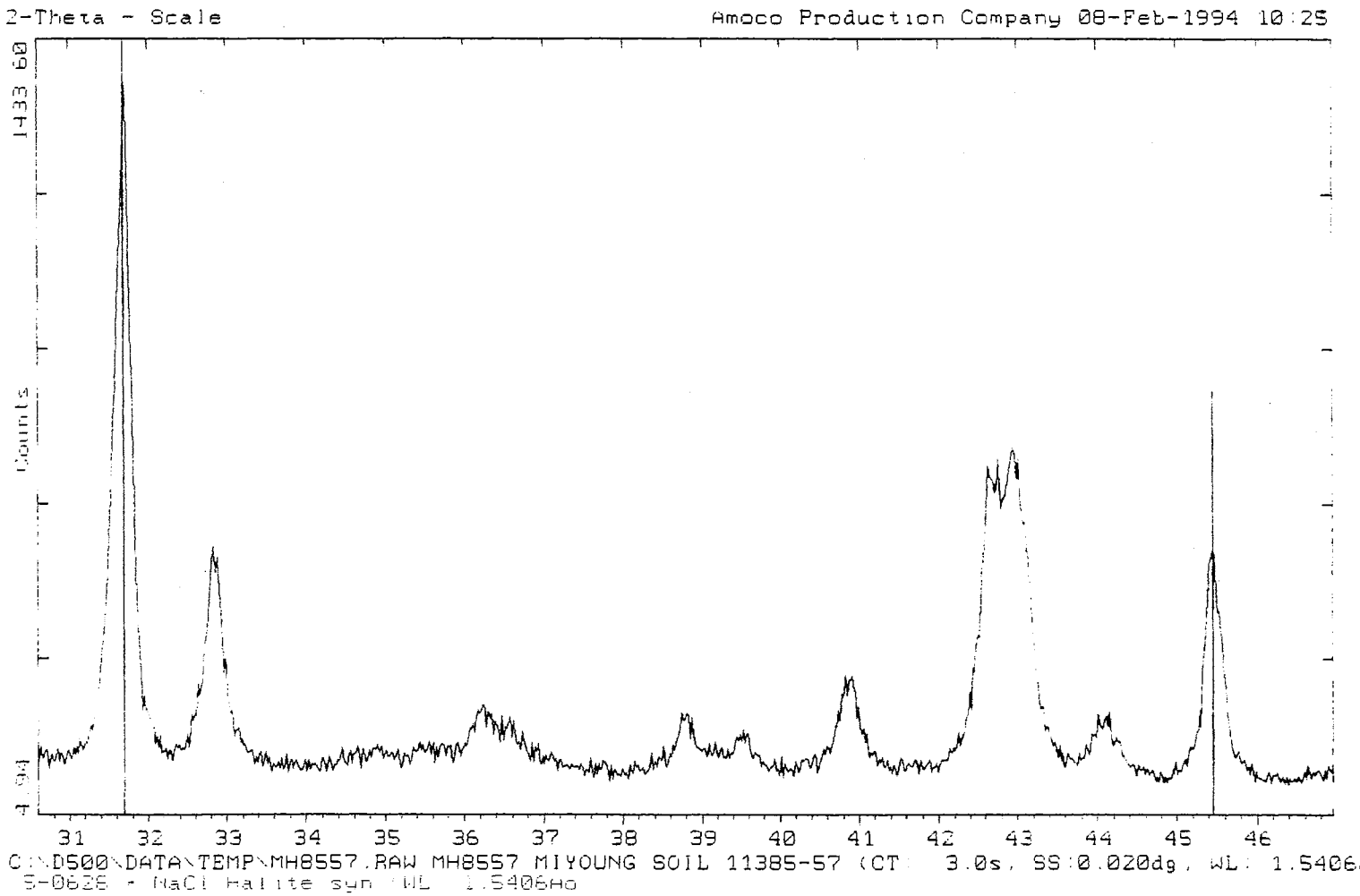
2-Theta - Scale
Amoco Production Company 08-Feb-1994 10:25
1433.60
Counts
4.94
31
32
33
34
35
36
37
38
39
40
41
42
43
44
45
46
C:\D500\DATA\TEMP\MH8557.RAW MH8557 MIYOUNG SOIL 11385-57 (CT: 3.0s, SS:0.020dg, WL: 1.5406Ac
S-0628 - NaCl Halite syn WL: 1.5406Ao

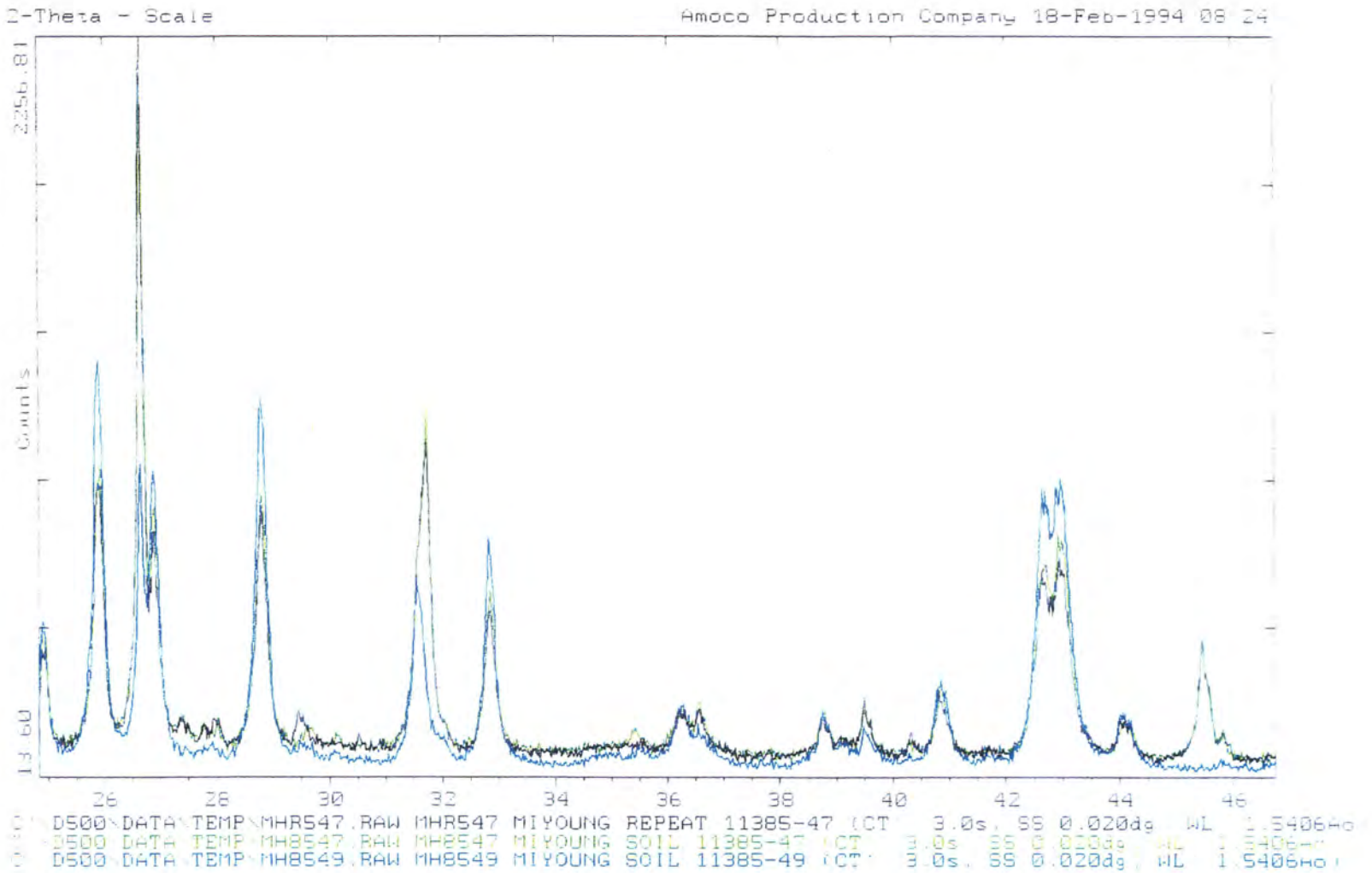
2-Theta - Scale
Amoco Production Company 18-Feb-1994 08:24
2256.81
Counts
13.60
26
28
30
32
34
36
38
40
42
44
46
D500\DATA\TEMP\MHR547.RAW MHR547 MIYOUNG REPEAT 11385-47 (CT 3.0s, SS 0.020dg, WL 1.5406Ho
D500\DATA\TEMP\MH8547.RAW MH8547 MIYOUNG SOIL 11385-47 (CT 3.0s, SS 0.020dg, WL 1.5406Ho
D500\DATA\TEMP\MH8549.RAW MH8549 MIYOUNG SOIL 11385-49 (CT 3.0s, SS 0.020dg, WL 1.5406Ho

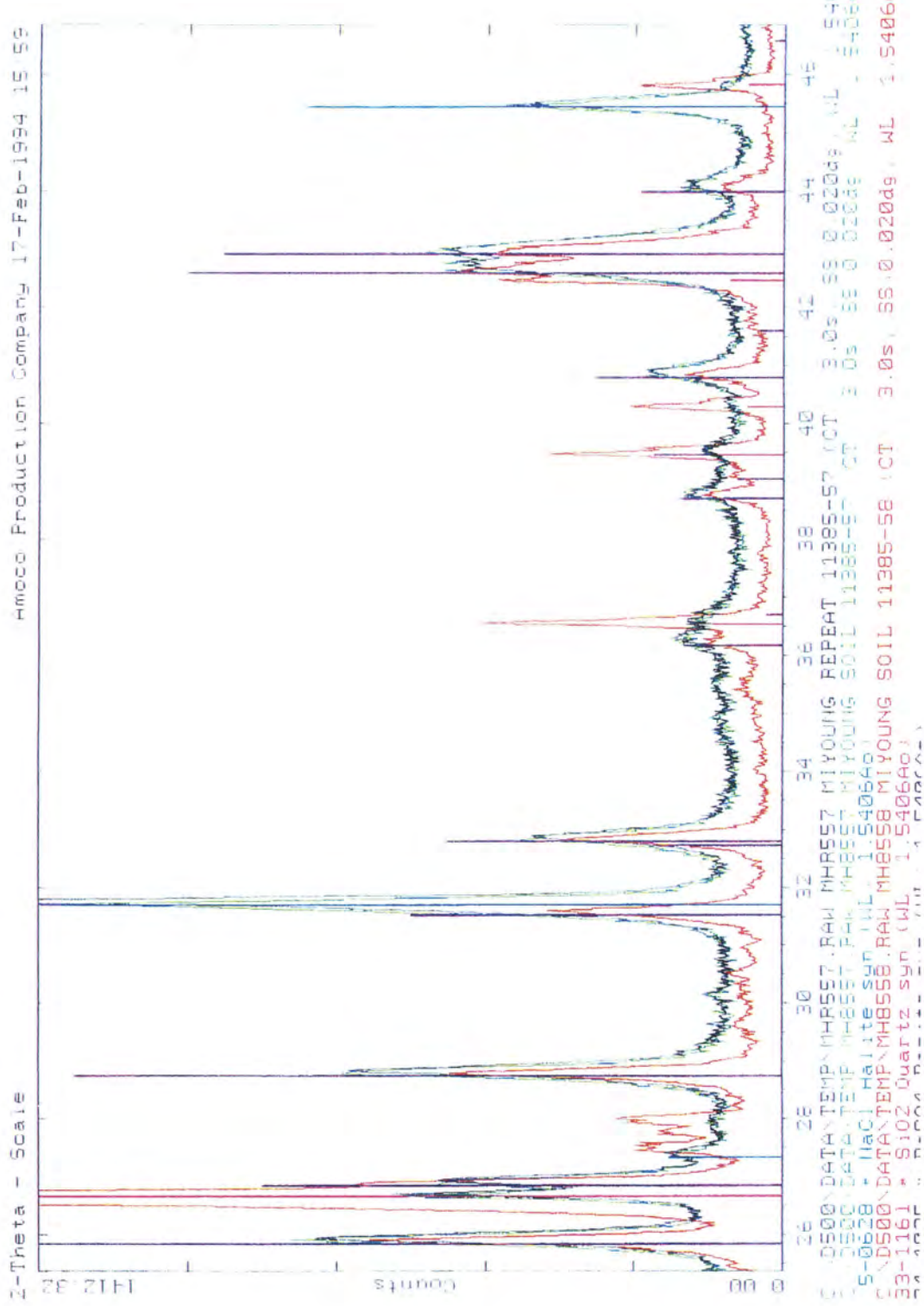
Amoco Production Company 17-Feb-1994 15:59
2-Theta - Scale
Counts
1412.32
0.00
26
28
30
32
34
36
38
40
42
44
46
D500\DATA\TEMP\MH8557.RAW MH8557 MIYOUNG REPEAT 11385-57 CT 3.0s, 58 0.020d, WL 1.5406Ac
D500\DATA\TEMP\MH8558.RAW MH8558 MIYOUNG SOIL 11385-58 CT 3.0s, 58 0.020d, WL 1.5406Ac
5-0628 * NaCl Halite syn (WL 1.5406Ac)
33-1161 * SiO2 Quartz syn (WL 1.5406Ac)

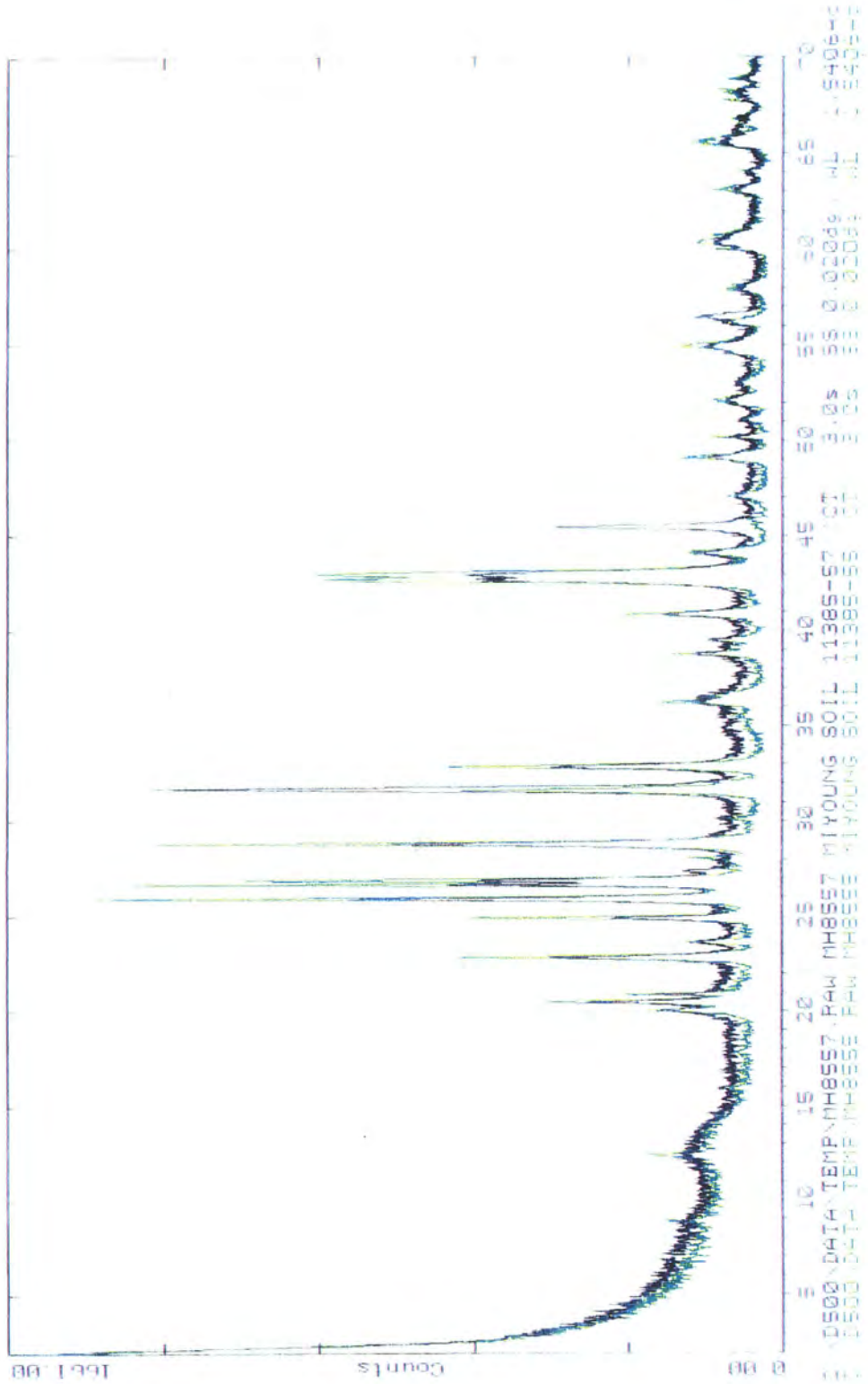
Counts
1661.00
0.00
0
5
10
15
20
25
30
35
40
45
50
55
60
65
70
D500\DATA\TEMP\MH8557.RAW MH8557 MIYOUNG SOIL 11385-57 CT 3.0s 56 0.020d6 HL
D500\DATA\TEMP\MH8558.RAW MH8558 MIYOUNG SOIL 11385-58 CT 3.0s 56 0.020d6 HL

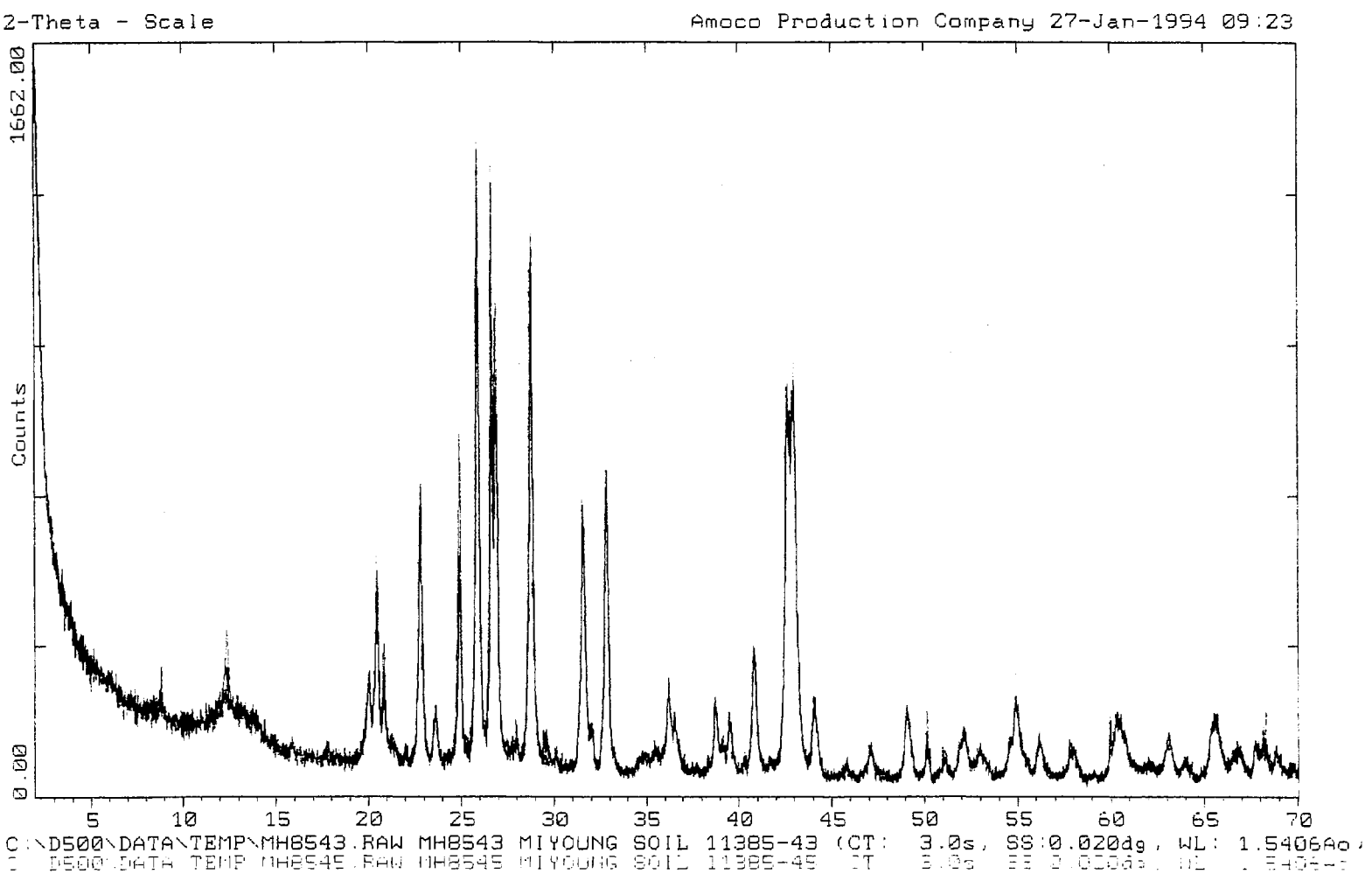
2-Theta - Scale
Amoco Production Company 27-Jan-1994 09:23
1662.00
Counts
0.00
5
10
15
20
25
30
35
40
45
50
55
60
65
70
C:\D500\DATA\TEMP\MH8543.RAW MH8543 MIYOUNG SOIL 11385-43 (CT: 3.0s, SS:0.020dg, WL: 1.5406Ao

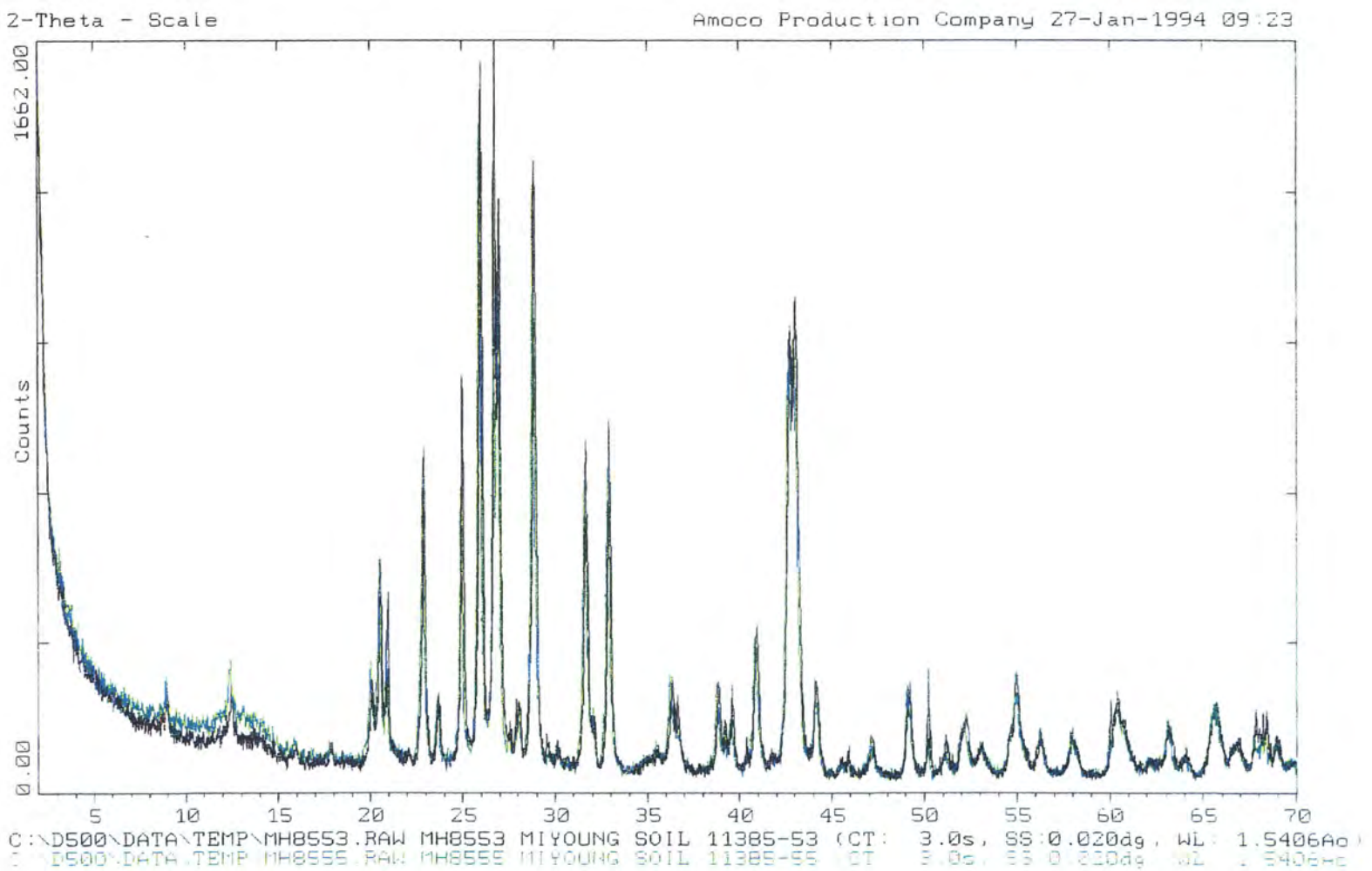
2-Theta - Scale
Amoco Production Company 27-Jan-1994 09:23
1662.00
Counts
0.00
5
10
15
20
25
30
35
40
45
50
55
60
65
70
C:\D500\DATA\TEMP\MH8553.RAW MH8553 MIYOUNG SOIL 11385-53 (CT: 3.0s, SS:0.020dg, WL: 1.5406Ao)

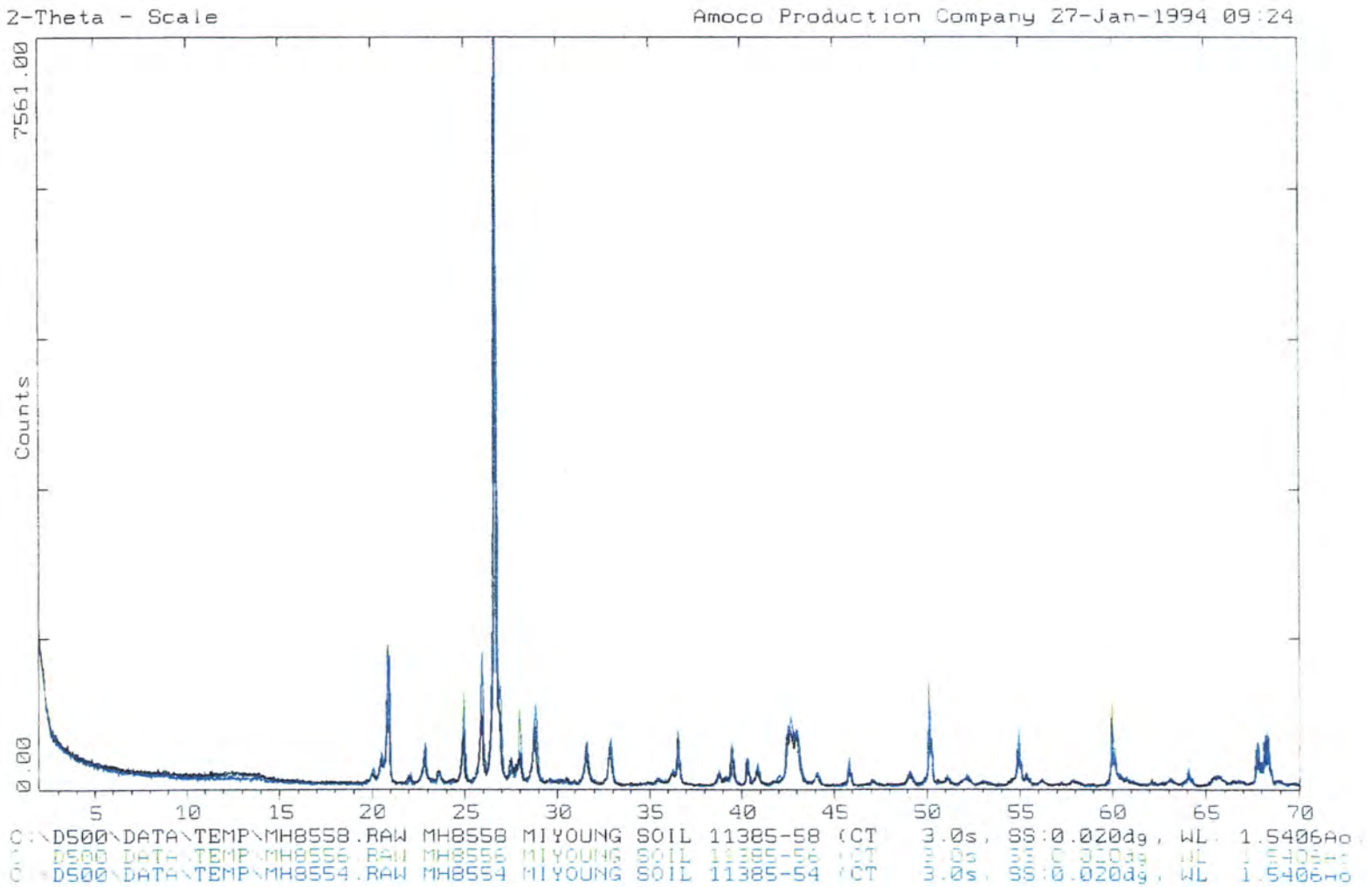
2-Theta - Scale
Amoco Production Company 27-Jan-1994 09:24
7561.00
Counts
0.00
5
10
15
20
25
30
35
40
45
50
55
60
65
70
C:\D500\DATA\TEMP\MH8558.RAW MH8558 MIYOUNG SOIL 11385-58 (CT 3.0s, SS:0.020dg, WL: 1.5406Ao
C:\D500\DATA\TEMP\MH8556.RAW MH8556 MIYOUNG SOIL 11385-56 (CT 3.0s, SS:0.020dg, WL: 1.5406Ao
C:\D500\DATA\TEMP\MH8554.RAW MH8554 MIYOUNG SOIL 11385-54 (CT 3.0s, SS:0.020dg, WL: 1.5406Ao

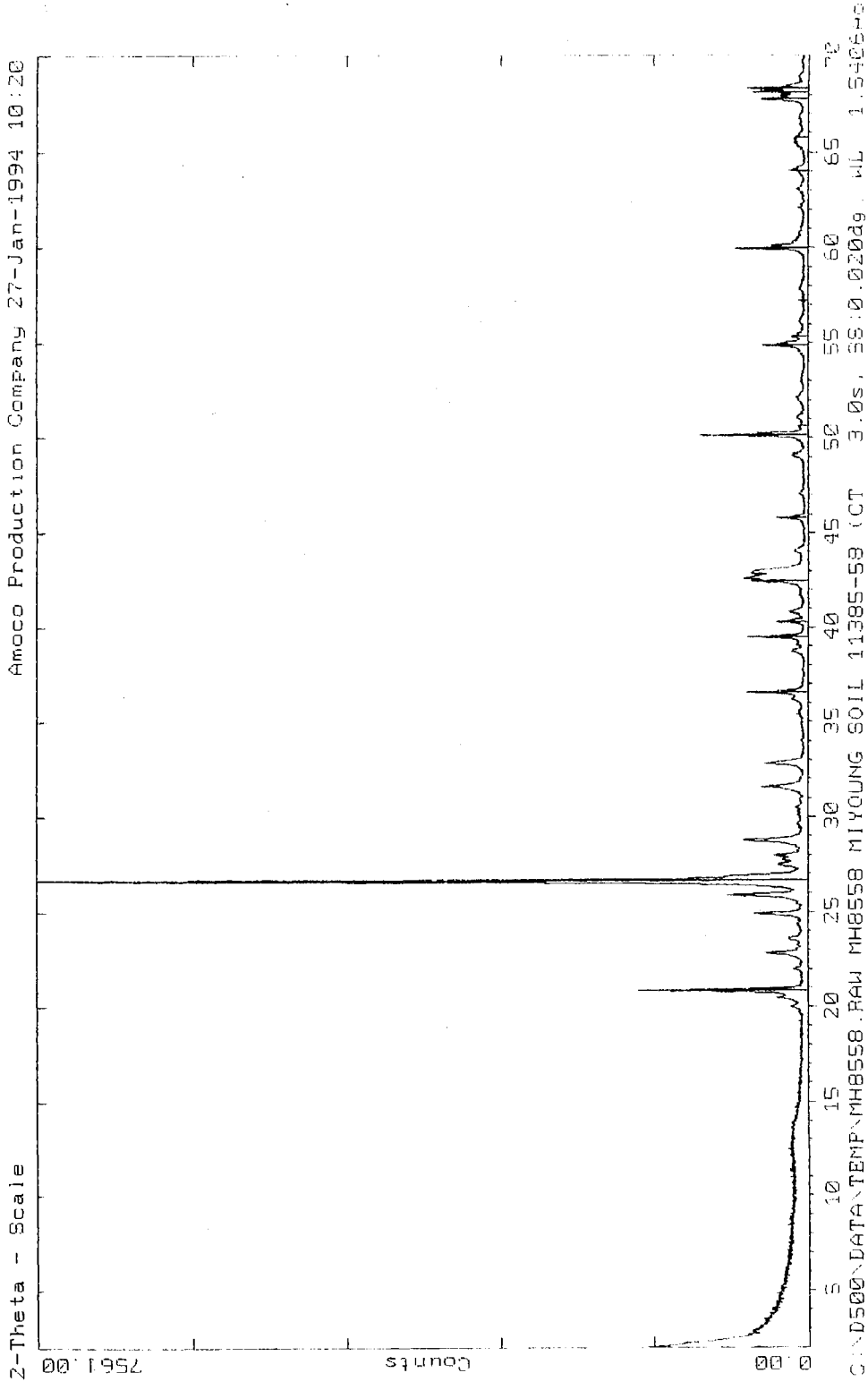
Amoco Production Company 27-Jan-1994 10:20
2-Theta - Scale
Counts
7561.00
0.00
0
5
10
15
20
25
30
35
40
45
50
55
60
65
72
C:\D500\DATA\TEMP\MH8558.RAW MH8558 MIYOUNG SOIL 11385-59 CT 3.0s, SS:0.0200 WL 1.5406
33-1161 * SiO2 Quartz

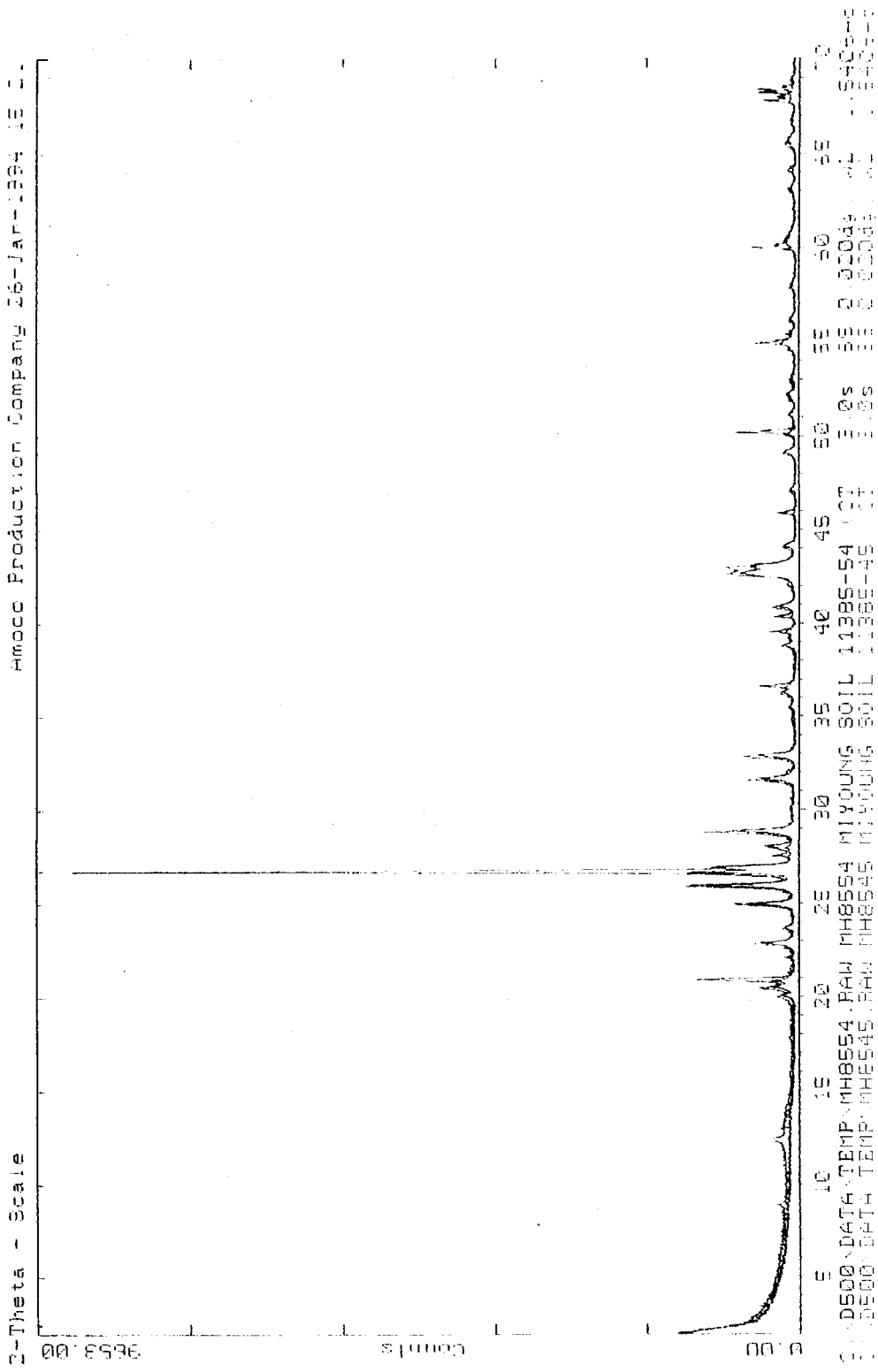
Amoco Production Company 26-Jan-1994 13 C.
2-Theta - Scale
Counts
9653.00
0.00
5
10
15
20
25
30
35
40
45
50
55
60
D500\DATA\TEMP\MH8554.RAW MH8554 MIYOUNG SOIL 11385-54
D500\DATA\TEMP\MH8545.RAW MH8545 MIYOUNG SOIL 11385-45

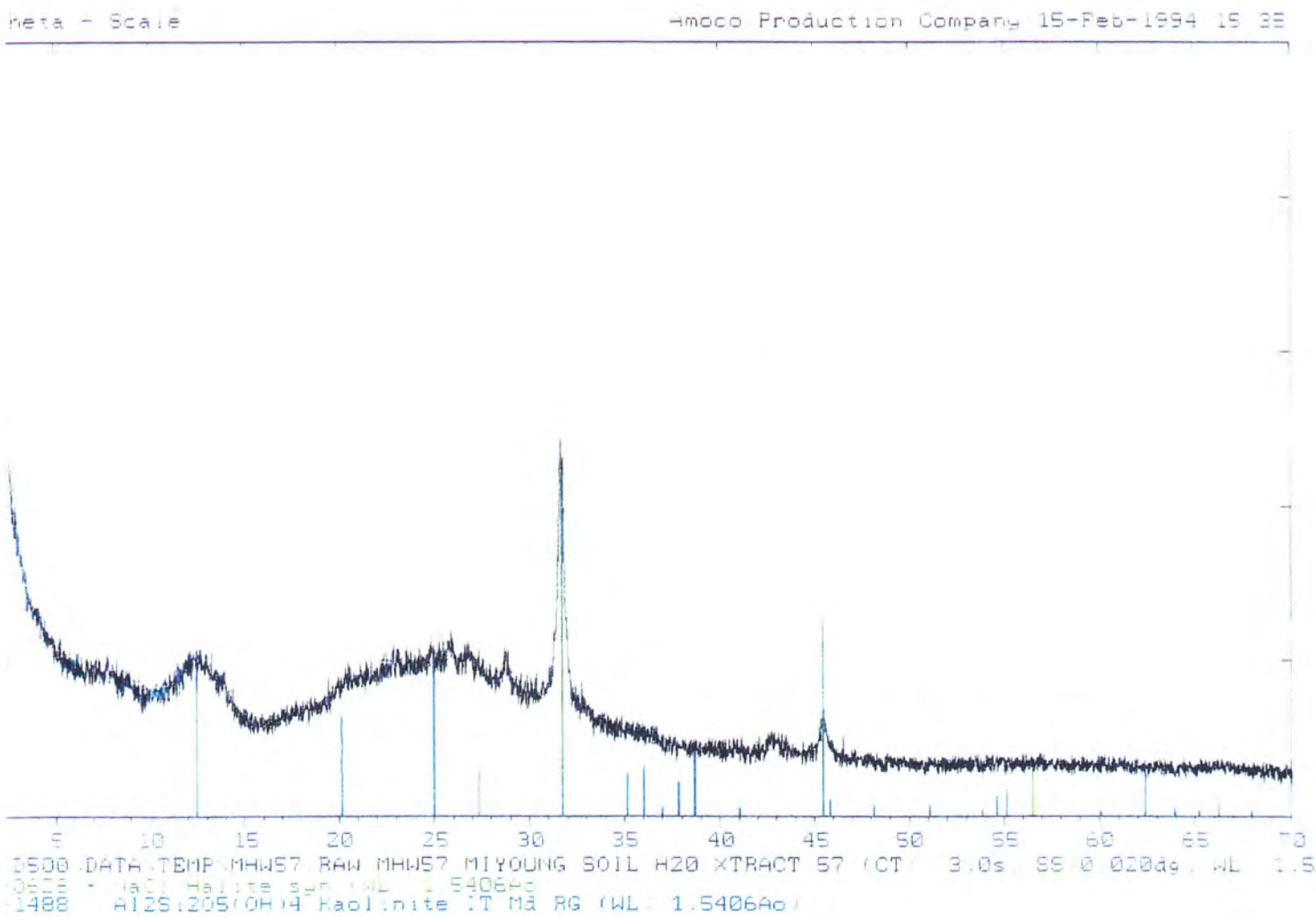
neta - Scale
Amoco Production Company 15-Feb-1994 15 35
5 10 15 20 25 30 35 40 45 50 55 60 65 70
1500 DATA TEMP MHW57 RAW MHW57 MIYOUNG SOIL H20 XTRACT 57 (CT 3.0s SS 0 020dg WL 1.5406Ao
0525 * NaCl Halite syn (WL 1.5406Ao
1488 Al2Si2O5(OH)4 Kaolinite 1T Ma RG (WL: 1.5406Ao)

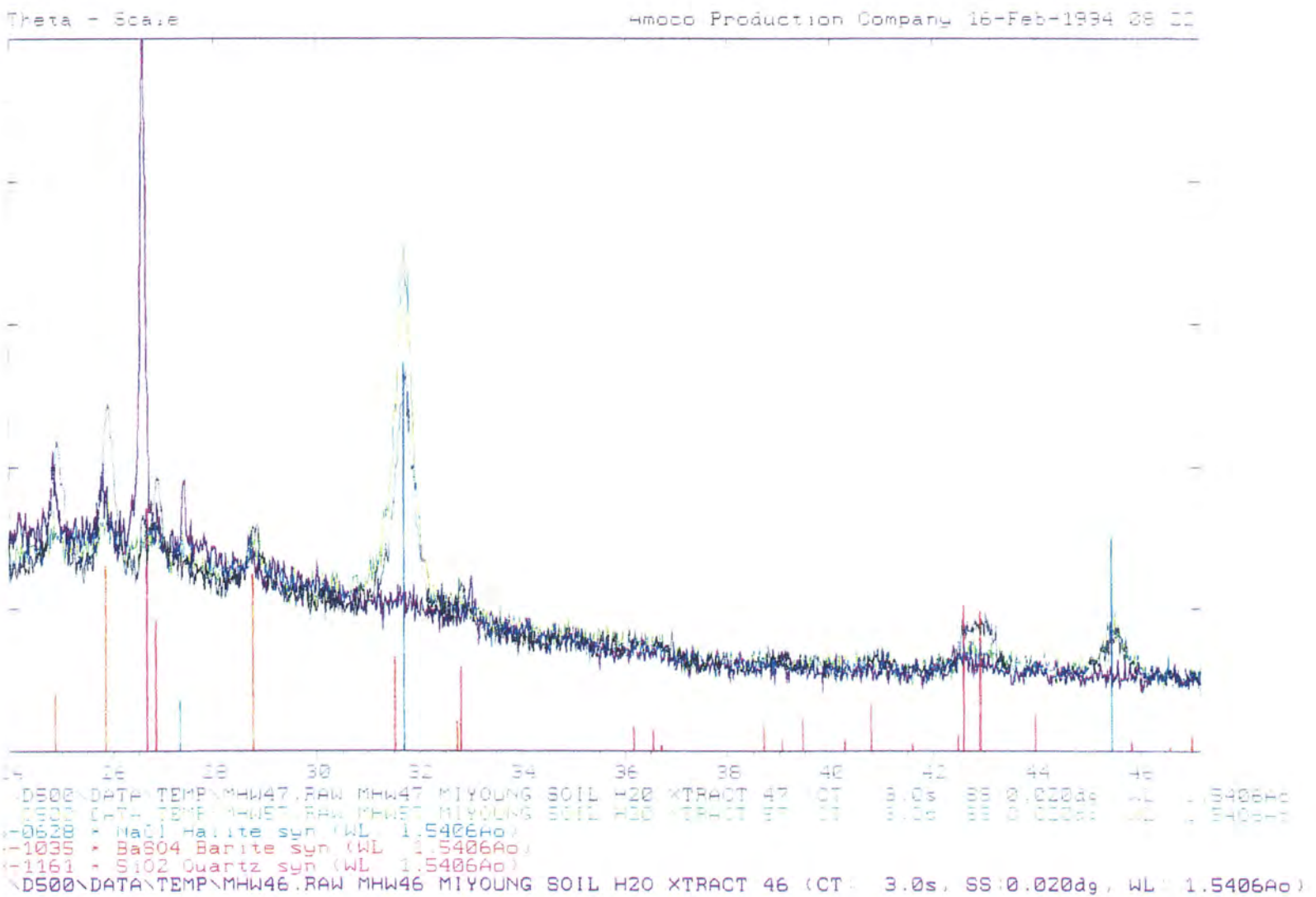
Theta - Scale
Amoco Production Company 16-Feb-1994 08:22
26
28
30
32
34
36
38
40
42
44
46
D500\DATA\TEMP\MHW47.RAW MHW47 MIYOUNG SOIL H20 XTRACT 47 (CT
-0628 - NaCl Halite syn (WL: 1.5406Ao)
-1035 - BaSO4 Barite syn (WL: 1.5406Ao)
-1161 - SiO2 Quartz syn (WL: 1.5406Ao)
\D500\DATA\TEMP\MHW46.RAW MHW46 MIYOUNG SOIL H20 XTRACT 46 (CT: 3.0s, SS:0.020dg, WL: 1.5406Ao)

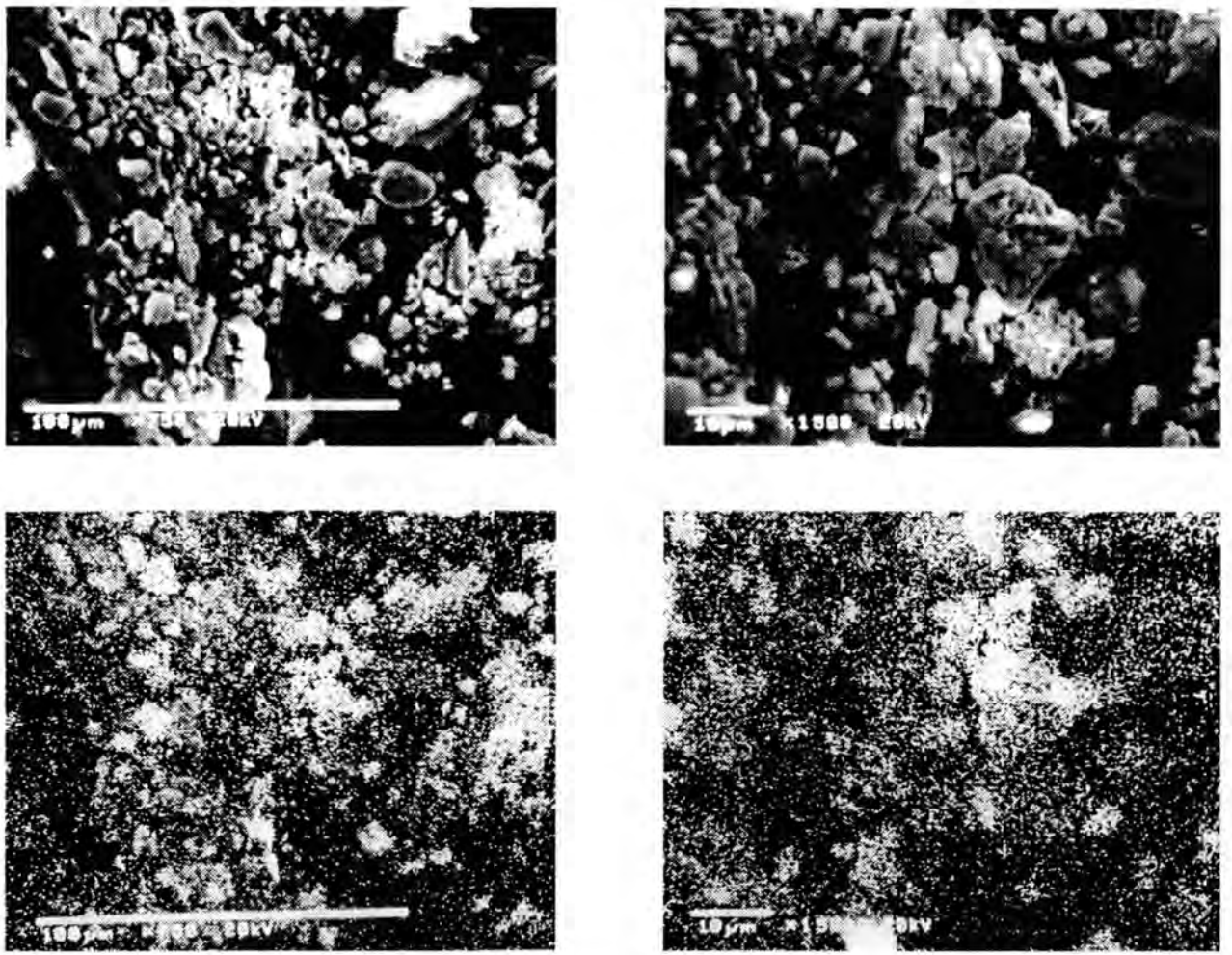

SEM photographs of solids obtained from the overflow of the hydrocyclone of sample treated with dispersant and dispersator (11385-45). (A) x750 image showing particle morphologies. (B) x1500 image showing detailed particle morphologies. (C) x750 image showing barium X-ray map of inage shown in (A). (D) x1500 image showing barium X-ray map of image shown in (B).

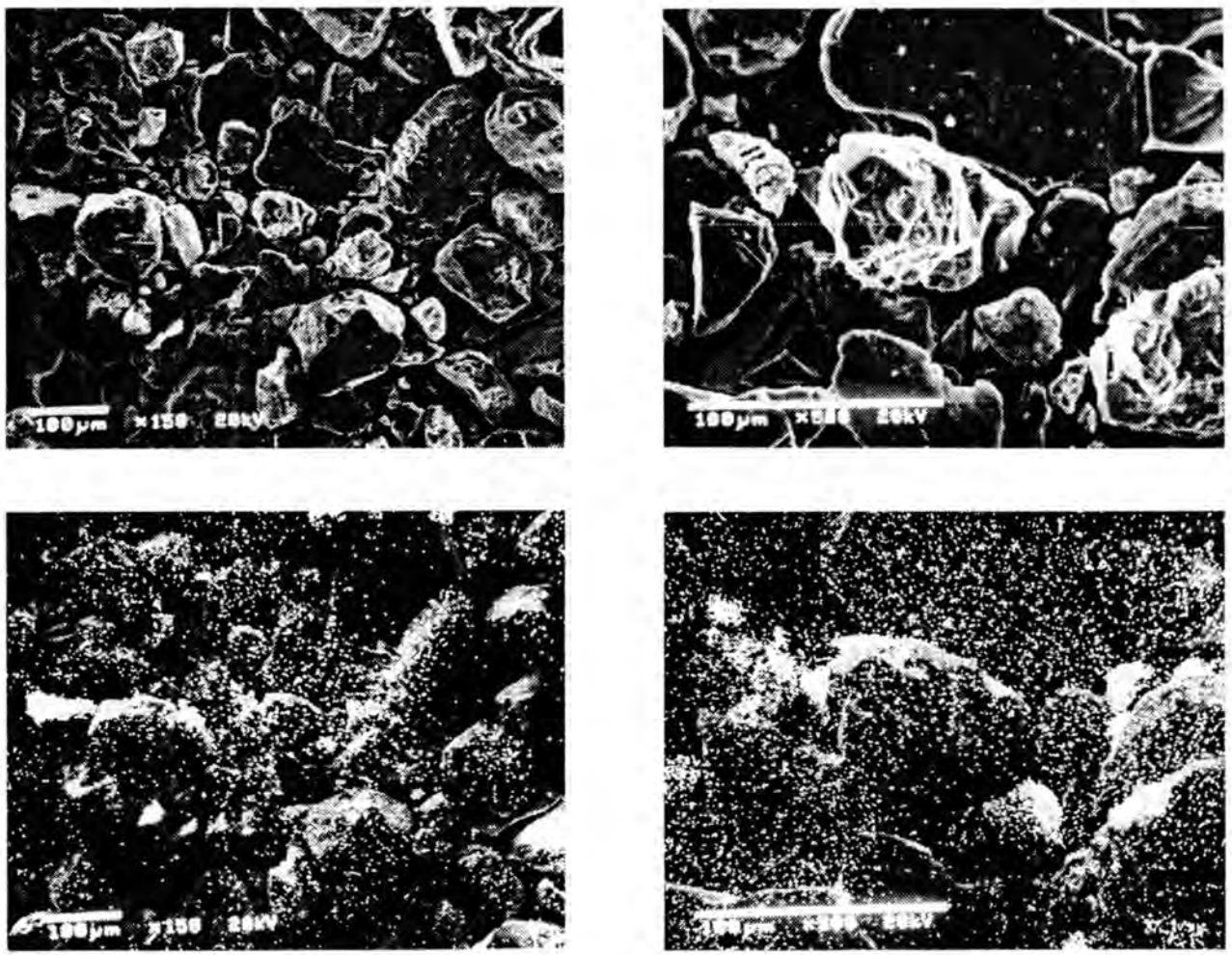

SEM photographs of solids obtained from the underflow of the hydrocyclone of sample treated with dispersant and dispersator (11385-46). (A) x150 image showing particle morphologies. (B) x500 image showing detailed particle morphologies. (C) x150 image showing barium X-ray map of inage shown in (A). (D) x500 image showing barium X-ray map of image shown in (B).

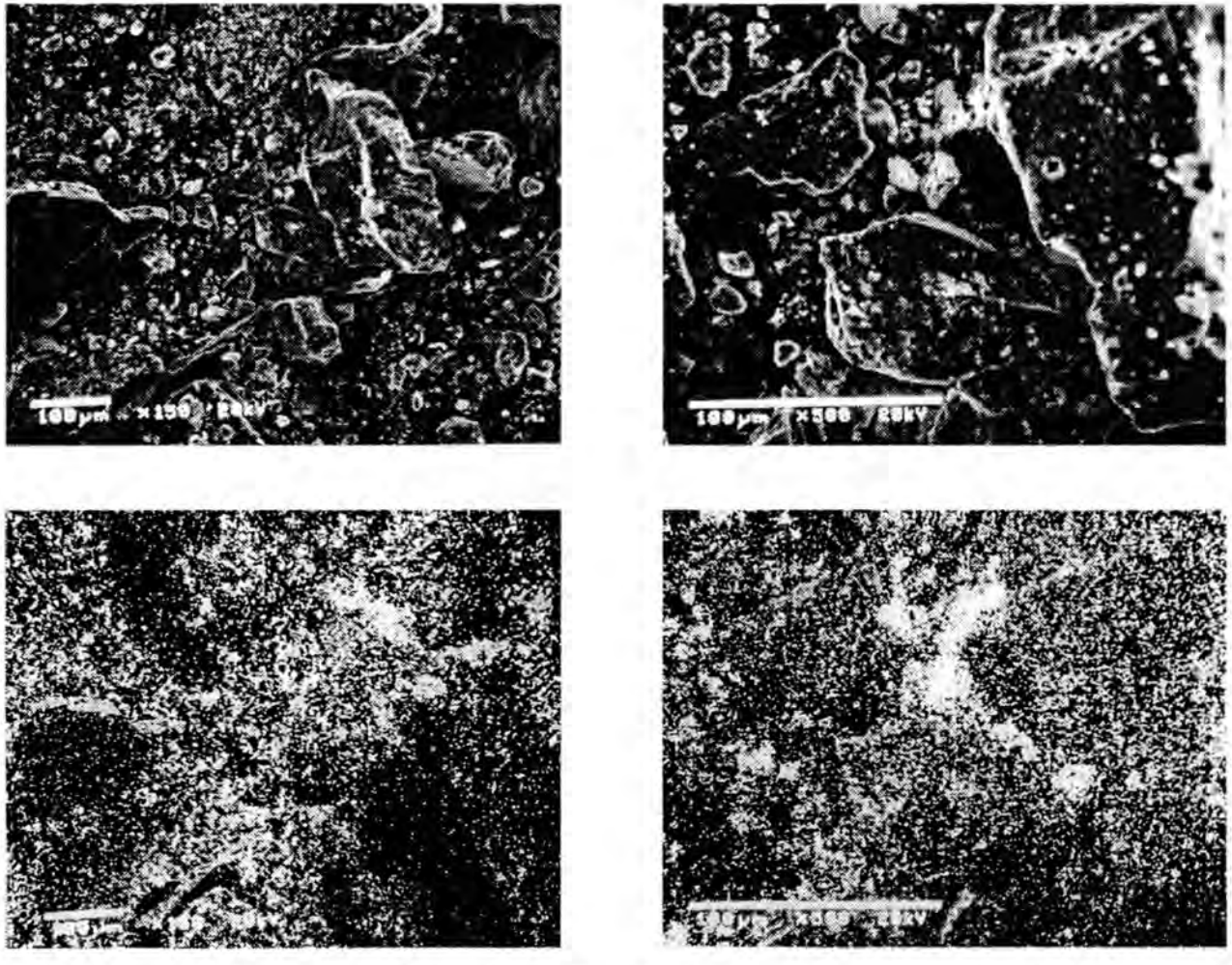

SEM photographs of solids obtained from the overflow of the hydrocyclone of sample treated with dispersant and dispersator (11385-47). (A) x150 image showing particle morphologies. (B) x500 image showing detailed particle morphologies. (C) x150 image showing barium X-ray map of inage shown in (A). (D) x500 image showing barium X-ray map of image shown in (B).

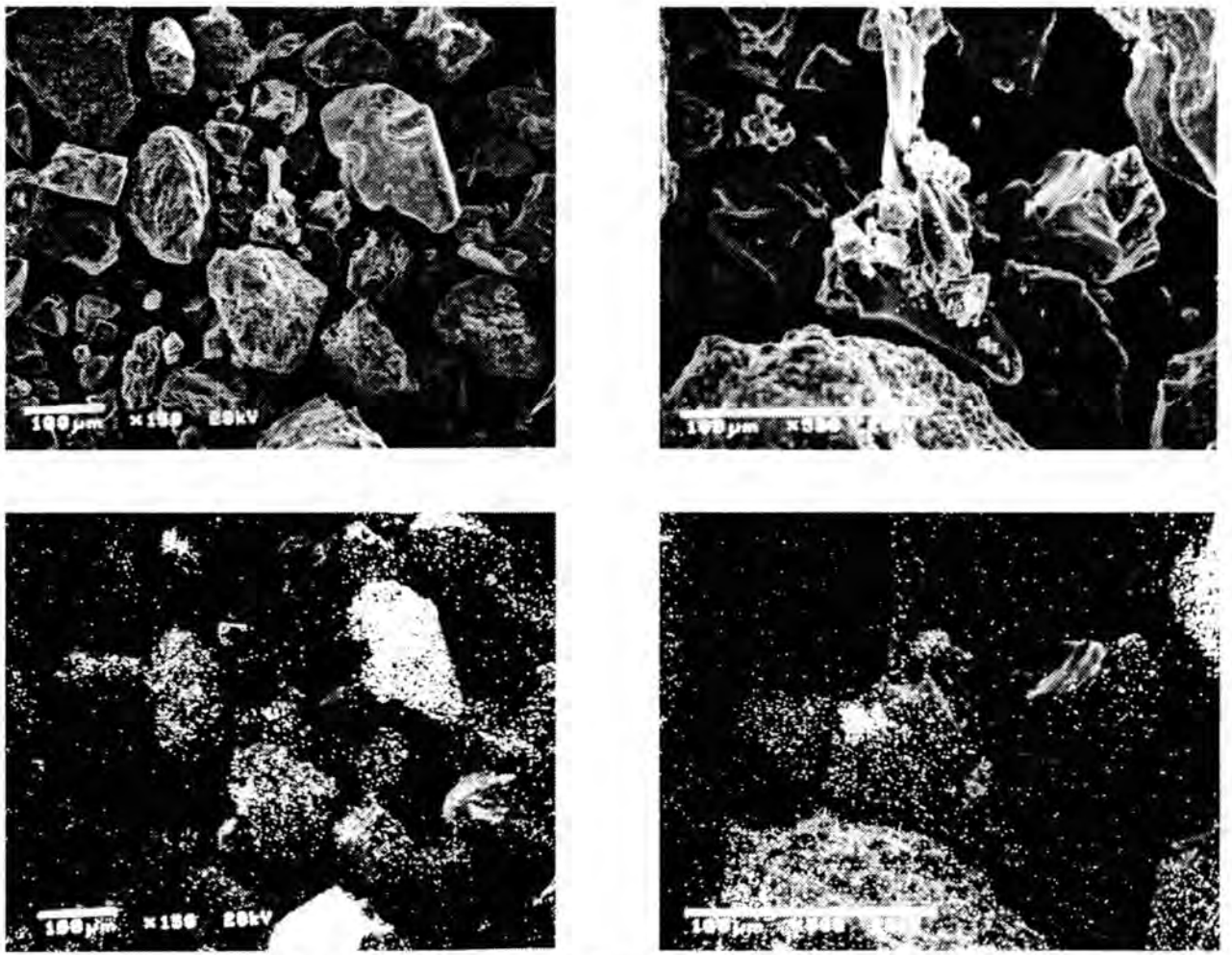

SEM photographs of solids obtained from the underflow of the hydrocyclone of sample treated with dispersant and dispersator (11385-48). (A) x150 image showing particle morphologies. (B) x500 image showing detailed particle morphologies. (C) x150 image showing barium X-ray map of inage shown in (A). (D) x500 image showing barium X-ray map of image shown in (B).

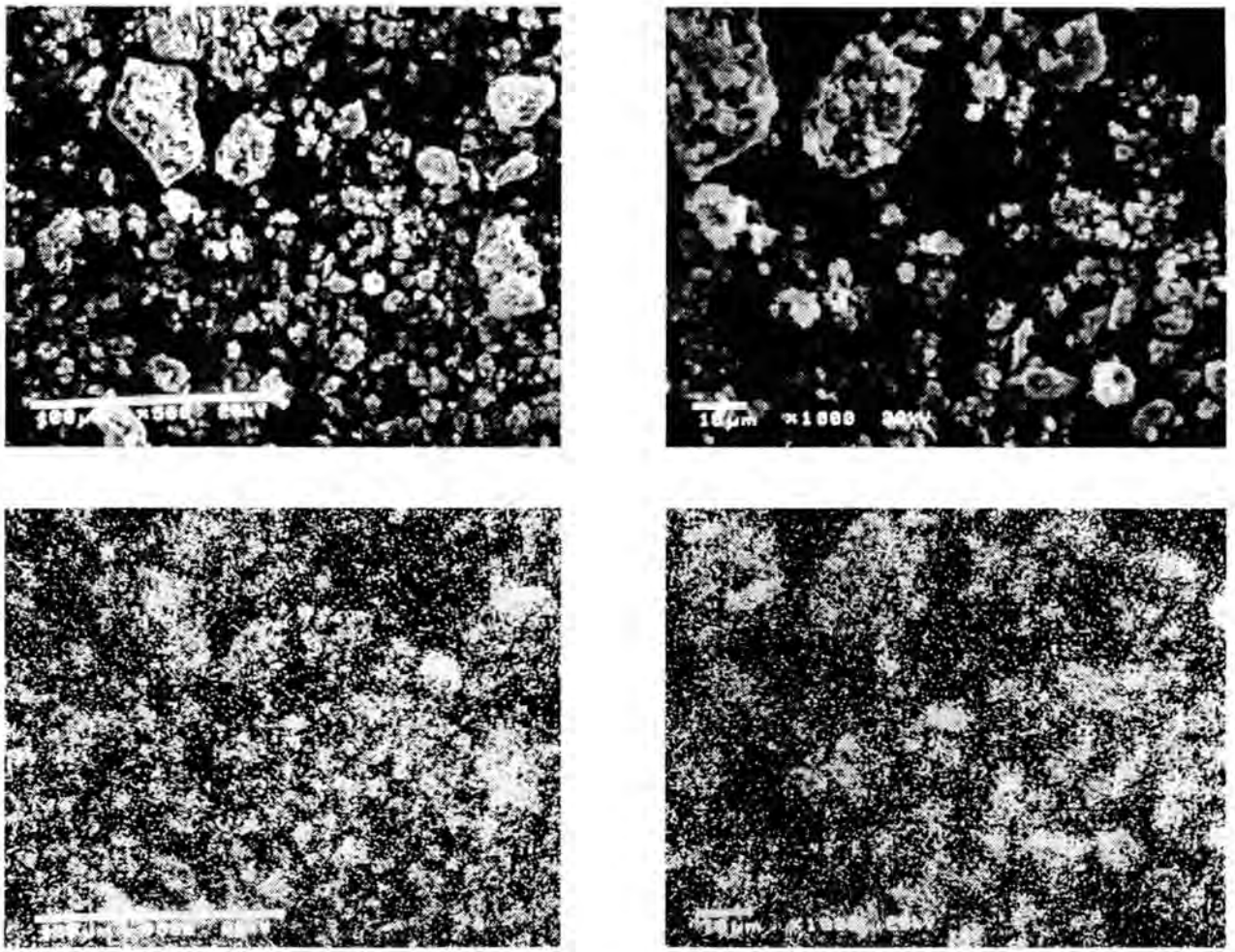

SEM photographs of solids obtained from the overflow of the hydrocyclone of sample treated with dispersant and dispersator (11385-49). (A) x500 image showing particle morphologies. (B) x1000 image showing detailed particle morphologies. (C) x500 image showing barium X-ray map of inage shown in (A). (D) x1000 image showing barium X-ray map of image shown in (B).

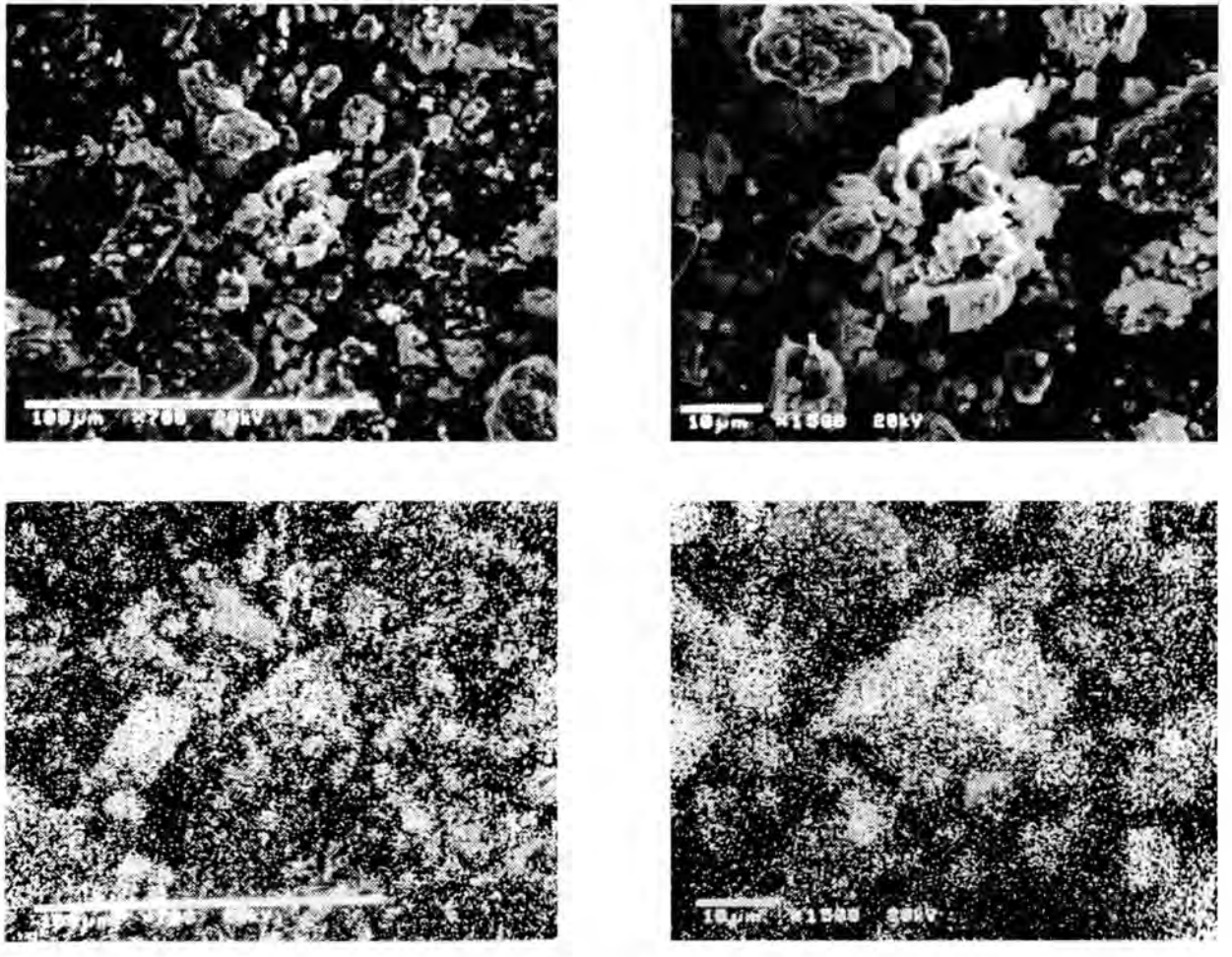

SEM photographs of solids obtained from the overflow of the hydrocyclone of sample treated with dispersant and dispersator (11385-53). (A) x700 image showing particle morphologies. (B) x1500 image showing detailed particle morphologies. (C) x700 image showing barium X-ray map of inage shown in (A). (D) x1500 image showing barium X-ray map of image shown in (B).

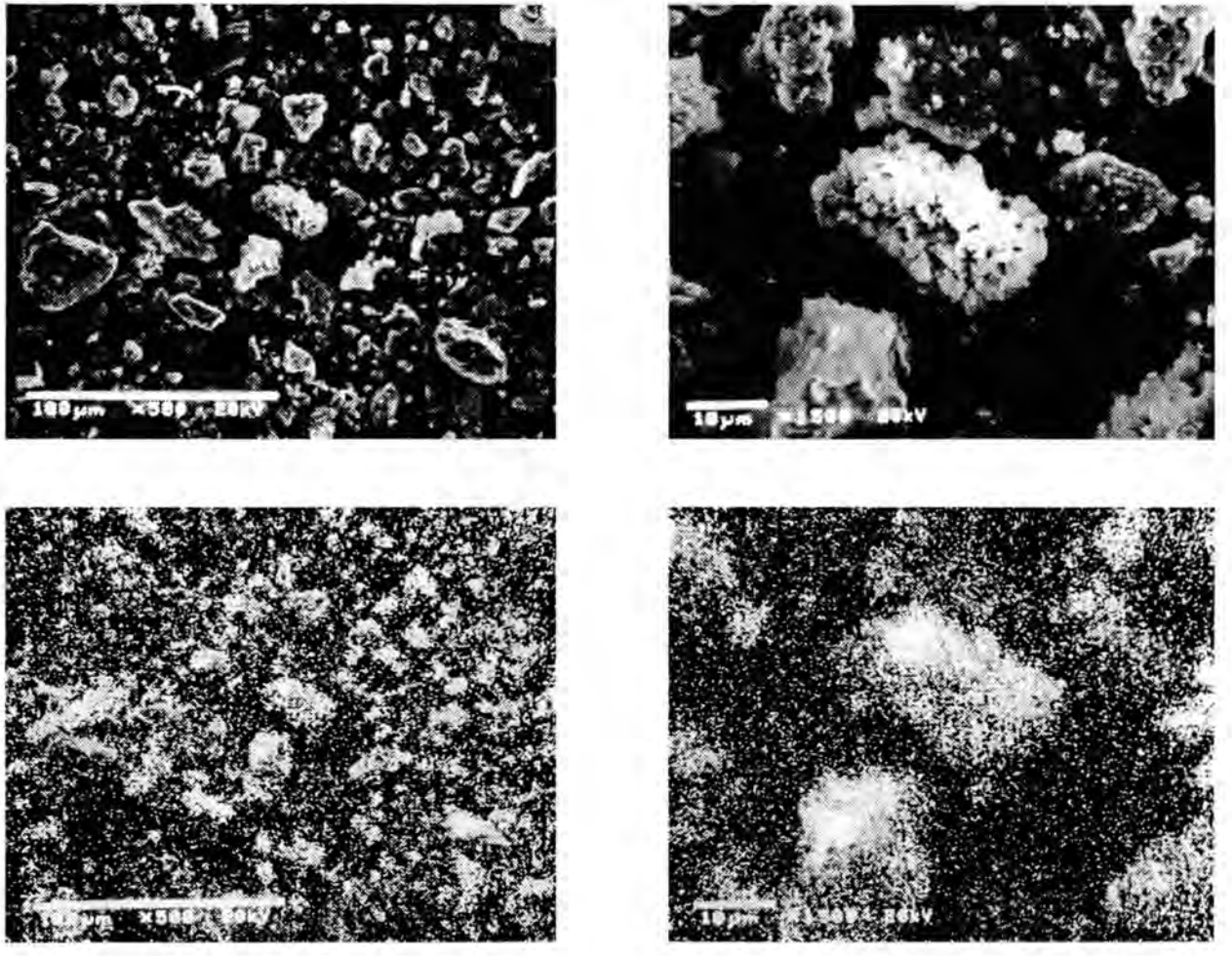

SEM photographs of solids obtained from the overflow from second run of the hydrocyclone of sample treated with dispersant and dispersator (11385-53b). (A) x500 image showing particle morphologies. (B) x1500 image showing detailed particle morphologies. (C) x500 image showing barium X-ray map of inage shown in (A). (D) x1500 image showing barium X-ray map of image shown in (B).

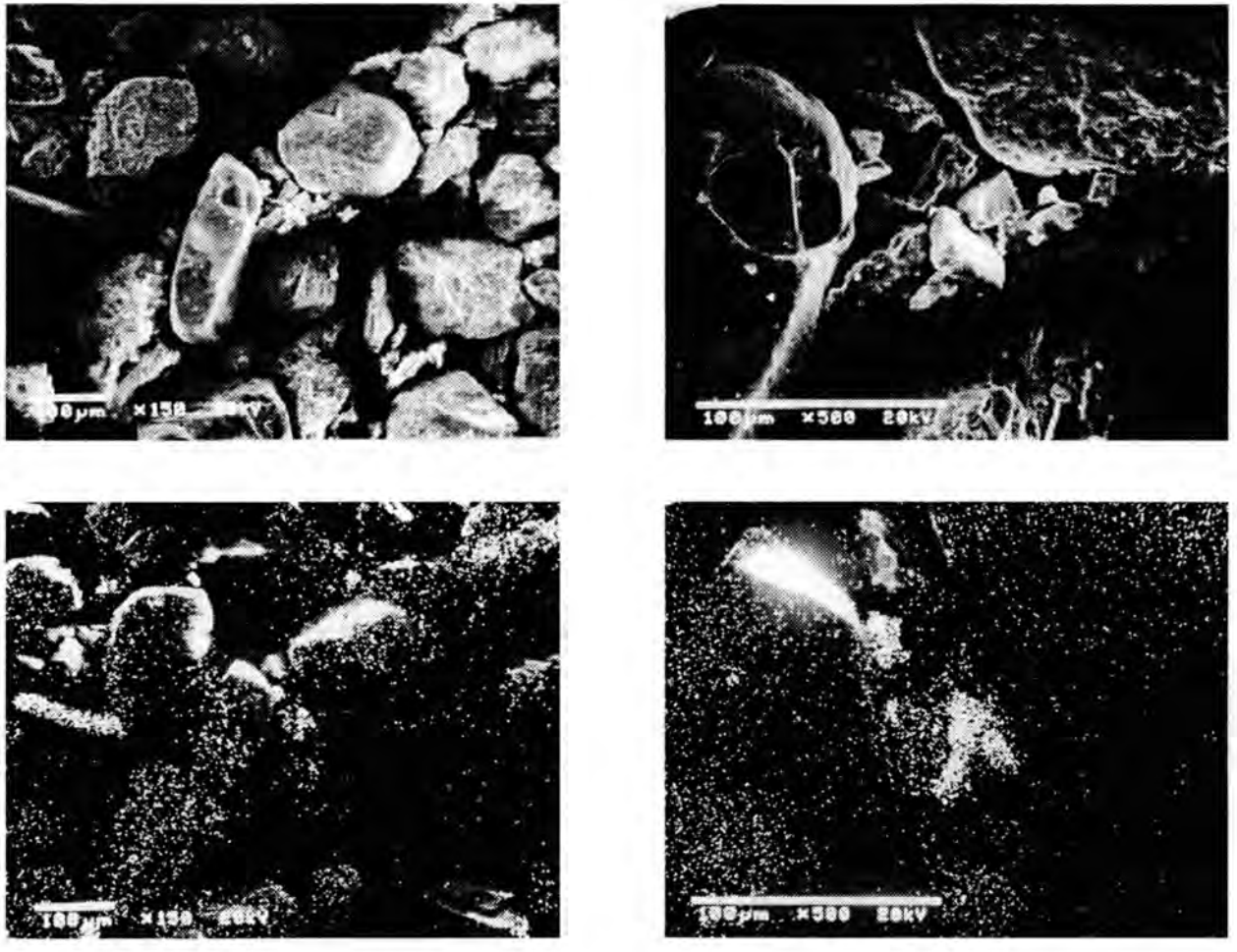

SEM photographs of solids obtained from the underflow of the hydrocyclone of sample treated with dispersant and dispersator (11385-54). (A) x150 image showing particle morphologies. (B) x500 image showing detailed particle morphologies. (C) x150 image showing barium X-ray map of inage shown in (A). (D) x500 image showing barium X-ray map of image shown in (B).

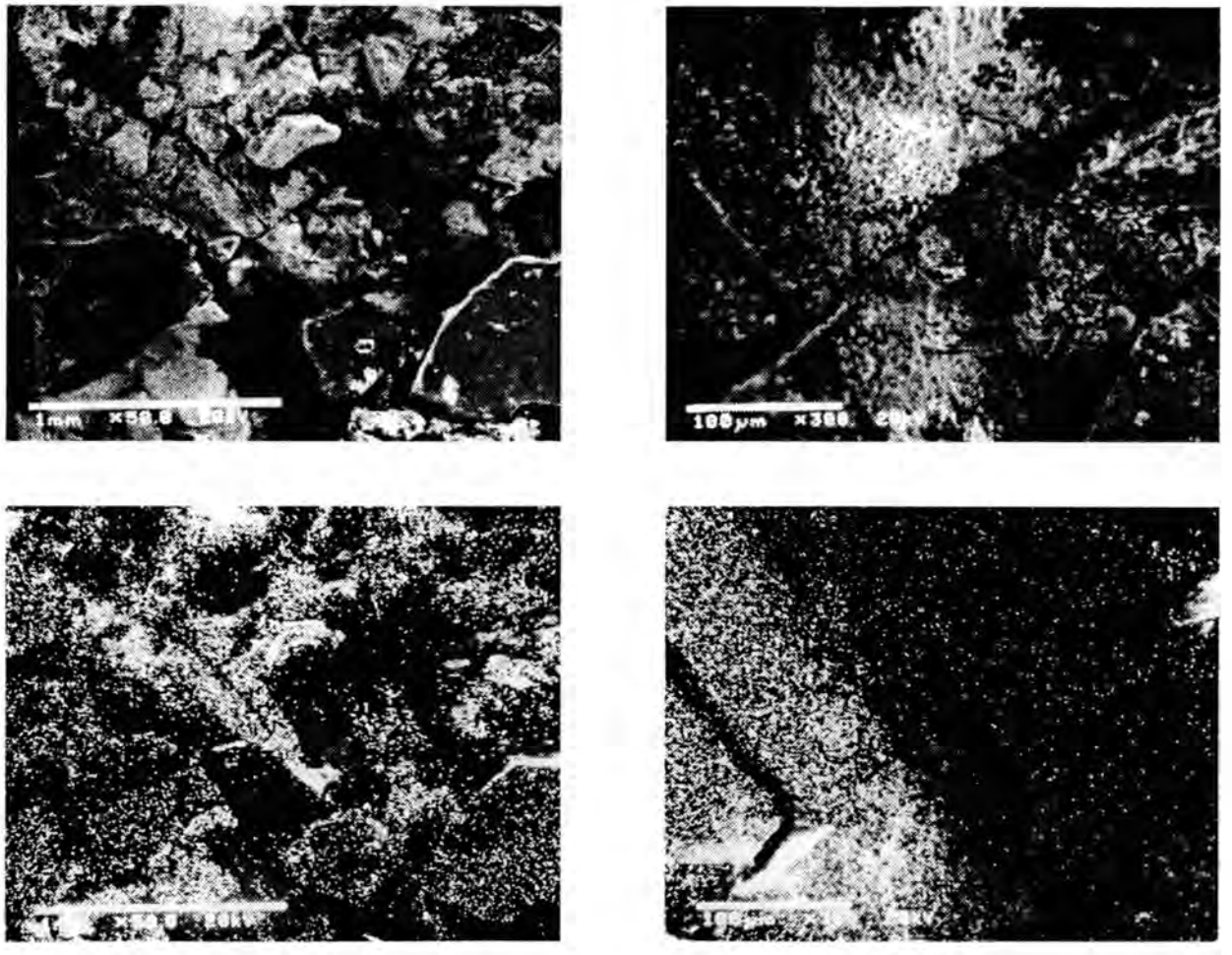

SEM photographs of solids obtained from the overflow of the hydrocyclone of sample treated with dispersant and dispersator (11385-57). (A) x50 image showing particle morphologies. (B) x300 image showing detailed particle morphologies. (C) x50 image showing barium X-ray map of inage shown in (A). (D) x300 image showing barium X-ray map of image shown in (B).

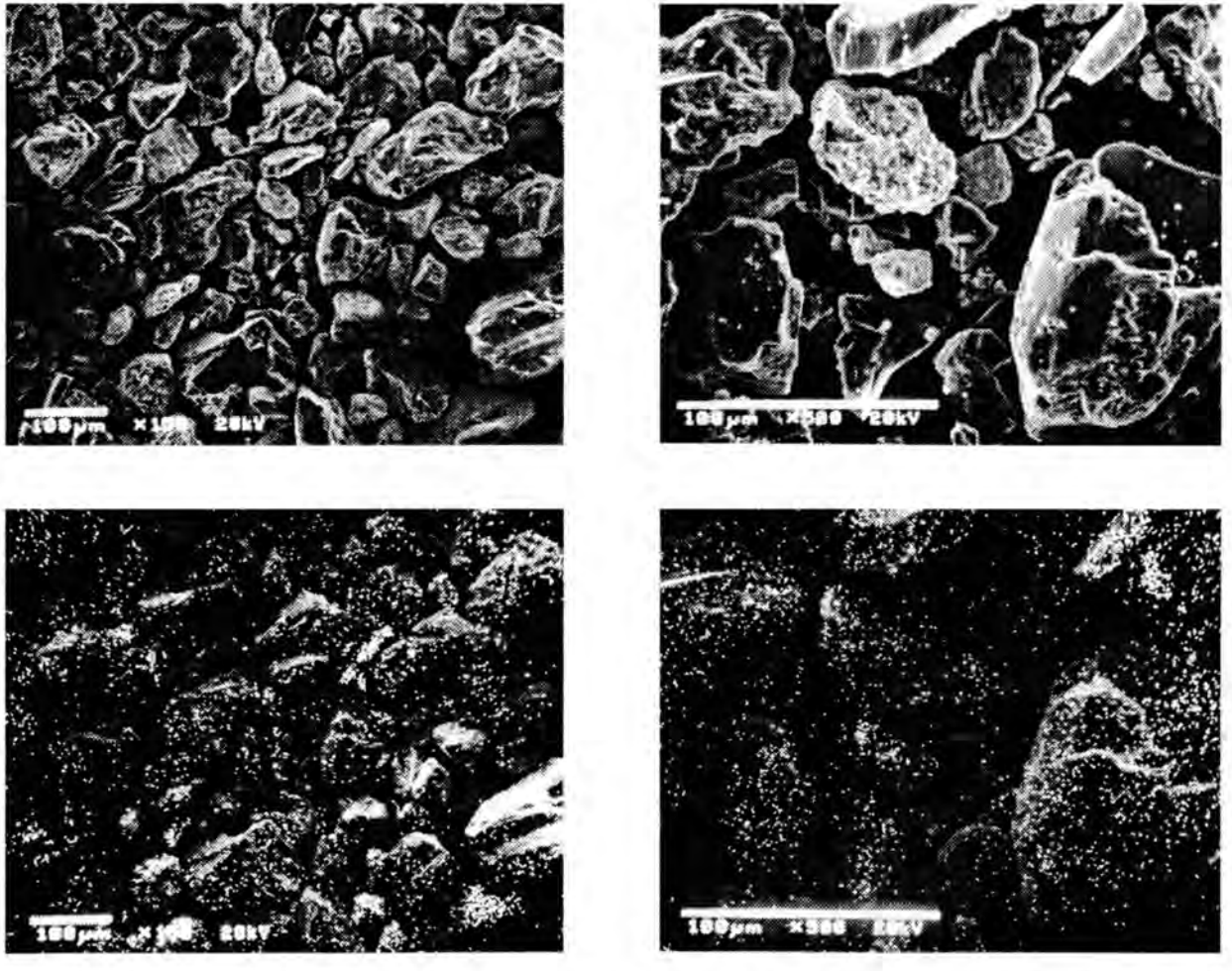

SEM photographs of solids obtained from the underflow of the hydrocyclone of sample treated with dispersant and dispersator (11385-58). (A) x150 image showing particle morphologies. (B) x500 image showing detailed particle morphologies. (C) x150 image showing barium X-ray map of inage shown in (A). (D) x500 image showing barium X-ray map of image shown in (B).

File: AM355321
AMOCO 11385-43 (93-553)

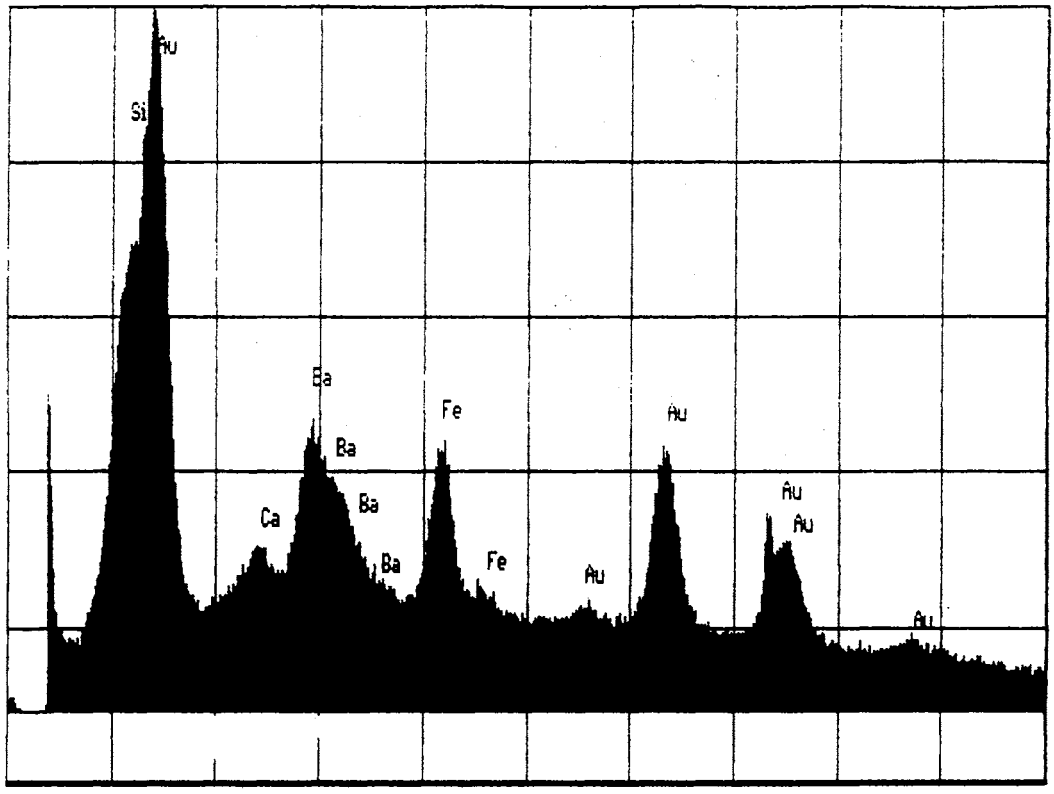

<- 0.0150 15.3600 ->
12/15/93 11:38 am

Data From: AM355321 Comments: AMOCO 11385-43 (93-553)
Time: 12/15/93 11:38 am

Net Area	Normalized Area	Comments
162.25	33.68	Si
37.69	7.83	Ca
124.79	25.91	Ba
156.97	32.59	Fe

File: AM355311
AMOCO 11385-44 (93-553)

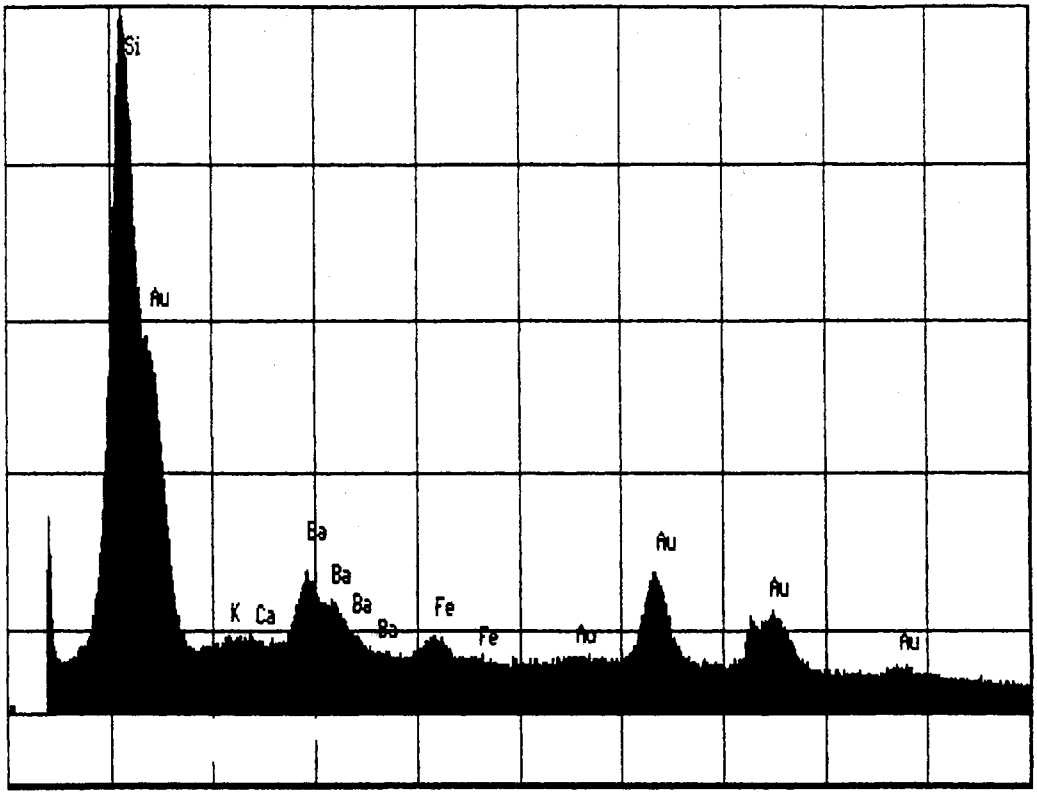

<- 0.0150 15.3600 ->
12/10/93 11:50 am

Data From: AM355311 Comments: AMOCO 11385-44 (93-553)
Time: 12/10/93 11:50 am

Net Area	Normalized Area	Comments
1093.64	88.55	Si
4.53	0.37	K
4.87	0.39	Ca
104.62	8.47	Ba
27.45	2.22	Fe

File: AM355324
AMOCO 11385-45 (93-553)

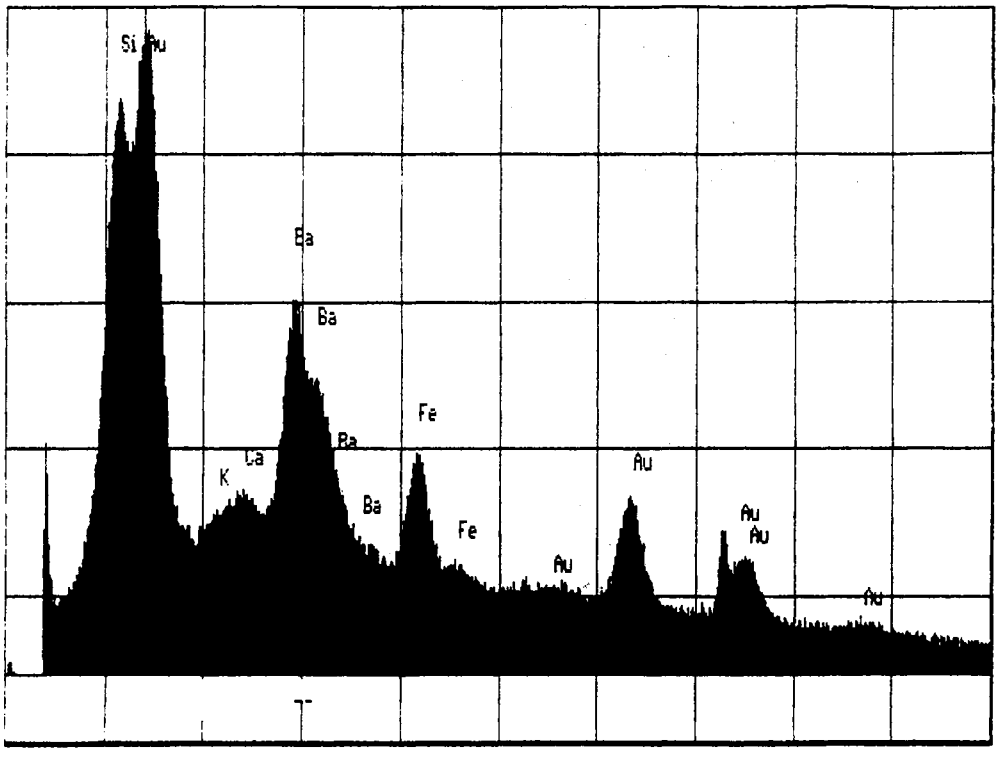

<- 0.0150 15.3600 ->
12/15/93 12:51 pm

Data From: AM355324 Comments: AMOCO 11385-45 (93-553)
Time: 12/15/93 12:51 pm

Net Area	Normalized Area	Comments
483.39	51.24	Si
25.39	2.69	
31.44	3.33	Ca
262.43	27.82	Ba
140.61	14.91	Fe

File: AM355313
AMOCO 11385-46 (93-553)

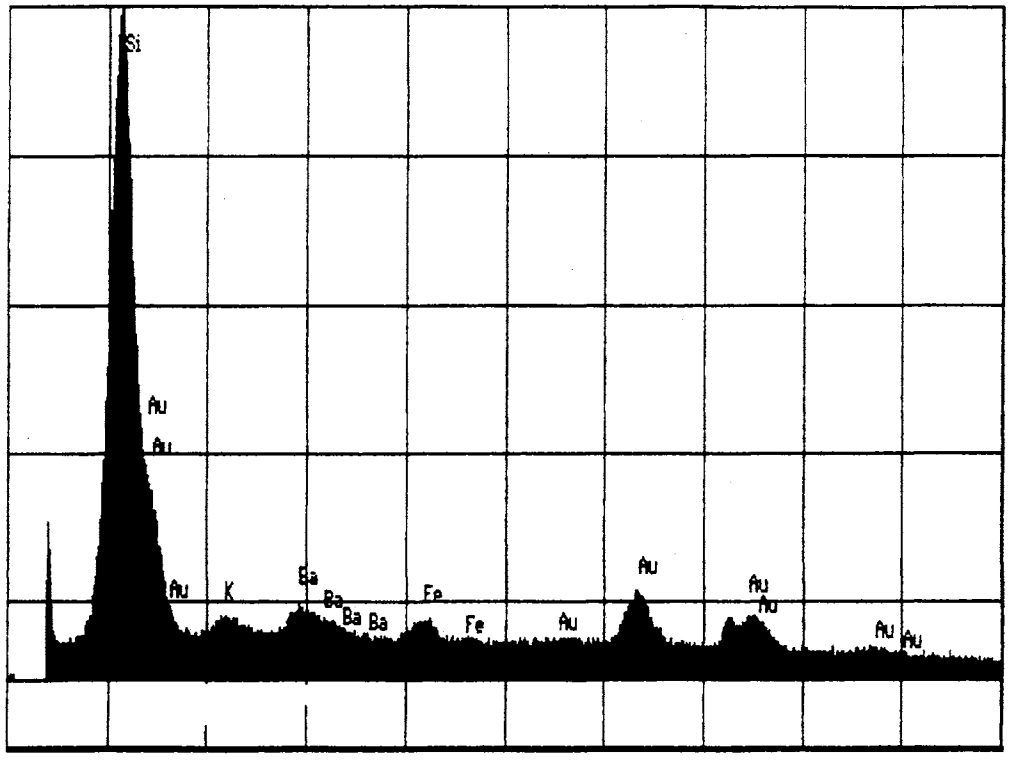

<- 0.0150 15.3600 ->
12/10/93 12:45 pm

Data From: AM355313 Comments: AMOCO 11385-46 (93-553)
Time: 12/10/93 12:45 pm

Net Area	Normalized Area	Comments
1434.01	92.89	Si
23.20	1.50	K
29.05	1.88	Ba
57.53	3.73	Fe

File: AM355314
AMOCO 11385-47 (93-553)

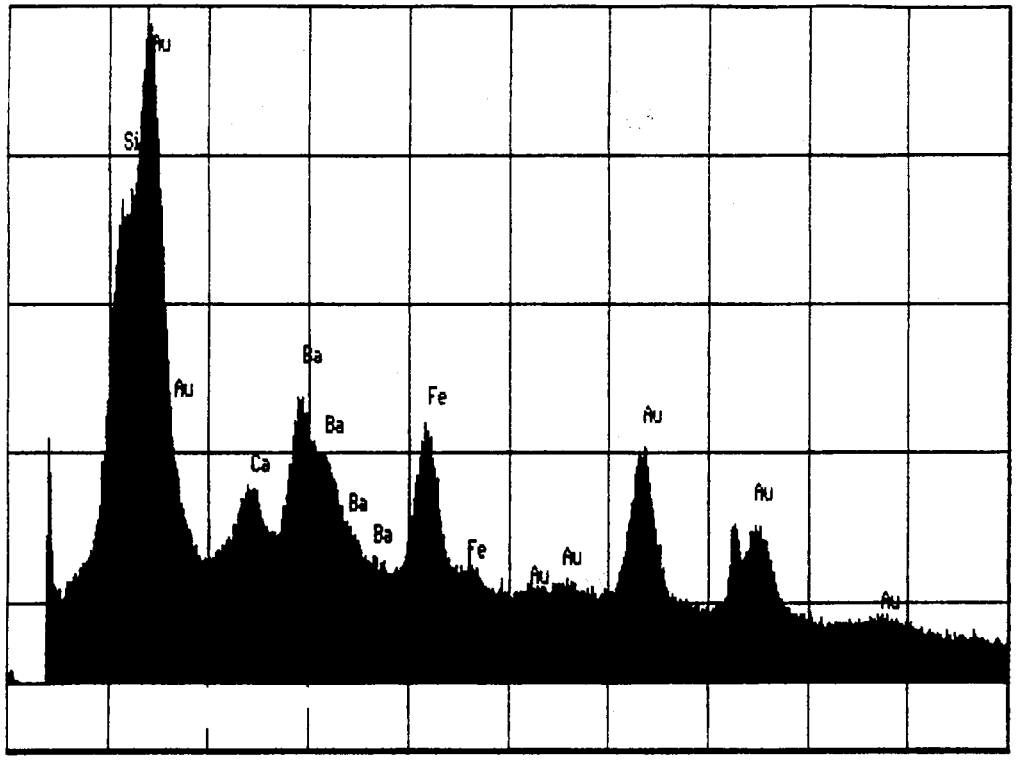

<- 0.0150 15.3600 ->
12/10/93 1:17 pm

Data From: AM355314 Comments: AMOCO 11385-47 (93-553)
Time: 12/10/93 1:17 pm

Net Area	Normalized Area	Comments
188.16	31.65	Si
80.89	13.61	Ca
146.84	24.70	Ba
178.64	30.05	Fe

File: AM355316
AMOCO 11385-49 (93-553)

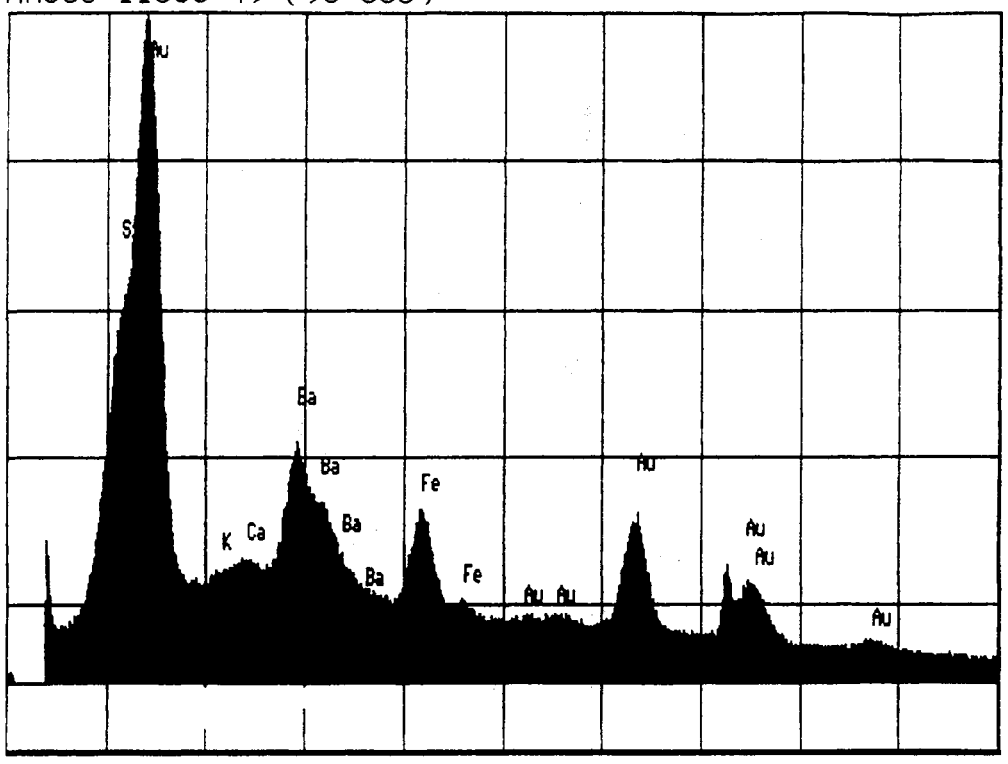

<- 0.0150 15.3600 ->
12/10/93 2:08 pm

Data From: AM355316 Comments: AMOCO 11385-49 (93-553)
Time: 12/10/93 2:08 pm

Net Area	Normalized Area	Comments
101.95	12.96	Si
3.39	0.43	K
15.86	2.02	Ca
415.15	52.78	Ba
250.25	31.81	Fe

File: AM355317
AMOCO 11385-50 (93-553)

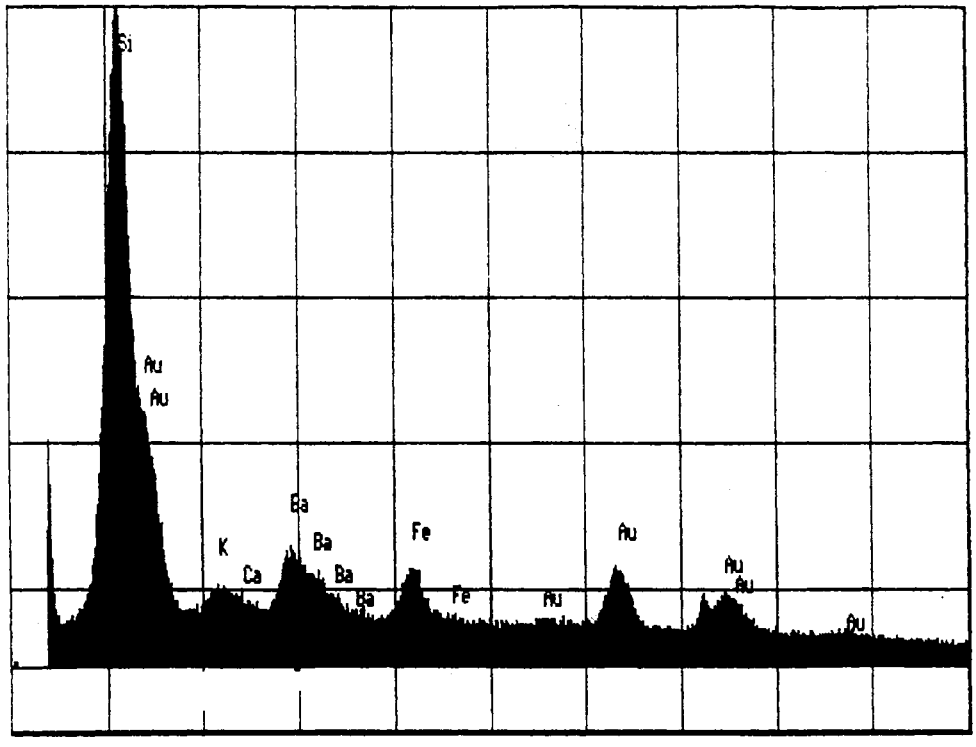

<- 0.0150 15.3600 ->
12/10/93 8:35 pm

Data From: AM355317 Comments: AMOCO 11385-50 (93-553)
Time: 12/10/93 8:35 pm

Net Area	Normalized Area	Comments
989.29	86.69	Si
16.25	1.42	K
66.97	5.87	Ba
68.69	6.02	Fe

File: AM355322
AMOCO 11385-53 (93-553)

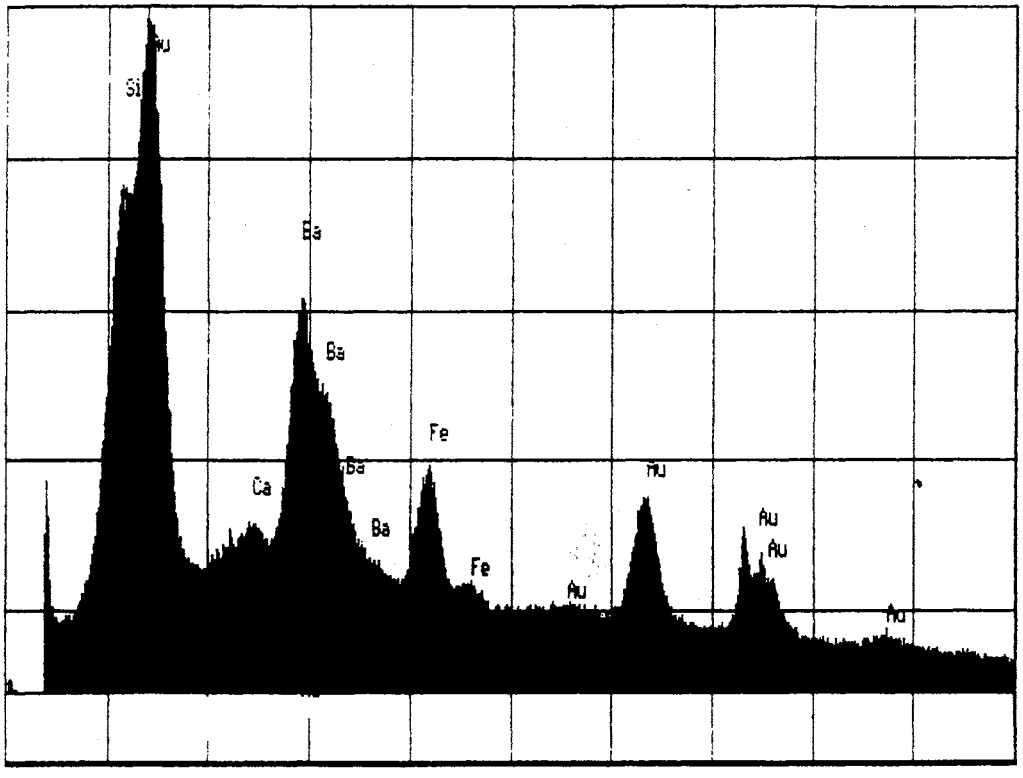

(- 0.0150 15.3600 ->
12/15/93 12:03 pm

Data From: AM355322 Comments: AMOCO 11385-53 (93-553)
Time: 12/15/93 12:03 pm

Net Area	Normalized Area	Comments
350.25	32.00	Si
56.88	5.20	Ca
530.68	48.48	Ba
156.83	14.33	Fe

File: AM355323
AMOCO 11385-53B (93-553)

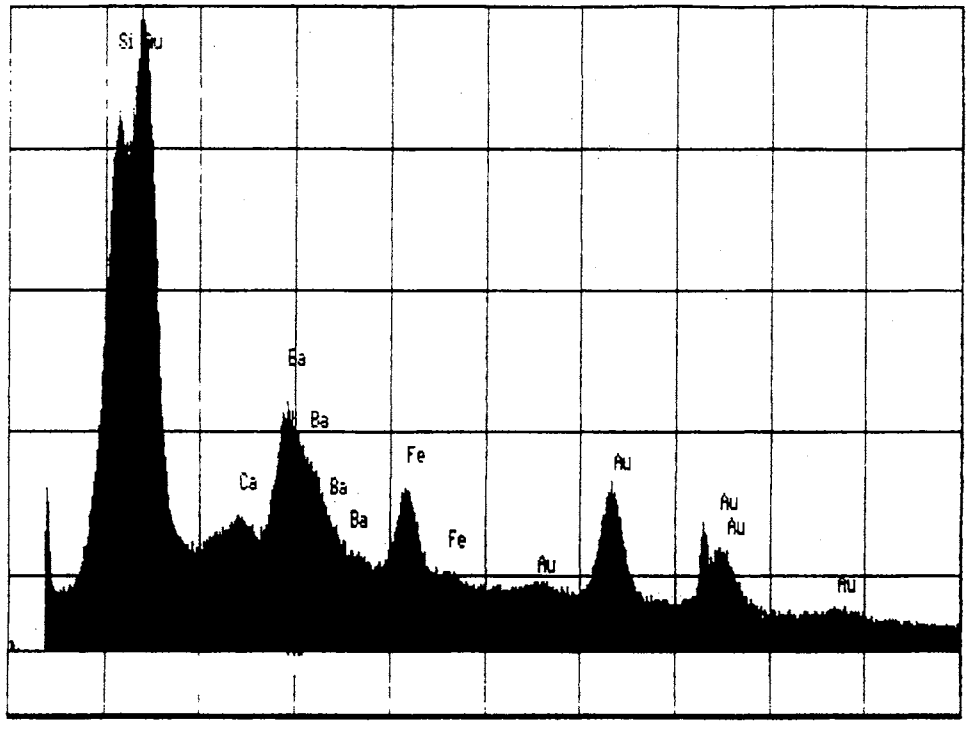

(- 0.0150 15.3600 ->
12/15/93 12:23 pm

Data From: AM355323 Comments: AMOCO 11385-53B (93-553)
Time: 12/15/93 12:23 pm

Net Area	Normalized Area	Comments
569.19	56.37	Si
30.92	3.06	Ca
281.61	27.89	Ba
127.94	12.67	Fe

File: AM355318
AMOCO 11385-54 (93-553)

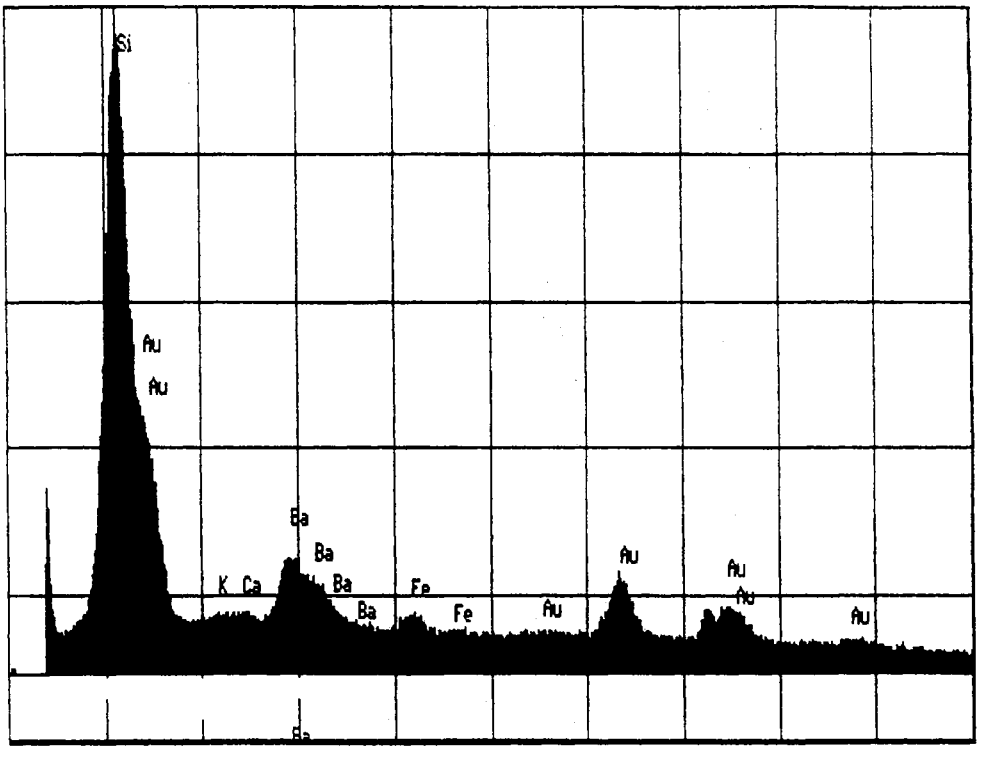

(- 0.0150 15.3600 ->
12/10/93 9:01 pm

Data From: AM355318 Comments: AMOCO 11385-54 (93-553)
Time: 12/10/93 9:01 pm

Net Area	Normalized Area	Comments
1012.91	89.66	Si
3.66	0.32	K
11.44	1.01	Ca
77.03	6.82	Ba
24.69	2.19	Fe

File: AM355319
AMOCO 11385-57 (93-553)

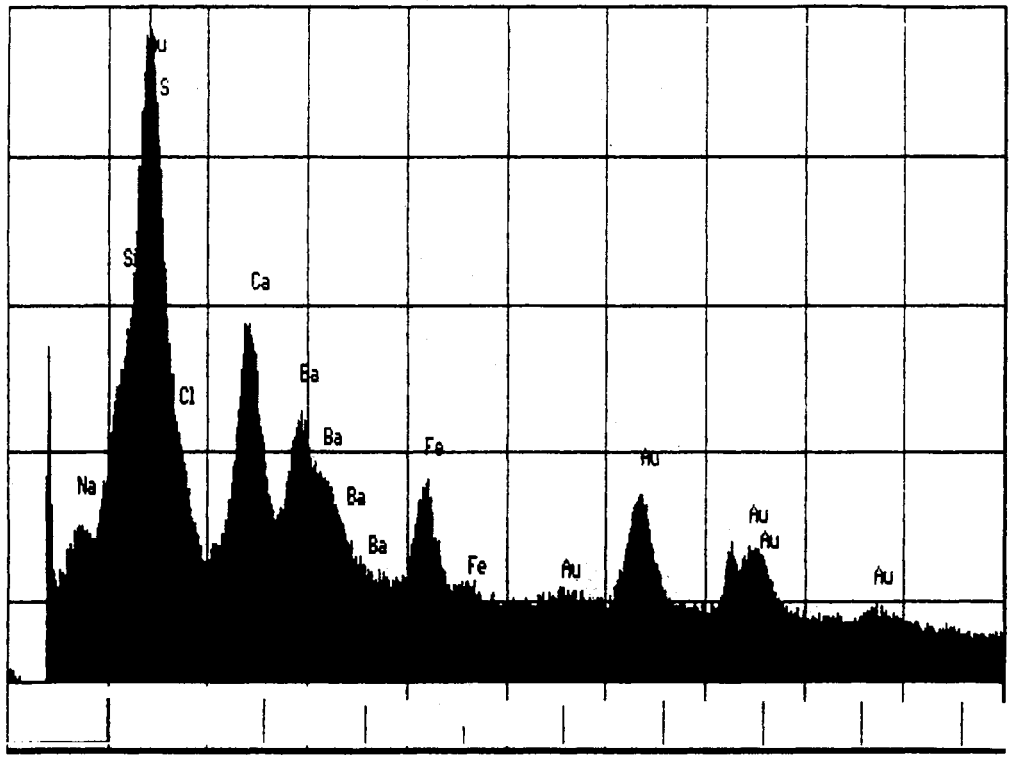

<- 0.0150 15.3600 ->
12/10/93 9:52 pm

Data From: AM355319 Comments: AMOCO 11385-57 (93-553)
Time: 12/10/93 9:52 pm

Net Area	Normalized Area	Comments
53.10	10.98	Na
7.57	1.57	Si
252.26	52.15	Ca
85.33	17.64	Ba
85.43	17.66	Fe

File: AM355319
AMOCO 11385-57 (93-553)

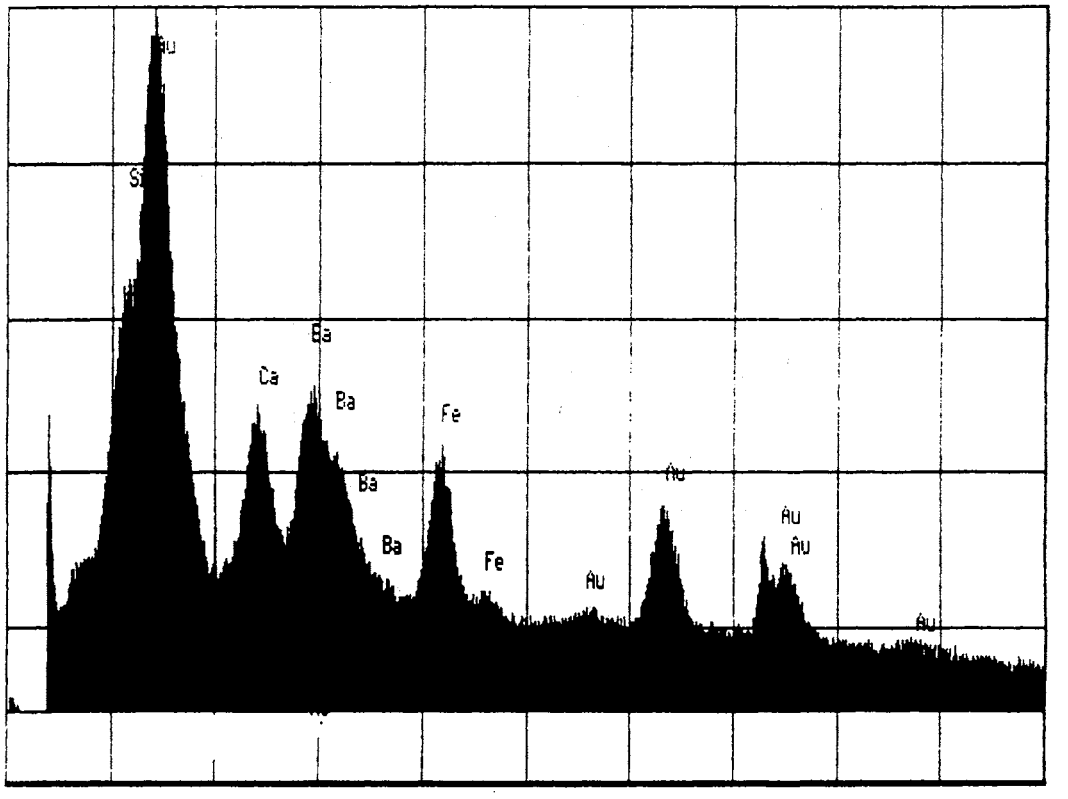

<- 0.0150 15.3600 ->
12/15/93 1:21 pm

Data From: AM355319 Comments: AMOCO 11385-57 (93-553)
Time: 12/15/93 1:21 pm

Net Area	Normalized Area	Comments
102.64	15.68	Si
215.91	32.99	Ca
172.67	26.38	Ba
163.30	24.95	Fe

APPENDIX E

ORIGINAL DATA PERTAINING TO DISSOLUTION EXPERIMENT

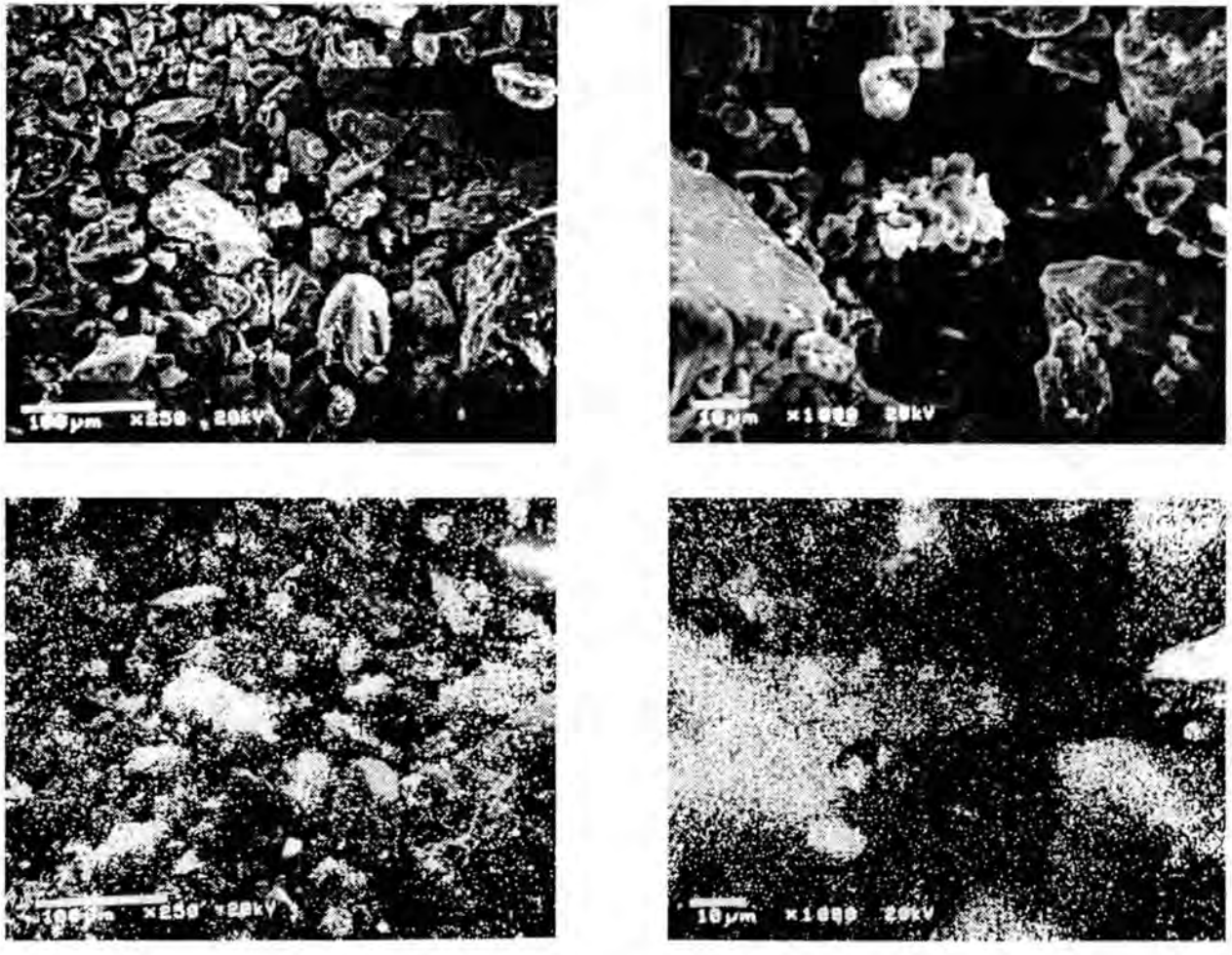

SEM photographs of sample from dissolution experiment performed at room temperature with DTPA and oxalic acid solution (11374-32F). (A) x250 image showing particle morphologies. (B) x1000 image showing detailed particle morphologies. (C) x250 image showing barium X-ray map of image shown in (A). (D) x1000 image showing barium X-ray map of image shown in (B).

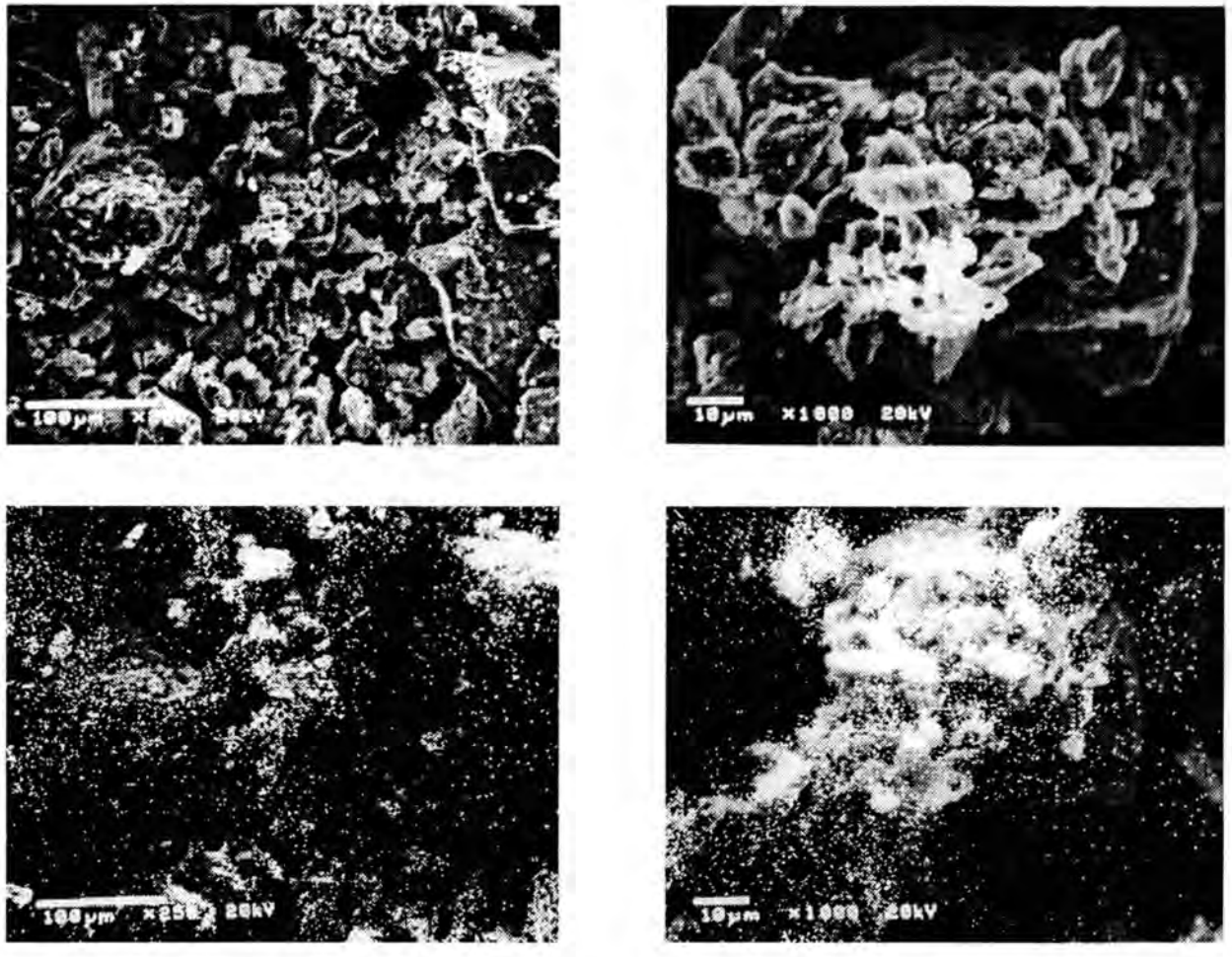

SEM photographs of sample from dissolution experiment performed at room temperature with Calnox S-271 (11374-32F). (A) x100 image showing particle morphologies. (B) x1000 image showing detailed particle morphologies. (C) x100 image showing barium X-ray map of image shown in (A). (D) x1000 image showing barium X-ray map of image shown in (B).

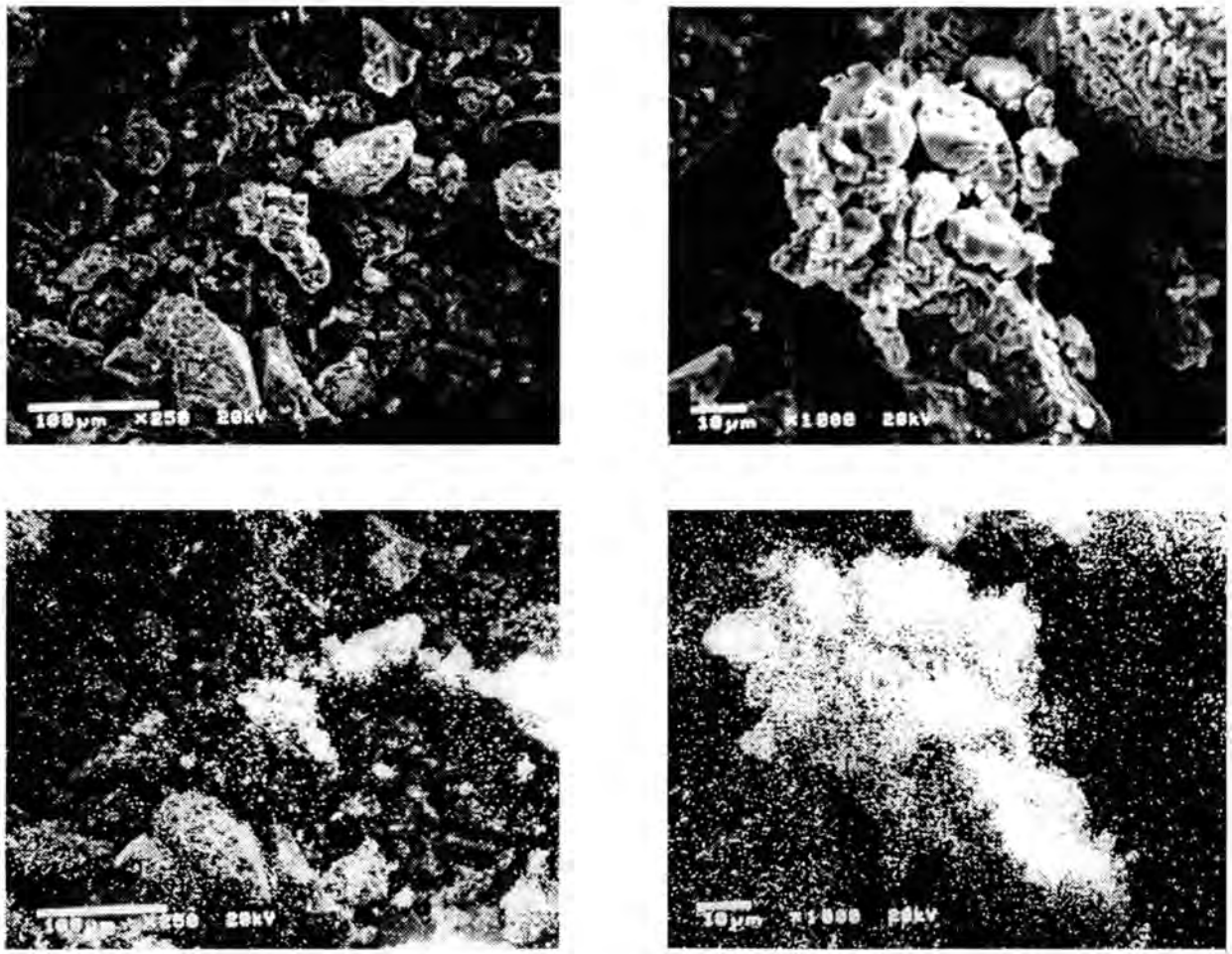

SEM photographs of sample from dissolution experiment performed at elevated temperature with Calnox S-271 (11374-33H). (A) x250 image showing particle morphologies. (B) x1000 image showing detailed particle morphologies. (C) x250 image showing barium X-ray map of image shown in (A). (D) x1000 image showing barium X-ray map of image shown in (B).

VITA 2

Miyoung Hammond

Candidate for the Degree of

Master of Science

Thesis: CHARACTERIZATION AND POTENTIAL TECHNOLOGIES FOR HAZARD AND WASTE VOLUME REDUCTION FOR NORM-CONTAMINATED OIL-FIELD PROCESS VESSEL SOLIDS AND CONTAMINATED SOILS

Major Field: Environmental Engineering

Biographical:

Personal Data: Born in Inchon, Korea, September 17, 1963, the daughter of Henry H. and Nancy Hammond.

Education: Graduated from Judson High School, Converse, Texas, in May 1982; received Bachelor of Science degree in Petroleum Engineering from Texas A&M University, College Station, Texas; completed requirements for the Master of Science degree at Oklahoma State University in July 1994.

Professional Experience: Engineer, Amoco Production Company, Houston, Texas, September 1988 to September 1989. Engineer, Phillips Petroleum Company, Bartlesville, Oklahoma, October 1989 to May 1992.